TAMPEREEN TEKNILLINEN YLIOPISTO
TAMPERE UNIVERSITY OF TECHNOLOGY

Sarang Thombre

Test Bench Solutions for Advanced GNSS Receivers: Implementation, Automation, and Application

Julkaisu 1200 • Publication 1200

Tampere 2014

Tampereen teknillinen yliopisto. Julkaisu 1200
Tampere University of Technology. Publication 1200

Sarang Thombre

Test Bench Solutions for Advanced GNSS Receivers: Implementation, Automation, and Application

Thesis for the degree of Doctor of Science in Technology to be presented with due permission for public examination and criticism in Tietotalo Building, Auditorium TB224, at Tampere University of Technology, on the 4th of April 2014, at 12 noon.

Tampereen teknillinen yliopisto - Tampere University of Technology
Tampere 2014

Supervisors:

Jari Nurmi, Dr. Tech., Professor
Department of Electronics and Communications Engineering,
Tampere University of Technology,
Tampere, Finland.

Mikko Valkama, Dr. Tech., Professor
Department of Electronics and Communications Engineering,
Tampere University of Technology,
Tampere, Finland.

Pre-examiners:

Gérard Lachapelle, Dr.Tech., Professor

Professor and CRC/iCORE Chair in Wireless Location.
University of Calgary, Department of Geomatics Engineering,
2500 University Dr NW
Calgary, Alberta, Canada T2N 1N4.

Marco Lisi, Dottore ingegnere.

GNSS Services Engineering Manager,
Special Advisor of the European Commission.
European Space Research & Technology Centre (ESTEC),
Keplerlaan 1, 2201 AZ Noordwijk, The Netherlands.

Opponents:

Marco Lisi, Dottore ingegnere.

GNSS Services Engineering Manager,
Special Advisor of the European Commission.
European Space Research & Technology Centre (ESTEC),
Keplerlaan 1, 2201 AZ Noordwijk, The Netherlands.

Jari Syrjärinne, D.Sc.(Tech)

HERE, a Nokia business
PL 14, 33721 TAMPERE
Finland.

ISBN 978-952-15-3259-7 (printed)
ISBN 978-952-15-3263-4 (PDF)
ISSN 1459-2045

ABSTRACT

Considerable study has been devoted to the implementation of GNSS receivers for diverse applications, and to finding solutions to some of the non-idealities associated with such receivers. However, not much research is devoted to innovations in their performance evaluation, even though this is an integral step in the overall implementation process. This research work attempts to address this issue through three different perspectives: by focusing on innovation in the testing procedures and test-bench implementation, its automation and its application to advanced multi-frequency, multi-constellation GPS and Galileo receivers. Majority of this research was conducted within the GREAT, GRAMMAR, and FUGAT projects funded by EU FP6/FP7 and TEKES respectively, during which the author was responsible for designing test-scenarios and performing validations of the implemented receiver solution.

The first part of the research is devoted to the study and design of sources of test signals for an advanced GNSS receiver test-bench. An in-depth background literature study was conducted on software-based GNSS signal simulators to trace their evolution over the past two decades. Keeping their special features and limitations in view, recommendations have been made on the optimum architecture and essential features within such simulators for testing of advanced receivers. This resulted in the implementation of an experimental software-based simulator capable of producing GPS L1 and Galileo E1 signals at intermediate frequency. Another solution investigated was a GNSS Sampled Data Generator (SDG) based on wideband sampling. This included designing the entire radio front-end operating on the bandpass-sampling principle. The low noise amplifier designed as part of this SDG has been implemented on a printed circuit board.

Phase noise (PN) from the radio front-end's local frequency generator (LFG) is a source of error that has hitherto not been included in any GNSS signal simulator. Furthermore, the characterization of the baseband tracking loops in presence of this phase noise has not yet been included in the typical receiver test scenarios. The second part of this research attempts to create mathematical models representing the LFG's phase noise contribution,

first for a free running oscillator and later for a complete phase-locked loop (PLL). The effect of such phase noise was studied on the baseband correlation performance of GPS and Galileo receivers. The results helped to demonstrate a direct relation between the PN and the baseband tracking performance, thus helping to define guidelines for radio front-end PLL circuit design in order to maintain a minimum baseband tracking performance within the GNSS receiver.

The final part of this research work focusses on describing the automated test-bench developed at Tampere University of Technology (TUT) for analyzing the overall performance of multi-frequency multi-constellation GNSS receivers. The proposed test-bench includes a data capture tool to extract internal process information, and the overall controlling software, called automated performance evaluation tool, that is able to communicate between all modules for hands-free, one-button-click testing of GNSS receivers. Furthermore, these tools have been applied for the single frequency GPS L1 performance testing of the TUTGNSS receiver, with recommendations on how they can be adapted to testing of advanced multi-frequency, multi-constellation receivers.

PREFACE

The work presented in this thesis has been carried out under the supervision of Prof. Jari Nurmi and Prof. Mikko Valkama during the years 2010 - 2013 within the Department of Computer Systems and its successor, the Department of Electronics and Communications Engineering of the Tampere University of Technology, Finland.

I am grateful towards Prof. Nurmi for allowing me the research freedom during the past years to investigate a topic which is quite ubiquitous within the industrial domain, yet not fully explored within academic circles. He has been very supportive and encouraging, offering me new vistas for applying skills that I have attempted to gather over the past few years. It has been a real pleasure for me to be a part of his research group. I would also like to appreciate the technical advice and supervision provided to me by Prof. Mikko Valkama, who is most appropriate to verify whether a particular research idea possesses sound technological feasibility. Prof. Gérard Lachapelle and Dr. Marco Lisi have been the external reviewers for this manuscript, and I would like to acknowledge them for their valuable feedback and suggestions on improvements. Finally, I would like to thank Dr. Jari Syrjärinne and Dr. Marco Lisi for agreeing to be the opponents at my Doctoral dissertation, and through it providing me with constructive criticism while I defended my research work.

In addition to my direct supervisors, other experts who have guided me during the formative years of my Doctoral research career are Dr. Heikki Hurskainen, Associate Prof. Elena Simona Lohan, Dr. Stephan Sand, Dr. Nikolay N. Tchamov, Ernesto Perez Serna, Marco Detratti, Dr. L. Enrique Aguado, Ignacio Fernández Hernández, Ari Asp, Dr. Tiiti Kellomäki, Dr. Martti Kirkko-Jaakkola and Prof. John Raquet. I would like to sincerely thank them for their valuable and timely insights into matters of technology.

This research work would not have been possible without the financial support from the Tampere University of Technology, Tampere Doctoral Programme in Information Science and Engineering (TISE), Nokia Foundation and Ulla Tuominen Foundation. It has also been partially supported by the Finnish Funding Agency for Technology and Innovation (TEKES) under the project “Future GNSS Applications and Techniques (FUGAT)", and

the European Union Framework Programme (EU FP6, FP7) under the projects “Galileo Ready Advanced Mass Market Receiver (GRAMMAR)” and “Galileo Receiver for Mass Market (GREAT)”. I wish to convey my special gratitude to the Finnish Geodetic Institute, where I was able to complete the concluding phase of this thesis work while while working on the topics of multi-GNSS and COMPASS/Beidou receiver design.

Now comes the fun part! A career in research involves long periods of thinking, planning, waiting, and patience between short bursts of activity and breakthroughs. It is during these intervals of inactivity that you most require peer motivation, encouragement, support, and above all entertainment. I am eternally grateful to my (cramped) colleagues, Tommi Paakki, Francescantonio Della Rosa, and Jussi Raasakka from room TH310 for the countless lunches, funny anecdotes and videos, career highs and lows that we shared during the past years in the midst of Finnish rock music blaring on the radio. I am also thankful to the other members of Team Nurmi, for their company and support with technical and/or administrative matters during the past years. My special acknowledgement goes to Dr. Saku Suuriniemi with our orienteering excursions every Monday, and to all members of the Indian Community for the homely atmosphere they helped to create for me in this beautiful city of Tampere!

To my Mother (Aai) and Father (Baba), I wish to say that, “I would not be where I am today if it were not for your blessings, encouragement and eternal love. We may be thousands of kilometers away, but your thoughts are always with me”. To the other members of my family, I would like to appreciate their support and motivation during all these years. My little daughter Nishka has been the most beautiful distraction during my Doctoral research work. Her innocent eccentricities compelled me to leave my worries and anxieties at the workplace and instead join forces with her in scribbling, and LEGO-ing. Perhaps that was her little part in ensuring I ended each day on a high note. My final appreciation goes to my wife Pooja for her love and devotion. She believed in me and my ability to successfully accomplish this task, even during times of self-doubt when the light bulb of ideas was unlit. Thank you for providing me a warm and welcoming home and family to return to after a day of (mild) hard work!

Tampere, 4th April, 2014
Sarang Thombre

TABLE OF CONTENTS

ABSTRACT iii
PREFACE v
TABLE OF CONTENTS vii
LIST OF PUBLICATIONS xi
LIST OF ABBREVIATIONS xiii
LIST OF SYMBOLS xvii
LIST OF FIGURES xix
LIST OF TABLES xxi
1. INTRODUCTION 1
1.1 Background and Motivation 1
1.2 Research Objectives and Scope 2
1.3 Linking the Thesis Topic to the Chapters and Publications 3
1.4 Research Methodology 5
1.5 Main Contributions 6
1.6 Thesis Outline 7
2. BASICS OF GNSS 9
2.1 Concept of Satellite Positioning 9
2.2 GNSS Signal Structure 12
2.3 GNSS Signal Spectrum 12
2.4 GNSS Receiver Structure 14
2.5 RF Front-end Architecture Evolution 14
2.6 Receiver Radio Front-end Architectures 16
2.6.1 Direct conversion Architecture 16
2.6.2 Superheterodyne Architechture 17
2.6.3 Direct Bandpass-Sampling Architecture 18
3. SOFTWARE-BASED GNSS SIGNAL SIMULATORS 19

3.1 Introduction and background 19
3.2 Signal Generation Module 20
3.3 Error Generation Module 22
3.3.1 Receiver Clock Error 22
3.3.2 Satellite Clock Error 23
3.3.3 Ionospheric Delay Error 24
3.3.4 Tropospheric Delay Error 25
3.3.5 Doppler Frequency Offset 25
3.4 Transmission Channel Module 26
3.5 Radio Frequency Front-End Module 27
3.6 Satellite Geometry Module 27
4. BANDPASS-SAMPLING BASED GNSS RECEIVER RF FRONT-ENDS 29
4.1 Introduction and background 29
4.2 Antenna 29
4.3 Low Noise Amplifier (LNA) 30
4.4 RF Filter 31
4.5 Direct RF bandpass-sampling 31
4.5.1 Concept and numerical analysis 31
4.5.2 Benefits 35
4.5.3 Challenges 36
5. EFFECTS OF PHASE NOISE ON GNSS TRACKING PERFORMANCE 39
5.1 Introduction and Background 39
5.2 Basics of Phase Noise 39
5.3 Simulation Scenarios 41
5.4 Simulation Results 42
5.4.1 SNR of correlation peak versus VCO PN 44
5.4.2 Phase component of correlation peak versus VCO PN 45
5.5 Results Analysis 45
5.6 Endnote about Phase Noise and Allan Variance 46

6. TEST SCENARIOS FOR ADVANCED GNSS RECEIVERS 53
6.1 Introduction and Background 53
6.2 Receiver Settings 53
6.3 Time to First Fix (TTFF) Tests 54
6.3.1 Nominal Cold Start, Warm Start and Hot Start TTFF 54
6.3.2 Low Power Cold Start TTFF 54
6.4 Acquisition Sensitivity in Cold Start 56
6.5 Accuracy 57
6.6 Tracking Sensitivity 57
6.7 Availability 57
6.8 Receiver Dynamics 58
6.9 Reacquisition Time 58
6.10 Multipath Mitigation 59
6.11 Radio Frequency Interference (RFI) 59
6.12 Ionosphere errors 59
7. OVERVIEW OF PUBLICATIONS 61
7.1 Research Problems and Proposed Solutions 61
7.2 Relating Publications to the Research Work 62
7.3 Author's Contribution to the Publications 63
7.4 Impact of Publications 65
8. CONCLUSIONS 67
8.1 Main Contributions of the Research 67
8.2 Future Work 68
BIBLIOGRAPHY 69
PUBLICATIONS 81

LIST OF PUBLICATIONS

This thesis is a compilation of the following publications, referred to as [P#] and are appended in the concluding half of the thesis.

[P1] **S. Thombre**, E. S. Lohan, J. Raquet, H. Hurskainen, J. Nurmi, "Software-based GNSS Signal Simulators: Past, Present and Possible Future", Proceedings of the *2010 European Navigation Conference (ENC GNSS 2010)*, October 2010 in Braunschweig, Germany.

[P2] **S. Thombre**, H. Hurskainen, J. Nurmi, "Wideband, High Gain, High Linearity, Low Noise Amplifier for GNSS Frequencies with Compensation for Low Frequency Instability", Proceedings of the *Advanced Satellite Multimedia Systems Conference (ASMS 2010)*, September 2010 in Cagliari, Italy.

[P3] **S. Thombre**, J. Nurmi, "Bandpass-Sampling based GNSS Sampled Data Generator – A Design Perspective", Proceedings of the *International Conference on Localization and GNSS (ICL-GNSS 2012)*, June 2012 in Starnberg, Germany.

[P4] E. P. Serna, **S. Thombre**, M. Valkama, S. Lohan, V. Syrjälä, M. Detratti, H. Hurskainen, J. Nurmi, "Local Oscillator Phase Noise Effects on GNSS Code Tracking", *InsideGNSS*, Nov/Dec 2010, pg 52-62.

[P5] **S. Thombre**, J. Raasakka, M. Valkama, S. Lohan, H. Hurskainen, J. Nurmi, "Local Oscillator Phase Noise Effects on Phase Angle Component of GNSS Code Correlation", Proceedings of the *2011 International Conference on Localization and GNSS (ICL-GNSS 2011)*, June 2011 in Tampere, Finland.

[P6] **S. Thombre**, N. N. Tchamov, S. Lohan, M. Valkama, J. Nurmi, "Effects of Radio Front-end PLL Phase Noise on GNSS Baseband Correlation", accepted for publication in *NAVIGATION, Journal of the Institute of Navigation*, 21st March, 2014.

[P7] **S. Thombre**, J. Raasakka, T. Paakki, F. Della Rosa, M. Valkama, J. Nurmi, "Automated Test-bench Infrastructure for GNSS Receivers – Case Study of the

TUTGNSS Receiver", Proceedings of the *Institute of Navigation's GNSS+ (ION GNSS+ 2013)*, Nashville, Tennessee, USA, September 16-20, 2013.

LIST OF ABBREVIATIONS

2D	Two-dimensional
3D	Three-dimensional
ADC	Analog-to-Digital Converter
AutoPET	Automated Performance Evaluation Tool
AV	Allan Variance
AWGN	Additive White Gaussian Noise
BW	Bandwidth
BPF	Bandpass Filter
C/A	Coarse Acquisition
CHPLL	Charge Pump PLL
CNR	Carrier to Noise Ratio
DC	Direct Current
dCAP	Data Capture Tool
DLR	German Aerospace Center
ENC	European Navigation Conference
ELT	Department of Electronics and Communications Engineering
ESA	European Space Agency
EU FP	European Union Framework Programme
FDR	Frequency Division Ratio
FLL	Frequency Locked Loop
FPGA	Field Programmable Gate Array
FRO	Free Running Oscillator
FUGAT	Future GNSS Applications and Techniques
GALILEO	European Satellite Navigation System
GLONASS	Globalnaya Navigatsionnaya Sputnikovaya Sistema
GNSS	Global Navigation Satellite System
GPS	Global Positioning System
GRAMMAR	Galileo Ready Advanced Mass Market Receiver
GREAT	Galileo Receiver for Mass Market

HI	Human Interface
HSSP	High Speed Signal Processing unit
HW	Hardware
ICD	Interface Control Document
IEEE	Institute of Electrical and Electronics Engineers
IC	Integrated Circuit
IF	Intermediate Frequency
ION	Institute of Navigation
IRNSS	Indian Regional Navigation Satellite System
LC	Local Control unit
LFG	Local Frequency Generator
LNA	Low Noise Amplifier (Ampl.)
LPF	Low Pass Filter
LSSP	Low Speed Signal Processing Unit
LO	Local Oscillator
PFD	Phase and Frequency Detector
PIT	Pre-detection Integration Time
PLL	Phase locked Loop
PN	Phase Noise
PRN	Pseudo Random Noise
PS	Protocol Stack
PSD	Power Spectral Density
PVT	Position Velocity Time
QZSS	Japanese Quasi-zenith Satellite System
RF FE	Radio Frequency Front-end
RO	Reference Oscillator
RS-232	Recommended Standard – 232 (serial port)
RUT	Receiver Under Test
SDG	Sampled Data Generator
SDR	Software Defined Radio
SNR	Signal-to-Noise Ratio
SW	Software

TEKES	Finnish Funding Agency for Technology and Innovation
TTFF	Time to First Fix
TUT	Tampere University of Technology
TUTGNSS	TUT's Prototype GNSS Receiver
TUTGSSS	TUT's Prototype GNSS Signal Simulator in Software
USB	Universal Serial Bus
VCO	Voltage Controlled Oscillator
VHDL	Very High Speed Integrated Circuit Hardware Description Language

LIST OF SYMBOLS

ρ_s	Pseudorange between one satellite and the user
(x_s, y_s, z_s)	Coordinates of satellite position
(x_u, y_u, z_u)	Coordinates of user position
c	Speed of light
t_u	Time offset between satellite system and the user receiver clocks
$I_{carrier}$	In-phase component of the carrier signal
$Q_{carrier}$	Quadrature-phase component of the carrier signal
A	Signal Amplitude
$f_{carrier}$	Carrier frequency
$t_{carrier}$	Time parameter of the carrier signal
t_{code}	Time parameter of code signal
$AV(\tau)$	Allan Variance computed over time τ
M	Number of samples over which Allan Variance is computed
$y(\tau)_i$	Value of i^{th} sample
dt	Satellite clock error
a_0	Satellite clock time offset in seconds
a_1	Fractional satellite clock frequency offset
a_2	Fractional satellite clock frequency drift
t	Time
t_{oc}	Reference epoch in seconds
$n(h)$	Electron density at height h
n_{max}	Peak electron density
h_{max}	Height of peak electron density
B	Thickness of the ionospheric layer
$dTropo^{MH}$	Tropospheric delay using the Modified Hopfield model
$dTropo^{GG}$	Slant tropospheric delay with the Goad & Goodman model
$P(t)$	Time variant pressure parameter
$T(t)$	Time variant temperature parameter

$H(t)$	Time variant humidity parameter
$El(t)$	Elevation angle
w	Gaussian white noise
T_r^S	Tropospheric error in meters
N	Refractive index along the signal path
a	Upper limit of tropospheric boundary in meters
b	Lower limit of tropospheric boundary in meters
$r_{E1}(t)$	Galileo E1 received signal after the transmission channel
α_i	Complex path coefficient for path *i*
τ_i	Path delay for path *i*
n	Additive white Gaussian noise
f_{ci}	Center frequency of band *i*
f_{smin}	Minimum sampling frequency
f_{IFi}	Intermediate frequency of band *i*
f_s	Sampling frequency
$_{BWi}$	Bandwidth of band *i*
$Rem\left(\frac{X}{Y}\right)$	Remainder after dividing *X* with *Y*
Int[x]	Largest integer smaller than or equal to *x*
n_i	Signal spectrum segment number
f_{Hi}	Higher frequency limit of the signal band
f_{Li}	Lower frequency limit of the signal band
m	Replica number of the sampled band
N_{Phase}	Phase noise
K	Boltzmann constant
T	Temperature in Kelvin
P_{Signal}	Power of the signal under consideration (in absolute values)
ω_0	Center frequency of the signal under consideration in radians/sec
Q	Quality factor of the resonator in the local oscillator
$\Delta\omega$	Frequency offset from center frequency at which PN is computed
Ø	Phase noise

LIST OF FIGURES

Fig. 1.1	Block Diagram of a typical GNSS receiver test-bench…….....	4
Fig. 2.1	GPS Space, User and Control segments and their inter-relation……	10
Fig. 2.2	Estimating the position of a receiver by trilateration with three satellites…….....	10
Fig. 2.3	Concept of GNSS operation…….....	11
Fig. 2.4	GNSS frequency spectrum…….....	13
Fig. 2.5	Block diagram of a typical GNSS receiver…….....	14
Fig. 2.6	Current state of wireless receiver architecture…….....	15
Fig. 2.7	Ideal SDR architecture…….....	16
Fig. 2.8	Block diagram of direct downconversion receiver…….....	17
Fig. 2.9	Block diagram for superheterodyne receiver…….....	17
Fig. 2.10	Block diagram of direct bandpass-sampling receiver architecture….	18
Fig. 3.1	Block diagram of a software-based GNSS signal simulator….....	21
Fig. 3.2	Internal block diagram of one channel of the simulator…….....	21
Fig. 3.3	Simulink model for generating Galileo E1B primary PRN code……	23
Fig. 3.4	Internal block diagram of transmission channel module…….....	28
Fig. 4.1	Frequency spectrum of the proposed SDG…….....	30
Fig. 4.2	Frequency spectrum of a complex signal before and after sampling..	32
Fig. 4.3	Frequency spectrum showing harmful aliasing between different IF bands…….....	32
Fig. 4.4	Frequency spectrum showing different IF bands without aliasing….	32
Fig. 4.5	Frequency spectrum of two complex RF signal bands…….....	33
Fig. 4.6	First possibility of arranging the sampled and original bands….....	34
Fig. 4.7	Second possibility of arranging the sampled and original bands……	34
Fig. 4.8	Block diagram of complex bandpass-sampling…….....	35
Fig. 5.1	Experimental set-up to study the effect of phase noise on baseband tracking performance…….....	38
Fig. 5.2	Definition of phase noise…….....	38

Fig. 5.3	Phase Locked Loop Block Diagram…….....	41
Fig. 5.4	Block schematic showing the mechanism to add phase noise in the signal stream…….....	42
Fig. 5.5	Correlation SNR vs VCO PN...	45
Fig. 5.6	Correlation Phase vs VCO PN…….....	47
Fig. 6.1	Typical testing procedure for GNSS receivers…….....	53
Fig. 6.2	Rectangular (racetrack) trajectory for dynamics testing…….....	57

LIST OF TABLES

Table 1.1	Linking the Thesis topic to the chapters and publications…….....	4
Table 2.1	Evolution of radio transceiver with respect to integration on silicon…….....	15
Table 3.1	Typical values of GNSS signal errors…….....	22
Table 5.1	Constituent blocks of a PLL and typical values of their significant design parameters…….....	41
Table 5.2	Maximum phase noise (dBc/Hz) in order to maintain minimum correlation SNR of 50 dB for different values of loop BW, PIT and frequency division ratio (N)…….....	49
Table 5.3	Maximum phase noise (dBc/Hz) in order to maintain minimum correlation SNR of 30 dB for different values of loop BW, PIT and frequency division ratio (N)…….....	49
Table 6.1	Advanced GNSS receiver operating modes…….....	54

1. INTRODUCTION

1.1 Background and Motivation

Global Navigation Satellite Systems (GNSS) include the American NAVSTAR Global Positioning System (GPS), European GALILEO, Russian GLONASS, and the Chinese BeiDou-2/COMPASS system. Satellite navigation systems that are planned to be regional in their geographic scope include the Indian Regional Navigation Satellite System (IRNSS), and Japanese Quasi-zenith Satellite System (QZSS). The architecture of each of these systems is similar, consisting of three segments – Space, Ground, and User [29], [30], [31]. The Space Segment consists of a constellation of satellites which transmit the radio-navigation signals towards the Earth, the Ground Segment consists of a network of ground-based monitoring, control, tracking and uplink stations, and the User Segment consists of the receivers that provide the position, velocity, time (PVT) and navigation solutions.

Receiver design and innovation has attracted considerable attention and effort from the GNSS research community. This also includes research in overcoming limitations of power, size, speed, and cost, finding solutions to errors introduced due to atmospheric composition and multipath, and innovations in multi-frequency, multi-constellation receiver design. However, in-depth discussions, studies, and debates on the testing and performance evaluation of GNSS receivers are sorely missing from industrial and academic discourses. This has resulted in a considerable growth in the diversity of testing procedures, and yet the number of receiver parameters to be tested or innovation in the methodology of performing these testing procedures has remained limited and even

primitive in some cases. It has been noticed from a background literature review that very few research manuscripts are dedicated to innovations in testing and performance evaluation of GNSS receivers.

The prototype Global Navigation Satellite System receiver (TUTGNSS) [1], developed at the Department of Electronics and Communications Engineering (ELT) of Tampere University of Technology, is now in the performance testing phase. TUTGNSS is a GPS L1/L5 + Galileo E1/E5a dual-frequency dual-constellation receiver, jointly developed by TUT and its international partners under two European Union and a TEKES research grant. These included the Galileo Ready Advanced Mass Market Receiver (GRAMMAR), Galileo Receiver for Mass Market (GREAT), and Future GNSS Applications and Techniques (FUGAT) projects, aimed at a highly innovative approach to developing a prototype consumer–grade dual-frequency dual-constellation GNSS receiver, targeted at mass market applications with the widest potential exploitation (this is also the definition of 'advanced' GNSS receivers that is henceforth targeted in this manuscript).

With the advent of such advanced GNSS receivers capable of multi-frequency, multi-constellation operations, it is no longer sufficient to continue using the testing procedures and the related test-bench infrastructure that was used until now for 'simple' single frequency single constellation receivers.

Therefore, it was during the implementation of these projects that the author had the opportunity to conduct research on advanced GNSS receiver technology and contribute towards the creation of an innovative test plan, design the corresponding test scenarios and test facility, execute receiver testing, document test results and the user manual, troubleshoot the dual-frequency, dual-constellation prototype receiver, and facilitate the approval of the project from the external reviewers. This thesis manuscript is an accumulation of the experiences and scientific publications emanating from working on these projects, technologies and ideas during the past four years.

1.2 Research Objectives and Scope

Three major questions related to test-bench solutions for advanced GNSS receivers were addressed during the progress of this research:

- Is it possible to design innovative sources of test signals?
- Is it possible to locate new test parameters within the receiver that could offer new view-points for determining its performance?
- Is it possible to automate the entire testing process to improve reliability, accuracy and efficiency?

Therefore, the primary objective of this research work was to investigate novel techniques for performance evaluation of GNSS receivers. Building on this objective, the research scope included investigating innovative sources of test signals, inclusion of new parameters to test, adapting the test-cases and procedures for multi-frequency, multi-constellation receivers, and introducing automation and open-box testing (where it is possible to access the signal-flow within the system) into the overall test-plan. As mentioned in Section 1.1, the TUTGNSS receiver is capable of GPS L1/L5 + Galileo E1/E5a operation and consequently, this combination of frequencies and constellations sets the scope of the research work. Some of the research results are presented for the GPS L1 mode due to limitations of test-infrastructure within the research group.

The scope of the research was also bounded by the limitations of time, and the need for investigating multiple leads in an effort to diversify the research area. As an example, the radio front-end is the source of a number of RF non-linearities. However, here the scope is limited to the study of how the phase noise from its local frequency generator affects the receiver performance. It would be interesting for the future to investigate, e.g., the effect of differential group delay on the position accuracy of a multi-frequency receiver.

1.3 Linking the Thesis Topic to the Chapters and Publications

A block-diagram schematic of a typical GNSS receiver test-bench is shown in Fig. 1.1 Block 1 represents the source of test signals for Block 2, which denotes the receiver-under-test (RUT). Block 3 represents some intelligence, either human or machine, which

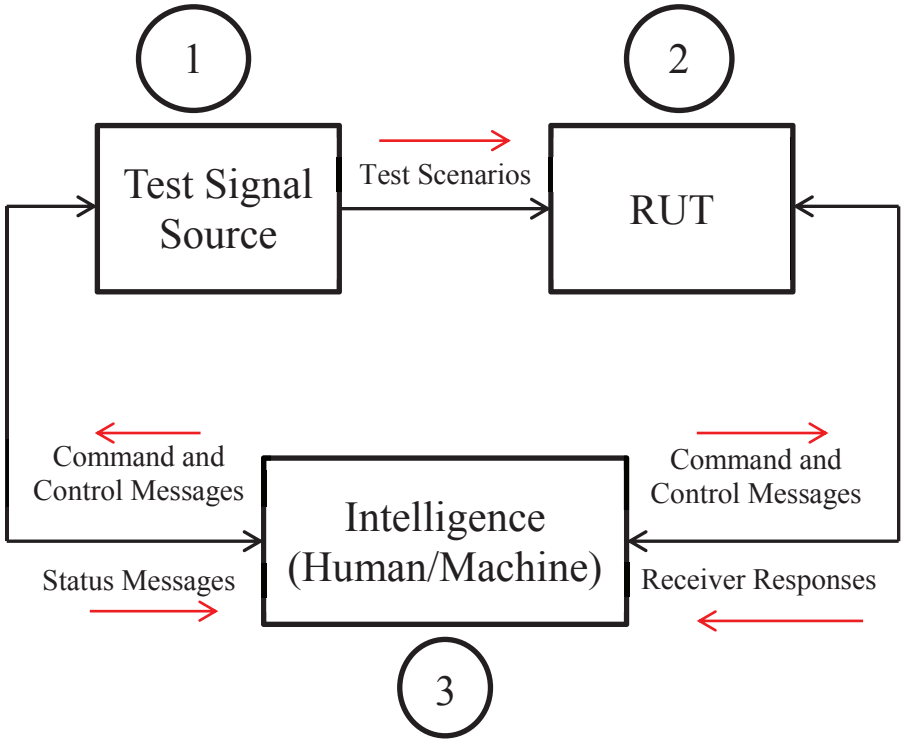

Fig. 1.1 Block Diagram of a typical GNSS receiver test-bench

Table 1.1 Linking the Thesis topic to the chapters and publications

Block	**Chapters**	**Publications**
Block 1	3, 4	[P1], [P2], [P3]
Block 2	5	[P4], [P5], [P6]
Block 3	6	[P7]

controls the entire testing process. It provides the test-scenarios and individual test-commands to Block 1, and simultaneously receives the responses from Block 2. In case of GNSS receivers, the communication between Blocks 1 and 2 and Block 3 can be full-duplex. This thesis work deals with innovation within each of these three Blocks. The Chapters within this manuscript are dedicated to describing the basic theory about these Blocks, while the novel research is then presented within the attached Publications [P1] – [P7]. The relation between the Publications, Thesis Chapters and the Block that each refers to is shown in Table 1.1

1.4 Research Methodology

This research utilized mostly a practical implementation methodology to reach the stated objectives and results. The research topic focusses more on innovations in the peripheral technologies associated with a GNSS receiver such as, source of test signals, test procedures, and test automation, rather than core signal processing tasks such as, acquisition, tracking and PVT computation. As can be deduced, the scope for innovation is more towards how these peripheral processes can be implemented with better efficiency and accuracy, and how they can be adapted for advanced receivers. This required working with software tools such as Matlab, Simulink, C language, VHDL, Agilent ADS, Qt, etc. and practically implementing the solutions. The need for creating breakthrough knowledge in the theoretical domain was out of scope of the research problem. However, the thesis does create new theoretical knowledge about the effect of phase noise on signal tracking, as this was necessary to demonstrate the need for proposing new parameters for more complete receiver characterization.

Another aspect of the methodology has been the focus on research collaboration. Due to the wide scope and inter-disciplinarity of the research topic, it was necessary to perform work-breakdown and delegate within the research group individual tasks related to the receiver design, development and performance evaluation. Furthermore, in situations where expert advice was necessary, as in the case of Simulink-based GNSS simulator implementation, and phase noise studies, collaborations with external research groups was

emphasized. The benefit has been a thorough peer-review of all the work performed and of every publication, and inclusion of best practices due to diversity of ideas. It should be noted however, that the bulk of the research work was performed by this researcher, as described in more detail in Chapter 7.

1.5 Main Contributions

This research has addressed the problem of innovations in GNSS receiver performance validation through three different perspectives - innovations in implementation of a test-bench, its automation techniques and application methodologies. The following are the main contributions and outcomes from this thesis work:

1. It presents an in-depth study of the state-of-art in software-based simulators for GNSS signals, including their evolution through three distinct generations [P1].

2. It describes essential modules and components of such simulators for testing advanced GNSS receivers, and proposes some mathematical models for their implementation [P1].

3. Based on this study, a GNSS signal simulator in software, called TUTGSSS and capable of producing GPS L1 and Galileo E1 B/C signals was implemented [P1].

4. The thesis describes an alternate solution for generating test-signals for performance testing of advanced GNSS receivers: a bandpass-sampling based sampled data generator, which is essentially a radio front-end capable of processing multiple GNSS frequencies [P2], [P3].

5. Implementation of the LNA within this radio front-end is described. The design, simulation, implementation and test results prove that the LNA successfully satisfied requirements of wide bandwidth, high gain, high linearity, frequency stability and low noise figure, and compares very well with the state-of-art in such amplifiers [P2].

6. The design and simulation of the filter stage and frequency planning for the bandpass-sampling analog-to-digital converter (ADC) of the radio frequency front-end (RF FE) is presented next. Optimum sampling frequency was computed to be

538.5 MHz and the resulting digital intermediate frequencies were 28.25 MHz and 155 MHz [P3].

7. This thesis presents an analytical approach to the evaluation of the effects of the RF FE's local frequency generator phase noise on the baseband tracking performance of a GNSS receiver, both in terms of a free running oscillator (FRO) and a PLL [P4], [P5], [P6].

8. The relation between integration time, PLL parameters and phase noise has been shown, and a criterion for radio front-end design has been presented [P4], [P5], [P6].

9. During this study a PLL phase noise model for GNSS applications was implemented which included PN contributions from each of its constituent building blocks [P6].

10. It includes a study on state-of-art in multi-frequency, multi-system GNSS receiver performance testing scenarios [P7].

11. An Automated Performance Evaluation Tool (AutoPET) was implemented for automated testing of GNSS receivers [P7].

12. A Data Capture Tool (dCAP) was implemented to access the signals at every stage of signal processing from inside the receiver hardware to identify the origin of signal anomalies [P7].

13. This thesis demonstrates the results of the GPS L1 performance evaluation of the TUTGNSS prototype receiver using the AutoPET and dCAP. Recommendations are made on how this testing can be enhanced to cover more advanced dual-frequency dual-constellation operating modes of the receiver [P7].

1.6 Thesis Outline

Because the thesis focus is on three different modules within the overall test-bench, the Chapters may at first glance appear as disjointed or unrelated to each other. It is hoped that Fig. 1.1 and Table 1.1, which describe how the individual Chapters within this thesis manuscript contribute to the overall research theme, will help the reader to view each Chapter as part of the whole.

Chapter 2 introduces the fundamental theory of satellite-based global navigation systems, including an introduction to the different receiver architectures. **Chapter 3** describes the software-based GNSS signal simulators. This includes a description of the various modules and components that constitute a typical software-based simulator. **Chapter 4** presents the background information about bandpass-sampling based receiver radio front-end design. **Chapter 5** presents an introduction to our study on the effects of radio front-end PLL phase noise on GNSS receiver performance. **Chapter 6** describes the state-of-art in GNSS receiver testing. The most important parameters-to-test of a typical receiver are listed, followed by the commonly used procedures for testing each of these parameters. This chapter also describes how these procedures can be adapted for a multi-frequency, multi-constellation receiver testing environment. **Chapter 7** is a summary of the scientific publications emanating from this research work. The manuscript concludes with a summary of the main results and proposals for future work in the continuation of this research direction.

2. BASICS OF GNSS

2.1 Concept of Satellite Positioning

As discussed in Section 1.1, a typical satellite-based navigation system consists of three segments, viz. Space segment, User segment and Control segment. The Space segment consists of man-made satellites revolving in medium-Earth orbits. These satellites continuously transmit digital navigation data modulated on fixed analog frequencies. The User segment consists of electronic receivers that receive signals transmitted by the satellites and extract the digital navigation data which is then used in complex processing algorithms to calculate accurately the position and velocity of the user on the surface of the Earth. The Control segment consists of ground stations that control the movement and well-being of the satellites and also the signals they transmit. The Control segment also monitors the satellites continuously to record their real time 'health' and sends correction data to the satellites in case there is a slight error in their position. Figs. 2.1 [34], 2.2 [35] and 2.3 [36] explain exactly how the three segments work to help a user know his current position velocity and time (PVT) using GNSS.

The satellites transmit accurate timing and self-identification information. This information helps the receiver know exactly when the signal was transmitted (and hence calculate the delay in propagation from the satellite to the Earth) and which satellite transmitted it. The receiver receives such signals simultaneously from all satellites currently visible in the sky overhead. To determine the position of the user, the receiver must compute the solution for four variables: x, y, z and Δt (3D location and the receiver clock bias). This is performed using the process of trilateration.

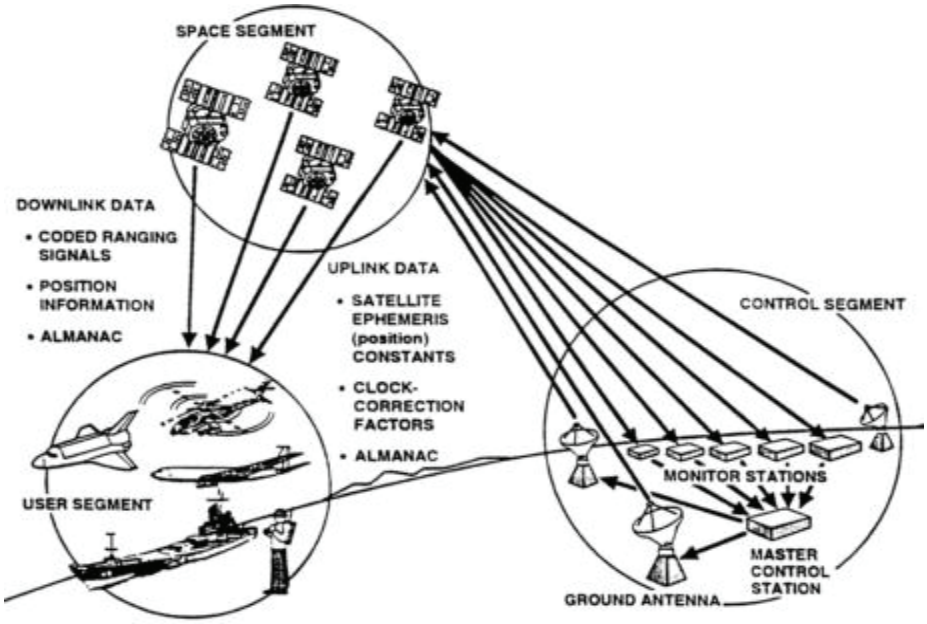

Fig. 2.1 GPS Space, User and Control segments and their inter-relation

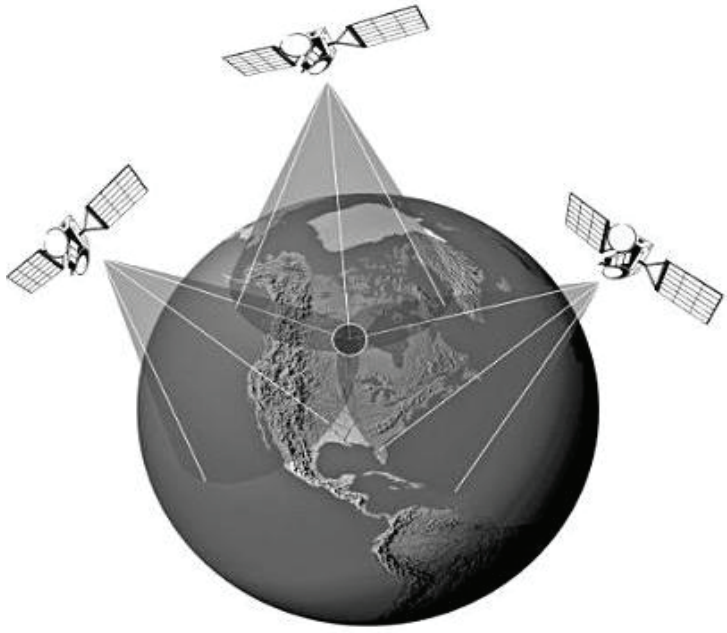

Fig. 2.2 Estimating the position of a receiver by trilateration with three satellites

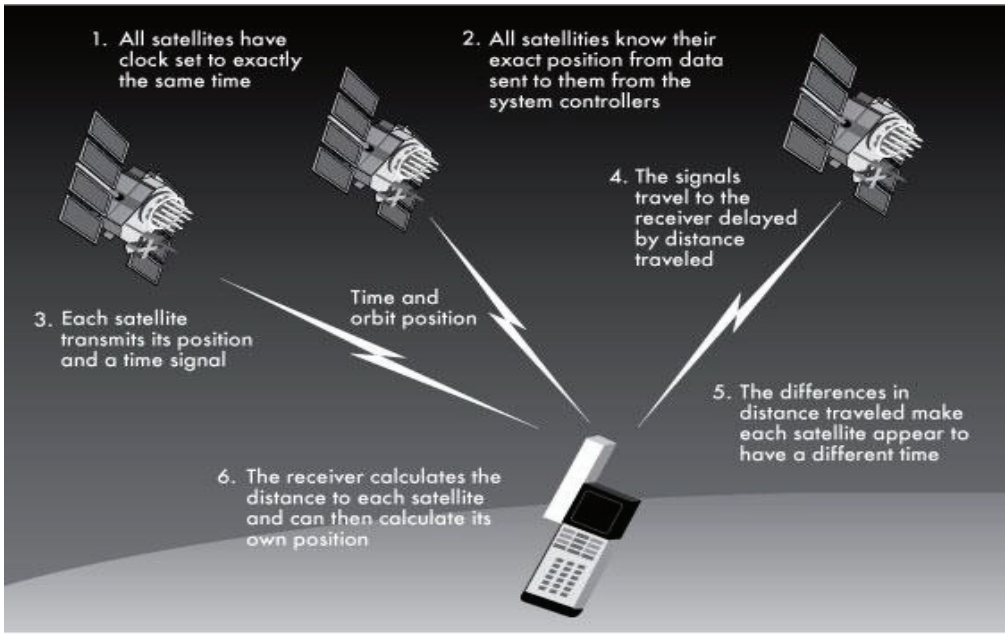

Fig. 2.3 Concept of GNSS operation

The locus of all points equidistant from one 'visible' satellite is a circle on the surface of the earth. Similar circles can be drawn for other 'visible' satellites once their distance from the receiver is measured. The exact location of the receiver is at the point where all such circles meet. Since there are four unknowns, information from four satellites is necessary and enough for estimation of receiver position. The distance between the receiver and one satellite is called the pseudorange. It is expressed by (1) [31]:

$$\rho_s = \sqrt{(x_s - x_u)^2 + (y_s - y_u)^2 + (z_s - z_u)^2} + ct_u \qquad (1)$$

where ρ_s is the pseudorange between one satellite and the user, x_s, y_s, z_s are the coordinates of satellite position, x_u, y_u, z_u are the coordinates of user position, c is a constant that defines the speed of light, and t_u is the offset between satellite system and the user receiver clocks. Once the distance between the user and at least four satellites is established, this information can be used to find the three dimensional position of the user (that is, to solve

(1) and determine values for coordinates of user position x_u, y_u, z_u) and solve for time offset between the receiver and satellite clocks.

2.2 GNSS Signal Structure

The various signals and codes that make up the composite GNSS signals vary from one constellation to another, and are described in detail in the following references [37], [38], [39], [40], [41], [42], and shown in Fig. 2.4 here. These references provide considerable information on the structure and description of various GNSS signals, and hence are not discussed again here.

2.3 GNSS Signal Spectrum

Fig. 2.4 [43] shows the overall frequency spectrum of the various satellite-based navigation system signals currently in the planning and/or completion stages throughout the world. As the figure shows, the frequency band of interest is from 1164 MHz to 1615.5 MHz resulting in a total bandwidth of 451.5 MHz. However, there is a 259 MHz band in between Galileo E6 and Galileo E2 (1300 MHz and 1559 MHz) that is not of interest (if we ignore the Galileo search and rescue (SAR) signal at 1544 MHz). Therefore, the entire spectrum of interest can be divided into two sub-spectrums of bandwidth 136 MHz and 56.5 MHz respectively. This relaxes the sampling frequency requirement considerably, as shown in Section 4.

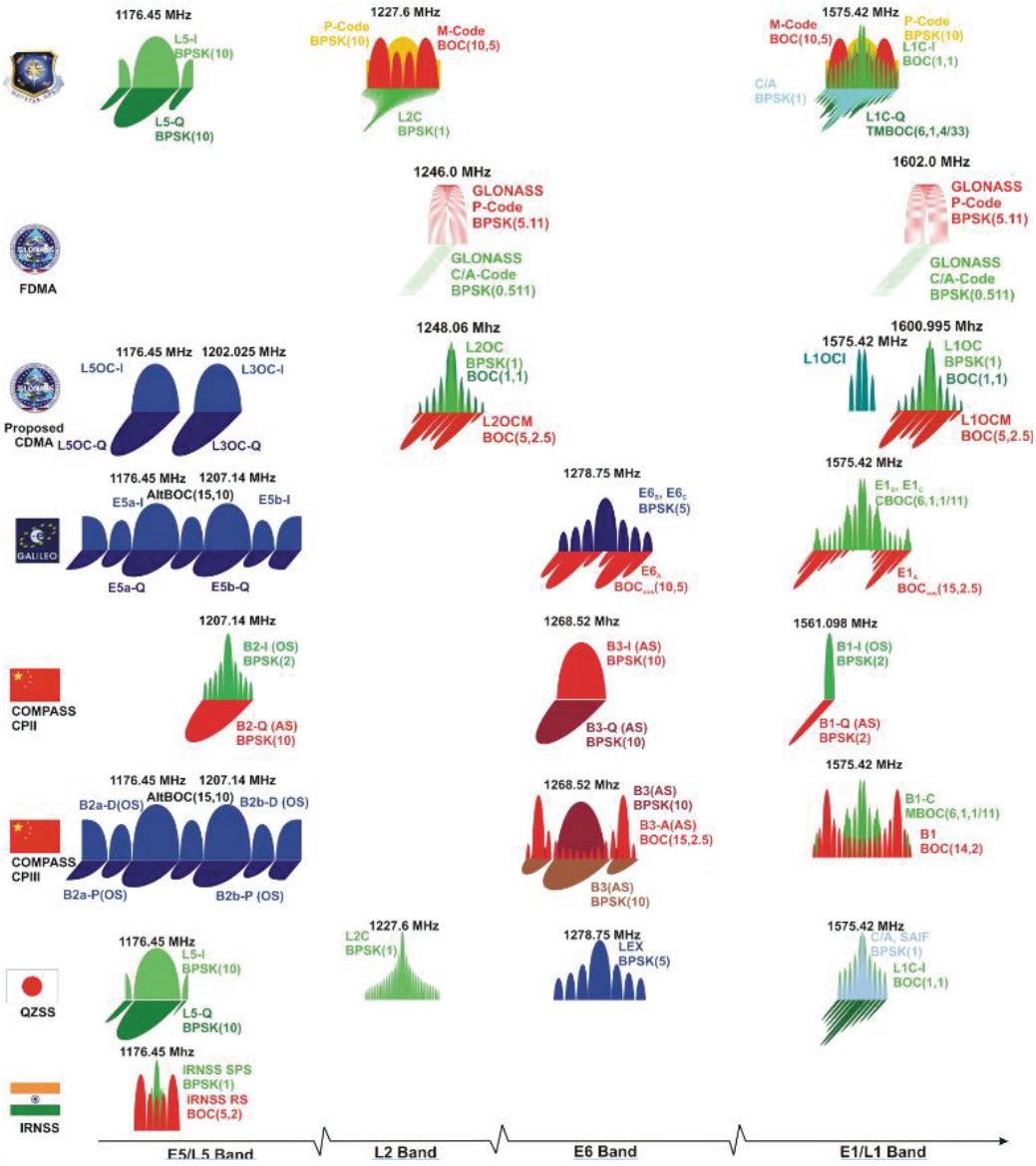

Fig. 2.4 GNSS frequency spectrum

2.4 GNSS Receiver Structure

The User segment consists of a GNSS receiver which receives signals from the satellites and/or other sources, e.g., cellular base stations [14]. A block schematic of a typical GNSS receiver is shown in Fig. 2.5 [44].

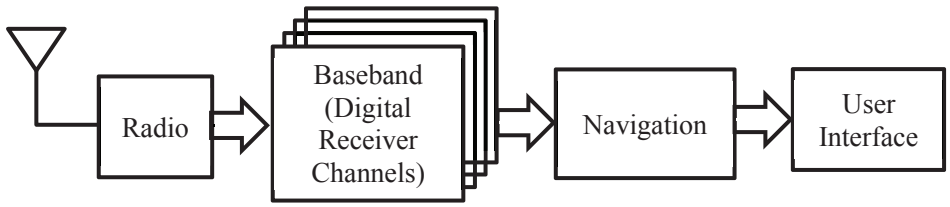

Fig. 2.5 Block diagram of a typical GNSS receiver

The antenna receives the signals from the satellite and forwards them into the analog radio front-end. The radio front-end is responsible for signal amplification, filtering out of band noise, frequency downconversion from RF to an intermediate frequency (IF), and analog to digital conversion. The digitized signal is then passed to the baseband processing unit, where the satellite acquisition and carrier and code signal tracking processes are performed. Acquisition is a process during which the receiver searches for visible satellites in the sky, and when found, the tracking process will keep track of the acquired satellites during their relative motion with respect to the receiver. Tracking the satellite is necessary to be able to demodulate the navigation message from the composite signal and measure pseudoranges for subsequent navigation processing [45], [46], and [47].

2.5 RF Front-end Architecture Evolution

Wireless transceiver implementation began with the development of the Monodyne receiver in 1890's, followed by the invention of the Superheterodyne receiver in 1915. Since then, the evolution has been concentrated on developing advanced information modulation and encoding schemes and simultaneously developing hardware and software capable enough to implement these schemes [48], [49]. The current state of wireless

receiver architecture can be described by Fig. 2.6. The evolution of radio transceiver with respect to integration on silicon can be described by the comparative study presented in Table 2.1.

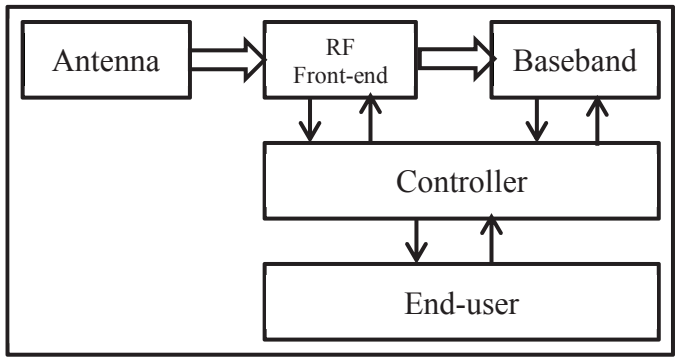

Fig. 2.6 Current state of wireless receiver architecture

Table 2.1 Evolution of radio transceiver with respect to integration on silicon

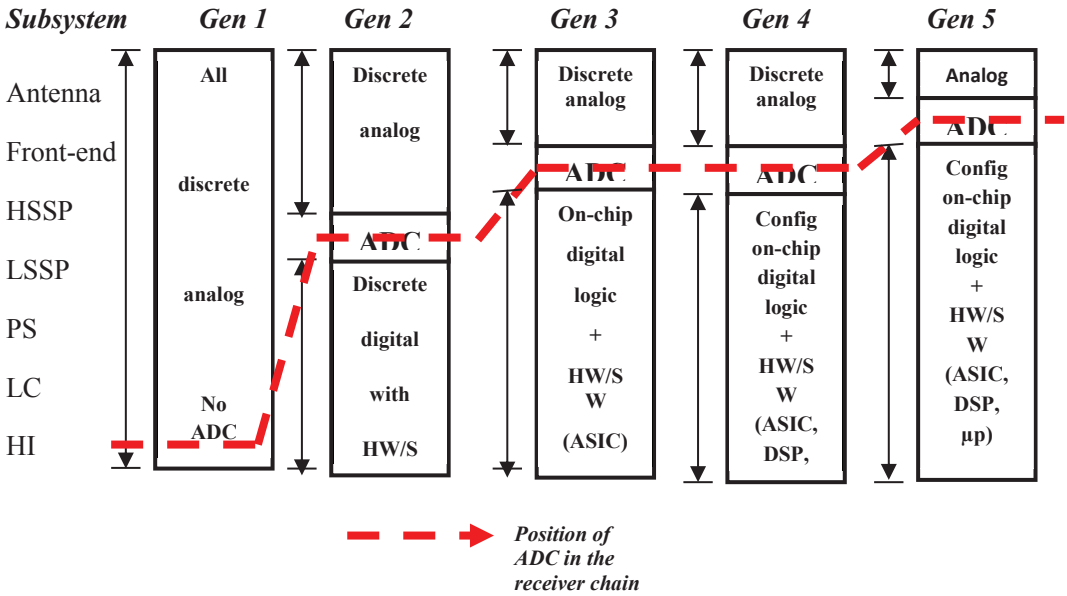

A typical receiver is considered to consist of an antenna, RF front-end, High Speed Signal Processing (HSSP) unit, Low Speed Signal Processing (LSSP) unit, Protocol Stack (PS), Local Control (LC) unit and finally, a Human Interface (HI) unit. One can clearly distinguish a pattern in the evolution; with each new generation, there is an attempt to move the ADC closer to the antenna.

The ideal software defined radio (SDR) architecture is given in Fig. 2.7. In this architecture, the behavior of the radio in the physical layer is defined in software, thus enabling on-the-air software upgrades of the physical layer behavior. Consequently, the analog front-end is configurable to support wide range of frequencies and applications.

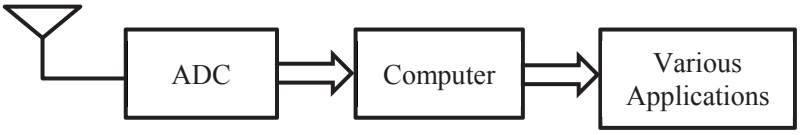

Fig. 2.7 Ideal SDR architecture

2.6 Receiver Radio Front-end Architectures

This section describes briefly the various radio front-end architectures such as direct conversion, superheterodyne, and the direct bandpass-sampling, which are used in typical communications receivers.

2.6.1 Direct conversion Architecture

Direct conversion receivers perform downconversion of the high frequency carrier signal directly to the baseband frequency or zero frequency (also called direct current (DC)), as shown in Fig. 2.8 [50]. It does not contain an intermediate frequency processing stage. Its benefits are reduced component count, better suitability for integration on silicon, and the ease of frequency planning. The most important drawbacks of this architecture are pink noise (flicker or 1/f noise) that usually affects low frequency signals, and local oscillator (LO) leakage creating a DC offset that can potentially drive the successive stages into non-linearity. The Low IF architecture attempts to overcome these disadvantages. It has an IF stage where the RF carrier is downconverted to a non-zero, yet very low IF.

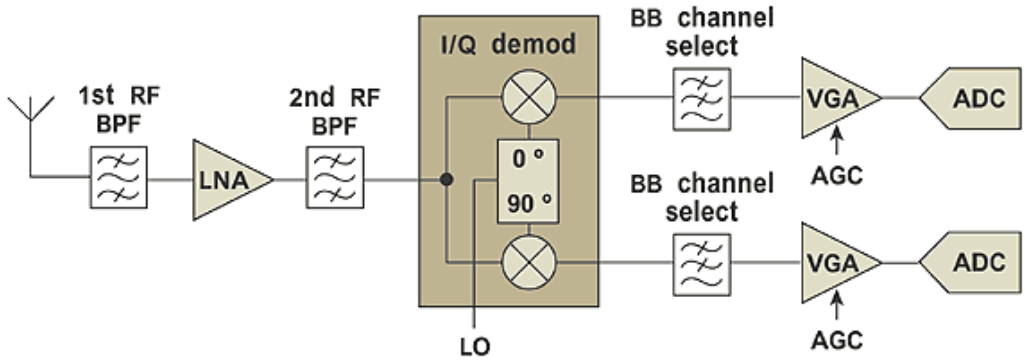

Fig. 2.8 Block diagram of direct downconversion receiver

This ensures that channel selection can be done with highly selective filters and yet the signal is not contaminated by pink noise or DC offset.

2.6.2 Superheterodyne Architechture

In this architecture, the RF carrier signal is first downconverted to an intermediate frequency, usually much higher than the baseband frequency. The benefit of this architecture is that sufficient SNR is maintained, and it is also possible to achieve good selectivity in the IF filters. Drawbacks include, image frequency problems, difficulty to integrate on silicon because of the bulky RF filters, and necessity for complex frequency planning. Fig. 2.9 shows a typical architecture for superheterodyne receivers.

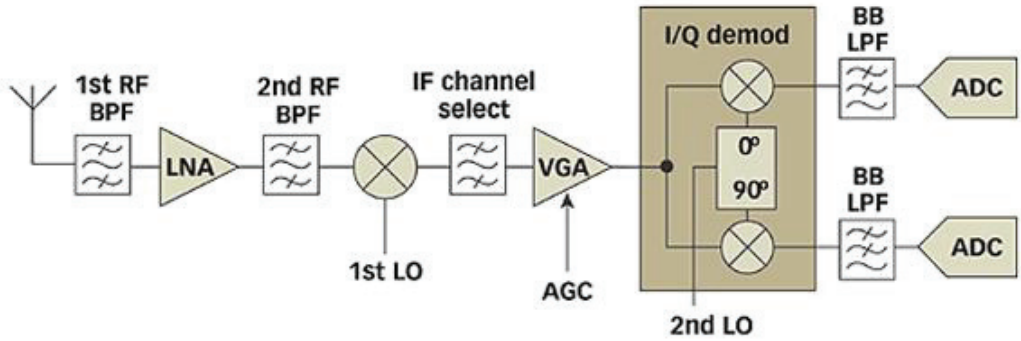

Fig. 2.9 Block diagram for superheterodyne receiver

2.6.3 Direct Bandpass-Sampling Architecture

This architecture directly samples the RF signal bandwidth and converts it to digital IF using the principle of intentional, yet non-destructive aliasing. The RF signal from the antenna is filtered to remove any out of band noise, amplified and then directly digitized using a high speed ADC. After the ADC, digital filters are employed to separate the IF bands to be demodulated in the baseband processor. Fig. 2.10 shows the block diagram of a bandpass-sampling RF front-end [51]. The design principle of this architecture is described in detail in Section 4.

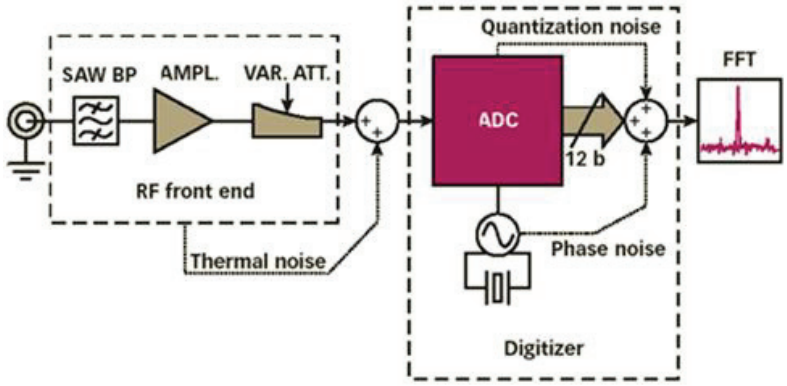

Fig. 2.10 Block diagram of direct bandpass-sampling receiver architecture

3. SOFTWARE-BASED GNSS SIGNAL SIMULATORS

3.1 Introduction and background

Another solution to investigate novel sources for test GNSS signals was to use a software-based GNSS signal simulator. The primary motivation for investigating this solution was the ease with which it could be designed and implemented within the research group without the need for expensive commercial components. This Chapter presents the general introduction to the theory, including an overview of the essential components of such simulators. Publication [P1] extends this discussion by describing a detailed literature review of state-of-art in software-based simulators. This is followed with information about the first results of the TUT's GNSS Signal Simulator in Software (TUTGSSS) developed in the research group using the Matlab programming environment.

GNSS signal simulators are used for imitating the satellite signals arriving at a receiver under test. They provide a deterministic and repeatable source of signals, independent of satellite constellations available and visible at the time of testing [72] – [110]. Simulators have a modular design, where each module is responsible for a particular functionality. The different modules include (but not limited to): The signal generation module, including error signals generation, the transmission channel module, the satellite constellation module, and the receiver RF FE module. Fig. 3.1 shows the block diagram of a typical software-based GNSS simulator. The satellite constellation module gives a real-time view of the geometry of the satellites in the sky. Based on this geometry, signals from the visible satellites are generated at an intermediate frequency and combined to

form a composite navigation signal-in-space, e.g., Galileo E1 or GPS L1. This composite signal flows through the transmission channel module, which simulates non-idealities and other effects, e.g., interference and multipath signals, and additive white Gaussian noise, within a typical transmission path between the satellite and receiver. The RF FE module simulates the effects of the radio frequency front-end of a typical GNSS receiver on the signal received from the sky. This includes filtering, amplification, local oscillator phase noise and ADC quantization effects. The following sections describe the implementation of a simple software-based simulator using the SIMULINK tool.

3.2 Signal Generation Module

The signal generation module is composed of a number of channels, as shown in Fig. 3.2. Each channel simulates one signal, either a legitimate positioning signal or an interference signal, and the various timing errors affecting this signal. The sampled time generator creates time samples from a continuous time source by sampling at a user desired sampling frequency. In the error signal generation block the sampled time is contaminated with various clock errors and atmospheric timing errors. The most common timing errors and their typical values [14], [33] are given in Table 3.1. These typical values are generalizations of the average value of these errors over a long time and wide areas, and may be considered accurate enough only for simple simulators for academic purposes. For higher accuracy, complex mathematical error models are used, which attempt to replicate real-world situations faithfully.

The digital and analog components of the GNSS signal are affected equally but in opposite manner by the ionosphere. It advances the carrier component while delays the code [32]. Hence, there is a need for two time sample streams, called $t_{carrier}$ and t_{code}. These streams are then used in the creation of the digital pseudorandom noise (PRN) code and navigation data, and the radio frequency carrier. To create the digital components, the easiest approach is to create them as memory codes in look-up tables as shown in Fig. 3.3. The $t_{carrier}$ component is used to create the in-phase and quadrature (I/Q) components of the analog high frequency carrier signal, using (2) and (3). Using software tools, it is not possible to handle signals with large sample rates. Hence, it is more convenient to

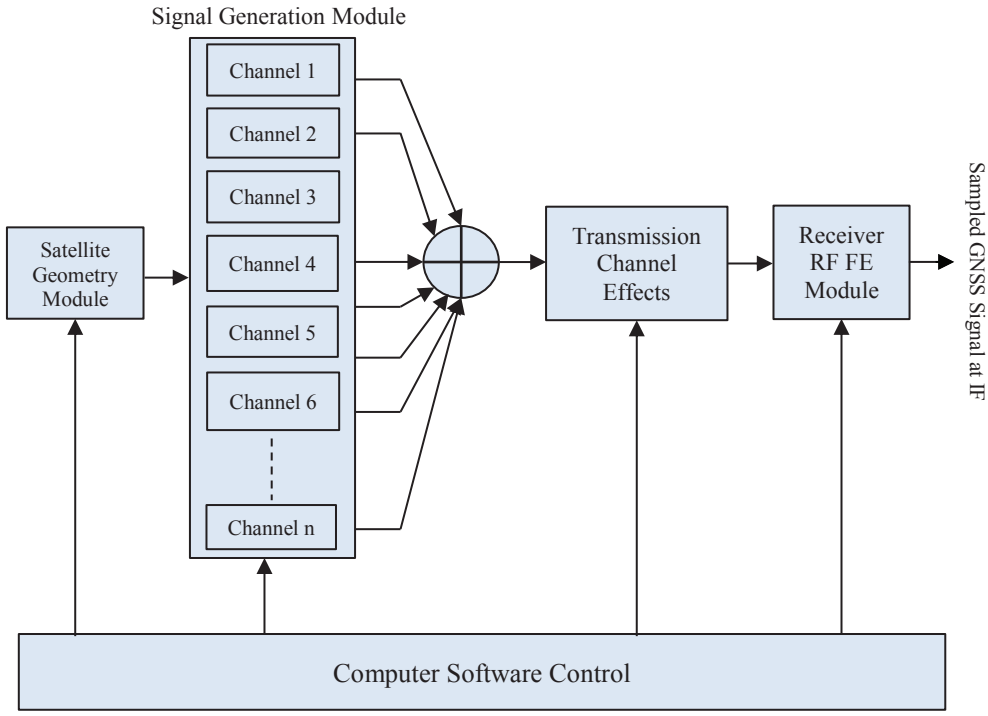

Fig. 3.1 Block diagram of a software-based GNSS signal simulator

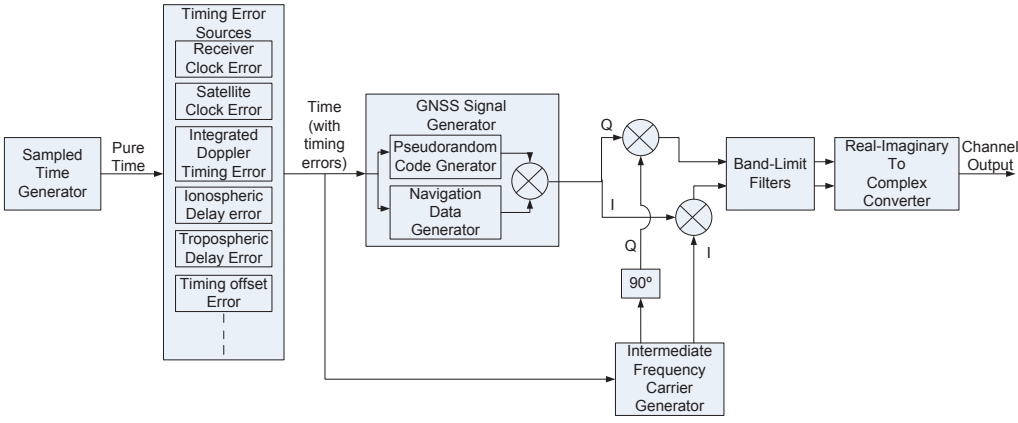

Fig. 3.2 Internal block diagram of one channel of the simulator

Table 3.1 Typical values of GNSS signal errors

Parameter	Typical Value
Receiver clock error	15 ns
Satellite clock error	7 ns
Ionosphere error	17 ns
Troposphere error	2 ns
Timing signal offset error	few ns
Doppler frequency offset	±12 kHz

simulate GNSS signal-in-space at a lower intermediate frequency, e.g., in the range 2 MHz to 5 MHz, rather than the actual 1.5 GHz.

$$I_{carrier} = A\ cos(2\pi f_{carrier} t_{carrier}) \tag{2}$$

$$Q_{carrier} = A\ sin(2\pi f_{carrier} t_{carrier}) \tag{3}$$

3.3 Error Generation Module

The error generation module consists of a number of sources of timing and power variation errors that affect the GNSS signal during its travel from the satellite to the terrestrial receiver, and also within the receiver signal processing chain. Here, we explain the most common error sources, e.g., receiver and satellite clock errors, atmospheric delay errors, transmission channel effects and radio front-end effects. The accuracy of the signal simulator is directly dependent on the number and sophistication of the error sources that it can model.

3.3.1 Receiver Clock Error

The time offset between the receiver's clock and the standard GPS (or Galileo) time is called the receiver clock error. Receiver clocks are usually constructed using crystal oscillators, which suffer from higher rates of drift yet are more affordable than the ultra-

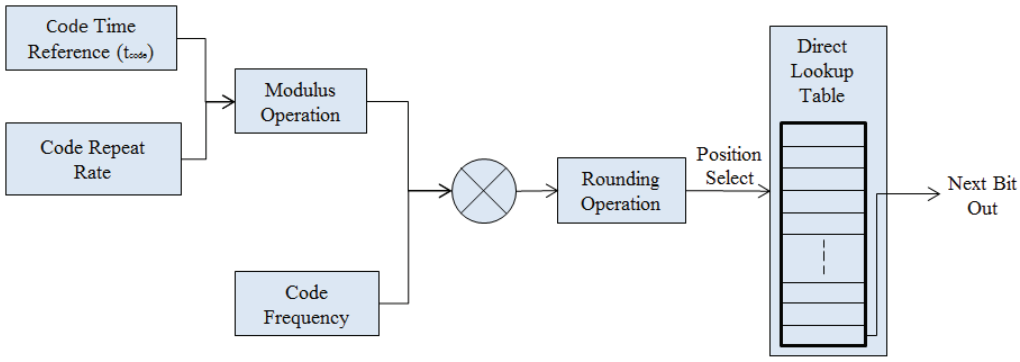

Fig. 3.3 Simulink model for generating Galileo E1B primary PRN code

stable atomic clocks used in the GNSS satellites. The receiver clock error is a combination of systematic and random errors [2]. Examples of systematic errors are the constant time and frequency offsets, defined in units of parts per million (ppm). The Allan Variance (AV) [3] commonly characterizes the remaining frequency errors. The AV gives the measure of frequency instability of the clock over consecutive samples. Using M samples, AV can be modeled by (4) [4]:

$$AV(\tau) = \frac{1}{2(M-1)} \sum_i (y(\tau)_{i+1} - y(\tau)_i)^2 \tag{4}$$

where τ is the time period over which AV is calculated and $y(\tau)_i$ is the i^{th} sample value.

3.3.2 Satellite Clock Error

The time offset between the satellite's clock and standard GPS time is called the satellite clock error. Satellites have highly accurate and precise atomic clocks, with small frequency drift. The ground control segment monitors this drift at regular intervals and a correction parameter is transmitted by the satellites through the navigation message. Navigation messages transmitted by the satellites are available on the internet [5] in various file formats such as YUMA, SP3, and RINEX. Historical values of the satellite clock correction parameter can be studied using these files, and with reverse-engineering, the satellite clock error can be modeled. As an alternate, URA/SISA parameters [6], [7]

can be used to model the satellite clock errors in a similar way. The equation for the satellite clock error is given by (5) [8].

$$dt = a_0 + a_1(t - t_{oc}) + a_2(t - t_{oc})^2 \quad (5)$$

where t_{oc} is the reference epoch in seconds, a_0 is the satellite clock time offset in seconds, a_1 is the fractional satellite clock frequency offset and a_2 is the fractional satellite clock frequency drift.

3.3.3 Ionospheric Delay Error

The ionosphere is the outermost layer of the atmosphere, lying between 50 km to more than 1000 km from the Earth's surface. This layer consists of free ions which collide with the electromagnetic waves of the GNSS signals passing through it, causing the waves to refract or bend. This introduces a time error in the carrier and the code components of the signal. This error is highly dependent on the signal frequency and on the number of free ions in the ionosphere. A parameter that gives information on the current condition of the ionosphere is the Total Electron Content (TEC). The value of TEC is dependent on the geographic location of the receiver and the time of day. TEC values over a particular area and at a particular time of day are available from the internet [9]. These TEC values can be used to model the ionospheric errors.

Usually for GPS, the Klobuchar model is used using the 'ION ALPHA' and 'ION BETA' parameters from GPS RINEX files available on the internet [10]. For Galileo signals, the NeQuick model is preferred, which builds on the formulation for the electron density function in the Epstein layer of the ionosphere given by (6) [11]:

$$n(h) = \frac{4n_{max}}{\left(1+exp\left(\frac{h-h_{max}}{B}\right)\right)} exp\left(\frac{h-h_{max}}{B}\right) \quad (6)$$

where $n(h)$ is the electron density at height h, n_{max} is the peak electron density, h_{max} is the height of peak electron density, and B is the thickness of the layer. Once the electron

density in the ionosphere above the receiver is computed, it can be used to calculate the delay and phase errors affecting the various satellite signals passing through it.

3.3.4 Tropospheric Delay Error

The troposphere is the layer of atmosphere up to 20 km from the Earth's surface. This layer also introduces delays in the GNSS signal propagation but unlike the ionosphere, this delay is independent of signal frequency. There are many models to simulate the troposphere. However, the most popular is the Modified Hopfield model, which is based on a model for the wet and the dry zenith tropospheric delays and a slant delay transformation. The equation for tropospheric error (in meters) using this model is given by (7) [12]:

$$dTropo^{MH}\big(P(t),T(t),H(t),El(t)\big) = dTropo^{GG}\big(P(t),T(t),H(t),El(t)\big) + w \qquad (7)$$

where $dTropo^{GG}$ is the slant tropospheric delay (in seconds) generated using the Goad and Goodman tropospheric model, $P(t)$ is time variant pressure parameter, $T(t)$ is time variant temperature parameter, $H(t)$ is time variant humidity parameter, $El(t)$ is elevation angle, and w is Gaussian white noise. An alternate equation for tropospheric error (in meters) is given by (8) [8]:

$$T_r^S = 10^{-6}\int_a^b N ds \qquad (8)$$

where $N = (n-1)*10^6$ is the refractive index along the signal path and a and b define the limits of tropospheric boundary in meters. Increased accuracy of modeling the atmospheric errors is possible if the obliquity factor is included. However, in that case the signal generation module needs to take into account the satellite geometry and user position information into the error generation [13].

3.3.5 Doppler Frequency Offset

Doppler phenomenon is the change in frequency of a signal incident upon a target from a source, one or both of which are in motion. The signal frequency changes at a rate which

is dependent on the speed and direction of relative motion between them. The usual range of Doppler offset in GNSS signals is about ±12.5 kHz. This includes the satellite relative velocity, the receiver clock frequency offset, and the receiver velocity [14]. The PRN code frequency is also affected by the Doppler offset, but since this frequency is much lower than the RF carrier frequency, the offset will be much smaller - typically in the order of a few Hz. If the receiver is able to accurately identify the amount of this Doppler offset, the relative velocity, acceleration and jerk between the receiver and satellite can be determined.

From a simulator point of view, altering the carrier and code frequency of every channel within their respective ranges stated above and based on the satellite positions and trajectories, a Doppler offset can be introduced into the simulator output. An additional Doppler offset would help to simulate receiver motion. Therefore, by a right combination of Doppler frequencies over different intervals of time, a dynamic (receiver-in-motion) scenario can be simulated.

3.4 Transmission Channel Module

The internal block diagram of the transmission channel module is shown in Fig. 3.4. Three errors that are typically introduced in this module are interference and multipath signals, and additive white Gaussian noise (AWGN). More than one channel can be dedicated to simulating the interference and multipath signals, usually from the left-over channels from the Signal Generation module. Interference signals are characterized by the modulation type (e.g. FM, AM, DVB etc.), frequency offset from the GNSS signal-of-interest, and the signal power. Important parameters in the case of Multipath error are the number of multipath components, and the magnitude and the delay (in samples) of each component with respect to the fundamental component. AWGN can be generated as random noise with zero mean, and variance equivalent to the maximum noise power required to maintain the carrier to noise ratio (CNR) defined for each channel. The basic function of the transmission channel for the Galileo E1 signal in terms of the sub-carrier can be modeled as shown in (9).

$$r_{E1}(t) = \sum_{i=1}^{l} \alpha_i(t)\, S_{E1}(t - \tau_i) + n \quad (9)$$

where $r_{E1}(t)$ is the Galileo E1 received signal after the transmission channel, α_i and τ_i are the complex path coefficient and path delay for the i^{th} path respectively, and n is the AWGN.

3.5 Radio Frequency Front-End Module

Some state-of-art software simulators have the capability to model different antenna patterns and signal power profiles [15]. Typically though, only RF filtering effects, amplification, and analog to digital (ADC) conversion losses are considered. The RF filter is similar to the band-limited filter used in each channel of the signal generation module, as shown in Fig. 3.2. The filter bandwidth depends upon the signals being received. The various filtering effects that can be simulated include band-limiting, insertion loss, passband ripple and group delay. The low noise amplifier includes gain and noise figure effects. Simulating noise figure is equivalent to introducing additional AWGN before the output of the amplifier. ADC quantization causes degradation in signal to noise ratio (SNR) of the received signal [16]. Additionally, an important contribution of this thesis work is to demonstrate how to include the effects of phase noise from the radio front-end's local frequency generator within the received signal [P4], [P5], [P6].

3.6 Satellite Geometry Module

The satellite geometry module is responsible for controlling the individual channels according to the currently visible satellite positions and trajectories. The signal strength and pseudorange are controlled depending on the elevation angle of the satellite, while the Doppler frequency offset is decided based on the rate of change of pseudorange, which is based on direction of satellite motion with respect to the simulated receiver position. Publication [P1] describes the solutions and techniques used by state-of-art software-based GNSS simulators in simulating the satellite geometry. They answer important questions such as, from where does this module get the current (real-time) picture of the satellite positions and trajectories in the sky? What are its inputs and which data-formats are supported?

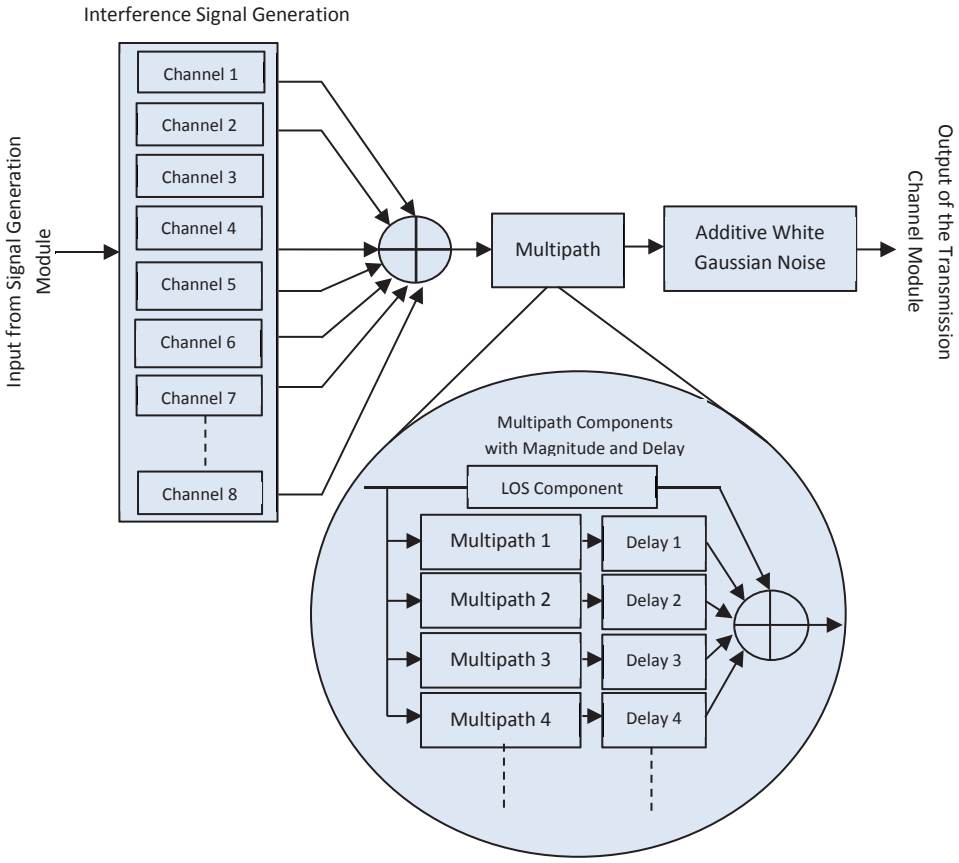

Fig. 3.4 Internal block diagram of transmission channel module

4. BANDPASS-SAMPLING BASED GNSS RECEIVER RF FRONT-ENDS

4.1 Introduction and background

One of the solutions proposed towards investigating novel sources of test signals for GNSS receivers was a bandpass-sampling based radio front-end capable of processing all planned GNSS signals, called here the Sampled Data Generator (SDG). As defined in Section 2.3, the composite bandwidth of the GNSS signals extends from 1164 MHz to 1300 MHz, and from 1559 MHz to 1615.5 MHz, and is shown in Fig. 4.1 [115]. The bandpass-sampling architecture is built around the concept of direct digital conversion of a band of RF frequencies using a wideband ADC, followed by channel selection in the digital domain using digital filters. The ADC is a critical element and some of its desirable properties for this particular application are high speed, low jitter, low power consumption and low resolution. Publications [P2] and [P3] describe in detail the background literature study about general theory of wide-bandwidth sampling, and previous cases of its implementation in the GNSS domain. Here we briefly present some of the essential components of such radio front-ends (please refer to Fig. 2.10), which include the antenna, low noise amplifier, and RF Filter and ADC for the actual bandpass-sampling.

4.2 Antenna

The antenna to be used for this architecture would need to be wideband, capable of receiving signals from 1164 MHz up to 1615.5 MHz. We propose here, few good commercial antenna options, e.g., the Zephyr 2 and Zephyr Geodetic 2 antennas from

Trimble [52], Satellite Navigation Antenna from Roke Manor Research [53] and Universal GNSS Antenna designed at the Wang Electro-Opto Corporation (WEO) [54].

4.3 Low Noise Amplifier (LNA)

The antenna is connected to a low noise amplifier using a 50 Ohm interface. A low noise amplifier is a device that amplifies incoming signals while introducing little noise of its own. Because of this property (high amplification but low noise injection), it is usually placed as the first component in a receiver chain. According to Friis' formula for overall noise factor of a receiver chain, the first component's noise and gain heavily influence the overall noise factor of the receiver chain [55], [56], [57]. Publication [P2] describes the design and implementation of an LNA within the Sampled Data Generator, capable of operating on the entire GNSS frequency band of interest. It also describes the design and software simulations of RF filters and the bandpass-sampling ADC, used subsequent to the LNA stage.

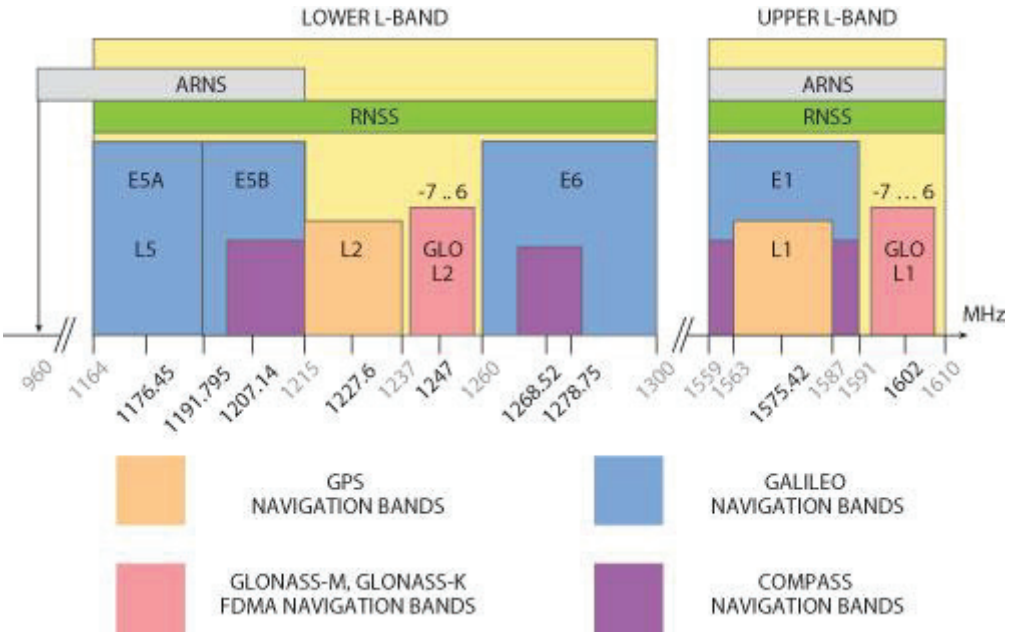

Fig. 4.1 Frequency spectrum of the proposed SDG

4.4 RF Filter

To isolate the two GNSS bands as stated in Section 3.1, it requires one RF bandpass filter (1164 MHz to 1615.5 MHz) followed by an RF bandstop filter (1300 MHz to 1559 MHz). These filters were designed as seventh-order LC Chebyshev filters in order to trade-off sharpness of filter cut-off with complexity and cost of final design. The design methodology adopted was as follows: first, the seventh-order low pass Chebyshev filter was designed, followed by the transformation from low pass to bandpass or bandstop filter using the principle of component transformations. Publication [P3] describes the design and simulation results of these two filters in detail.

4.5 Direct RF bandpass-sampling

The primary concept of direct bandpass-sampling based GNSS receiver front-end is to achieve digitization of the complete RF band of interest into digital intermediate frequency, thus eliminating the need for an analog mixer. The following describe the numerical analysis of this method, its benefits and drawbacks. The following research papers [58] - [71] are cited as references in support of this discussion, and are listed in the reference section of this thesis work. More details are provided in the Publication [P3].

4.5.1 Concept and numerical analysis

Upon sampling of a band of frequencies, the resulting spectrum consists of the original band replicated at integer multiples of the sampling frequency as shown in Fig. 4.2. Furthermore, to avoid any destructive aliasing (Fig. 4.3) it is necessary to sample at a frequency greater than twice the bandwidth (Fig. 4.4). This relaxes the sampling frequency requirement and also does not compromise on the data content in the sampled output.

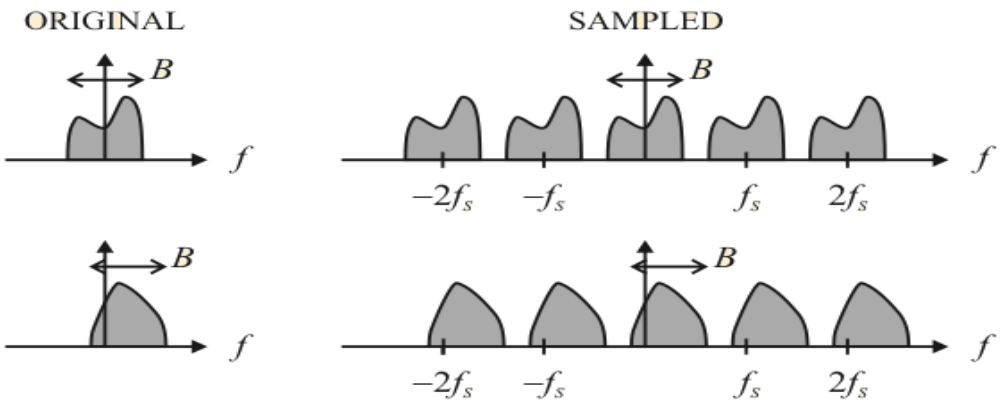

Fig. 4.2 Frequency spectrum of a complex signal before and after sampling

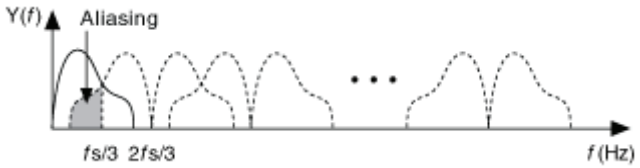

Fig. 4.3 Frequency spectrum showing harmful aliasing between different IF bands

Fig. 4.4 Frequency spectrum showing different IF bands without aliasing

For a set of two real distinct bands (as in the case of the proposed SDG), appropriate sampling frequency can be computed based on the simultaneous fulfillment of certain conditions as given by (10) to (17).

$$\text{Bandwidth of interest} = (1300\ MHz - 1164\ MHz) + (1615.5\ MHz - 1559\ MHz) = 192.5\ MHz \quad (10)$$

Center frequency of band 1 $(f_{c1}) = 1232\ MHz$ (11)

Center frequency of band 2 $(f_{c2}) = 1587.25\ MHz$ (12)

Minimum sampling frequency $(f_{smin}) = 2*($Bandwidth of interest$)$ (13)

$$\text{Intermediate frequency } (f_{IFi}) \begin{cases} = Rem\left(\frac{f_{ci}}{f_s}\right) & if\ Int\left[\frac{f_{ci}}{\frac{f_s}{2}}\right] = even \\ = f_s - Rem\left(\frac{f_{ci}}{f_s}\right) & If\ Int\left[\frac{f_{ci}}{\frac{f_s}{2}}\right] = odd \end{cases} \quad (14)$$

$$f_{IFi} > \frac{BWi}{2} \quad (15)$$

$$f_{IFi} < \frac{f_{s-BWi}}{2} \quad (16)$$

$$|f_{IF1} - f_{IF2}| \geq \frac{BW_1 - BW_2}{2} \quad (17)$$

where *Int[x]* is largest integer smaller than or equal to *x*, and *i* = The frequency band number (Band 1 = 1164 MHz to 1300 MHz and Band 2 = 1559 MHz to 1615.5 MHz). Further computation of possible sampling frequencies is described in Publication [P3]. If the GNSS signals are converted into complex/analytic by using Hilbert transformer and then sampled, the sampling frequency requirement is further relaxed. Fig. 4.5 shows the frequency spectrum of two complex signals with all important frequency points marked on the diagram.

Fig. 4.5 Frequency spectrum of two complex RF signal bands

Equations (18) to (21) give the criteria that must be simultaneously satisfied by the sampling frequency in case of complex GNSS signals.

$$n_1 \leq Int\left[\frac{f_{c1}}{BW_1 + BW_2}\right] \tag{18}$$

$$Int\left[\frac{n_1 * f_{c2}}{f_{c1}}\right] \leq n_2 \leq Int\left[n_1 * \left(\frac{f_{c2}}{f_{c1}}\right) + \frac{f_{c2}}{f_{c1}}\right] \tag{19}$$

$$\frac{f_{H2} - f_{L1}}{n_2 - n_1 + 1} \leq f_s \leq \frac{f_{L2} - f_{H1}}{n_2 - n_1} \tag{20}$$

$$\frac{f_{H2} - f_{L1}}{n_2 - n_1} \leq f_s \leq \frac{f_{L2} - f_{H1}}{n_2 - n_1 - 1} \tag{21}$$

Equation (20) should be used if the position of the resulting sampled bands should be as shown in Fig. 4.6. While if their positions should be as in Fig. 4.7, then (21) should be used. The solid trapezoid denotes spectra of original signal and the dashed trapezoid denotes a replica after sampling the original band.

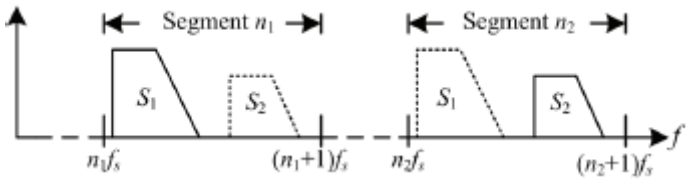

Fig. 4.6 First possibility of arranging the sampled and original bands

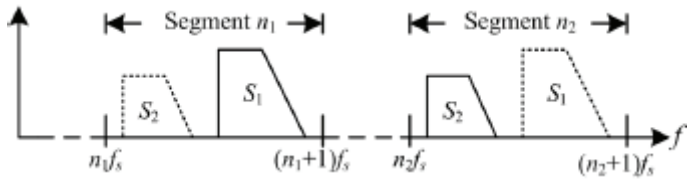

Fig. 4.7 Second possibility of arranging the sampled and original bands

Thus the procedure for obtaining a range of valid sampling frequency for two complex RF signals is: first, choose an appropriate n_1 using (18); next, choose an appropriate n_2 using (19), and last, using (20) or (21) compute the range of sampling frequencies. Equation (22) gives the new position of the sampled IF band when complex GNSS signals are considered.

$$f_c^m = m*f_s + rem(f_c, f_s) \qquad for\ (m = 0, \pm1, \pm2, \pm3 \ldots ....) \tag{22}$$

where f_c^m is the center frequency of the m^{th} replica of the sampled band, and $rem(f_c, f_s)$ is the remainder from the ratio of f_c and f_s. A drawback in the case of complex signal processing is the need to replicate the ADC in both the signal branches (I/Q), as shown in Fig. 4.8.

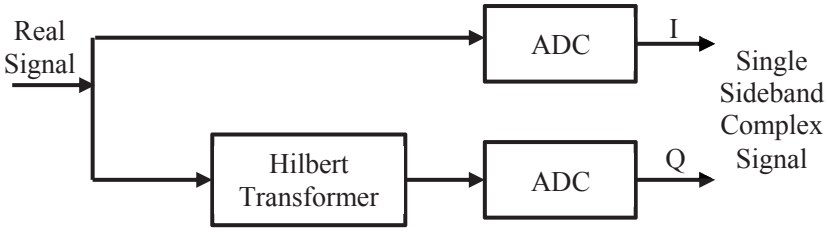

Fig. 4.8 Block diagram of complex bandpass-sampling

4.5.2 Benefits

Using the bandpass-sampling technique, a band of frequencies may be sampled at a rate that is twice the bandwidth, rather than twice the highest frequency component. This offers considerable relaxation in the sampling frequency requirement through the process of non-destructive aliasing. This also eliminates the need for a separate analog mixer. The intermediate frequencies are in digital domain and hence can be separated by digital filters instead of expensive and bulky analog channel select filters. This in turn helps in placing the ADC as close as possible to the antenna, a primary requirement of true software defined radio architecture.

4.5.3 Challenges

There are a number of challenges that must be analyzed and overcome to design a bandpass-sampling receiver front-end architecture.

ADC dynamic range and spurious free dynamic range - due to the wide bandwidth requirement, it is possible that there is considerable difference in the strengths of the signals received at different frequencies within this band. This complicates the decision about the ADC resolution and consequently, also complicates the estimations of the quantization noise. If a low resolution ADC is used, any high power frequency components will be 'clipped'. Such clipping in turn, produces spurious frequency components in the spectrum of the sampled signal.

SNR degradation due to noise aliasing - during bandpass-sampling, out of band noise from around integer multiples of sampling frequency is also aliased onto the desired frequency band after digitization [67]. This causes the degradation in SNR, and this degradation is proportional to the sub-sampling factor as given by (23). A solution to this degradation in SNR due to noise aliasing is to have sufficient amplification in the initial stages of the RF front-end.

$$Sub\text{-}sampling\ factor = \frac{f_{center}}{f_{sampling}} \tag{23}$$

SNR degradation due to clock jitter – The quality of the sampling clock is a major concern as the bandwidth to be digitized increases. In [117] and related works for example, the authors have performed a theoretical analysis of the power of the jitter noise, and the consequent degradation in the signal to noise ratio. Based on this study, a relation for jitter threshold in terms of the useful signal frequency, oversampling factor and power of any possible interferers was proposed. A set of acceptable sampling rates sufficient for Galileo reception were then computed based on this jitter threshold.

Analog to digital conversion is a computationally heavy process - Therefore, the ADC is a bottle-neck in the entire receiver front-end chain, especially for the bandpass-sampling architecture. It consumes most of the time and power allocated to the front-end and in the process generates a lot of heat that can be self-destructing if not dissipated effectively. For this reason, the ADC should have high speed of operation, low power consumption, and yet be affordable. Additionally, it needs to be carefully cooled to keep its temperature during operation within the safe operational limits [69]. The flash ADC architecture offers the fastest conversion speeds. Their only limitations are lower resolution and higher costs. For GNSS applications, lower resolution is not a primary concern and therefore, the flash architecture is worth further investigation in spite of the higher costs involved [68].

5. EFFECTS OF PHASE NOISE ON GNSS TRACKING PERFORMANCE

5.1 Introduction and Background

One of the objectives of this thesis work was to propose novel methods to improve the diversity of receiver characterization. This study proposes a new perspective for GNSS designers, which quantifies the performance loss in the baseband signal's correlation product due to phase noise from the radio front-end frequency source. These performance bounds may then be used as the basis for local oscillator design. Extensive simulations are used to validate results, while drawing conclusions regarding the relationship between phase noise, correlation time, and loss in the carrier-to-noise ratio. The experimental setup is shown in Fig. 5.1.

This Chapter is an introduction to the results provided in Publications [P4], [P5] and [P6], which describe this relationship, first for a free running oscillator case, and then for the more realistic PLL scenario. The actual phase noise models of the free running oscillator and PLL are described in the publications. Here we only provide a brief overview of the study and present some of the intermediate results using a recreation of the simulation scenarios described in the publications.

5.2 Basics of Phase Noise

In typical GNSS receivers, the signal received from a satellite is compared with an internally generated replica of its corresponding code at different code phases until the correlation product is maximized. This provides an indirect measurement of the pseudo-

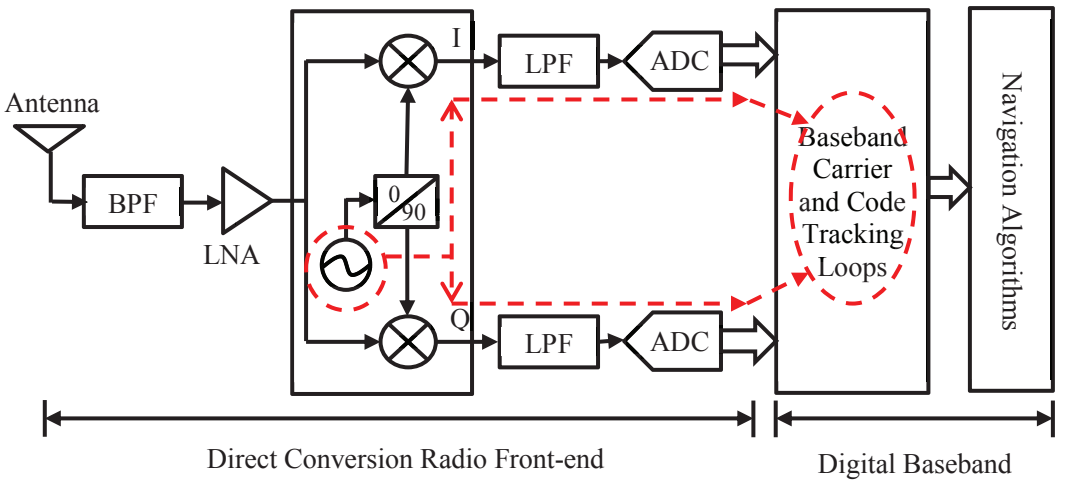

Fig. 5.1 Experimental set-up to study the effect of phase noise on banseband tracking performance

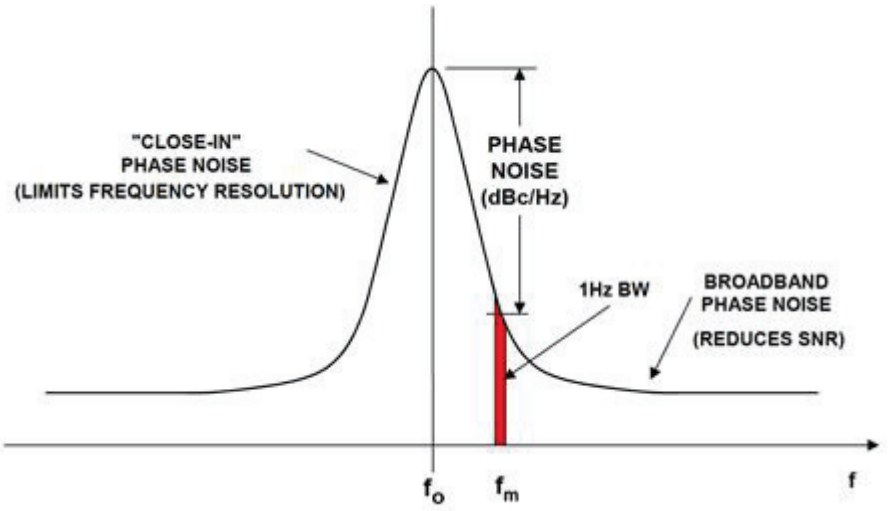

Fig. 5.2 Definition of phase noise

range between the receiver and the satellite. One of the performance limiting factors of GNSS receivers is the imperfection of the radio frequency (RF) oscillator, often referred to as phase noise. Phase noise is the random, rapid short-term phase fluctuations of the radio front-end's local frequency generator [27]. As shown in Fig. 5.2 [83], the phase noise is measured in a bandwidth of 1 Hz at a defined frequency offset from the center frequency. The unit for measuring the phase noise is dBc/Hz. The normalized single side-band phase noise spectral density is given by (24) [28].

$$N_{Phase}(dBc/Hz) = 10log_{10}[\frac{2KT}{P_{Signal}} * (\frac{\omega_0}{2Q\Delta\omega})^2] \quad (24)$$

where N_{phase} is the phase noise within the bandwidth of 1Hz at a frequency offset of $\Delta\omega$, K is the Boltzmann constant of 1.38 x 10-23 J/K, T is the Temperature in Kelvin, P_{signal} is the power of the signal under consideration (in absolute values), ω_0 is the center frequency of the signal under consideration in radians/sec, and Q is quality factor of the resonator in the local oscillator.

The receiver oscillator phase noise adversely affects the frequency down conversion and analog to digital conversion processes, thus diminishing the achievable carrier-to-noise ratio (C/No). Consequently, the correlation outputs in the code-tracking loop and the carrier phase tracking jitter are also adversely affected. Furthermore, longer integration intervals can make integration (correlation) comparatively less effective in the presence of this phase noise. In this study, we attempt to investigate the answers to the following questions: What is the maximum acceptable phase noise level as required by an RF designer in order to achieve a minimum pre-defined C/No? How do correlation losses relate to phase noise levels? Answers to these questions will ultimately help in justifying the addition of this phenomenon in the overall characterization of GNSS receiver performance.

5.3 Simulation Scenarios

In the first part of this study [P4] and [P5], we proposed an analytical approach using a mathematical phase noise model for a simple free running oscillator. Our results provided

a first estimate of the noise floor requirements for a receiver given a particular baseband implementation. However, the FRO model is not well suited to represent practical receiver frequency synthesizers and hence, its direct use for specification of receiver designs is not appropriate. Therefore, the second part of this study [P6], presented the subsequent observations of receiver performance by utilizing the PLL as a practical frequency synthesizer. The results reveal that, there are both quantitative and qualitative differences in performance when compared to the FRO scenario. Here we present a summary of the study in [P6] and show some intermediate results which are then refined and extended in the publication.

The PLL model shown in Fig. 5.3 was used to create sampled phase noise signal vectors (called 'realizations') of duration 200 ms each. These signal vectors were created for different combinations of a range of typical GNSS front-end PLL parameters, as described in Table 5.1. This allowed studying the effect of each PLL parameter upon the GNSS baseband correlation performance. One hundred such realizations were generated for every combination so that the results could be averaged over a considerable size of data samples. The overall PLL phase noise is dependent on the sum of phase noise contributions of its constituent blocks. The contribution of each block is in turn dependent upon various parameters, as shown in Table 5.1. In each realization, only one parameter was varied while keeping all others constant, so that the effect on code correlation due to that parameter (and hence due to that constituent block) could be studied. The method for adding the PN into the signal stream is shown in Fig. 5.4.

5.4 Simulation Results

Fig. 5.5 shows how the SNR of correlation peak degrades with increasing thermal PN of the PLL VCO for different loop filter bandwidths, frequency division ratios (FDR, denoted by N) and PIT values while Fig. 5.6 shows the relation between phase component of correlation peak and the PLL PN. As mentioned earlier, these results are refined and extended in publication [P6].

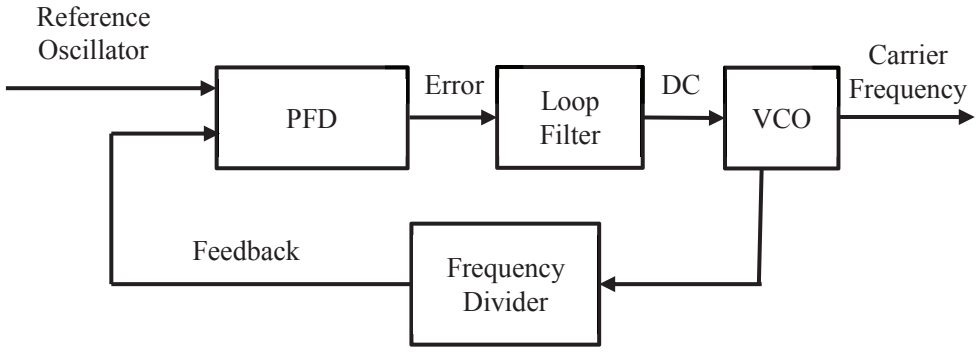

Fig. 5.3 Phase Locked Loop Block Diagram

Table 5.1 Constituent blocks of a PLL and typical values of their significant design parameters

Constituent Block	**Important Parameter**	**Typical Value(s)/Range**
Crystal RO	PN (at 10 kHz offset)	-150 dBc/Hz
PFD	PN (at 1 MHz offset)	-265 dBc/Hz
Loop Filter	Order	2^{nd} order
	Bandwidth	1 kHz → 100 kHz
VCO	PN (at 1 MHz offset)	-130 dBc/Hz → -100 dBc/Hz
FD	Division Ratio (N)	64, 200

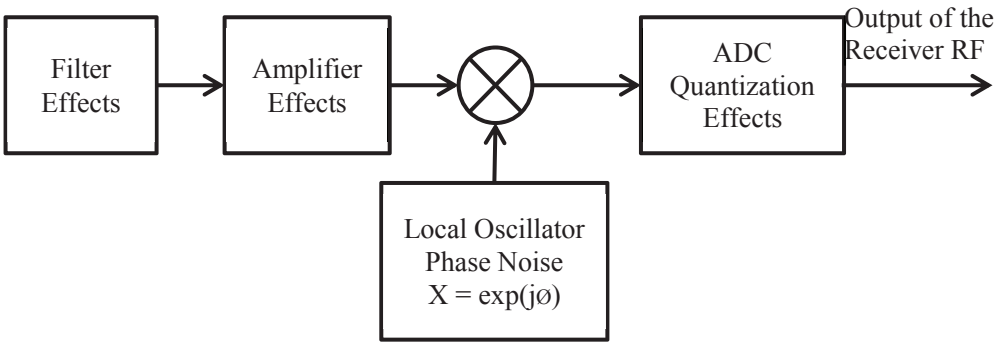

Fig. 5.4 Block schematic showing the mechanism to add phase noise in the signal stream

5.4.1 SNR of correlation peak versus VCO PN

Fig. 5.5 shows that the SNR of correlation peak degrades with increasing thermal PN of the PLL VCO. This degradation is more rapid at higher PLL bandwidths and is approximately 10 dB per every 5 dBc/Hz increase in PN. It should be noted that, the SNR values obtained here are greater than those observed in typical GNSS receivers because the simulation environment does not assume any receiver thermal noise floor. Consequently, this makes the noise-free post-correlation SNR to be infinite.

The dynamic range of the SNR extends from 0 dB to 110 dB for the chosen range of PLL BW and VCO phase noise values; however, its absolute value for a given PN is inversely proportional to the loop filter bandwidth. Therefore, loss in SNR due to PN can be at least partially compensated by increasing the filter BW. This observation is expected, as the VCO PN contribution to the overall PLL PSD is diminished for higher bandwidths. However, there is a limit to which the increase in bandwidth translates to an improvement in SNR. Very large PLL bandwidths would also result in more noise and spurious signals flowing into the signal stream, thus adversely affecting the baseband correlation SNR.

Additionally, increasing the PLL bandwidth propagates the reference oscillator (RO) PN to the output PLL PN, thus making it the bottleneck for improving the SNR. This phenomenon can be observed in the case where both, bandwidth and PIT are large. Comparison between the two frequency division ratios shows that the slope of degradation

remains similar, but there is a noticeable degradation in SNR for a given PN if the FDR is increased to 200. The SNR may even drop to zero in case of small filter BW and high PIT.

5.4.2 Phase component of correlation peak versus VCO PN

The objective is to maintain the standard deviation of phase angle of the correlation result over consecutive epochs below 10 degrees so that the tracking loop PLL can keep track of the correlation product. Fig. 5.6 shows that, although increasing VCO PN degrades the phase angle stability, this degradation is not significant for bandwidths greater than 5 kHz. GNSS radio front-end PLLs usually have filter bandwidths in excess of 5 kHz and therefore, PLL phase noise should not be a major problem in maintaining correlation product's phase angle stability.

The degradation in angular stability for lower bandwidths is quite significant. A PLL with zero bandwidth acts as a free-running oscillator. This is where the RO is rejected entirely from the loop while at the same time passing the VCO only to the output as a free-running oscillator. Hence its behavior resembles the results obtained in [P4], which used a FRO for all its simulations. Otherwise, the standard deviation is inversely proportional to the loop bandwidth, which means that the deviations in phase angle over consecutive epochs can be reduced if the PLL loop bandwidth is increased. Increasing the frequency division ratio of the PLL worsens the overall phase angle stability for given values of VCO PN and PLL bandwidth. Nevertheless, it is still possible to easily maintain maximum phase deviations under 10 degrees for almost all the loop bandwidths typically used in commercial GNSS radio front-end PLLs.

5.5 Results Analysis

Table 5.2 and Table 5.3 describe the maximum PLL phase noise allowed at different combinations of loop bandwidth, frequency division ratio and integration time to maintain SNR above 50 dB and 30 dB respectively. To better interpret the values in Table 5.2, consider the case of bandwidth 30 kHz (shaded). For frequency division ratio N = 64, as the PIT is increased, the maximum phase noise allowed to maintain SNR above 50 dB also increases, or in other words, more phase noise is acceptable. If the frequency division

ratio is increased to 200, for the same PIT (e.g., 4 ms), to maintain SNR above 50 dB the phase noise requirement becomes more stringent (-112.5 dBc/Hz as compared to -105 dBc/Hz for FDR of N = 64). It can be observed that as we reduce the PLL loop bandwidth to 1 kHz, it starts to behave increasingly like a free running oscillator, and shows characteristics opposite to the higher BW cases. As an example, the SNR at a given PN reduces as the PIT is increased from 4 ms to 100 ms for bandwidth equal to 1 kHz. This conforms very well with the results obtained in [P4] and [P5], both of which used a FRO model as the frequency source.

5.6 Endnote about Phase Noise and Allan Variance

Oscillator manufacturers usually represent the performance of their products in terms of phase noise as a function of frequency difference from the center frequency, with units of dBc/Hz. Phase noise is a simple way to evaluate the performance of an oscillator as it is very easy to visualize on paper. However, it is debatable if this is indeed an informative metric for a GNSS receiver designer who may rather require a metric that will evaluate the oscillator performance in the time domain. Usually, the Allan Variance (AV) [112], [113], [114] is considered as a metric to provide such information, which is a derivative of the phase noise measurements over consecutive sample points. Would it be of interest to investigate the carrier and code tracking jitter as a function of oscillator AV as well, particularly:

- Is it possible to recreate this study using Allan Variance instead of Phase Noise?
- Is it possible to simulate overall Allan Variance of the PLL taking into account Allan Variance of each sub-block within the PLL?

In our opinion, AV and jitter measurements are computed using the phase noise power spectral density (PSD). It is possible that different PSDs can result in the same AV. Furthermore, the same AV (even though from different PSDs) may result in different bit error rate (BER). Hence, the PN PSD is more explicit measure that is nevertheless easily convertible to AV.

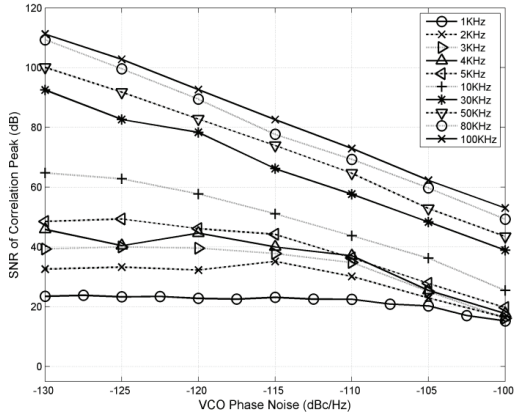
1KHz
2KHz
3KHz
4KHz
5KHz
10KHz
30KHz
50KHz
80KHz
100KHz
SNR of Correlation Peak (dB)
VCO Phase Noise (dBc/Hz)
120
100
80
60
40
20
0
-130
-125
-120
-115
-110
-105
-100

(a)

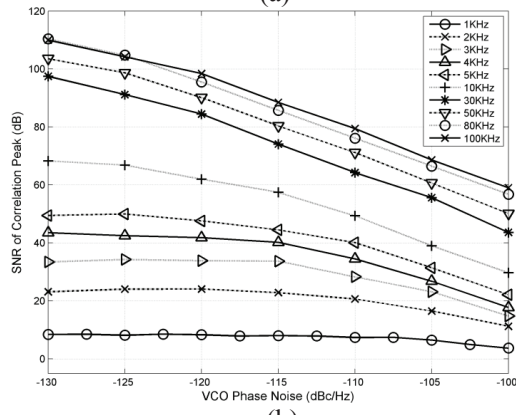
1KHz
2KHz
3KHz
4KHz
5KHz
10KHz
30KHz
50KHz
80KHz
100KHz
SNR of Correlation Peak (dB)
VCO Phase Noise (dBc/Hz)
120
100
80
60
40
20
0
-130
-125
-120
-115
-110
-105
-100

(b)

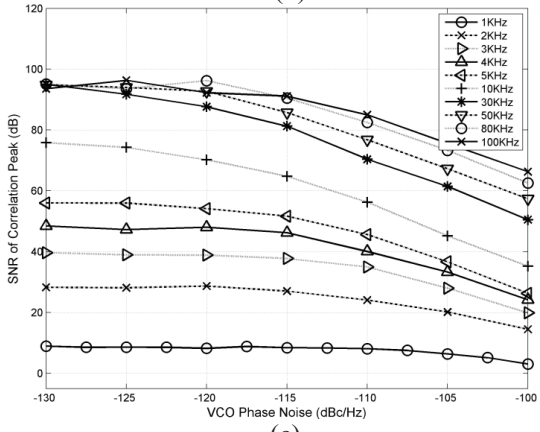
1KHz
2KHz
3KHz
4KHz
5KHz
10KHz
30KHz
50KHz
80KHz
100KHz
SNR of Correlation Peak (dB)
VCO Phase Noise (dBc/Hz)
120
100
80
60
40
20
0
-130
-125
-120
-115
-110
-105
-100

(c)

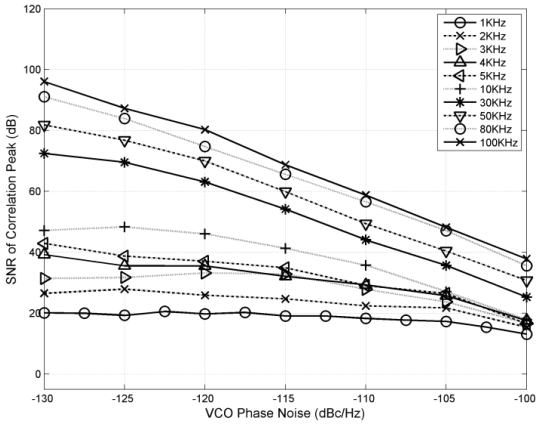

(d)

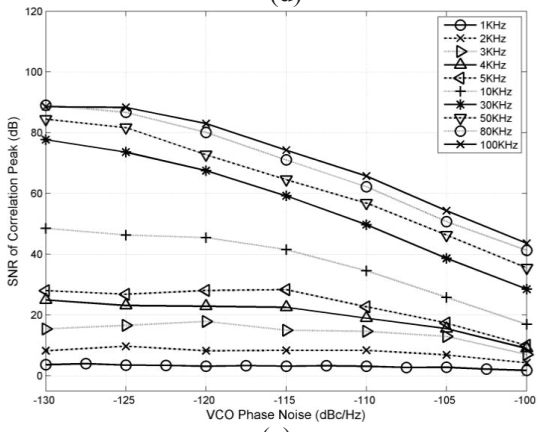

(e)

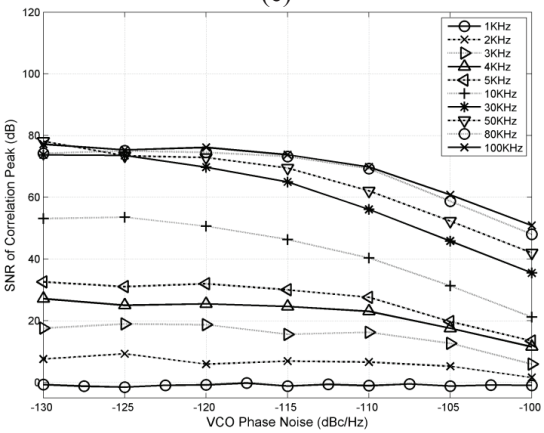

(f)

Fig. 5.5 Correlation SNR vs VCO PN with N = 64 and PIT = a) 4ms b) 20ms c) 100ms. N = 200 and PIT = d) 4ms e) 20ms f) 100ms

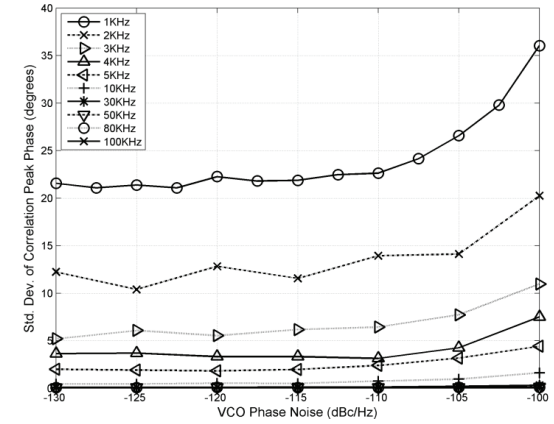
1KHz
2KHz
3KHz
4KHz
5KHz
10KHz
30KHz
50KHz
80KHz
100KHz
Std. Dev. of Correlation Peak Phase (degrees)
VCO Phase Noise (dBc/Hz)
40
35
30
25
20
15
10
5
0
-130
-125
-120
-115
-110
-105
-100

(a)

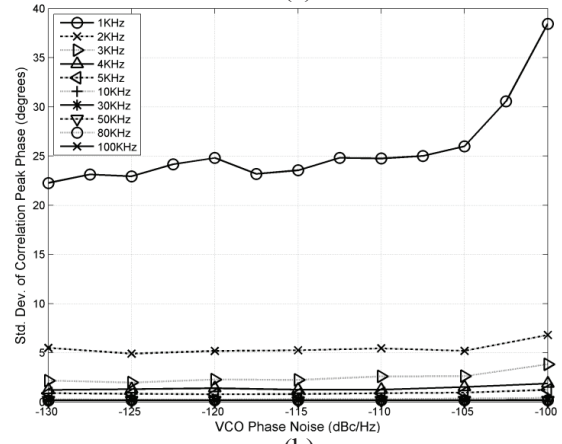
1KHz
2KHz
3KHz
4KHz
5KHz
10KHz
30KHz
50KHz
80KHz
100KHz
Std. Dev. of Correlation Peak Phase (degrees)
VCO Phase Noise (dBc/Hz)
40
35
30
25
20
15
10
5
0
-130
-125
-120
-115
-110
-105
-100

(b)

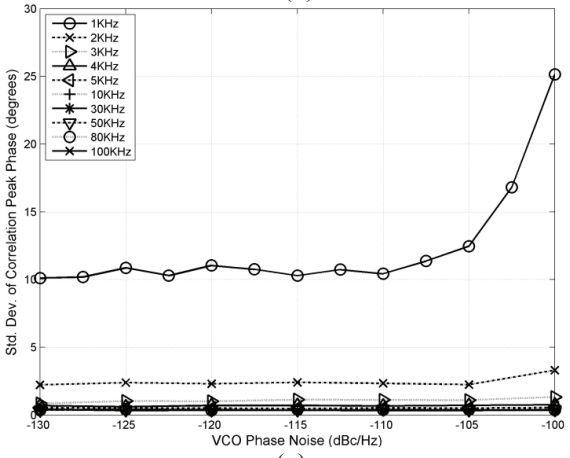
1KHz
2KHz
3KHz
4KHz
5KHz
10KHz
30KHz
50KHz
80KHz
100KHz
Std. Dev. of Correlation Peak Phase (degrees)
VCO Phase Noise (dBc/Hz)
30
25
20
15
10
5
0
-130
-125
-120
-115
-110
-105
-100

(c)

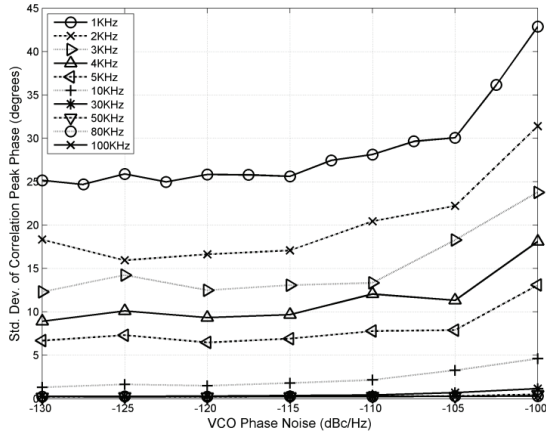

(d)

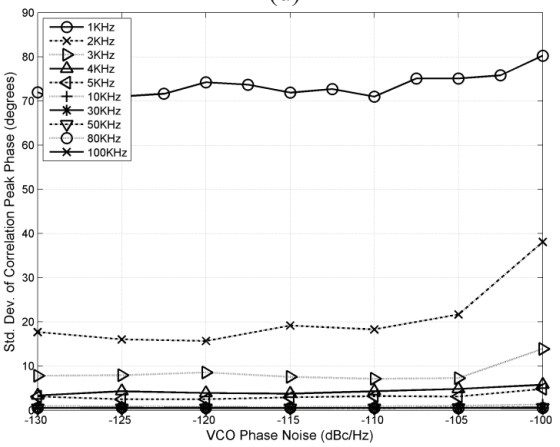

(e)

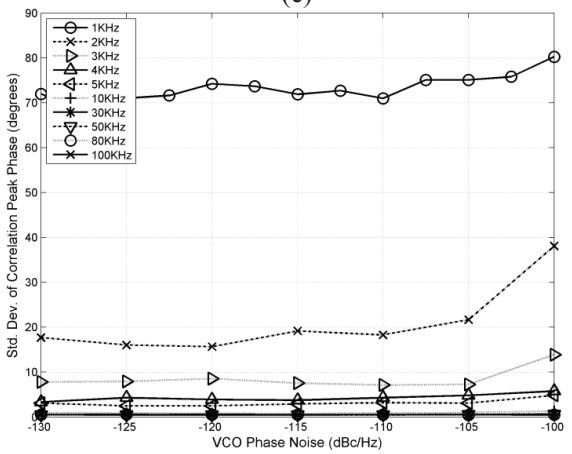

(f)

Fig. 5.6 Correlation Phase vs VCO PN with Freq Div = 64 and PIT = (a) 4ms (b) 20ms (c) 100ms. Freq Div = 200 and PIT = (d) 4ms (e) 20ms (f) 100ms

Table 5.2 Maximum phase noise (dBc/Hz) in order to maintain minimum correlation SNR of 50 dB for different values of loop BW, PIT and frequency division ratio (N)

BW (kHz)	***N* = 64**			***N* = 200**		
	PIT = 4msec	**PIT = 20msec**	**PIT = 100msec**	**PIT = 4msec**	**PIT = 20msec**	**PIT = 100msec**
5	-125	-125	-113	-	-	-
10	-115	-110	-107	-	-	-119
30	-105	-102.5	-100	-112.5	-110	-107
50	-102.5	-100	> -100	-110	-107	-104
80	-100	> -100	> -100	-105	-105	-101
100	> -100	> -100	> -100	-105	-103	-100

Table 5.3 Maximum phase noise (dBc/Hz) in order to maintain minimum correlation SNR of 30 dB for different values of loop BW, PIT and frequency division ratio

BW (kHz)	**FDR = 64**			**FDR = 200**		
	PIT = 4msec	**PIT = 20msec**	**PIT = 100msec**	**PIT = 4msec**	**PIT = 20msec**	**PIT = 100msec**
1	-	-	-	-	-	-
2	-110	-	-	-	-	-
3	-107.5	-111	-106	-112	-	-
4	-107	-107	-103	-111	-	-
5	-106	-104	-102	-111	-	-115
10	-102	-100	> -100	-107	-107.5	-104.5
30	> -100	> -100	> -100	-102	-101	> -100
50	> -100	> -100	> -100	-100	> -100	> -100
80	> -100	> -100	> -100	> -100	> -100	> -100
100	> -100	> -100	> -100	> -100	> -100	> -100

6. TEST SCENARIOS FOR ADVANCED GNSS RECEIVERS

6.1 Introduction and Background

The objective of this section is to serve as a guideline for the testing and performance validation of GNSS receivers. We follow the typical testing procedure for GNSS receivers as shown in Fig. 6.1 and the test scenarios described in [17]-[26]. However, the aim is to adapt these scenarios, (which are targeted primarily towards simple receivers) to the more advanced multi-frequency, multi-constellation GPS L1/L5, Galileo E1/E5a TUTGNSS prototype receiver. Publication [P7] extends this discussion further by demonstrating how these test cases can be incorporated into an automated test-bench. Together, this information describes our work in investigating novel solutions for Block 3 from Fig. 1.1.

6.2 Receiver Settings

Two configuration settings in the receiver control the mode of operation and the manner in which it has to be turned ON via a 32-bit control word. Table 6.1 describes the various options and the digital control word corresponding to each option. There are eight possible modes of operations which would require 3 bits to be uniquely represented. However, it is recommended to use 5 bits in order to accommodate any future increase in operating modes. Similarly, there are three ways to turn ON a receiver, which can be uniquely represented by 2 bits. Therefore, out of the 32 available bits, only 7 bits are currently utilized, leaving the rest in reserve for future use. The mode selection bits are in the least significant bit (LSB) position of the control word. As an example, if the receiver should

perform position fix after a warm start using GPS L1 and Galileo E1 signals, the 32-bit control word would be “00000000_0000000_00000000_00100010”. Using such a control word at the beginning of every test, it is possible to use the following scenarios to test a basic single constellation or more advanced multi-constellation receiver.

6.3 Time to First Fix (TTFF) Tests

The amount of time it takes the receiver after switching ON to compute the first valid position fix is called time-to-first-fix or TTFF. Depending upon the initial conditions, there are four start modes for a typical GNSS receiver: cold start, warm start and hot start [14]. In cold start, the receiver has no a-priori information about the on the approximate time, ephemeris, almanac or last computed position, and TTFF may take around 60 seconds under nominal signal power. In warm start conditions, the receiver has a-priori information about the approximate time, last computed position, oscillator offset and a valid copy of the almanac is stored in memory. The ephemeris is yet to be decoded and hence the time-of-week information is missing, resulting in a TTFF close to 30 seconds. In hot start conditions, the receiver has a-priori information about all data required for a position fix. Valid ephemeris and almanac are available for all visible satellites, along with approximate time, oscillator offset, and last position fix, resulting in a TTFF of about 1 second.

6.3.1 Nominal Cold Start, Warm Start and Hot Start TTFF

The aim of this test is to verify receiver’s cold start, warm start and hot start TTFF performances under nominal signal conditions, typically assumed as satellite signal power equal to or greater than -130dBm.

6.3.2 Low Power Cold Start TTFF

The aim of this test is to verify the receiver’s cold start TTFF performance under low power input signal conditions, typically assumed as maximum satellite signal power equal to or less than -142 dBm.

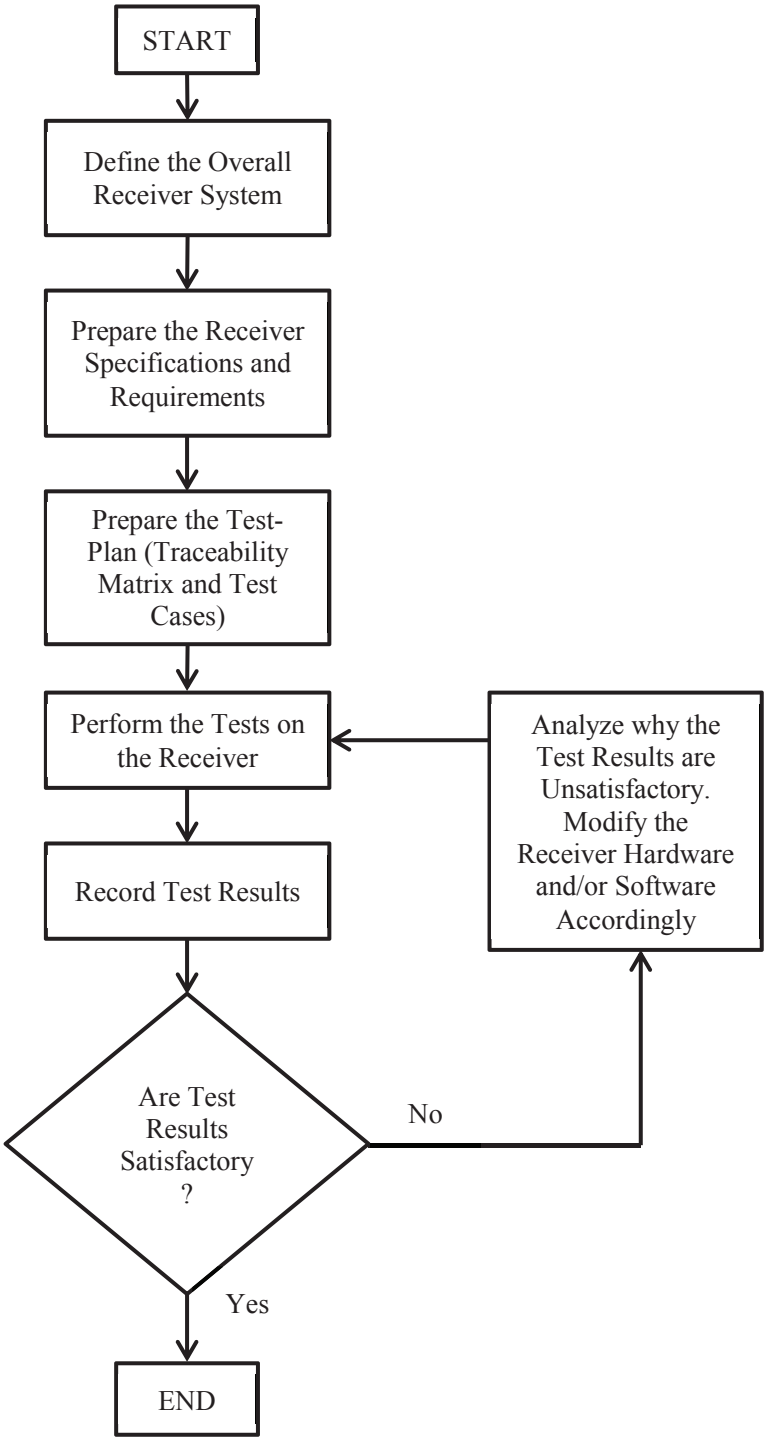

Fig. 6.1 Typical testing procedure for GNSS receivers

Table 6.1 Advanced GNSS receiver operating modes

	Example Options	**Binary Representation**
Example modes of operation	GPS L1 only	00000
	Galileo E1 only	00001
	GPS L1 + Galileo E1	00010
	GPS L1 + GPS L5	00011
	Galileo E1 + Galileo E5a	00100
	GPS L1 + GPS L5 + Galileo E1 + Galileo E5a	00101
	GPS L1 + GPS L5 + Galileo E1	00110
	GPS L1 + Galileo E1 + Galileo E5a	00111
Turn ON modes	Cold Start	00
	Warm Start	01
	Hot Start	10

6.4 Acquisition Sensitivity in Cold Start

The aim of this test is to verify the receiver's acquisition sensitivity. Acquisition sensitivity refers to the minimum satellite signal power level at which the receiver can still perform successful acquisition. To perform this test, one satellite in the simulator is maintained at a defined power level and required numbers of acquisition iterations are performed. In each iteration, acquisition is deemed successful only if the code delay and the Doppler offset estimated by the receiver acquisition is within ±1 chip (300m) and ±150Hz respectively from the correct (simulator) values. If the percentage of successful acquisitions is greater than a pre-determined threshold, the receiver is thought to acquire satellites successfully at this power level. The satellite signal power is then reduced and the test repeated.

6.5 Accuracy

Position accuracy is defined as the magnitude of the distance between the computed position of the receiver and the true position as defined in the simulator. 2-dimensional position accuracy is usually represented in terms of Circular Error Probability (CEP), while 3-dimension position accuracy is expressed in terms of Spherical Error Probability (SEP). CEP is the radius of a circle which encompasses half of the position fixes. Better the accuracy of the receiver, closer to the true position will be its repetitive position fixes, thus smaller will be the radius of the circle encompassing half of these points.

6.6 Tracking Sensitivity

Tracking sensitivity of a receiver is defined as the minimum satellite signal power at which the receiver can still continue tracking the satellite. To perform this test, the signal power of a visible satellite is switched between nominal and a low power level at regular intervals and over a number of iterations. The tracking performance, in terms of CNR of the satellite as measured by the receiver is continuously monitored over the power variations to ensure that it is indeed successfully tracking the satellite. In the next iteration, the low power level is reduced by 1 dB and the process is repeated. It is interesting to identify what benefits in tracking advanced receivers offer over single-frequency single-constellation receivers. Furthermore, when using GPS L5/Galileo E5a signals, it is necessary to specify whether this refers to only pilot signal tracking or to combined data and pilot signal tracking.

6.7 Availability

Availability refers to the percentage of time services of the GNSS receiver are useable. Differently put, it refers to the percentage of time valid position fix is computed by the receiver under diverse conditions of signal strength. Under this scenario, the receiver is subjected to diverse signal power, interference and multipath conditions, which attempt to recreate outdoor, urban canyon and indoor environments. Receiver motion is simulated by changing the simulator signal characteristics at regular intervals. Throughout the scenario, the receiver performance is monitored to ensure that it continues to provide a valid

position solution. The percentage of time that the receiver experiences an ‘outage’ is then used to compute the availability of the receiver.

6.8 Receiver Dynamics

This scenario is used to test the performance of the GNSS receiver when in motion. The important parameters of motion are speed, direction, acceleration, jerk and instantaneous position. Typically, receiver dynamics are tested for speeds up to 120 km/h. [18] proposes a circular trajectory, while [17] proposes a racetrack trajectory (also called a rectangular trajectory with rounded corners), as shown in Fig. 6.2. This figure also shows some example values for the top/bottom path distance = 1440m, left/right path distance = 940m, corner radius = 20m, position of starting point = left hand top corner, direction of rotation = clockwise, acceleration distance = 500m, minimum speed = 30 km/h on turn, and maximum speed = 120 km/h on straight path. Moving over the selected route three times allows a more general idea of receiver performance under dynamic stress. If the receiver is capable of mapping the route as it is in motion, this is convenient for post-processing of the positioning accuracy and availability during the dynamic scenario.

6.9 Reacquisition Time

Reacquisition time is defined as the time necessary for a receiver to reacquire all visible satellites and make a position fix after a sudden drop in signal power causes all previously tracked satellite signals to be lost. Quick reacquisition time is important, e.g., in vehicle navigation systems. To perform this scenario, the receiver is first allowed to make a stable position fix under nominal satellite signal power conditions. Next, all the visible satellite signals from the simulator are turned OFF until the receiver no longer is tracking any of them. Finally, all the signals are turned ON simultaneously at nominal power level. The amount of time it takes for the receiver to re-obtain stable position fix is measured as the reacquisition time.

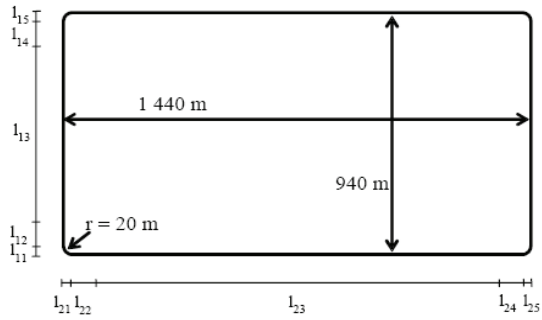

Fig. 6.2 Rectangular (racetrack) trajectory for dynamics testing

6.10 Multipath Mitigation

The objective of this test is to determine the ability of the receiver in mitigating the effect of multipath errors, including Non Line-Of-Sight (NLOS) multipath components. Signal simulators have inbuilt support for a number of realistic multipath scenarios and models, which can be used for performing this test. Multipath errors are a significant source of receiver performance degradation, considering that the number of satellite navigation receivers in smartphones/Personal Navigation Devices (PNDs) is continuously rising, and majority of such receivers are typically used in urban high-multipath conditions.

6.11 Radio Frequency Interference (RFI)

The objective of this test is to determine the ability of the receiver to operate in the presence of interfering signals, including non-intentional and intentional (jamming) interferers. The most convenient option is to check whether in presence of radio frequency interference of up to -60 dBm, the receiver continues to maintain stable position fix. Testing can be performed for interference mitigation on a single GNSS frequency band or on all frequency bands processed by the receiver.

6.12 Ionosphere errors

The objective of this test is to investigate the performance of the dual-frequency receiver approach in compensating for the ionosphere error and improving the accuracy of position

fix. This scenario can be performed by computing the receiver accuracy in single-frequency mode of operation, followed by the dual-frequency mode. The benefit of using dual-frequency can be quantified in terms of meters of improved accuracy. Signal simulators are capable of generating ionosphere errors based on one or more mathematical models, which can be used for performing this test. However, it should be noted that, using the same mathematical model to generate ionosphere errors in the simulator as that used for ionospheric error compensation within the receiver can result in an unrealistically improved performance of the receiver.

7. OVERVIEW OF PUBLICATIONS

7.1 Research Problems and Proposed Solutions

During the course of this thesis work, the research group was presented with a number of challenges emanating from the performance testing of the TUTGNSS receiver in the final stages of the GRAMMAR project. This necessitated the design of an overall test-plan and development of the individual test-cases for the important performance parameters. The solutions to these challenges were compiled and gradually evolved into the composition of this manuscript.

During the test-plan, it was noticed that the research group at TUT did not possess a GNSS signal source capable of producing the multiple frequencies and multiple constellations necessary for full performance evaluation of the advanced TUTGNSS receiver. Consequently, it was planned to investigate the possibility of developing a software-based signal simulator capable of generating the required signals. The first step towards this was a background study of important performance parameters of GNSS receivers and their typical test-scenarios. Also included in this study was a literature study of state-of-art in software-based GNSS simulators within the academic and industrial domains. Simultaneously, it was decided to investigate another novel solution for a GNSS signal source, which was to implement a radio front-end capable of receiving all possible GNSS signals from the sky using the concept of wideband sampling.

During the actual testing of the TUTGNSS receiver, it was observed that manual intervention was unsuitable for repetitive testing as it was inefficient and introduced errors into the test results. Moreover, without an internal view of the signal processing chain at every stage of the receiver, it was difficult to locate the cause of receiver performance

anomalies. Therefore, the next challenge was to design an automated test-bench that would remove the need for human control, and a data capture tool for accessing intermediate results from within the receiver processing chain.

The third and final challenge addressed by this thesis was to study the degrading effect of phase noise from the radio front-end's local frequency generator on the baseband tracking performance of the GNSS receiver. The objective of this study was to demonstrate that there exists possibility to design innovative test scenarios for GNSS receivers through the study of new performance metrics. The solution to this problem included designing mathematical models for simple free running oscillators and consequently, a more realistic PLL, in terms of their phase noise contributions, which were then used to study the performance of typical carrier and code tracking loops under diverse operating environments.

7.2 Relating Publications to the Research Work

The publications included in this manuscript are referred to as [P1] – [P7] in the following paragraphs. Fig. 1.1 and Table 1.1 describe how the individual Publications contribute to the overall research theme. Publications [P1], [P2] and [P3] describe the work done towards implementing novel sources of test signals for GNSS receivers. Two solutions are proposed for this problem: a software-based signal simulator with multi-frequency, multi-constellation capability, and a bandpass-sampling based sampled data generator. These publications build upon the introduction about general theory of software-based simulators and wide-band sampling provided in Chapters 3 and 4 respectively.

Chapter 5 presents a brief introduction and background to the concept of phase noise, and our proposed study on its effects on GNSS tracking performance. Further details of this study are presented in publications [P4], [P5] and [P6]. In [P4] and [P5], a simple free-running oscillator phase noise model is used as the noise source, and its effects on a GPS and Galileo code and carrier tracking channel are investigated in terms of the signal to noise ratio and phase component of the correlation product. In [P6], the study is extended to include the effect of a more realistic PLL PN model on a GPS code tracking channel.

As described earlier, these publications deal with investigating novel applications for the test-bench and identifying novel parameters to characterize receiver performance.

Chapter 6 describes the typical test cases and test scenarios for the performance evaluation of GNSS receivers. An attempt has been made to adapt these scenarios so that they can be applied to more advanced multi-frequency, multi-constellation receivers. Publication [P7] describes the tool that assists in the automated performance evaluation of the receiver based on scenarios introduced in Chapter 6. It also describes a data capture tool to capture the internal process parameters from within the TUTGNSS receiver hardware.

Together, these publications describe the novel solutions that we propose for improving the efficiency, accuracy and diversity of GNSS receiver performance evaluation, which is the main theme of this thesis work.

7.3 Author's Contribution to the Publications

The author has been the lead contributor to a majority of the publications included in this manuscript. However, as in any research activity, collaboration between internal and external research partners has been a significant driver for these publications. Here we attempt to specify the actual contribution of this author to each one of the listed publications [P1] – [P7].

In [P1], this author formulated the research problem based on the prevailing situation in the research group with regards to the testing of the TUTGNSS prototype receiver. This was followed with an in-depth literature review of the state-of-art software-based simulators, including categorizing them in three generations based on their year of creation, listing their constituent components, strengths and weaknesses, and identifying a pattern in the evolution of such simulators over the past 20 years. By extrapolating this pattern, a set of criteria for an advanced software-based simulator were proposed. A Simulink-based model was developed which attempted to incorporate some of the components of such advanced simulators. The co-authors assisted in the formulation of the research problem, suggested additional parameters on which the simulators could be compared and helped to review the publication manuscript.

In [P2] and [P3], this author prepared the design for the Sampled Data Generator in collaboration with research supervisors (who were also the co-authors) after a detailed literature review of multi-frequency GNSS receivers and the general theory of bandpass-sampling. The low noise amplifier design, simulations, and PCB-based implementation were accomplished by this researcher. Testing of the LNA was performed in collaboration with a supervisor from the RF Department. This was followed by Matlab-based simulations of the bandpass-sampling theorem to identify the most suitable sampling frequency for the proposed SDG. The composition of these publication manuscripts was accomplished by this author with peer-reviews provided by the co-authors.

In [P4], the original idea for the research direction was suggested by two of the co-authors, who also contributed to the theoretical formulation of the research problem. They performed the time-domain and frequency-domain analysis of the effect of free running oscillator phase noise on a typical GNSS code tracking loop. This author designed the Matlab-based simulations, performed experiments to verify that the effect of phase noise on code tracking was in conformance to the theoretical stipulations, recorded the results, and made conclusions from the analysis about the nature of the relationship between tracking performance and radio front-end phase noise. In [P5] the idea to extend the analysis from [P4] to carrier tracking loops was proposed by a co-author. This author extended the mathematical models for the code tracking loops to incorporate also carrier tracking (phase angle information of the correlation product) in a similar analysis using Matlab-based simulations.

In [P6], the publication was a result of equal collaboration between this author and the next significant co-author. The RF research group was involved in implementing a detailed mathematical model of a charge-pump PLL, including the phase noise contribution of its constituent blocks. This author was responsible for implementing the GNSS tracking and correlation model in Matlab and simulating the effect of the phase noise on the tracking loop performance, which resulted in detailed guidelines about radio front-end PLL circuit design for GNSS receivers. This study was more comprehensive than the previous studies using free running oscillator PN models. The analysis of the results provided for more practically useful metrics and thresholds for receiver designers.

In [P7], two major themes are addressed: automation of the overall receiver testing using a custom software tool called the AutoPET, and introducing the capability to characterize the signal processing chain using the data capture tool called dCAP. The AutoPET is a software program in the Qt platform and C++ language that communicates between the GNSS receiver, the test signal source and a control computer to achieve human-independent testing of the receiver. The entire assembly, including the communication between the entities was designed and implemented by this researcher. The data capture tool called dCAP, was implemented in hardware by the next significant co-author. The integration of these tools into the overall test-bench, and composing the publication was accomplished by this author.

7.4 Impact of Publications

There has been a conscious attempt by the author to propose the results of the thesis work for publication at high quality, high impact conferences and journals in accordance with the Finnish Publication Forum (Julkaisufoorumi – Jufo, for short) [111]. In case of publications in venues not listed in the forum, the author has chosen recommended conferences from the field of navigation and positioning. Additionally, Chapter 3 of this manuscript has been adapted as a book chapter in [116]. Below is a list of publications and their respective venues, supporting the earlier remarks:

[P6] - Jufo Level 2 Journal

[P5] & [P3] - Jufo Level 1 Conferences

[P1] - European Navigation Conference (ENC-GNSS)

[P7] - Institute of Navigation's GNSS+ Conference (ION GNSS+)

[P4] - InsideGNSS

[P2] - IEEE, ESA, and DLR Co-sponsored Conference

8. CONCLUSIONS

8.1 Main Contributions of the Research

The principle contributions of this research work are towards GNSS receiver performance evaluation through innovations in implementation of a test-bench, its automation techniques and application procedures. After an in-depth study of the state-of-art in GNSS software-based signal simulators, showing that such simulators have evolved through three distinct generations, a further study was conducted on multi-frequency, multi-system GNSS receiver performance testing and its necessary simulator architectures. Based on this study, a GNSS signal simulator in software capable of producing GPS L1 and Galileo E1 B/C signals was implemented.

Another contribution of this thesis is a bandpass-sampling based sampled data generator capable of processing multiple GNSS frequencies. Implementation of the constituent LNA is covered in detail. The design, simulation, implementation and test results prove that the LNA successfully satisfied requirements of wide bandwidth, high gain, high linearity, frequency stability and low noise figure and compares very well with the state-of-art in such amplifiers. The process for calculating the optimum sampling frequency and resultant intermediate frequencies for the bandpass-sampling ADC was automated for all possible input signal conditions. Both, real and complex sampling was addressed.

A third contribution of this research work is the automation in receiver testing through the implementation of the AutoPET and dCAP. These tools are portable (software platform-independent), easy to install and execute on any computer with the basic scientific software and enable highly efficient and accurate testing of GNSS receivers. From an academic point of view, the dCAP is useful for teaching the spectral characteristics of

GNSS signals at every stage from deep inside the receiver to researchers or university students in laboratory exercises. In other words, the proposed research has a practical as well as academic appeal.

As an application of the test bench, the effects of an FRO and a PLL phase noise on the tracking performance of a GNSS receiver were analyzed. A mathematical model for the PLL PN incorporating the PN contributions from its constituent sub-blocks was implemented and validated using Matlab and Simulink based GPS and Galileo correlators. The relation between integration time, PLL parameters and phase noise has been shown, and a criterion for radio front-end frequency generator design has been presented.

8.2 Future Work

In the duration of this research work, some ideas, concepts and implementation paths were left to be resolved in the future due to time and task prioritization. It is hoped that the receiver testing and the GNSS research community in general would be interested in following-up on the leads that this thesis has provided.

A number of challenges in the implementation of the sampled data generator have yet to be fully addressed. As an example, SNR degradation due to jitter, noise aliasing, quantization and high power consumption leading to ADC thermal issues have yet to be quantified and can be a subject of further research along with possible solutions to mitigate their effects. The PLL phase noise model in Matlab can be integrated with the software-based GNSS signal simulator as an additional source of receiver error. It can also be converted into a physical device using programmable hardware logic and VHDL coding. This physical PLL (P-PLL) can then be integrated with a VHDL-based GNSS signal simulator and their combined signals can be studied using the TUTGNSS prototype. With regards to the automated test-bench, there is a need for further study on the testing procedures employed for receivers used in more diverse applications of satellite-based positioning receivers, e.g., military, indoor navigation and high-accuracy positioning. These test cases can be added to the library of the AutoPET and dCAP tools, thus expanding their application areas.

BIBLIOGRAPHY

[1] T. Paakki, J. Raasakka, F. Della Rosa, H. Hurskainen, J. Nurmi, TUTGNSS University based hardware/software GNSS receiver for research purposes, Proceedings of the 2010 Ubiquitous Positioning Indoor Navigation and Location Based Service (UPINLBS 2010), vol. 1, no. 6, pp. 14-15, Oct. 2010.

[2] U. Weinbach, S. Schön, "GNSS receiver clock modeling when using high-precision oscillators and its impact on PPP", Journal on Advances in Space Research, January 2011, Volume 47 Issue 2, pp 229-238.

[3] D. W. Allan, "Statistics of Atomic Frequency Standard", Proceedings of the IEEE, Vol 54, No. 2, Feb 1966, pp. 221–230.

[4] W. Stockwell, "Bias Stability Measurement: Allan Variance", Crossbow Technology Inc. Available at: http://www.xbow.com/pdf/Bias_Stability_Measurement.pdf.

[5] NASA Goddard Space Flight Center, "GNSS Data Sets", Crustal Dynamics Data Information System (CDDIS). Available at: http://cddis.nasa.gov/gnss_datasum.html.

[6] "EU-U.S. Cooperation on Satellite Navigation", Working Group C, ARAIM Technical Subgroup, Interim Report, Issue 1.0, December 19th, 2012.

[7] Federal Aviation Administration, "Phase II of the GNSS Evolutionary Architecture Study", February 2010. Available at: http://www.faa.gov/about/office_org/headquarters_offices/ato/service_units/techops/navservices/gnss/library/documents/media/GEASPhaseII_Final.pdf

[8] A. M. A. Farah, "GPS/Galileo simulation for reduced dynamic LEO satellite orbit determination", University of Nottingham PhD Thesis 2004, UK.

[9] Jet Propulsion Laboratory, California Institute of Technology, "Global Ionospheric (TEC) Maps". Available at: http://www.gdgps.net/products/tec-maps.html.

[10] Magellan Professional, "Manually Downloading US National Geodetic Survey CORS data", January 2007. Available at: ftp://ftp.ashtech.com/Mobile%20Mapping/MobileMapper%20Office%20for%20MMCX%20&%20MMPro/Application%20Notes/Manually%20downloading%20US%20NGS%20CORS%20data.pdf.

[11] Y. Memarzadeh, "Ionospheric Modeling for Precise GNSS Applications", Delft University of Technology Ph.D. Thesis, the Netherlands, December 2009. Available at: http://www.ncg.knaw.nl/Publicaties/Geodesy/pdf/71Memarzadeh.pdf.

[12] A. Dolgansky, A. Szeto and S. Bisnath "Software Simulation Of Multiple Global Navigation Satellite System Measurements", Proceedings of the IEEE Toronto International Conference – Science and Technology for Humanity 2009 (TIC-STH 2009), September 2009, Toronto, Canada.

[13] S. Pullen, J. Rife, "Differential GNSS: Accuracy and Integrity", from the book GNSS Applications and Methods, (Eds.) S. Gleason, D. Gebre-Egziabher, Artech House, 2009, ISBN-13: 978-1-59693-329-3.

[14] F. van Diggelen, "A-GPS: Assisted GPS, GNSS, and SBAS", Edition 1, March 2009, ISBN- 10: 1596933747, ISBN-13: 978-1596933743.

[15] Fernández, J. Diez, A. Caramagno, "GRANADA-Galileo Receiver Analysis and Design Application", ESA-GJU Workshop on Tools and Facilities for Galileo Receivers, March 2006.

[16] B. Shen, Q. Zhang, "A New Method for Analyzing the Quantization Effect of ADC in Broadband QAM Receiver", Proceedings of the 2002 IEEE International

Conference on Communications, Circuits and Systems and West Sino Expositions, June 2002, pp 1262-1266.

[17] 3rd Generation Partnership Project (3GPP); 'TS34.171'; Technical Specification, V6.5.0 (2006-10).

[18] A. Mitelman, P. Nomark, M. Reidevall, S. Strickland, "Apples to Apples - Standardized Testing for High-Sensitivity Receivers", GPS World, January 1, 2008.

[19] Spirent Communications, "Testing GNSS System Errors", Application Note: DAN002, Issue 1-01.

[20] Spirent Communications, "Fundamental GNSS Receiver Characterisation", Application Note DAN003, Issue 1-01.

[21] Agilent Technologies, "Typical GPS Receiver Verification Tests Using a GPS Signal Simulator", Application Note, May 2008.

[25] Spirent Communications, "Simulation versus Real World Testing - How to undertake controlled testing of your GNSS receiver design". Available at: http://www.insidegnss.com/special/elib/Spirent_Simulation_vs_Real_World_Testing.pdf.

[26] National Instruments, "The Case for GPS Simulation". Available at: http://www.insidegnss.com/special/elib/NI_GPS_Simulation.pdf.

[27] Alliance for Telecommunications Industry Solutions, ATIS Telecom Glossary 2007 (Updated version of Federal Standard 1037C). Available at: http://www.atis.org/glossary/.

[28] T. H. Hee, A. Hajimiri, "Oscillator Phase Noise: A Tutorial" IEEE Journal on Solid-State Circuits, March 2000, vol. 35, no. 3, pp. 326-336.

[29] P. Misra, P. Enge, "Global Positioning System: Signals, Measurements, and Performance", Second Edition, 2006, ISBN: 0-9709544-1-7.

[30] B. Parkinson, J. Spilker (Editors), "Global Positioning System: Theory and Applications", Volume 1, ISBN: 1-56347-106-X.

[31] E. Kaplan, C. Hegarty (Editors), “Understanding GPS: Principles and Applications”, Second Edition, ISBN-10: 1-58053-894-0.

[32] R. Giffard, “Estimation of GPS Ionospheric Delay Using L1 Code and Carrier Phase Observables”, Proceedings of the 31st Annual Precise Time and Time Interval (PTTI) Planning Meeting, 7-9 December 1999, Dana Point, CA.

[33] Kowoma.de, “The GPS System: Sources of Errors in GPS”, November 2013. Available at: http://www.kowoma.de/en/gps/errors.htm.

[34] Navstar GPS, “Navstar GPS User Equipment Introduction”, September 1996. Available at: http://www.navcen.uscg.gov/pubs/gps/gpsuser/gpsuser.pdf.

[35] J. Mendizabal S. J. M. Lagunilla, R. B. Perez, “GPS and Galileo: Dual RF Front-end Receiver and Design, Fabrication, and Test”, McGraw Hill 2009, ISBN 978-0-07-159869-9.

[36] Aerospace Corporation, “How GPS Works, GPS Primer”. Available at: http://www.aero.org/education/primers/gps/howgpsworks.html

[37] R. B. Langley, “Why is the GPS signal so complex?”, GPS World, May/June 1990.

[38] Navstar GPS, “Global Positioning System Standard Positioning Service Signal Specification”, Second Edition, 2nd June, 1995.

[39] Navstar GPS, “Global Positioning System Interface Control Document, IS-GPS-200G”, 5th September, 2012.

[40] European Commission, “Galileo Open Service, Signal in Space Interface Control Document, (OS SIS ICD)”, Draft 1.1, September 2010.

[41] “Global Navigation Satellite System (GLONASS), Interface Control Document”, Edition 5.1, Coordination Scientific Information Center, Moscow, 2008.

[42] China Satellite Navigation Office, "BeiDou Navigation Satellite System, Signal in Space Interface Control Document, Open Service Signal B1I", Version 1.0, December 2012.

[43] S. Wallner, European Space Agency (ESA), Navipedia, “GNSS Signal”, November, 2013. Available at: http://www.navipedia.net/index.php/GNSS_signal.

[44] H. Hurskainen, T. Paakki, Z. Liu, J. Raasakka, J. Nurmi, “GNSS Receiver Reference Design”, in Proceedings of 4th Advanced Satellite Mobile Systems (ASMS) conference 2008, Aug 26-28, 2008, Bologna, Italy, Pages: 204-209.

[45] ESA Navipedia, “Tracking Loops”, Available at: http://www.navipedia.net/index.php/Tracking_Loops.

[46] V. G Dikshit, “Development of Global Navigation Satellite System (GNSS) Receiver”, DRDO-IISc. Program on Mathematical Engineering Workshop, Bangalore, September 2007. Available at: http://pal.ece.iisc.ernet.in/PAM/work07.html.

[47] M. S. Braasch, A. J. Van Dierendonck, “GPS Receiver Architectures And Measurements”, Invited paper, Proceedings of the IEEE, Vol. 87, No. 1, January 1999.

[48] M. Cummings, T. Cooklev, “Software Defined Radio (SDR) Technologies”, Tutorial, International Symposium on System-On-Chip (SoC 2008), Tampere, 2008.

[49] SDR Forum, “What is Software Defined Radio?”. Available at: http://www.sdrforum.org/pages/aboutSdrTech/SoftwareDefinedRadio.pdf

[50] V. Dvorkin, J. Wong, M. Zou, “Quad Demodulators Arm Direct-Conversion Receivers”, Microwaves and RF, Feb 2004. Available at: http://mwrf.com/Articles/ArticleID/7470/7470.html

[51] U. Mavric, "Digitizer Provides Direct Sampling Of RF Signals: Employing a simple RF signal chain, many potential limiting factors can be eliminated when directly sampling RF signals with high-speed analog-to-digital converters (ADCs)", Microwaves and RF, April 2006. Available at: http://mwrf.com/systems/digitizer-provides-direct-sampling-rf-signals

[52] Trimble, Datasheet for Zephyr and Zephyr Geodetic GNSS antennas, 2007. Available at: http://www.navtechgps.com/assets/1/7/Zephyr_DS.pdf

[53] Roke Manor Research/Siemens, Datasheet for Triple GNSS Geodetic-grade Antenna, 2006. Available at: http://www.roke.co.uk/resources/datasheets/042-gnss-antenna.pdf

[54] J. Wang, D. Triplett (Wang Electro-Opto Corporation), "High-Performance Universal GNSS Antenna Based on SMM Antenna Technology", Proceedings of the IEEE 2007 International Symposium on Microwave Antenna Propagation and EMC Technologies for Wireless Communications, August 2007.

[55] H. T. Friis, "Noise figures of radio receivers", Proceedings of I.R.E, July 1944.

[56] L. E. Larson, "RF and Microwave Circuit Design for Wireless Communications", Artech House 1996, ISBN 0890068186.

[57] C. Chien, "Digital Radio Systems on a Chip - A Systems Approach", First Edition, Springer 2001, ISBN 0792372603.

[58] Jie-Cherng Liu, "Bandpass Sampling of Multiple Single Sideband RF Signals", Proceedings of the 2008 International Symposium on Communications, Control, and Signal Processing (ISCCSP 2008), Malta, 12-14 March 2008.

[59] Ching-Hsiang Tseng, Sun-Chung Chou, "Direct Downconversion of Multiband RF Signals Using Bandpass Sampling", IEEE Transactions on Wireless Communications, Vol. 5, No. 1, January 2006.

[60] Yi-Ran Sun, "Generalized Bandpass Sampling Receivers for Software Defined Radio", PhD Thesis, Royal Institute of Technology, Stockholm 2006.

[61] M. L. Psiaki, D. M. Akos, J. Thor, "A Comparison of "Direct RF Sampling and Down-Convert & Sampling GNSS Receiver Architectures", Proceedings of the 2003 ION GPS/GNSS, 9-12 September 2003, USA.

[62] D. M. Akos, M. Stockmaster, J. B. Y. Tsui, J. Caschera, "Direct Bandpass Sampling of Multiple Distinct RF Signals", IEEE Transactions on Communications, Vol. 47, No. 7, July 1999.

[63] R. G. Vaughan, N. L. Scott, D. R. White, "The Theory of Bandpass Sampling", IEEE Transactions on Signal Processing. Vol. 39, No. 9. September 1991.

[64] M. Psiaki, S. Powell, H. Jung, P. Kintner, "Design and Practical Implementation of Multifrequency RF Front Ends Using Direct RF Sampling", IEEE Transactions on Microwave Theory & Techniques, Vol. 53, No. 10, October 2005.

[65] A. Latiri, L. Joet, P. Desgreys, P. Loumeau, "A Reconfigurable RF Sampling Receiver For Multistandard Applications", Académie Des Sciences, 2006.

[66] N. Wong, Tung-Sang Ng, "An Efficient Algorithm for Downconverting Multiple Bandpass Signals Using Bandpass Sampling", Proceedings of the IEEE International Conference on Communications (ICC), June 2001, Helsinki, Finland.

[67] M. Renfors, "Sampling and Multirate Techniques for Complex and Bandpass Signals", Lecture notes, Receiver architectures and signal processing, Tampere University of Technology.

[68] T. J. Rouphael, "RF and Digital Signal Processing for Software-Defined Radio - A Multi-standard multi-mode approach", Elsevier Inc. 2009, ISBN 978-0-7506-8210-7.

[69] N. Gray, "ABCs of ADCs – Analog to Digital converter Basics", National Semiconductor, June 2006. Available at: http://www.national.com/appinfo/adc/files/ABCs_of_ADCs.pdf

[70] Invocom, Complex Signals and Sampling, Sampling and Multirate Processing of Bandpass and Complex (I/Q) Signals (Lesson 1), Invocom Tutorials, TUT. Available at: bruce.cs.tut.fi/invocom/p3-2/p3-2_3_1.htm

[71] National Instruments, "Rational Resampling (Digital Filter Design Toolkit)", LabVIEW 8.6, Digital Filter Design Toolkit Help. Available at: http://zone.ni.com/reference/en-XX/help/371988B-01/lvdfdtconcepts/rational_resampling/

[72] P. M. Corbell, M. M. Miller, "Design and Analysis of a Matlab Based Digitized IF GPS Signal Simulator and a Simulink Based Configurable GPS Receiver", Proceedings of ION GPS 2000, 19-22 September 2000, Salt Lake City, UT.

[73] M. M. Miller, P. M. Corbell, J. F. Raquet, "Design and Validation of Digitized Intermediate Frequency GPS Signal and Receiver Software Models for Developing and Comparing Advanced GPS Receiver Technologies", Proceedings of ION GPS 2000, 19-22 September 2000, Salt Lake City, UT.

[74] A. Brown, N. Gerein, K. Taylor, "Modeling and Simulation of GPS Using Software Signal Generation and Digital signal Reconstruction", Proceedings of the ION National Technical Meeting, January 2000, Anaheim, CA.

[75] A. Brown and N. Gerein, "Advanced GPS Hybrid Simulator Architecture", Proceedings of ION 57th Annual Meeting, Albuquerque, NM, June 2001.

[76] P. M. Corbell, M. M. Miller, "A Configurable GPS Accumulated I and Q Signal Component Simulator in Matlab", Proceeding of ION NTM 2001, 22-24 January 2001, Long Beach, CA.

[77] T. H. Tan, "Global Positioning System Signal Simulation", Bachelor of Electrical Engineering (Honours) Thesis, The University of Queensland, Australia, October 2003.

[78] L. Dong, "IF GPS Signal Simulator Development and Verification", Master of Science Thesis, University of Calgary, Canada, November 2003.

[79] A. Nunes, T. Ferreira, J. Borràs, F. Nunes, F. Sousa, G. Seco, "Signal Generator and Receiver Toolbox for Galileo/GPS Signals", Proceedings of 2nd ESA Workshop on Satellite Navigation, Navitech 2004.

[80] O. Julien, B. Zheng, L. Dong, G. Lachapelle, "A Complete Software-Based IF GNSS Signal Generator for Software Receiver Development", Proceedings of ION GNSS 2004, Sept. 21-24, Long Beach, CA.

[81] L. Dong, C. Ma, G. Lachapelle, "Implementation and Verification of a Software-Based IF GPS Signal Simulator", Proceedings of National Technical Meeting, Institute of Navigation, 26-28 January 2004, San Diego.

[82] C. Seynat, A. Kealy, K. Zhang, "A Performance Analysis of Future Global Navigation Satellite Systems", Journal of Global Positioning Systems (2004) Vol. 3, No. 1-2: 232-241.

[83] W. Kester, "Converting Oscillator Phase Noise to Time Jitter", Digi-Key Corporation, Techzone. Available at: http://www.digikey.com/us/en/techzone/wireless/resources/articles/converting-oscillator-phase-noise-to-time-jitter.html

[84] A. Pósfay, T. Pany, B. Eissfeller, "First Results of a GNSS Signal Generator Using a PC and a Digital-to-Analog Converter", Proceedings of ION GNSS 18th International Technical Meeting of the Satellite Division, 13-16 September 2005, Long Beach, CA.

[85] T. Inzerilli, D. Lo Forti, V. Suraci, "Modeling and Simulation of GNSS with NS2", Proceedings of 14th IST Mobile and Wireless Communications Summit, Dresden, June 2005.

[86] Accord Software & Systems Pvt. Ltd, "GPSLAB". Available at: http://www.gpslab.us/datasheet/DataSheet-prof.pdf

[87] A. Constantinescu, R.Jr. Landry, I. Ilie, "Hybrid GPS/Galileo/GLONASS IF Software Signal Generator", Proceedings of ION GNSS 18th International Technical Meeting of the Satellite Division, 13-16 September 2005, Long Beach, CA.

[88] NAVSYS Corporation, "GPS Signal Simulation Toolbox". Available at: http://www.navsys.com/brochures/NAVSYS_Toolbox.pdf

[89] C. Abart, P. Berglez, G. Abwerzger, B. Hoffmann-Wellenhof, W. Cresens, T. Vandeplas, W. De Win, "Simulating GNSS Constellations - The GAMMA Signal

Generator", Proceedings of the 20th International Technical Meeting of the Satellite Division of The Institute of Navigation (ION GNSS 2007), Fort Worth, TX.

[90] Intecs, "gLAB GNSS Signal Analysis Tool". Available at: http://www.intecs.it/pdf/brochure_gLAB_01-02-2010.pdf

[91] VEGA IT GmbH, "Galileo System Simulation Facility (GSSF)". Available at: http://www.gssf.eu/Documents/GSSF%20V2.1%20Fact%20Sheet%20-%20Issue%201.pdf

[92] K. Borre,"The E1 Galileo Signal", Lecture at Stanford University. Available at: http://waas.stanford.edu/~wwu/papers/gps/PDF/Borre/galileo_sig.pdf

[93] C. Hu, M. Tsai, "The Implementation of an INS-GNSS Software Simulator", Proceedings of 28th Asian conference on Remote Sensing (ACRS 2007), November 2007, Kuala Lumpur, Malaysia.

[94] I. Joo, J. Lee, S. Lee, J. Kim, D. Lim, S. J. Lee, "S/W based IF Signal Simulator Prototyping for L1 C/A, L2C, and E1(B/C)", Proceedings of The 9th International Conference on Information and Communications Security (ICICS 2007), December 2007, Zhengzhou, China.

[95] C. Cosenza, Q. Morante, S. Corvo, F. Gottifredi, "GNSS Bit-True Signal Simulator-A Test Bed for Receivers and Applications", Satellite Communications and Navigation Systems, Signals and Communication Technology, 2008, 3, 447-460, DOI: 10.1007/978-0-387-47524-0_34.

[96] F. Schubert, R. Prieto-Cerdeira, A. Steingass, "GNSS Software Simulation System for Realistic High-Multipath Environments", Proceedings of 4th ESA Workshop on Satellite Navigation User Equipment Technologies (NAVITEC 2008), December 2008, Noordwijk, The Netherlands.

[97] J. Lee, T. Kim, S. Lee, J. Kim, "Development of Software GNSS Signal Generator", Proceedings of International Symposium on GPS/GNSS 2008, November 2008, Tokyo, Japan.

[98] S. Lim, D. Lim, M. Liu, S. W. Moon, C. Park, S. J. Lee, "Design of a Software-based Multi-Channel GNSS IF Signal Generator", Proceedings of International Conference on Control, Automation and Systems 2008, October 2008 in Seoul, Korea.

[99] German Aerospace Center (DLR), "Simulation of Satellite Navigation Signals and Channels (SNACKS)". Available at: http://snacs.sourceforge.net/index.html

[100] Fraunhofer Institute for Integrated Circuits IIS, "GNSS-SIGNAL-SIMULATOR". Available at: http://www.iis.fraunhofer.de/fhg/Images/07_GNSS-Signal_Simulator_neu_tcm278-158408.pdf

[101] TeleConsult Austria GmbH, "GNSS Multisystem Performance Simulation Environment (GIPSIE)". Available at: http://www.teleconsult-austria.at/download_public/GIPSIE.pdf

[102] Center for Remote Sensing Inc., "Software GNSS Signal Simulator". Available at: http://www.cfrsi.com/pdf/Software%20GNSS%20Signal%20Simulator.pdf

[103] Z. Y. Kou, Y. Huang, Z. Z. Qishan, "Architecture of software-based GNSS signal simulator and implementation of its IF signals generation", Journal of Beijing University of Aeronautics and Astronautics (2009-07), Available: http://en.cnki.com.cn/Article_en/CJFDTOTAL-BJHK200907004.htm

[104] C. Ouzeau, J. Korsakissok, "Performance Assessment of a Juzzle-Based GNSS Simulator", Proceedings of ENC GNSS 2009, May 2009, Naples, Italy.

[105] A. M. Smith, "Global Navigation Satellite System Signal Simulator - An Analysis of the Effects of the Local Environment and Atmosphere on Receiver Positioning", Doctor of Philosophy Thesis, University of Bath, UK, October 2007.

[106] University FAF Munich, "GNSS Software Simulation". Available at: http://www.ifen.unibw.de/research/gnss_simulator.htm

[107] Fernández, J. Diez, A. Caramagno, "GRANADA-Galileo Receiver Analysis and Design Application", ESA-GJU Workshop on Tools and Facilities for Galileo Receivers, March 2006.

[108] A. Dolgansky, A. Szeto and S. Bisnath “Software Simulation Of Multiple Global Navigation Satellite System Measurements”, proceedings of the IEEE Toronto International Conference – Science and Technology for Humanity 2009 (TIC-STH 2009) in Toronto Canada.

[109] L. Marradi, G. Franzoni et. al, “The GARDA Project – Building a Galileo Receiver”, InsideGNSS, November/December 2006, pp 40-53

[110] D. Boschen, “GPS C/A Code Generator”, Matlab Central, Jun 2010. Available at: http://www.mathworks.com/matlabcentral/fileexchange/14670-gps-ca-code-generator&watching=14670.

[111] Finland Publication Forum, Julkaisufoorumi. Available at: http://www.tsv.fi/julkaisufoorumi/

[112] P. C. Chang, H. M. Peng, S. Y. Lin, "Allan Variance Estimated by Phase Noise Measurements", 36th Annual Precise Time and Time Interval (PTTI) Systems and Applications Meeting, Washington DC on 7-9 Dec 2004.

[113] Wenzel Associates, Inc., "Spreadsheets/Programs", Available at: http://www.wenzel.com/documents/spread.htm

[114] F. Ramian, "Time Domain Oscillator Stability Measurement Allan Variance", Application Note, Rhode&Schwarz, Feb 2012.

[115] R. El Assir, "Global Navigation Satellite Systems and Their Applications", Microwave Journal, Vol. 55, No. 5, pp. 142-152, May 14, 2012.

[116] J. Nurmi, S. Lohan, S. Sand, H. Hurskainen, (Eds.), "GALILEO Positioning Technology", Signals and Communication Technology Series, Vol. 182, ISBN 978-94-007-1829-6.

[117] V. Syrjala, M. Valkama, M. Renfors, "Design considerations for direct RF sampling receiver in GNSS environment", proceedings of the 5th Workshop on Positioning, Navigation and Communication, 2008 (WPNC 2008), March 2008, Hannover Germany.

PUBLICATIONS

PUBLICATION 1

S. Thombre, E. S. Lohan, J. Raquet, H. Hurskainen, J. Nurmi, "Software-based GNSS Signal Simulators: Past, Present and Possible Future", Proceedings of the *2010 European Navigation Conference (ENC GNSS 2010)*, October 2010 in Braunschweig, Germany.

Software-Based GNSS Signal Simulators - Past, Present and Possible Future

Sarang Thombre[1], Elena Simona Lohan[2], Heikki Hurskainen[1], John F. Raquet[3], Jari Nurmi[1]
[1]Department of Computer Systems, Tampere University of Technology (TUT)
[2]Department of Communications Engineering, TUT
[3]Air Force Institute of Technology (AFIT), USA
{sarang.thombre, elena-simona.lohan, heikki.hurskainen, jari.nurmi}@tut.fi, john.raquet@afit.edu
P.O.Box 553, FI-33101 Tampere
Phone: +358 3 3115 3872, Fax: +358 3 3115 4561

***Abstract*— Software-based Global Navigation Satellite System (GNSS) signal simulators are essential in supporting education, research, and also development of advanced receivers. This paper presents a detailed literature study of state-of-the-art in such simulators. Thirty-six references (both commercial and academic) have been compared based on features including, but not limited to, the number of GNSS satellite constellations and signals modeled, the strategy of error modeling, the programming language used, the input and output data formats, and the modeling of the radio frequency front-end (RF FE) effects. Overall, it is observed that software-based generation of GNSS signals still has considerable potential for innovation especially through the use of C Sharp (C#) programming language and in the generation of Russian GLONASS signals. The next part of the paper describes the first results from the development of GNSS Signal Simulator in Software (TUTGSSS) at our university. This simulator is a Matlab, Simulink and C++ based Global Positioning System (GPS) L1 and Galileo E1 B/C signal simulator. Already incorporated into the TUTGSSS are the scenarios of step-wise increase and decrease of output power and Carrier to Noise Ratio (CNR), that were lacking in the state-of-the-art.**

Keywords-GNSS, software-based, simulator, receiver, literature study, test cases, pedestrian navigation

I. INTRODUCTION

Future GNSS signals are usually announced to the public before satellites begin transmitting them from the sky. This enables the users to be already equipped with compatible receivers by the time the signals are actually 'turned on live' from satellites. However, the major concern for manufacturers of such innovative-GNSS-signal-compatible receivers is their testing. How do you test whether a receiver is compatible to presently non-existent signals? One possible solution is to create replicas of those signals artificially in laboratories and to test the receivers with them. Devices that locally create such signals are called Simulators or Generators. If the receiver works fine under such 'simulated conditions' (which includes simulated signals and simulated environment) then it is safe to assume that they will work equally satisfactorily under real-life situations. The trick here is to make the simulated conditions as close to reality as possible. For example, if a receiver is intended to be stationed in a dense multipath environment in real-life, while testing in laboratory, the simulated signals should also contain high number of powerful multipath components. If not, the performance of the receiver will be unreliable when used in real-life. In addition to their application as a testing tool, simulators can be useful for education and research by gaining knowledge of the signal characteristics. This may also help in locating vulnerabilities in the signals and in designing suitable encryption or snooping technologies.

Such simulators for GNSS signals are already in existence and are of two types: hardware-based simulators and software-based simulators. Hardware-based simulators are physical devices containing an actual radio frequency transmitter chain generating physical signals at the output. Such simulators are often bulky and costly. Software-based simulators are built using software programming languages such as Matlab, Simulink, C, C++, etc. They output virtual signals in order to test receivers also designed using similar software. This study deals solely with software-based GNSS simulators and hence hardware-based simulators are not considered henceforth.

A brief outline of the paper is as follows: Section II deals with the study of already existent software-based simulators for GNSS signals. Thirty-six reference sources have been compared based on their features and functionality. These sources have been grouped into three categories or generations based on their year of publication: Generation 1 (2000 to 2003), Generation 2 (2004 to 2005) and Generation 3 (2006 onwards). The results show distinct patterns of evolution from one generation to the next and special features or trends in every generation are discussed.

Section III describes the first results from the development of GNSS Signal Simulator in Software (TUTGSSS) at our university. This simulator is a Matlab, Simulink and C++ based GPS L1 and Galileo E1 B/C signal simulator. The simulated signals have been verified using software receivers for GPS L1 and Galileo E1 generated in our university. Results are also described for the test scenarios related to sensitivity testing under conditions of increasing and decreasing signal power from satellite and noise interference.

II. LITERATURE REVIEW OF SOFTWARE-BASED GNSS SIGNAL SIMULATORS

Software-based signal simulators for GNSS are a relatively recent invention: pioneered in 1999-2000. After a considerable online survey, we have located thirty-six reference sources (both academic and commercial) from the last 10 years of their existence. However, it is possible that this may not be a completely exhaustive list and since such simulators are being designed and built with increasing frequency in the recent years, some new results may still enter the public domain by the time this paper is published. To place such a considerable number of similar devices in perspective, we have categorized these sources into three groups or generations, based on their year of publication. Generation I (2000 to 2003) sources are [1] to [7], Generation II (2004 to 2005) sources are [8] to [17] while Generation III (2006 to 2010) sources are [18] to [36]. Due to the considerable number of sources, comparison between them was done based on five factors only: GNSS signals simulated, used software platform, error sources modeling, space segment modeling and others. 'Others', includes any special or unique feature present in a particular reference, which would be worth mentioning. The comparison is presented in textual format (instead of tabular) because documents for the sources did not always contain all the required information. As a rule, almost all simulators (even the latest ones) upconvert the baseband GNSS signals to an Intermediate Frequency (IF) and not to the actual carrier frequencies since GHz range sampled signal generation is not yet possible with the current software platforms.

A. *GNSS signals simulated*

GPS was the first fully operational GNSS and hence the first generation simulators could simulate only GPS signals and that too only GPS L1. C/A codes for all satellite vehicles could be generated easily; however, P code could be generated only by [3], [4] and [5]. [4] could even generate M code at GPS L1. [5] also generated GPS L2 signals. Because they did not have the capability to generate actual navigation data, nor to read downloaded navigation files in Receiver Independent Exchange (RINEX) format, all simulators in Generation I used random bits to denote navigation data.

By the time of Generation II, details had been emerging about Galileo signal characteristics and also of the newer GPS signals. Hence, it is observed that in Generation II, the signals simulated had become more diverse, for example, GPS L1, L2, and L5, Galileo E1, and E5 were available. Notable exceptions are: [8] which could simulate also Galileo E6, while [16] has information about SBAS signal generation.

In Generation III, the signals became ever more diverse. All GPS (L1, L2, L5) and Galileo (E1, E5, E6) signals could be generated. In comparison to Generation II, many could simulate EGNOS signals as well. [22] could generate inertial measurement (IM) data while [30] and [31] could generate GLONASS (L1) data as well. [31] could generate also WAAS and pseudolite signals. The ability of these simulators to read navigation data from RINEX files is covered under the 'Others' topic, later in the paper.

B. *Software Platform*

The underlying software in which the simulators have been coded has also undergone an evolution from one generation to the next. During the time of Generation 1, Matlab was popular for engineering simulations and due to its ease of usage, most simulators from this generation are coded in Matlab, although [6] and [7] also had a few modules of Simulink and C respectively. In Generation II, C was more widely used, but always in addition with Matlab. Some of the simulators were later upgraded and were completely coded in C++. As an exception, [14] used Network Simulator 2 (NS2) coding while in [15] the simulator was encoded in FPGA in the final stage. In Generation III, most of the simulators were encoded using C++, owing to its greater object oriented programming capability. This probably enabled more resource efficient coding, faster generation and processing of data samples and greater modularity for increased flexibility. [10] and [14] used a graphical user interface (GUI) coded using Microsoft foundation class libraries (MFC). [33] used the Juzzle software platform for coding the simulator. Juzzle is a combination of Java and Puzzle platform and also contains traces of C, Matlab, FORTRAN, Ada, SystemC and Ptolemy. It has been observed that although C# has better memory management and more object oriented programming capability along with Microsoft (MS) .Net support for GUI [37], it has not yet been used for simulator design. Only [20] is

coded in MS .Net with some modules of C++ and C# and is compatible with Windows 2000 and Windows XP.

C. *Modelling of Error sources*

As mentioned in Section I, simulating the environment is just as essential as simulating the actual signals. In reality, the actual signals are always affected by various error sources during their travel from the satellite to the receiver and also inside both of them. Therefore, the more error sources simulated, the closer the output signal is to reality. In Generation I, many of the sources did not have error modeling, or used typical values or constants for describing the various error sources, for example, [1] used the values given in Spilker's clock error model. However, [3] and [4] could simulate jamming signal environment by creating Frequency Modulated (FM), Amplitude Modulated (AM), Phase Modulated (PM) and frequency swept jamming signals at L1 frequency. [7] had a fairly advanced error modeling scheme with satellite clock, ionosphere, troposphere and Doppler errors modeled. Ionosphere delay error was modeled by Spherical Harmonics (SH) and Grid model using Global Ionospheric Maps (GIM) of Total Electron Content (TEC). Troposheric error was simulated using the Hopfield model extended by the Black and Eisner model. It also generated additive white gaussian noise (AWGN) bandlimited to 2MHz.

Starting from Generation II, Multipath was considered the dominant error source and hence almost every simulator modeled it. [8] can simulate 7 multipath channels, each with a different amplitude, delay and phase using Rayleigh or Rice multipath fading models. [9] divides multipath error into Near and Far echoes. Near echoes are simulated using Brenner and Jahn models considering 500 small reflectors randomly located in a 100m radius circle around the receiver antenna. Far echo is modeled considering specular reflections. It assumes a smooth ground and uses Snell's laws of reflection. Effects of reflections, fading and blocking are calculated using an algorithm designed by their own researchers. On the other hand, [11] used an empirical model created by observation of multipath errors at a given location over time and then finding a definite pattern. It is able to model a low, medium and strong multipath environment.

Calculation of Ionosphere and Troposphere errors also becomes more complex (and hence more realistic) in Generation II. In [10], ionosphere error is 'constructed' from correction parameters extracted from RINEX files downloaded from the Crustal Dynamics Data Information Systems (CDDIS) website. In [11] and [14] ionospheric error is calculated from TEC obtained from the global NeQuick model or using vTEC from the more local Ionospheric Exchange (IONEX) files available from the internet and using the Appleton and Hartree model. While in [16], the Klobuchar model is used for Ionosphere delay modeling. For the troposphere delay modeling, [10], [11], [14] and [16] use the Hopfield model, usually aided by the Black and Eisner model. [14] also suggests other possible models for calculating the tropospheric error. Usually, these models are also aided by climate data accessible in RINEX format from the internet.

Clock errors (satellite and receiver) were also modeled, for example, [9] used the Winkle model along with Allan Variance for satellite oscillator errors. The receiver clock error was modeled the same way, but considering lower quality oscillators, such as quartz or temperature controlled crystal oscillators (TCXO). In [10] satellite clock error was constructed from correction parameter given in the RINEX file downloaded from the CDDIS website. Other error modeled were Doppler, thermal noise, interference, front-end effects and power loss. In [11], all these other errors were combined into a single parameter – User Equivalent Range Error. This is especially useful when the simulation is conducted over longer intervals or larger geographical areas.

In Generation III, some new error sources were modeled in addition to those inherited from the previous generations. New sources included for example, interference signal generation: continuous wave, pulsed, wideband, narrowband, air traffic control signals, tactical air navigation (TACAN) signals and distance measuring equipment signals (DME) were simulated. Different models for receiver clock errors are mentioned in [24]. This paper also proposes that the best model to calculate ionospheric error affecting GPS signals is the Klobuchar model while the NeQuick model is best suited for Galileo signals. It uses the Saastamoinen model for calculating tropospheric error. In [34], the ionosphere error is modeled using the International Reference Ionosphere Model (IRI) and then it is converted into scintillation and finally timing delay using the Wide Band model (WBMOD). For multipath, in Generation III, the models of the environment improved drastically, with even minute details being added and in some cases 3-dimensional (3D) models being created. In [25] the authors created an extensive urban multipath model using empirical means while in [33] Rice and Rayleigh distribution models were used. In [34] Ray Shooting algorithm was used to replicate the local multipath environment very close to reality. This algorithm is based on studying and recreating the local environment around the receiver and then

estimating the different multipath sources in this environment. It then generates the reflected signal vectors for every source of multipath. This algorithm is also used to create a Doppler profile for this simulator. A similar approach was adopted in [35] where 3D models of urban area and surrounding terrain were created for future receiver sites and then possible multipath sources were identified from these models.

D. *Space Segment Modelling*

This part deals with how satellite constellations have been developed for the simulators. This also includes information on satellite trajectory modeling and also receiver dynamics modeling. In Generation I, many simulators performed approximate modeling of satellite trajectories using spline smooth fitting or using user input of raw geometric parameters to create satellite dynamics data, for example in [1], [2] and [4]. [4] could also read GPS almanac and ephemeris files to recreate satellite position and dynamics as a function of time, same as in [3] and [5]. For user trajectory generation, [4] accepts set of user inputs of co-ordinates (latitude, longitude, altitude and time) and reconstructs user route.

In Generation II, simulators had the capability to read ephemeris files (usually in RINEX format) to construct entire constellation of satellites, for example in [9], [10], [13], [16], and [17]. The simulator in [13] can even read the research institute's own geometry file. It can even read the YUMA almanac files in case of GPS and use the Walker constellation parameters to simulate the Galileo space segment. The simulator in [11] can also read YUMA files and ephemeris files in SP3 format. It can also use Keplerian orbital parameters to calculate satellite co-ordinates as a function of time. The simulators in [12] and [15] can simulate Low Earth Orbit (LEO) satellite constellations and a comparison is made on signal quality using GPS only, GPS-Galileo and GPS Modernized-Galileo constellations. The simulator in [16] is also unique because it is the only simulator which proposes to simulate GLONASS constellation. It uses information from Right Ascension of Ascending Node (RAAN) and mean anomaly for this purpose. User trajectories include static and dynamic scenarios using user input of set of co-ordinates. Typical shapes of user trajectories are along straight line or circle with constant linear or angular velocity. Examples are [9], [10], [11], and [13]. Notable exceptions are [15], where complete 3D dynamics of user vehicle are simulated using user input of acceleration, direction and altitude information, and [16] which can simulate user trajectory from user inputs, Microsoft Flight Simulator software or X-Plane software.

In Generation III, major advancement was in the ability to read data in any of the co-ordinate systems (for example, WGS-84, ECEF etc) and to convert from one system to another. Also, a greater percentage of simulators (as compared to Generation I and II) has the capability to simulate complete satellite constellations and dynamics of multiple navigation systems. Methods employed are reading ephemeris files in RINEX or SP3 format, almanac files in YUMA format or using Keplerian elements. Satellite positions, their tracks, azimuth and elevation and velocity are computed as a function of time. At any given time, a complete list of visible satellites can be easily produced. In [35], weather data is combined with satellite orbit data to compute signal strengths from visible satellites.

E. *Other factors*

As mentioned before, this part will describe any features that are unique to any of the simulators or their generations. As a rule, almost all simulators have been validated using software GNSS receivers, usually developed at the same affiliation. In Generation I, [1], [2] and [3] use flight trajectory data to define receiver position. It is assumed that because data processing techniques were not as advanced, simulators were designed to store large amounts of data over longer simulation periods for example, in [3], [4] and [5]. In [5], another option is to generate 12 channel Early, Prompt and Late I/Q signal data using mathematical modeling of GPS. This allows more data to be generated over smaller simulation periods.

In Generation II, [8], [9], [10], [16] and [17] simulated radio frequency (RF) front-end effects, especially, analog to digital conversion (ADC) and quantization, filter, antenna gain etc. [8], [9], [10] and [13] allowed users to set the frequency plan (sampling frequency, intermediate frequency etc), simulation time, filter and ADC parameters etc. [11] also defined certain performance related figures of merit used in GNSS receivers. [8], [13], [15] and [16] had some form of graphical user interface (GUI) to interact with user. [13] is unique because it has the capability to convert virtual digital IF GNSS signals at its output into physical analog signals using a digital to analog converter. Similarly, [15] and [17] have capability to record simulated signals and replay them as scenarios later. One general limitation of this generation is the inability to handle data from different co-ordinate systems (for example, WGS-84, ECEF etc).

In Generation III, additional features offered by the simulators become so extensive and diverse that it is not possible to arrange them according to resources. It is best to list out the different features that include: steering software, indoor positioning

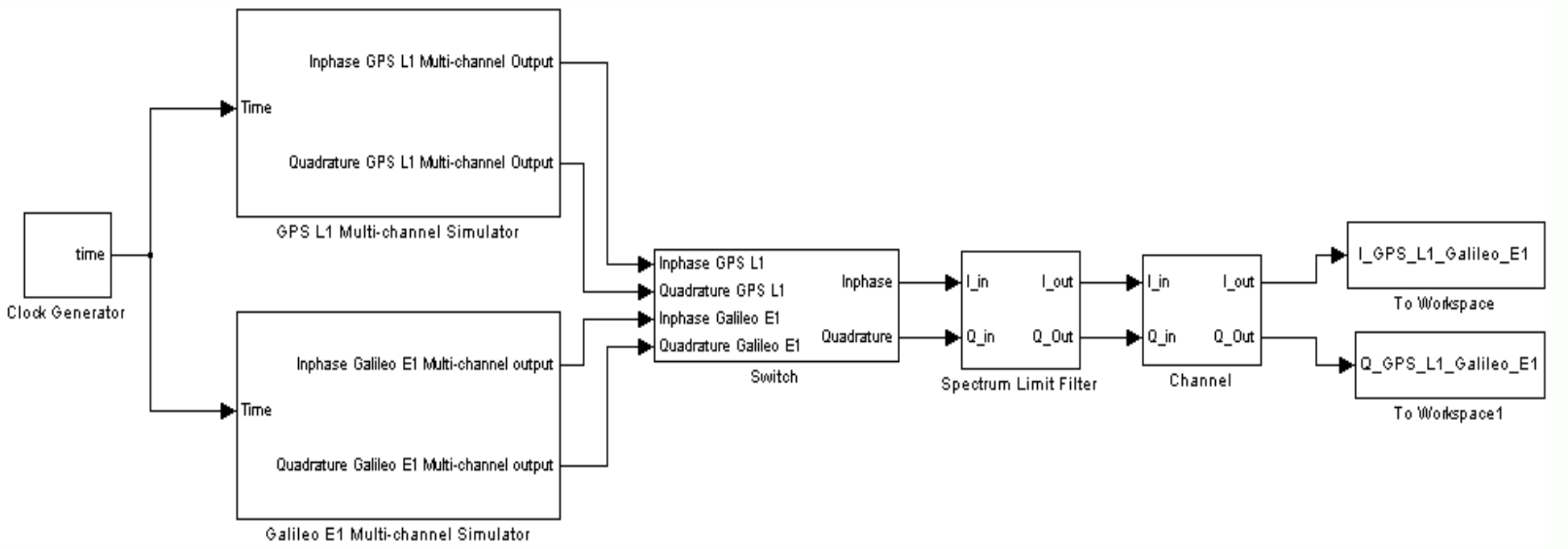

Figure 1. Block Diagram of the TUTGSSS

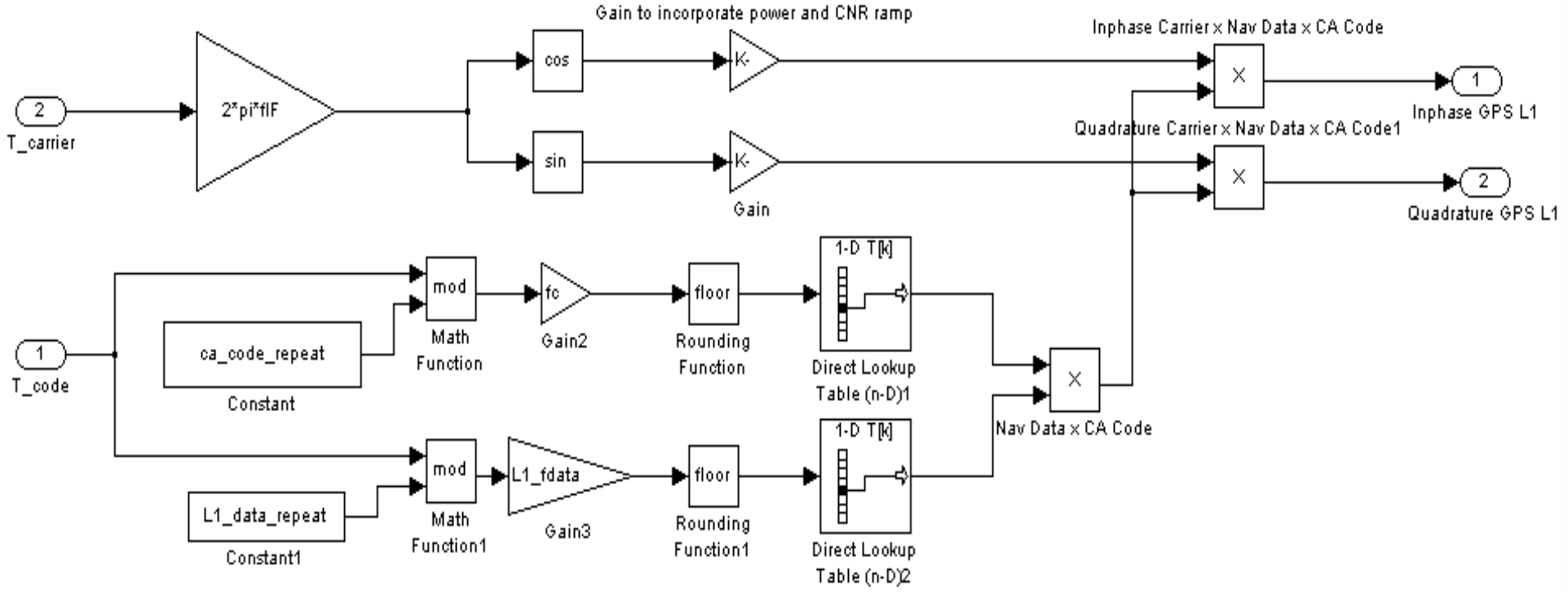

Figure 2. GPS L1 simulator module

capability, use of software defined radio (SDR) design principles, support for different RF FE architectures, flexible/user modifiable software platforms, support for 3D and contour maps, networking/multi-user capabilities (LAN, WAN) among others. Supported input data formats even include (Tropospheric Exchange) TROPEX files in addition to the usual IONEX and RINEX files. Data output can now be exported to files in different formats, for example log, binary and text formats. Real time processing capabilities are introduced with support for FPGA, VHDL, Windows, Linux etc. Correction terms are calculated for anomalies such as, orbit eccentricities in satellite trajectory or the Sagnac effect. GUI have become more advanced with not only a greater degree of freedom for the user to modify and redesign the software architecture of the simulators, but also access to inter-modular interfaces for easy testing and troubleshooting.

Table 1. Typical values of GNSS signal errors

Parameter	Typical Value
Receiver clock error	15nsec
Satellite clock error	10nsec
Ionosphere error	3m
Troposphere error	1.7m
Timing signal offset error	few nsec
Doppler frequency error	1000Hz

III. GNSS SIGNAL SIMULATOR IN SOFTWARE (TUTGSSS)

Using the information gathered during the literature review in Section I, we have begun building a Matlab-Simulink-C++ based dual-band (GPS L1, Galileo E1) GNSS simulator in software, called TUTGSSS. This section provides a brief explanation of the various blocks, features and certain assumptions for simplicity that make up the entire simulator. Preliminary results are also provided.

Figure 1 shows the overall block diagram of the TUTGSSS. Clock generator block generates the

Figure 3. Galileo E1 B/C simulator Module

time pulses at sampling frequency of 13 MHz. These time pulses are provided to the GPS L1 and Galileo E1 simulators. Currently for simplicity, only two channels each can be simulated for L1 and E1, which will be increased to 8 or 12 in future versions.

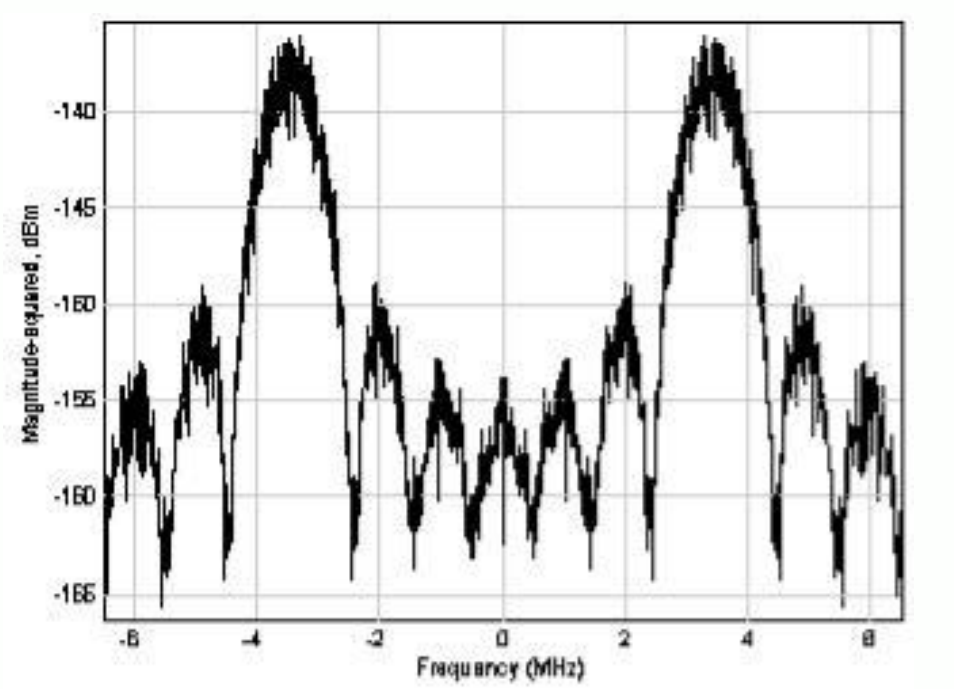

Figure 4. GPS Only - Before Filter

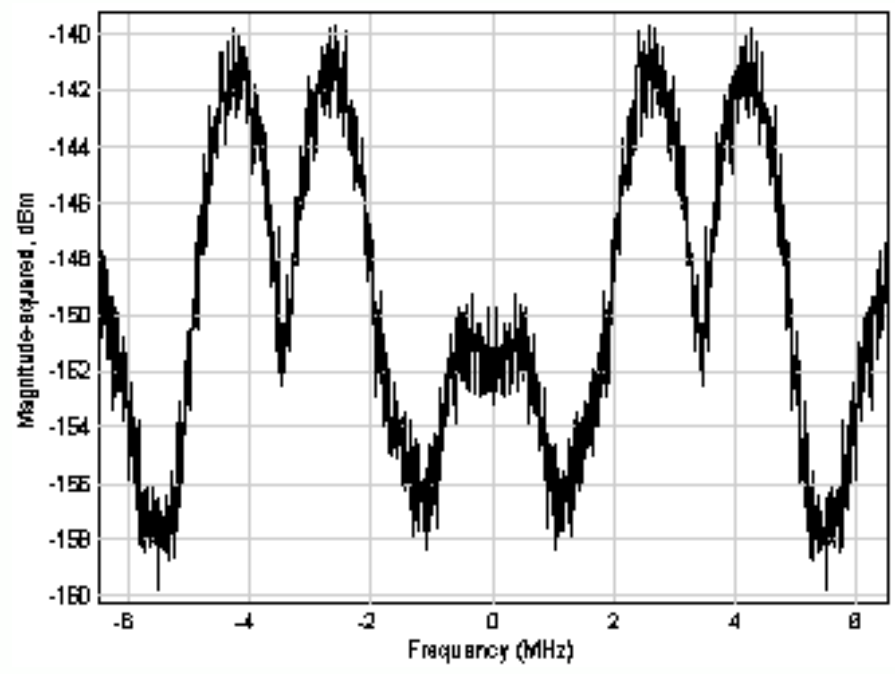

Figure 5. Galileo only - Before Filter

Each channel consists of a timing error block, where different error sources are simulated as disturbances in the timing pulses input to the actual signal simulator. The various error sources that can be simulated are: satellite vehicle clock error, doppler frequency error, tropospheric delay error, ionospheric delay error, other timing offset for the carrier and code time pulses and receiver clock error. All error sources can be independently programmed. If a single dual-band GPS L1 and Galileo E1 receiver is to be tested, the receiver clock error may be kept equal for all channels. For simplicity, all of these timing errors have been assigned their typical values as constants. They are mentioned in Table 1. The output of this block are two timing signals: ‘t_carrier’ and ‘t_code’ for the carrier and code respectively. Since this is the first version of TUTGSSS, we have yet to include any satellite orbital information or receiver trajectory and front-end effects. These features are planned under the upgrade to version 2 of TUTGSSS.

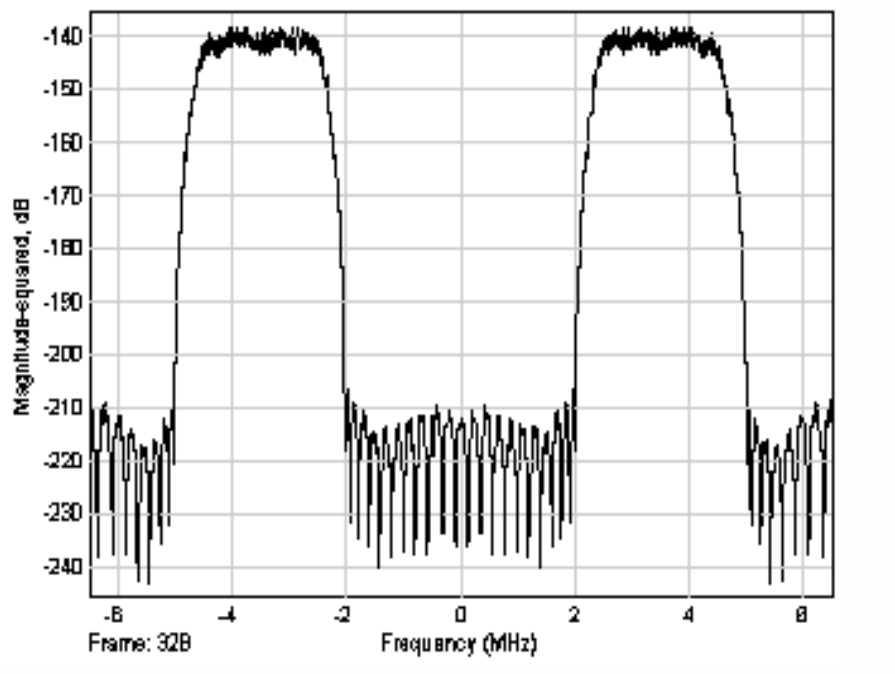

Figure 6. GPS + Galileo after filter

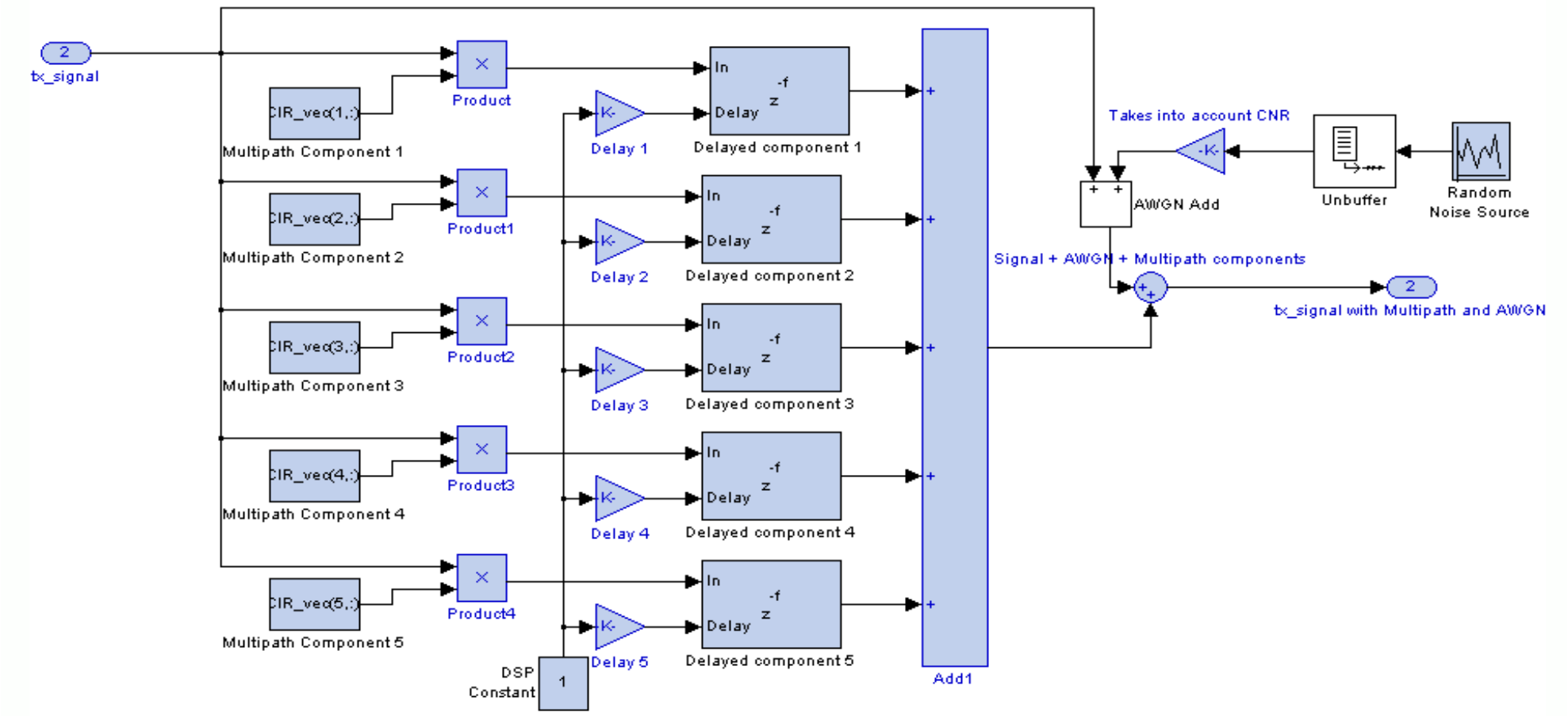

Figure 7. Multipath and AWGN channel model

Figure 2 shows the GPS L1 simulator. It consists of three branches, the carrier frequency generator, C/A code generator and navigation data generator.

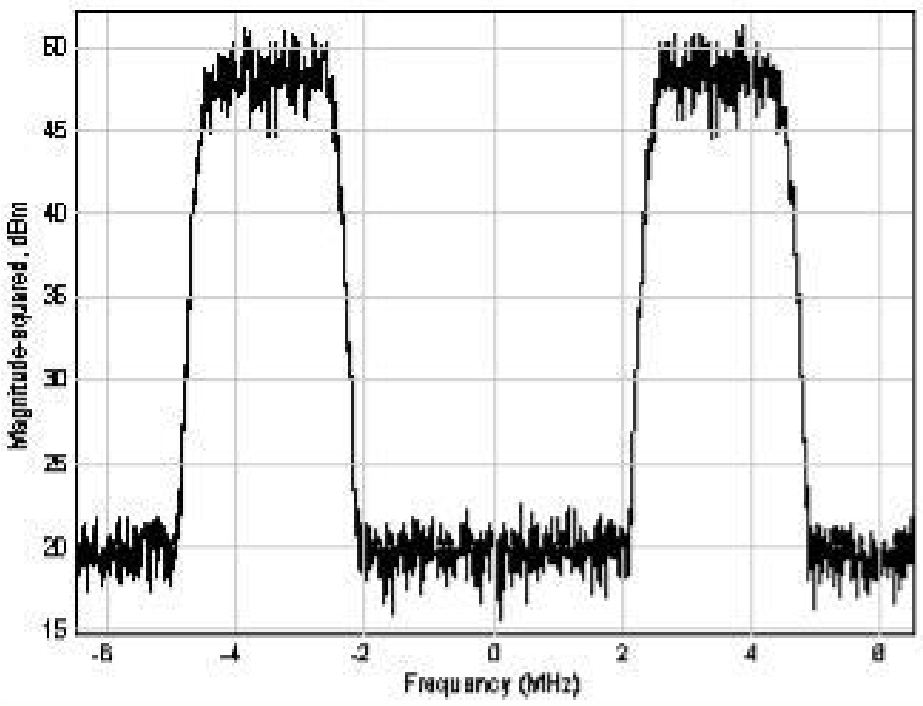

Figure 8. CNR = 50dB-Hz (GPS + Galileo)

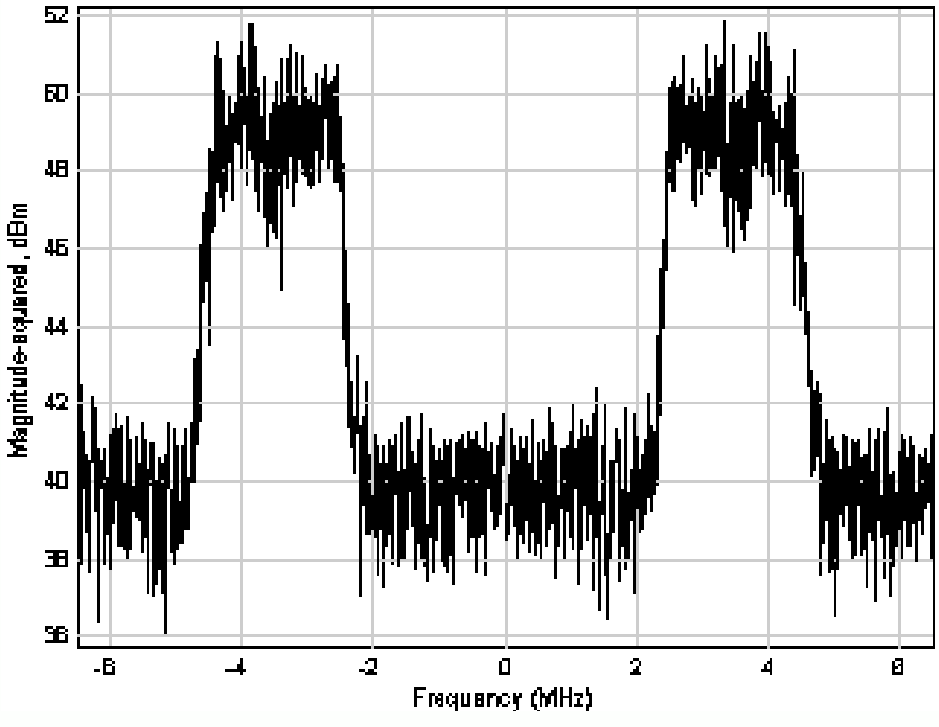

Figure 9. CNR = 30dB-Hz (GPS + Galileo)

P-code generator branch will be included in the future version. For simplicity, navigation data bits are a random vector of ±1 of 30 second duration and frequency of 50Hz. This navigation data is spread over 2MHz by multiplying with C/A code, which can be generated for every satellite vehicle. This combination of data and spreading code is then upconverted to an IF carrier at 3.42MHz, since it would be impossible to work with 1.57542GHz samples using Matlab-Simulink. The output of this block is the GPS L1 signal in Inphase (I) and Quadrature (Q) components. Similarly, Figure 3 shows the block diagram of the Galileo E1 generator. It contains a carrier generator, an E1B primary code generator, navigation data generator (random vector of ±1 with symbol rate of 125sps and page refresh rate of 2Hz), E1C primary code generator, CS25 secondary code generator and BOC11 and BOC61 generators. Here too, the carrier frequency is 3.42MHz and the output is in the IQ format. Figures 4 and 5 show the spectrum of the GPS L1 and Galileo E1 signals respectively as generated by TUTGSSS.

The next three blocks are a switch, spectrum limit filters and RF channel. The switch block is used to select which signals should propogate to the channel. Options are GPS only, Galileo Only or GPS and Galileo both. The spectrum limit filters are designed as equi-ripple, FIR bandpass filters with pass band ripple of 1dB and stop band attenuation of 60 dB. They help to limit the output spectrum to a bandwidth of 2MHz around the carrier frequency. Figure 6 shows the baseband spectrum of the combined GPS and Galileo signal at the output of the spectrum limit filter. The channel block simulates a multipath and AWGN channel. Five

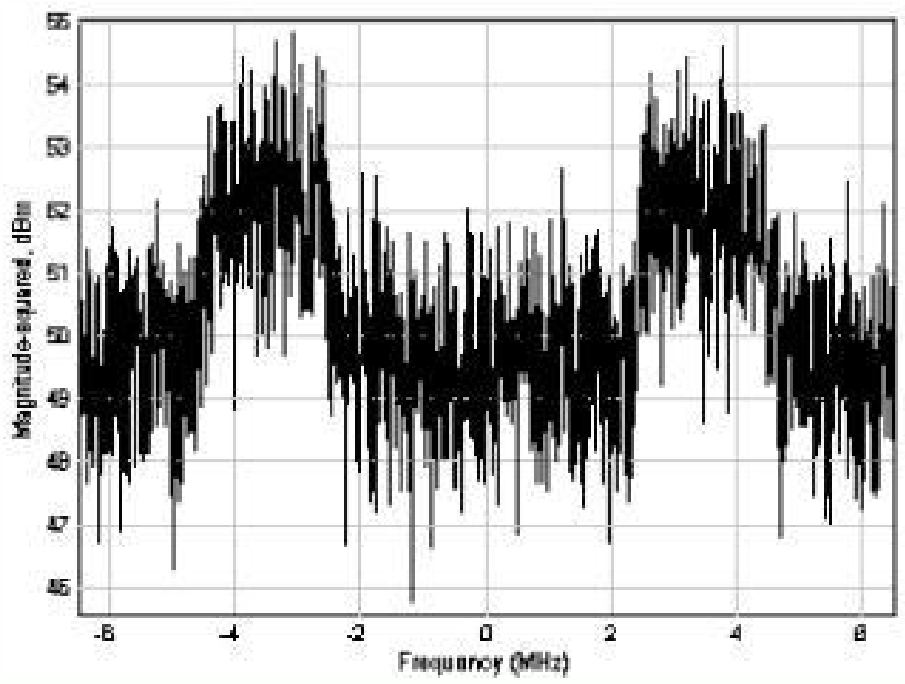

Figure 10. CNR = 20dB-Hz (GPS + Galileo)

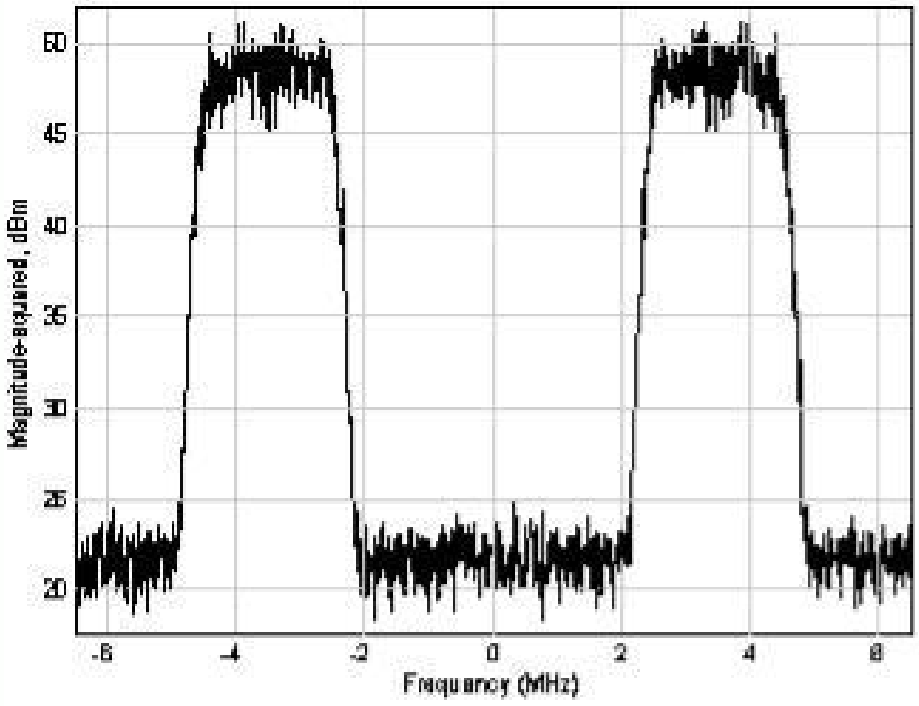

Figure 11. Power of signal (GPS + Galileo) = 40dBm

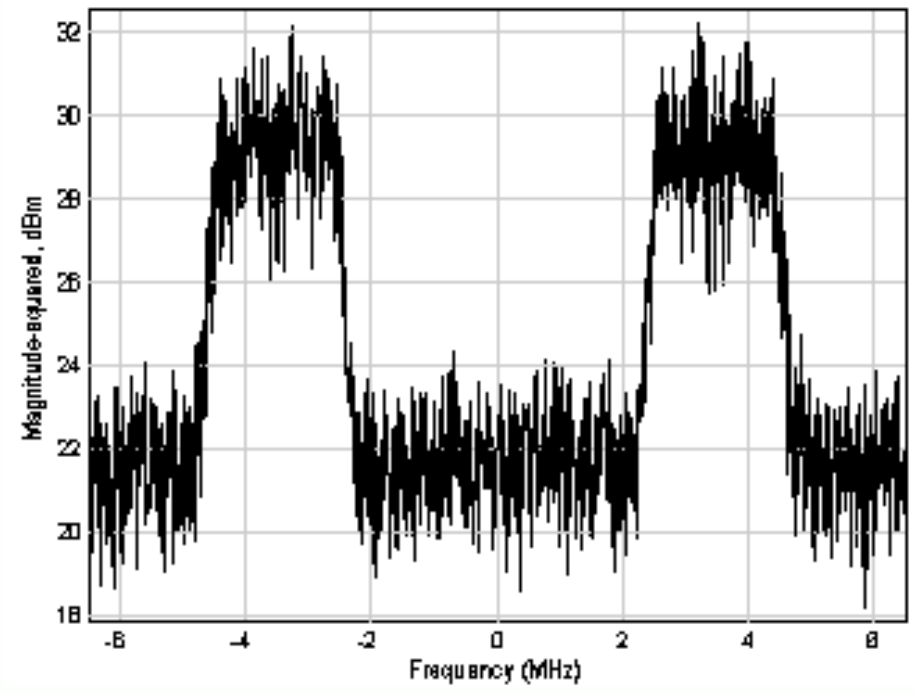

Figure 12. Power of Signal (GPS + Galileo) = 20dBm

multipath components are simulated. It is possible to independently set the gain and delay for each path. The AWGN added to the signal depends on the CNR, also selected by the user. Figure 7 shows the block diagram of the channel block. The IQ data is stored in two variables in the Matlab workspace from where they are copied into a bianry (.bin) file

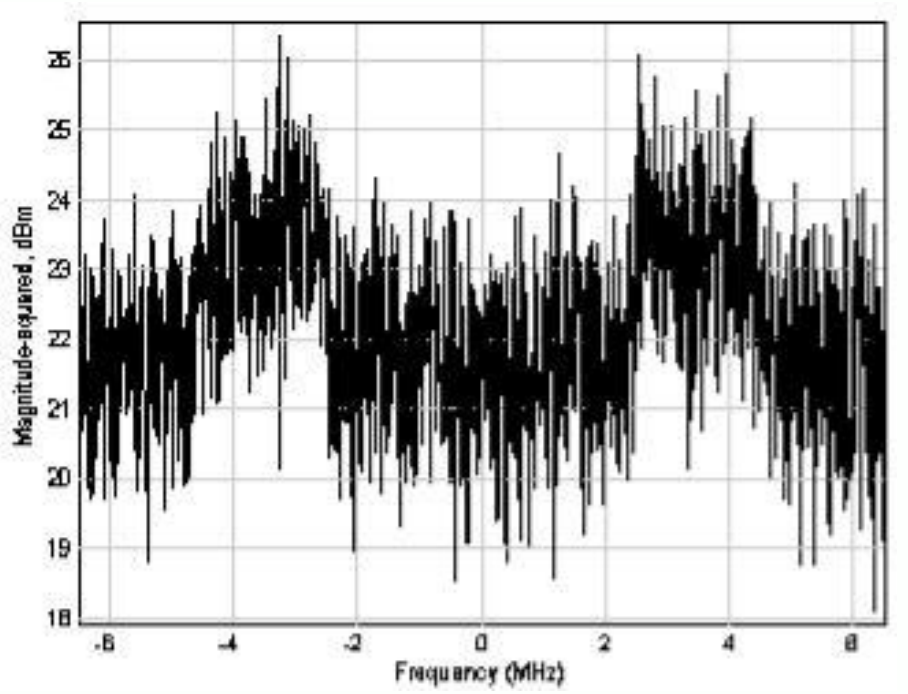

Figure 13. Power of signal (GPS + Galileo) = 10dBm

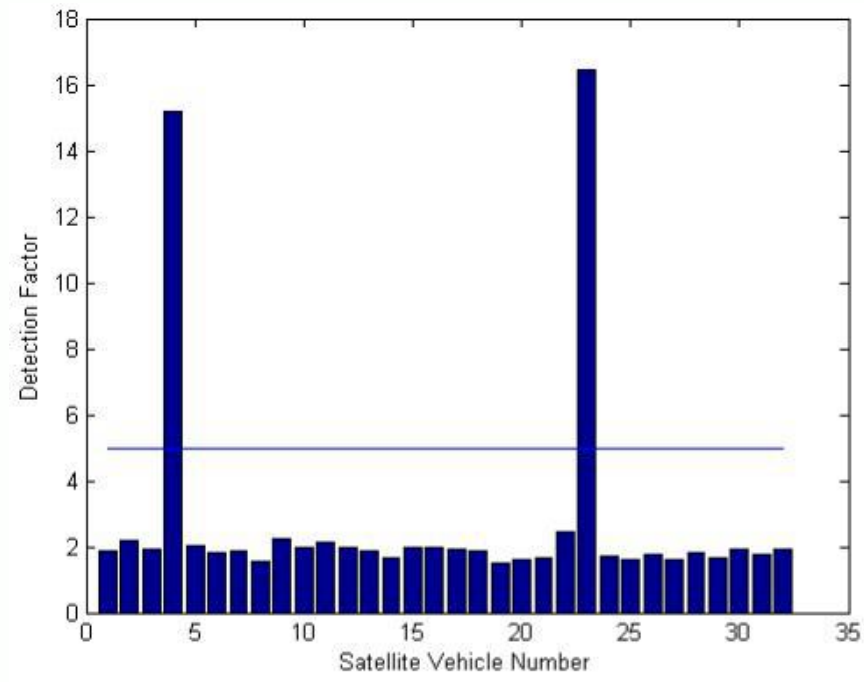

Figure 14. Acquisition profile of GPS Software Receiver. Satellite number 4 and 23 show peak values greater than detection threshold

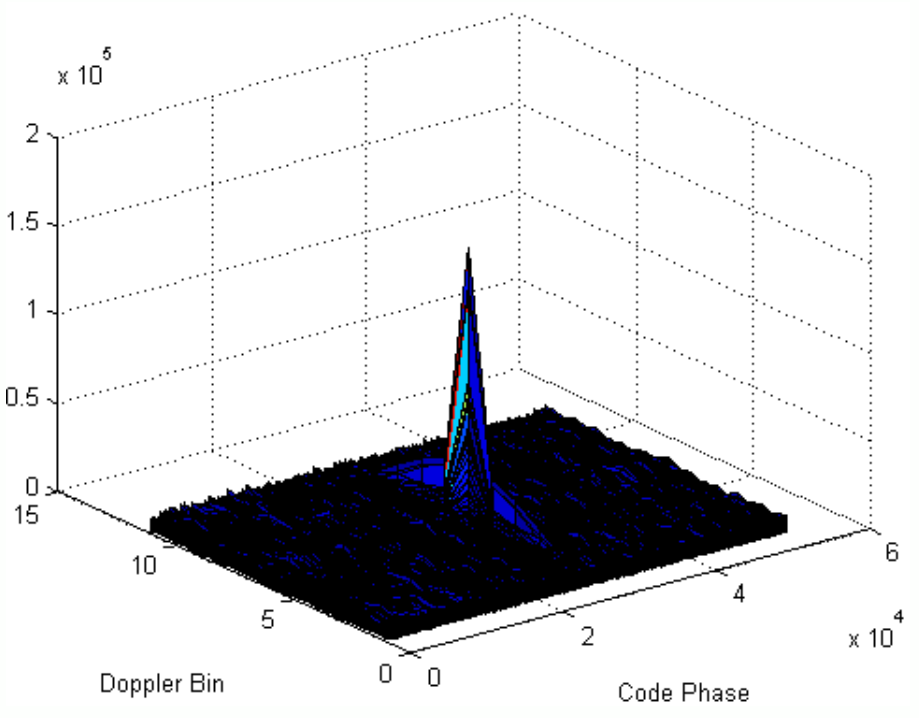

Figure 15. Galileo signal acquisition using software receiver and time bin step of 0.17 chips

by the background matlab program once the entire simulation is complete.

We have begun to incorporate some of the standard GPS test cases as scenarios within the TUTGSSS for effective and automated testing of

Table 2. TUTGSSS features in comparison to state-of-art simulators

Criteria	Present Capability	Possible Extensions
1. Signals simulated	GPS L1 (C/A), Galileo E1 (B/C)	GPS L1(P(Y), M), Galileo E5, E6, Glonass L1, L2, SBAS, IMU
2. Software platform	1. Matlab, Simulink, C++ 2. Open source simulator application	Some modules in C#
3. Error sources modeled	1. Satellite clock, receiver clock, troposphere delay, ionosphere delay, Doppler, code and carrier timing offset, AWGN, multipath, transmitter filter attenuation 2. Typical values as constants	1. Receiver RF FE effects (AWGN, phase noise, group delay, automatic gain control (AGC) effects, quantization errors, filter attenuation), jamming, interference 2. Accurate mathematical or empirical models instead of typical values as constants
4. Space segment modeling	Not yet implemented	1. Satellite constellation modeling (geometry and trajectory) for GPS and Galileo 2. Read data and files in different co-ordinate systems and formats
5. Other features	1. Two channels modeled 2. Signal validation using GPS and Galileo software receivers 3. Scenarios to test sensitivity and TTFF under ramp-wise increasing and decreasing power of satellite signal and noise contamination (in other words, carrier-to-noise ratio)	1. Receiver trajectory modeling 2. 12 channels modeling 3. GUI to accept user input and display output

GNSS receivers. Further information regarding various performance parameters and testing procedures realted to GPS receivers can be found from [38], [39], [40], [41], [42], [43], [44]. Currently, scenarios for testing Time to First Fix (TTFF) and receiver sensitivity can be simulated by a ramped variation of power of satellite signal and noise comtamination in the channel. Figures 8, 9 and 10 show the output under increasing noise conditions, evident from the increasing power of the noise floor, which eventually overwhelms the fixed signal power (Figure 10). While Figures 11, 12, 13 show the output under decreasing signal power conditions, which eventually falls below the fixed noise floor (Figure 13).

In order to test whether the TUTGSSS is really providing authentic and correct GNSS signals, we fed the data from the IQ binary files as input to GPS L1 and Galileo E1 software receivers, also developed in our University. As an example, GPS L1 signals were generated from satellite vehicles 4 and 23. Figure 14 shows the output of the acquisition code of the GPS software receiver. It clearly shows that the detection factor for satellite vehicles 4 and 23 are greater than the detection threshold set for the receiver. This proves that GPS signals are correctly generated by TUTGSSS. In case of Galileo signals, the acquisiton results from the receiver is shown in figure 15. The Galileo signals were generated with a doppler frequency of 0Hz. The receiver is capable of acquiring signals even with 1000 Hz of doppler on either side of the center frequency. This 2000 Hz frequency range is divided into 11 doppler ‘bins’, each 200Hz wide. Since the Galileo signal generated by the simulator has 0Hz doppler, it will reside in the 6^{th} doppler bin. Figure 15 clearly shows the acquisition peak at doppler bin 6. Thus, the signals generated by the simulators have been verified using software receivers. We are in the process of incorporating actual navigation data into TUTGSSS, and then it will be possible to verify the signals indisputably using even the tracking stages of the software receivers. The features of TUTGSSS in comparison to other state-of-art simulators is given in Table 2.

CONCLUSION

This paper presents the state-of-art in GNSS software-based signal simulators. From the various sources that were studied and compared, it is clear that such simulators have evolved through three distinct generations, with newer and more complex

features being added in each generation. This has enabled the signal generated by such simulators to closely resemble actual GNSS signals as transmitted by satellites or as per their intended design.

The authors have designed and built a GNSS signal simulator in software called TUTGSSS and its first results are presented in this paper. GPS L1 and Galileo E1 B/C signals were generated and their output spectrum was plotted. Two of the scenarios for testing pedestrian navigation capabilities namely, sensitivity under low received signal power from satellite and high noise environments have been incorporated in the simulator and their results have been presented. Considering these factors, we believe that this paper could prove to be a single point source of information and education for research teams wanting to build a GNSS signal simulator for testing receivers of current and future GNSS signals.

MORE INFORMATION

More information on this research work and its parent affiliations can be found at [46], [47], and [48].

ACKNOWLEDGMENT

The research leading to these results has received funding from the European Union's Seventh Framework Programme (FP7/2007-2013) under grant agreement number 227890 (GRAMMAR project). This work has also been supported by the Academy of Finland.

DISCLAIMER

The views expressed in this article are those of the authors and do not reflect the official policy or position of the United States Air Force, Department of Defense, or the U.S Government.

REFERENCES

[1] P. M. Corbell, M. M. Miller, "Design and Analysis of a Matlab Based Digitized IF GPS Signal Simulator and a Simulink Based Configurable GPS Receiver", proceedings of ION GPS 2000, 19-22 September 2000, Salt Lake City, UT

[2] M. M. Miller, P. M. Corbell, J. F. Raquet, "Design and Validation of Digitized Intermediate Frequency GPS Signal and Receiver Software Models for Developing and Comparing Advanced GPS Receiver Technologies", proceedings of ION GPS 2000, 19-22 September 2000, Salt Lake City, UT

[3] A. Brown, N. Gerein, K. Taylor, "Modeling and Simulation of GPS Using Software Signal Generation and Digital signal Reconstruction", Proceedings of the ION National Technical Meeting, January 2000, Anaheim, CA

[4] A. Brown and N. Gerein, "Advanced GPS Hybrid Simulator Architecture", Proceedings of ION 57th Annual Meeting, Albuquerque, NM, June 2001

[5] P. M. Corbell, M. M. Miller, "A Configurable GPS Accumulated I and Q Signal Component Simulator in Matlab", Proceeding of ION NTM 2001, 22-24 January 2001, Long Beach, CA

[6] T. H. Tan, "Global Positioning System Signal Simulation", Bachelor of Electrical Engineering (Honours) Thesis, The University of Queensland, Australia, October 2003

[7] L. Dong, "IF GPS Signal Simulator Development and Verification", Master of Science Thesis, University of Calgary, Canada, November 2003

[8] A. Nunes, T. Ferreira, J. Borràs, F. Nunes, F. Sousa, G. Seco, "Signal Generator and Receiver Toolbox for Galileo/GPS Signals", Proceedings of 2nd ESA Workshop on Satellite Navigation, Navitech 2004

[9] O. Julien, B. Zheng, L. Dong, G. Lachapelle, "A Complete Software-Based IF GNSS Signal Generator for Software Receiver Development", Proceedings of ION GNSS 2004, Sept. 21-24, Long Beach, CA

[10] L. Dong, C. Ma, G. Lachapelle, "Implementation and Verification of a Software-Based IF GPS Signal Simulator", Proceedings of National Technical Meeting, Institute of Navigation, 26-28 January 2004, San Diego

[11] C. Seynat, A. Kealy, K. Zhang, "A Performance Analysis of Future Global Navigation Satellite Systems", Journal of Global Positioning Systems (2004) Vol. 3, No. 1-2: 232-241

[12] A. M. A. Farah, "GPS/Galileo simulation for reduced dynamic LEO satellite orbit determination", PhD Thesis 2004, University of Nottingham, UK

[13] A. Pósfay, T. Pany, B. Eissfeller, "First Results of a GNSS Signal Generator Using a PC and a Digital-to-Analog Converter", Proceedings of ION GNSS 18th International Technical Meeting of the Satellite Division, 13-16 September 2005, Long Beach, CA

[14] T. Inzerilli, D. Lo Forti, V. Suraci, "Modeling and Simulation of GNSS with NS2", Proceedings of 14th IST Mobile and Wireless Communications Summit, Dresden, June 2005

[15] Accord Software & Systems Pvt. Ltd, "GPSLAB", Available at: http://www.gpslab.us/datasheet/DataSheet-prof.pdf

[16] A. Constantinescu, R.Jr. Landry, I. Ilie, "Hybrid GPS/Galileo/GLONASS IF Software Signal Generator", Proceedings of ION GNSS 18th International Technical Meeting of the Satellite Division, 13-16 September 2005, Long Beach, CA

[17] NAVSYS Corporation, "GPS Signal Simulation Toolbox", Available at: http://www.navsys.com/brochures/NAVSYS_Toolbox.pdf

[18] C. Abart, P. Berglez, G. Abwerzger, B. Hoffmann-Wellenhof, W. Cresens, T. Vandeplas, W. De Win, "Simulating GNSS Constellations - The GAMMA Signal Generator", Proceedings of the 20th International Technical Meeting of the Satellite Division of The Institute of Navigation (ION GNSS 2007), Fort Worth, TX

[19] Intecs, "gLAB GNSS Signal Analysis Tool", Available at: http://www.intecs.it/pdf/brochure_gLAB_01-02-2010.pdf

[20] VEGA IT GmbH, "Galileo System Simulation Facility (GSSF)", Available at: http://www.gssf.eu/Documents/GSSF%20V2.1%20Fact%20Sheet%20-%20Issue%201.pdf

[21] K. Borre,"The E1 Galileo Signal", Lecture at Stanford university, Available at: http://waas.stanford.edu/~wwu/papers/gps/PDF/Borre/galileo_sig.pdf

[22] C. Hu, M. Tsai, "The Implementation of an INS-GNSS Software Simulator", Proceedings of 28th Asian

conference on Remote Sensing (ACRS 2007), November 2007, Kuala Lumpur, Malaysia

[23] I. Joo, J. Lee, S. Lee, J. Kim, D. Lim, S. J. Lee, "S/W based IF Signal Simulator Prototyping for L1 C/A, L2C, and E1(B&C)", Proceedings of The 9th International Conference on Information and Communications Security (ICICS 2007), December 2007, Zhengzhou, China

[24] C. Cosenza, Q. Morante, S. Corvo, F. Gottifredi, "GNSS Bit-True Signal Simulator-A Test Bed for Receivers and Applications", Satellite Communications and Navigation Systems, Signals and Communication Technology, 2008, 3, 447-460, DOI: 10.1007/978-0-387-47524-0_34

[25] F. Schubert, R. Prieto-Cerdeira, A. Steingass, "GNSS Software Simulation System for Realistic High-Multipath Environments", Proceedings of 4th ESA Workshop on Satellite Navigation User Equipment Technologies (NAVITEC 2008), December 2008, Noordwijk, The Netherlands

[26] J. Lee, T. Kim, S. Lee, J. Kim, "Development of Software GNSS Signal Generator", Proceedings of International Symposium on GPS/GNSS 2008, November 2008, Tokyo, Japan

[27] S. Lim, D. Lim, M. Liu, S. W. Moon, C. Park, S. J. Lee, "Design of a Software-based Multi-Channel GNSS IF Signal Generator", Proceedings of International Conference on Control, Automation and Systems 2008, October 2008 in Seoul, Korea

[28] German Aerospace Center (DLR), "Simulation of Satellite Navigation Signals and Channels (SNACKS)", Available at: http://snacs.sourceforge.net/index.html

[29] Fraunhofer Institute for Integrated Circuits IIS, "GNSS-SIGNAL-SIMULATOR", Available at:
http://www.iis.fraunhofer.de/fhg/Images/07_GNSS-Signal_Simulator_neu_tcm278-158408.pdf

[30] TeleConsult Austria GmbH, "GNSS Multisystem Performance Simulation Environment (GIPSIE)", Available at:
http://www.teleconsult-austria.at/download_public/GIPSIE.pdf

[31] Center for Remote Sensing Inc., "Software GNSS Signal Simulator", Available at: http://www.cfrsi.com/pdf/Software%20GNSS%20Signal%20Simulator.pdf

[32] Z. Y. Kou, Y. Huang, Z. Z. Qishan, "Architecture of software-based GNSS signal simulator and implementation of its IF signals generation", Journal of Beijing University of Aeronautics and Astronautics (2009-07), Available at:
http://en.cnki.com.cn/Article_en/CJFDTOTAL-BJHK200907004.htm

[33] C. Ouzeau, J. Korsakissok, "Performance Assessment of a Juzzle-Based GNSS Simulator", Proceedings of ENC GNSS 2009, May 2009, Naples, Italy

[34] A. M. Smith, "Global Navigation Satellite System Signal Simulator - An Analysis of the Effects of the Local Environment and Atmosphere on Receiver Positioning", Doctor of Philosophy Thesis, University of Bath, UK, October 2007

[35] University FAF Munich, "GNSS Software Simulation", Available at: http://www.ifen.unibw.de/research/gnss_simulator.htm

[36] A. Fernández, J. Diez, A. Caramagno, "GRANADA-Galileo Receiver Analysis and Design Application", ESA-GJU Workshop on Tools and Facilities for Galileo Receivers, March 2006

[37] L Wilkens, "The joy of teaching with C#", Journal of Computing Sciences in Colleges, Volume 19, Issue 2, December 2003, Pages: 254 - 264, ISSN:1937-4771

[38] Point Inc., “Glossary”, Available at:
http://www.point-inc.com/glossary.php

[39] S. A. Malik, N. C. Shivaramaiah, A. G. Dempster, “Search Engine Trade-offs in FPGA-based GNSS Receiver Designs”, University of New South Wales, Sydney, Australia. Available at:
http://www.gmat.unsw.edu.au/snap/publications/malik_etal2009a.pdf

[40] 3rd Generation Partnership Project (3GPP), "TS34.171", V6.5.0 (2006-10)

[41] A. Grant, D. Last, N. Ward, "Marine Radiobeacon GNSS Service – Predicting Availability and Continuity", Proceedings of Institute of Navigation (ION) GPS 2002, September 2002, Portland, OR

[42] A. Grant, D. Last, N. Ward, "Enhanced Accuracy by Regional Operation of Europe’s New Radiobeacon Differential System", Proceedings of Institute of Navigation (ION) GPS 2002, September 2002, Portland, OR

[43] Spirent Communications, "Testing GNSS System Errors", Application Note: DAN002 Issue 1-01

[44] GLORIA - Gnss & LOran-c in Road and rall Applications, "Technical Achievements", Available at:
http://www.eu-gloria.org/technical%20results.htm

[45] A. Mitelman, P. Nomark, M. Reidevall, S. Strickland, "Apples to Apples - Standardized Testing for High-Sensitivity Receivers", GPS World, January 1, 2008

[46] GRAMMAR Project webpage:
http://www.kn-s.dlr.de/grammar/index.html

[47] GNSS Receiver group of the Department of Computer Systems, Tampere University of Technology webpage:
http://www.tkt.cs.tut.fi/research/gnss/

[48] Signal Processing for Wireless Positioning group of the Department of Communications Engineering, Tampere University of Technology webpage:
http://www.cs.tut.fi/tlt/pos/

PUBLICATION 2

S. Thombre, H. Hurskainen, J. Nurmi, "Wideband, High Gain, High Linearity, Low Noise Amplifier for GNSS Frequencies with Compensation for Low Frequency Instability", Proceedings of the *5th Advanced Satellite Multimedia Systems Conference (ASMS 2010)*, September 2010 in Cagliari, Italy.

Reprinted with kind permission.

Wideband, High Gain, High Linearity, Low Noise Amplifier for GNSS Frequencies with Compensation for Low Frequency Instability

Sarang Thombre, Heikki Hurskainen, Jari Nurmi
Department of Computer Systems
Tampere University of Technology (TUT)
Tampere, Finland
{sarang.thombre, heikki.hurskainen, jari.nurmi}@tut.fi

Abstract— **This paper presents the design methodology, simulation results and implementation details of a low noise amplifier (LNA) designed to operate over the whole range of Global Navigation Satellite System (GNSS) frequencies (1164MHz to 1615.5MHz). This LNA works over combined (but overlapping) frequency bands of all three GNSS constellations (GNSS consist of the American Global Positioning System (GPS), European Galileo system and the Russian GLONASS system). Designed to be unconditionally stable with gain of over 18dB and noise figure of 2dB over a considerable bandwidth of about 450MHz, the achieved results conformed quite well to the specifications. Final implementation results include a gain of 18.5dB at the centre frequency with a nominal variation of ±1.3dB over the desired bandwidth. The noise figure obtained is 2.18dB and the amplifier stability range extends from 0Hz to 9GHz. Very high degree of linearity is achieved with output 1dB compression at +13dBm and output third order intercept at +23dBm. This paper describes results at every stage of design, simulation and implementation along with a solution against typical low frequency instability by a small trade-off in noise figure.**

Keywords-wideband, high gain, high linearity, GNSS, LNA, amplifier, stability, RF, low frequency instability

I. INTRODUCTION

Most of the current GNSS receiver radio frequency (RF) front-ends are tuned for L1 band (centered at 1575.42MHz) reception, since it is one of the frequencies used by GPS. In future, the RF front-ends need to be more versatile and capable of receiving wider range of frequencies due to introduction of new satellite navigation systems, e.g. Galileo which transmits signals at E1 (centered at 1575.42 MHz), E5 (centered at 1191.795MHz) and E6 (centered at 1278.75MHz) [1]. Modernized GPS will add civilian signal to L2 (centered at 1227.6MHz) and L5 (centered at 1176.45MHz) [2] and GLONASS system is using frequencies of L1 (centered at 1602MHz) and L2 (centered at 1246MHz) [3].

For some years there has been considerable interest in the bandpass sampling based RF front-end design. In [4], bandpass sampling of a single band of frequencies was considered which evolved to sampling multiple distinct RF bands in [5], [6] and [7]. In [8], bandpass sampling of multiple distinct single-sided (complex) RF bands was accomplished. In all these works, either GPS and GLONASS or GPS and GSM signals were integrated and that too, just L1 band signals in each case. [9] claims to use bandpass sampling and digital filtering for direct conversion of GPS L1 (C/A) and L1/L2 (P(y)) codes into digital intermediate frequency (IF).

The RF front-end architecture presented in Figure 1 is built around the concept of bandpass sampling of the entire GNSS frequency spectrum using a wideband LNA, filters and an analog to digital converter (ADC) and then performing the channel selection in the digital domain using digital filters and multi-rate signal processing. As the first step towards full implementation of this front-end architecture, the LNA was designed, simulated and implemented as a stand-alone circuit on printed circuit board (PCB). This paper details the results for this LNA.

Some research has already been performed towards designing LNAs working on or around the frequency range of interest. For example, in [10] a 65nm CMOS LNA for multi-standard radio applications between 100MHz and 6GHz is described. Its strengths are its wide bandwidth, low silicon area ($0.01mm^2$) and low power consumption (21mW). On the other hand, its gain and noise figure are 15dB and 3dB respectively. In [11], an LNA for GNSS frequencies is described. It is a PCB based design with a gain of 16.7dB. Similarly, in [12] a wideband LNA for GNSS frequencies is constructed. Here also, the LNA is a PCB based implementation with a gain of 15.5dB and power consumption of 2.2W.

Figure 2 shows the GNSS frequency spectrum on which the front-end and the LNA is designed to operate. The LNA is required to amplify a bandwidth of 451.5 MHz (1164MHz to 1615.5MHz). Power gain over this bandwidth should be atleast 18dB with a maximum deviation of ±1.5dB. Maximum noise figure should be 2dB and the minimum requirement for 50Ω impedance matching is that return loss at input and output

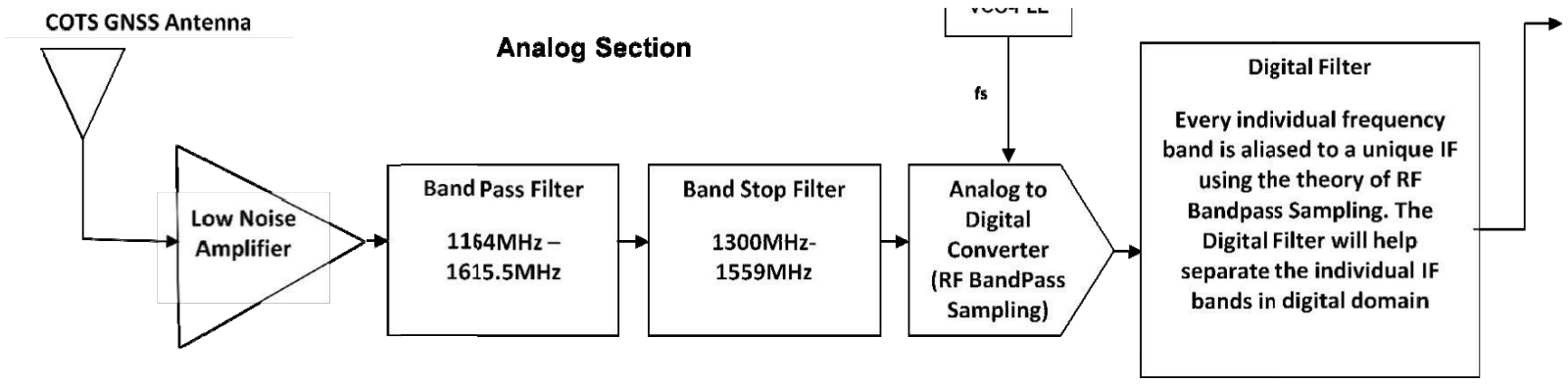

Figure 1. Block diagram of a bandpass sampling RF front-end for GNSS Receivers

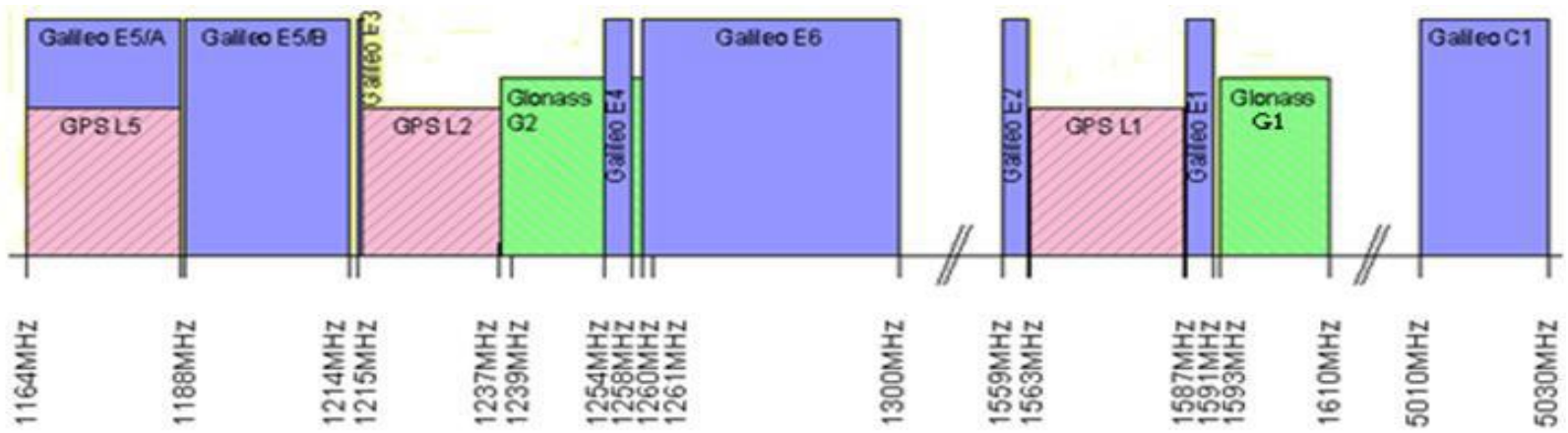

Figure 2. Future GNSS frequency spectrum [13]

should be less than -10dB. It should also be inherently stable over all frequencies, while output one-dB compression should be atleast +3dBm. A decision was made on using the BFP420 transistor from Infineon [14] because its gain and noise figure ratings were in conformance with the desired specifications. All simulations have been performed in Agilent ADS simulation software.

The outline of the paper is as follows. Section II describes the design of the support circuitry for the LNA. This includes the biasing, stabilization and input and output impedance matching circuits. Section III describes the simulation stage where the entire LNA circuit (including support structures and transmission line effects) were simulated using Agilent ADS software. Section IV describes the issue of and solution against low frequency instability typical to amplifiers that are impedance matched for high gain. The final implementation and PCB layout are described in Section V. The LNA structure was finalized only after many candidate structures were simulated and their limitations analyzed. These structures and their shortcomings are also described in this section. Section VI shows the results of the final implementation. It shows that this LNA is indeed wideband, high gain, highly linear, low noise and inherently stable over the GNSS frequency range.

II. Design Stage

The biasing network is responsible for setting the correct DC operating voltage and current for the transistor within an LNA circuit. The supply voltage and current was standardized at 5 volts and 20mA DC respectively. With proper design of biasing resistors, the desired operating voltage and current were achieved. An important point to note is the role of the emitter inductance. When the emitter of the amplifier is connected to ground via a hole in the PCB, this adds a certain inductance (usually assumed to be less than 1nH). It was found that this inductance lowers the gain of the amplifier by about 1-3dB and is unavoidable. Hence it should always accompany the transistor model in simulations.

The LNA is specified to be unconditionally stable from 0Hz to f_{max}. Here f_{max} is equal to the maximum frequency of oscillation of our transistor, BFP420, which is 25GHz. Since the S-parameter file for BFP420 had empirical data between 100MHz and 9GHz, it was possible to test the stability only within this frequency range. It is safe to assume that if the LNA is stable up to 9GHz, at higher frequencies the losses of the components and transmission line segments are so high that the reduced gain most probably negates any possibility of instability. Before a stabilization circuit was designed, the LNA was unstable after 3GHz. Therefore, a sub-circuit was designed that would take care of high frequency gain. One idea was to add a series resistance in the output circuit and tune all component values again to achieve best gain, noise figure and unconditional stability.

The amplifier should be impedance matched perfectly to 50 ohms at input and output. However, there are usually two methods by which impedance matching can be done, each with its unique advantage [15], [16]. It is possible to either match for maximum gain, using technique of simultaneous conjugate matching, or minimum noise figure using noise and available gain circles. It is even possible to match the input for minimum noise figure and output for maximum gain. It was decided to match the LNA for maximum gain using the principle of simultaneous conjugate matching. 'Matched' source (Γ_{ms}) and load (Γ_{ml}) reflection coefficients were plotted on Smith-Chart. Next, their value at the centre frequency was found and an appropriate LC matching network was designed using RFDude software [17] to match 50Ω input and output terminations to complex conjugates of these reflection

coefficients. Once the passive matching components are derived, they are inserted in the correct order starting from source and load impedances. Then the components are again tuned for best gain, noise figure and stability.

III. Simulation Stage

All the constituent blocks of the LNA were individually simulated and all the passive components were tuned to achieve perfect DC biasing conditions and maximum gain yet keeping all other parameters as close as possible to the specifications. The schematic was then re-simulated by considering all possible effects that may degrade the performance. There is one important effect that has to be taken into consideration - effect of transmission line (TL) segments in the RF path. When RF signals pass through the copper conductor, the conductor acts as a lossy TL and its effects have to be taken into account. TL effects are directly proportional to the physical dimensions of the TL segment. In the schematic of ADS, all copper conductors in the RF path were replaced with TL segments of length and width equal to that of the actual conductor. The width and length information can be obtained from the layout by placing a RULER component from the ADS Layout Tool at any conductor that is to be measured. The passive components were once again tuned for maximum gain.

Even though it is not possible to model all parasitic and TL effects perfectly, inclusion of the TL segments brings the simulation model very close to real world scenario. Figures 3, 4, 5, and 6 show final simulation results after designing all support circuitry and taking into account TL effects. Figure 3 shows the gain (given by S parameter S_{22}) of LNA versus frequency plot. At the desired center frequency, gain is 17.15 dB and very close to our specification of 18dB. This difference of 1dB between the desired and simulated gains was compensated for in the actual implementation as shown in Section V of this paper. Figure 4 shows the input reflection coefficient (S_{11}) versus frequency plot. It shows that perfect 50Ω matching at input is achieved over the entire desired bandwidth since S_{11} is less than -10dB in this region. Similarly, Figure 5 shows the output reflection coefficient (S_{22}) versus frequency plot. Here near-perfect output matching is also achieved over the entire desired bandwidth.

Figure 6 shows the noise figure of the simulated LNA. The curve nf(2), shows the actual noise figure and it is very close to our desired value of 2dB over the entire bandwidth. An interesting observation is that the gain falls drastically around 3.75GHz. Consequently, the noise figure is extremely high in the same frequency region. The reason can be found from figures 4 and 5 which show poor input and output impedance matching at the same frequency. This is most probably the consequence of TL effects considered in the final simulations. However, since 3.75GHz is very far from the GNSS band, we can safely ignore this phenomenon.

IV. Low Frequency Instability Issue

During the actual implementation, it was observed that the LNA was unstable at frequencies below 1GHz. The 'μ' stability factor derived for the source and load ends of the LNA has to be greater than unity over all frequencies for the LNA to be stable. However, as shown in Figure 7, the value of 'μ' goes

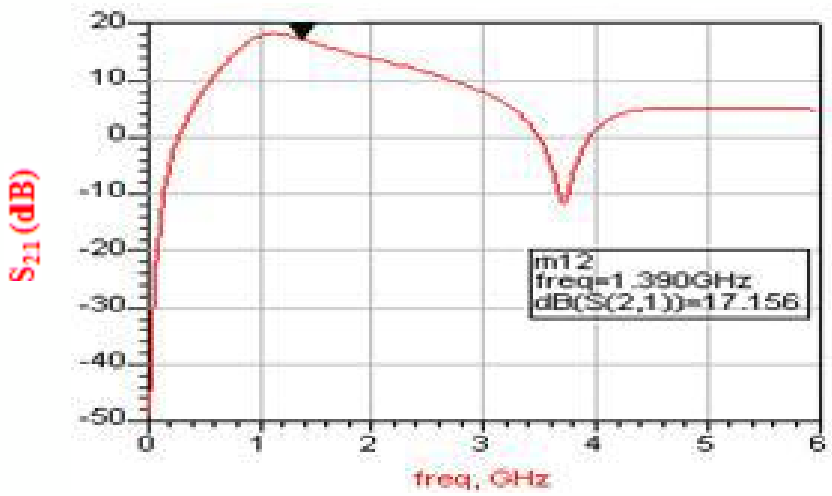

Figure 3. Gain VS Frequency after transmission line effects.

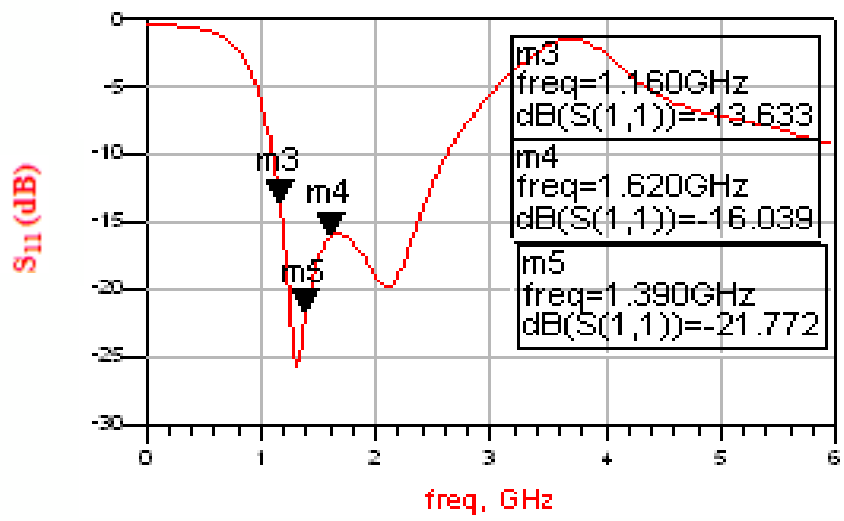

Figure 4. Input return loss curve after transmission line effects

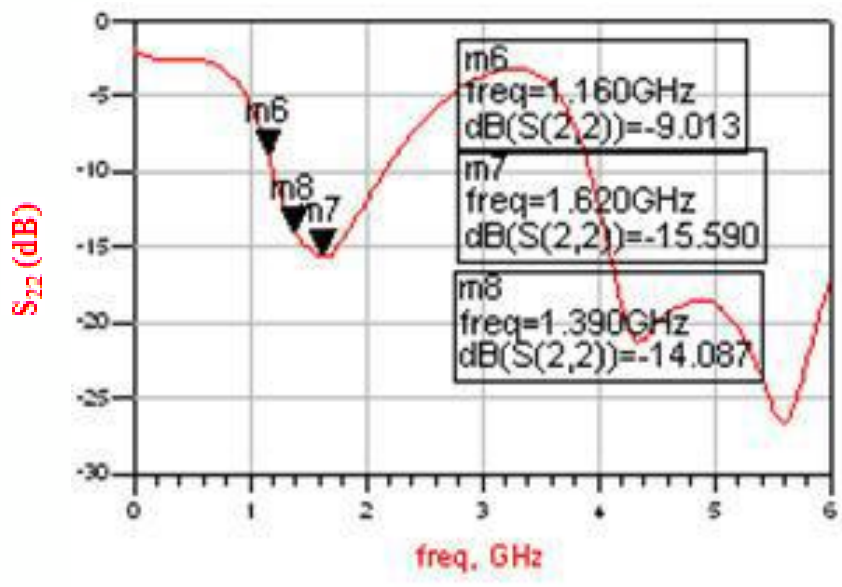

Figure 5. Output return loss after transmission line effects

below unity at around 1GHz. This instability issue was successfully solved by a slight compromise on the noise figure of the LNA.

Two possible solutions to this instability:

1. Parallel resonant circuit centered at about 500MHz.
2. Resistor stabilization.

Both options basically aim to lower the gain at low frequencies to remove the instability. They were prototyped one after the other. After implementing the resonant circuit the noise figure remained unchanged and the LNA became stable at low frequencies as expected. However, this also resulted in the input and output matching being disturbed and consequently, a reduced overall gain (16.5dB).

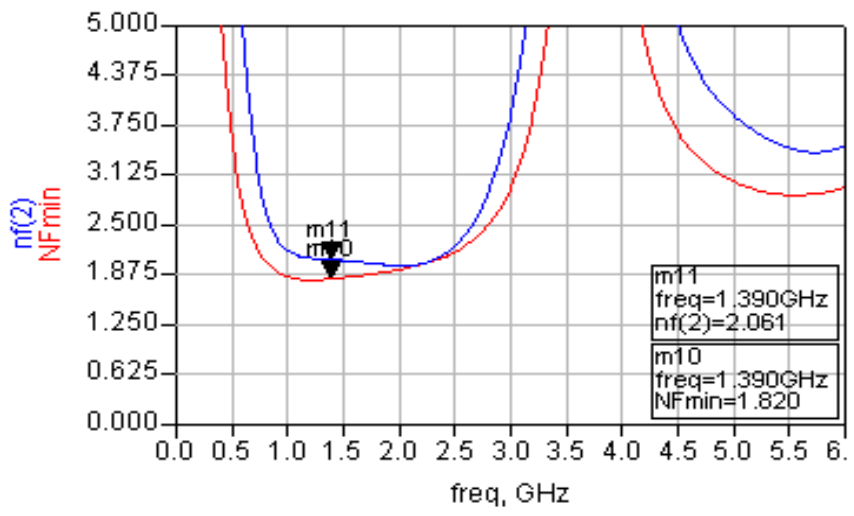

Figure 6. Noise figure VS frequency

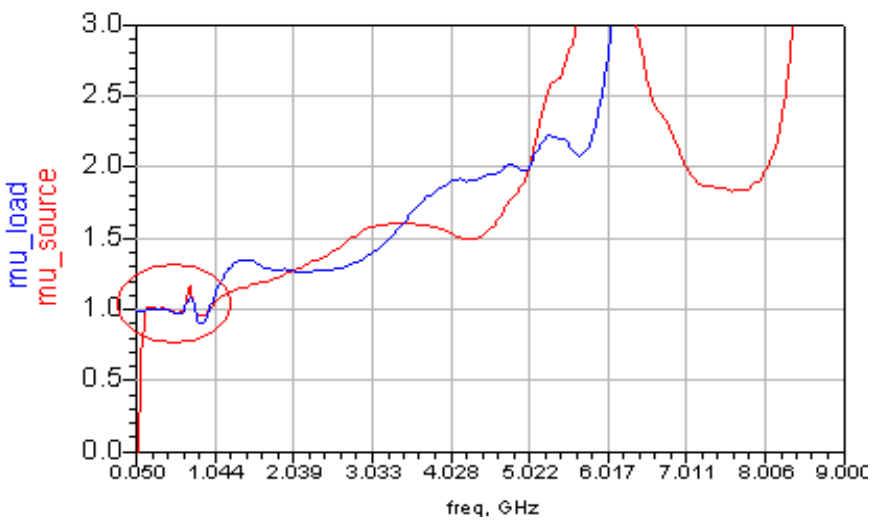

Figure 7. Plot of the 'μ' stability factor showing instability at low frequencies

In resistor stabilization, possible configurations are: a series resistor in input or output, parallel resistor in input or output and a combination of both in input or output. The parallel resistors disturb the matching quite a lot while resistors in the output had a limited effect on the matching. Hence, it was decided to use a single resistor in series in the input of the transistor. When the series resistor of 4.3Ω was used, the amplifier became stable at low frequencies, the gain reduced, but was still over the specified 18dB and the input and output matching improved. However, the series resistor added noise and the overall noise figure increased slightly to 2.18dB. Table 1 shows the various stabilization schemes tested and their results.

V. FINAL IMPLEMENTATION

Before the final implementation version could be reached, the LNA had to go through some initial test versions, each with its limitations that were identified and resolved in the subsequent versions. Version 1 had a gain of 8dB and noise figure in excess of 2.2dB. At this stage it was realized that taking into consideration TL effects in software simulation is necessary to design correct values of impedance matching elements. For version 2 of the LNA, new values of matching and stabilization elements were designed and consequently the gain nearly doubled to 15dB while noise figure dropped to 1.8dB. In spite of the encouraging results, it was observed that the impedance matching was not yet perfect as the input and output return loss was not below -10dB over the bandwidth. Therefore, in version 3 efforts were made to perfect the impedance matching sub-circuits. As a result, the gain increased to 19.2dB and noise figure further improved to 1.72dB. However, now the LNA was unstable at frequencies slightly below 1GHz due to the increased gain. Version 4 (final

TABLE 1. Various stabilization schemes attempted

Possible solution	Input or Output	Outcome	OK?
Series resonant circuit	Input	➢ Stability achieved, NF maintained ➢ Matching disturbed ➢ Gain degrades	No
Series resistor	Output	➢ Stability not achieved ➢ OIP3, P1dB disturbed ➢ NF, gain, matching maintained	No
Parallel resistor	Output	➢ Stability not achieved ➢ Matching disturbed	No
Parallel resistor	Input	➢ Stability not achieved ➢ Matching disturbed	No
Capacitor between VCC & ground	DC biasing circuitry	➢ Instability improved but not completely removed	No
Series resistor	Input	➢ Stability achieved ➢ Matching maintained ➢ NF disturbed	Yes

version) utilized the series resistor solution to improve stability as explained in section IV of this paper. At this point, the LNA had satisfied all design requirements.

The schematic of the final version of the LNA is shown in Figure 8. Resistors R2 and R1 are the biasing resistors while capacitor C1 is for grounding any RF energy that may enter the DC biasing circuit. Inductors L3 and L7 are RF chokes which also block any RF energy from entering the 'DC area' of the circuit. Resistor R3 is the series resistor added to compensate for low frequency instability as explained in section IV. Capacitor C3 is the output DC blocking capacitor. It does not allow DC energy to flow in the RF signal path in the direction of output. Capacitor C5 has a dual role – DC blocking and input impedance matching. Parallel combination of C6 and L6 form the output matching sub-circuit. Inductor L1 simulates the parasitic inductance of the hole in the PCB through which emitter pin of the transistor is grounded (explained in section II). Z_{in} and Z_{out} are dummy 50Ω source and load impedances respectively.

Figure 9 shows the layout of the final version to be etched on PCB. The RULERs are added to show the actual size of the final circuit PCB which is 5.5cm x 2.5cm. The LNA was created from an academic view point as a proof of concept for the bandpass sampling radio front-end and hence, only moderate effort was put into utilizing minimum area or integration on silicon. Similarly, minimization of power consumption was also not a critical requirement at present. We plan to design all individual blocks of the bandpass sampling RF front-end as stand-alone circuits on PCB and once the front-end is operational, future studies with more strenuous power consumption limits may follow.

VI. RESULTS

Results for the final implementation of the low noise amplifier are shown in Figures 10 to 13 and they show that the implementation of the design was successful not only at the centre frequency but also over the entire bandwidth of interest. The LNA centre frequency was 1389.75MHz (The desired band was from 1164MHz to 1615.5MHz) and the gain at this centre frequency is marked in Figure 10 by the s-parameter

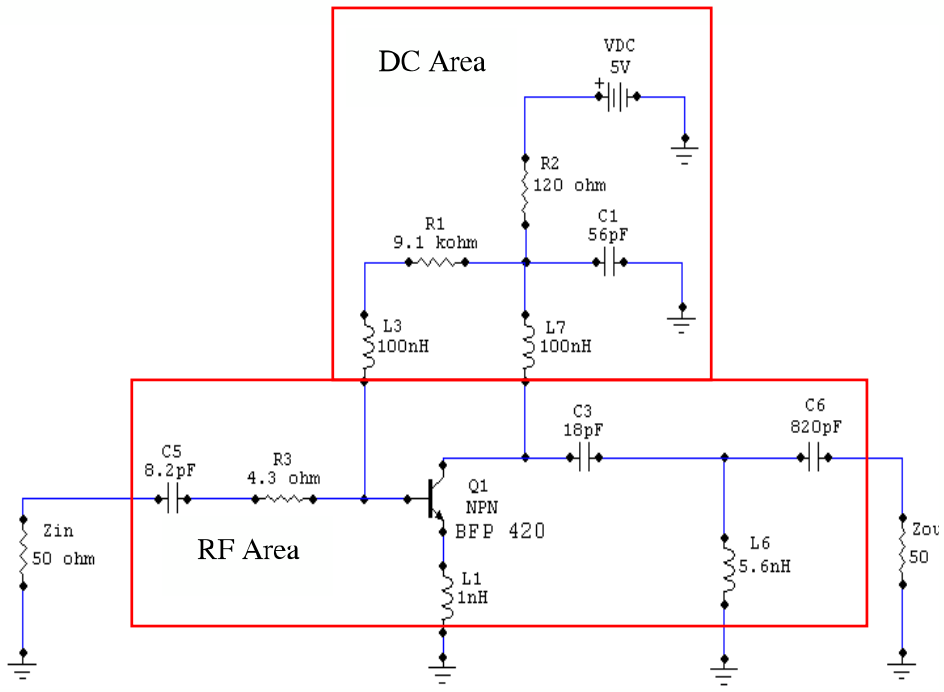

Figure 8. Simplified schematic of the final version of the LNA

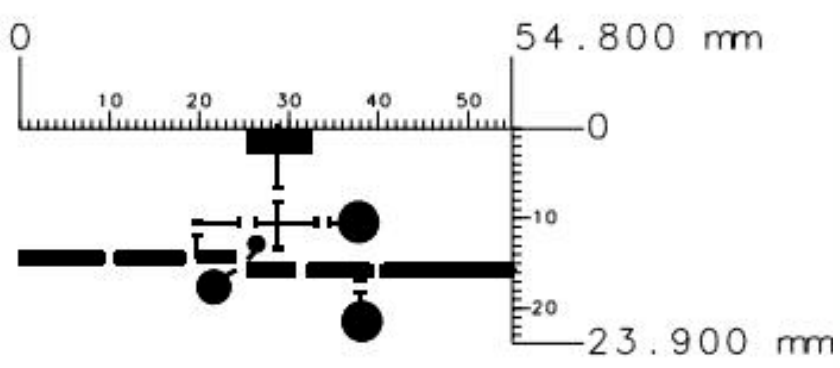

Figure 9. LNA layout used for PCB etching

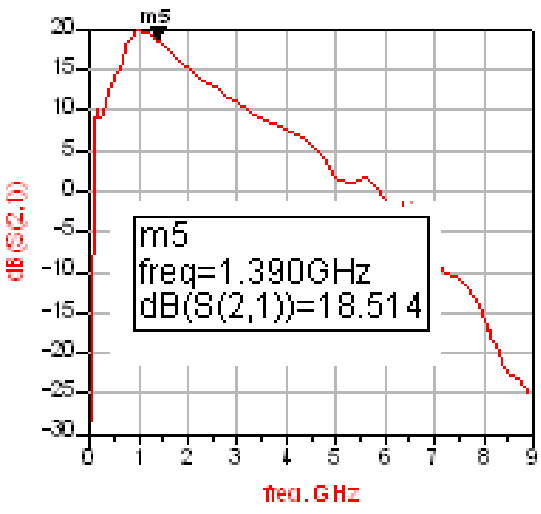

Figure 10. LNA Gain VS Frequency curve

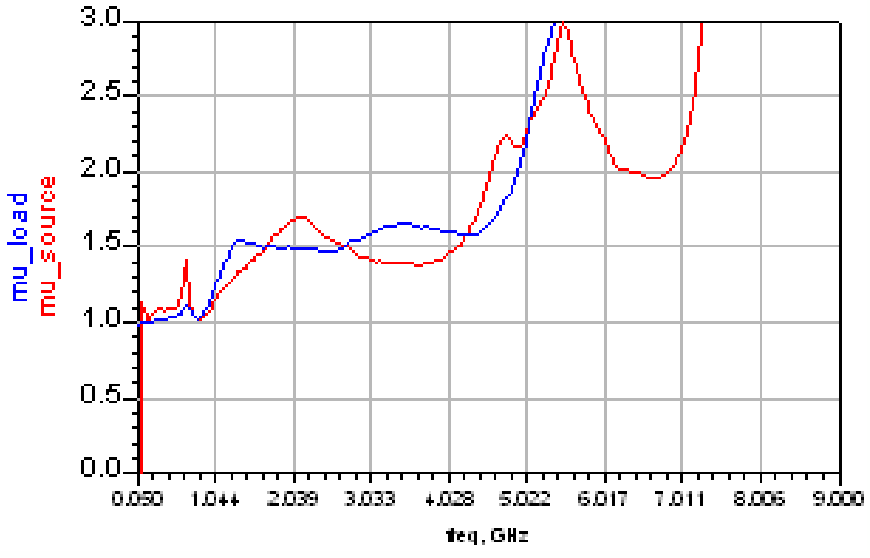

Figure 11. 'μ' stability factor

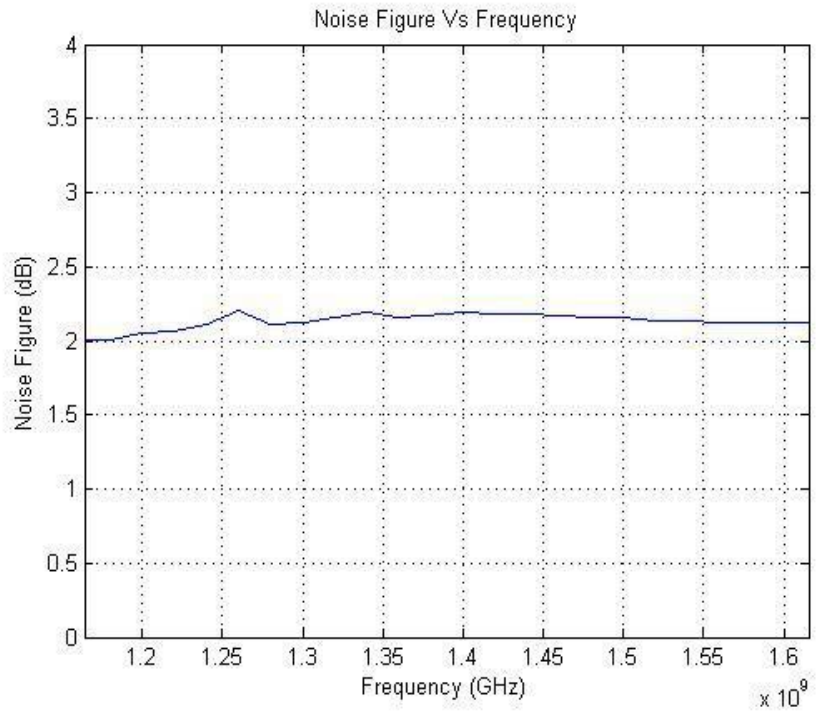

Figure 12. Plot of NF vs frequency in the entire bandwidth of the design

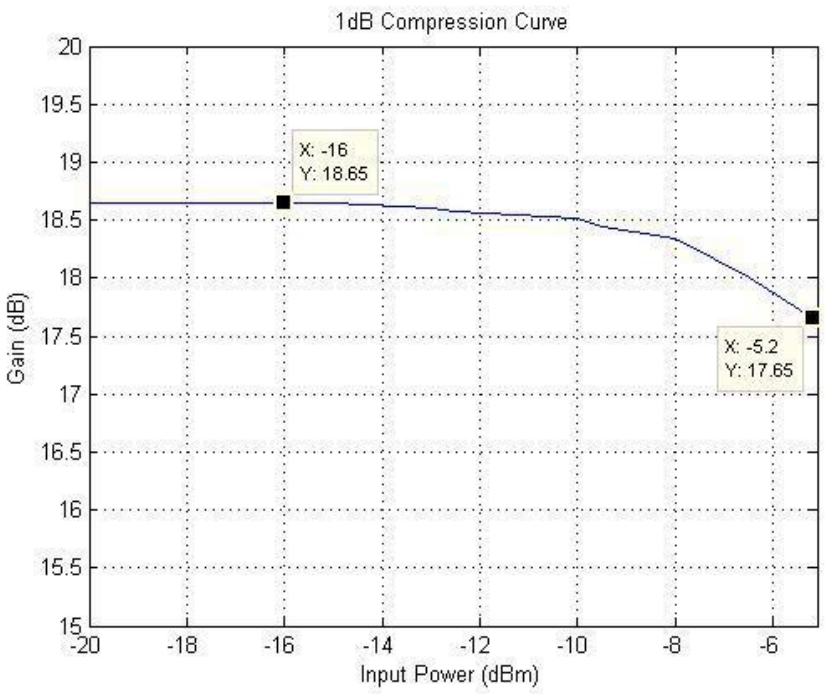

Figure 13. Input one dB compression curve. IP_{1dB} point is achieved at -5.2dBm

$|S_{21}|$. The gain of the LNA remains above the desired 18dB over the entire bandwidth. Figure 11 shows that the value of 'μ' on both the source and load impedance side is always greater than unity. Thus the LNA design is inherently stable at all frequencies. Figure 12 shows that noise figure is in the range from 2.0dB to 2.18dB over the entire bandwidth. Figure 13 shows the 1dB compression curve for the LNA. The input one dB compression point (P_{1dB}) is achieved at -5.2dBm. Therefore the output P_{1dB} can be calculated by (1).

$$P_{1dB\ output} = P_{1dB\ input}\ (dBm) + Gain\ (dB) \quad (1)$$

$$= -5.2 + 18.5 = 13.3dBm$$

A two-tone test was performed on the LNA and the results showed that when the power of the fundamental component was 0.22dBm the power of the third order intermodulation product was -46dBm. The output third order intercept point (OIP3) can be calculated from $P1dB_{\ output}$ by (2) and also from the two-tone test by (3). The value of OIP_3 obtained using both equations is the same, thus verifying the correctness of the result.

$$OIP_3 = P_{1dB\ output}\ (dBm) + 10dB = 13.3 + 10 = 23.3dBm \quad (2)$$

$$OIP_3 = \left(\frac{3}{2} * P_{input\ tones@output} - \frac{1}{2} * P_{3rd\text{-}order\ products}\right)$$

$$= (1.5*(0.22) - 0.5*(-46.0)) = 23.33dBm \quad (3)$$

TABLE 2. Final results compared with original design specifications of the LNA

Specification Name	Design Specification	Final Value
Centre frequency	1389.75MHz	1389.75MHz
Minimum bandwidth	451.5	451.5MHz
Maximum gain deviation over bandwidth	±1.5dB	±1.3dB
Small signal gain	18 – 21dB	18.5dB
Return loss (Input/Output)	<-10dB	Input = -11dB Output= -23.5dB
Noise Figure	2dB	2.18dB
Stability	0Hz to 9GHz	0Hz to 9GHz
P1dB	3dBm	13.5dBm
OIP3	13dBm	23.5dBm
Supply voltage	5V	5V
Current Consumption	20mA	18.6mA

Table 2 compares the final results with original specifications for the LNA implementation.

CONCLUSION

Design of the proposed LNA is the first step towards successful implementation of a bandpass sampling based RF front-end capable of receiving multiple GNSS frequencies. The design, simulation, implementation and test results prove that the LNA successfully satisfied requirements of wide bandwidth, high gain, high linearity and low noise figure and a solution was also found against low frequency instability. Furthermore, compared to other similar implementations, this work has a higher gain and yet has comparable noise figure, linearity and power consumption. Different methods of stabilization have been considered and their results tabulated. The implementation was perfected over a number of versions and the intermediate results of every version are also detailed. Future modifications could include addition of a linear RF filtering stage after the LNA to remove the unwanted frequency band from 1300MHz to 1559MHz. Work on such a filter has already begun at the GNSS Receiver Group of our university.

ACKNOWLEDGMENT

The research leading to these results has received funding from the European Community Seventh Framework Programme (FP7/2007-2013) under grant agreement number 227890.

REFERENCES

[1] Navstar GPS, Global Positioning System Interface Control Document, ICD-GPS-200D, 10th October, 1993

[2] Galileo Open Service, Signal in Space Interface Control Document, (OS SIS ICD, Draft 1), February 2008

[3] Global Navigation Satellite System (GLONASS), Interface Control Document, Coordination Scientific Information Center, Moscow, 2002

[4] Rodney G. Vaughan, Neil L. Scott, & D. Rod White, "The Theory of Bandpass Sampling", IEEE Transactions on Signal Processing. Vol. 39, No. 9. September 1991

[5] Dennis M. Akos, Michael Stockmaster, James B. Y. Tsui, & Joe Caschera, "Direct Bandpass Sampling of Multiple Distinct RF Signals", IEEE Transactions on Communications, Vol. 47, No. 7, July 1999

[6] Ngai Wong & Tung-Sang Ng, "An Efficient Algorithm for Downconverting Multiple Bandpass Signals Using Bandpass Sampling", IEEE International Conference on Communications Proceedings, Helsinki, Finland, June 2001, v. 3, p. 910-914

[7] Ching-Hsiang Tseng & Sun-Chung Chou, "Direct Downconversion of Multiband RF Signals Using Bandpass Sampling", IEEE Transactions on Wireless Communications, Vol. 5, No. 1, January 2006

[8] Jie-Cherng Liu, "Bandpass Sampling of Multiple Single Sideband RF Signals", ISCCSP 2008, Malta, 12-14 March 2008

[9] Mark L. Psiaki, Steven P. Powell, Hee Jung, & Paul M. Kintner, "Design and Practical Implementation of Multifrequency RF Front Ends Using Direct RF Sampling", IEEE Transactions on Microwave Theory and Techniques, Vol. 53, No. 10, October 2005

[10] S. Blaakmeer, E.A.M. Klumperink, B. Nauta, D.M.W. Leenaerts, "An Inductorless Wideband Balun-LNA in 65nm CMOS with Balanced Output", 33rd European Solid State Circuits Conference, ESSCIRC, 11-13 Sept. 2007 , München, Germany .

[11] Md. M. Hossain, "Design of RF Front End for Multi-Band Multi-System GNSS Receivers", M.Sc. Thesis, University of Gävle, January, 2008.

[12] P. Kovár, P. Kacmarík, F. Vejražka, "Universal Front End for Software GNSS Receiver", Proceedings of the 13th IAIN World Congress, Stockholm, 27-30 October 2009. Published by the Nordic Institute of Navigation

[13] Veena G Dikshit, "Development of Global Navigation Satellite System (GNSS) Receiver", DRDO-IISc Program on Mathematical Engineering Workshop, Banglore, September 2007

Available: http://pal.ece.iisc.ernet.in/PAM/work07.html

[14] Datasheet for BFP420 NPN Silicon RF Transistor, Infineon, April, 2007

[15] Reinhold Ludwig, Pavel Bretchko, RF Circuit Design – Theory and Applications, Prentice Hall 2000, ISBN 0130953237

[16] David M. Pozar, Microwave Engineering, Third Edition, Wiley 2004, ISBN 0471448788

[17] RFDude.com, RFdude.com LLC,

Available: http://tools.rfdude.com/RFdude_Smith_Chart_Program/RFdude_smith_chart_program.html

PUBLICATION 3

S. Thombre, J. Nurmi, “Bandpass-Sampling based GNSS Sampled Data Generator – A Design Perspective”, Proceedings of the *2012 International Conference on Localization and GNSS (ICL-GNSS 2012)*, June 2012 in Starnberg, Germany.

Bandpass-Sampling based GNSS Sampled Data Generator – A Design Perspective

Sarang Thombre, Jari Nurmi
Department of Computer Systems
Tampere University of Technology (TUT)
Tampere, Finland
{sarang.thombre, jari.nurmi}@tut.fi

Abstract— **This paper presents the design methodology and simulation results of a sampled data generator (SDG) designed to operate over the whole range of Global Navigation Satellite System (GNSS) frequencies (1164MHz to 1615.5MHz). An SDG is actually a radio front-end (RF FE) that generates digital samples at intermediate frequency (IF), which can be recorded and used in the future as test input to a baseband processing unit. The proposed SDG is based on the bandpass-sampling principle and works over combined (but overlapping) frequency bands of all three GNSS constellations (American Global Positioning System (GPS), European Galileo system and the Russian GLONASS system). It is observed that there is currently no commercially available multi-system multi-frequency GNSS SDG. This paper hopes to fill this gap. First, the overall architecture of the proposed SDG is described, followed by the detailed design of each block, namely, the bandpass & bandstop filters, and the frequency planning for the bandpass-sampling analog to digital converter (ADC).**

Keywords-Navigation, bandpass-sampling, sampled data generator

I. INTRODUCTION

The GNSS Receiver Research Group at Tampere University of Technology is engaged in the design and construction of an embedded dual-frequency, dual-system GNSS receiver. One of the challenges faced is the availability of test input. Hardware simulators of GNSS signals are very expensive and hence an alternate solution was needed. One possible solution was to record data samples from a temporarily accessible GNSS simulator. This spawned the idea for constructing a GNSS sampled data generator which would provide at the output a sampled data stream of the GNSS signal input from the simulator. Also, it would be really beneficial if a wideband architecture were used so that most of the GNSS signals could be accommodated.

For some years there has been considerable interest in bandpass-sampling as a means to digitize a wide spectrum of frequencies while keeping the sampling frequency at reasonable levels. In [1], bandpass sampling of a single band of frequencies was considered which evolved to sampling multiple distinct RF bands in [2], [3] and [4]. In [5], bandpass sampling of multiple distinct single-sided (complex) RF bands was accomplished. In all these works, either GPS and GLONASS or GPS and GSM signals were integrated and that too, just L1 band signals in each case. [6] claims to use bandpass sampling and digital filtering for direct conversion of GPS L1 (C/A) and L1/L2 (P(y)) codes into digital intermediate frequency (IF). Therefore, it can be observed that information on using bandpass-sampling to sample the entire GNSS band of frequencies is not yet covered in past literature. Research work has already begun towards this goal and [7] describes the design, construction and results of the low noise amplifier (LNA) to be used in the present SDG.

The layout of the paper is as follows: in Section II the overall block architecture of the SDG and the frequency spectrum of interest have been briefly described. It also presents a summary of the LNA developed in [7]. Then the design and simulation results of the bandpass and bandstop filters are presented in Section III. Section IV presents the frequency planning for the bandpass-sampling ADC. Finally, Section V contains the results of the SDG functional blocks discussed in the earlier sections.

II. BLOCK ARCHITECTURE OF BANDPASS-SAMPLING SDG

The bandpass-sampling architecture works on the principle of down-conversion to a digital IF by direct sampling of the RF signal bandwidth (BW) using intentional, yet non-destructive aliasing. The RF signal from the antenna is filtered (to remove out-of-band noise), amplified and then directly digitized using a high speed ADC. The clock frequency along with proper band-select filters allows selecting the right frequency band to downconvert from the received RF spectrum. After the ADC, either the digital data is stored on a hard-drive or digital filters are employed to separate the IF bands to be demodulated in the baseband processor.

Fig. 1 shows the block diagram of a bandpass-sampling SDG proposed in this research work. Fig. 2 shows the frequency spectrum over which this SDG is designed to operate. It includes all the GNSS frequency bands and extends from 1164MHz to 1300MHz and again from 1559MHz to 1615.5MHz. Frequencies between 1300MHz and 1559MHz are not interesting to us and this 'empty' band allows for the use of the bandpass-sampling technique.

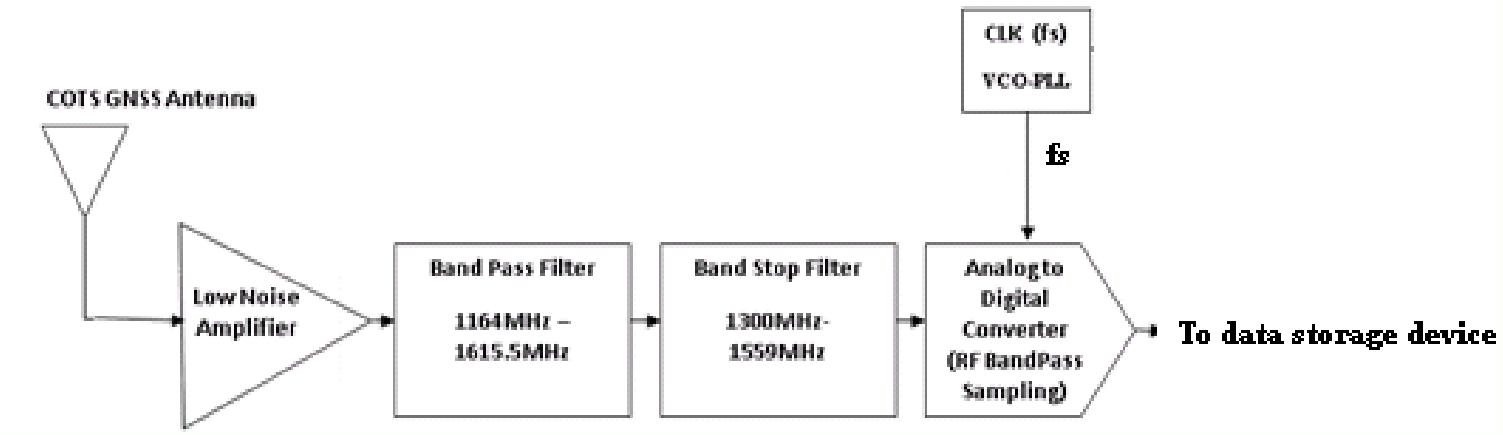

Fig. 1 Block-diagram of the proposed bandpass-Sampling SDG

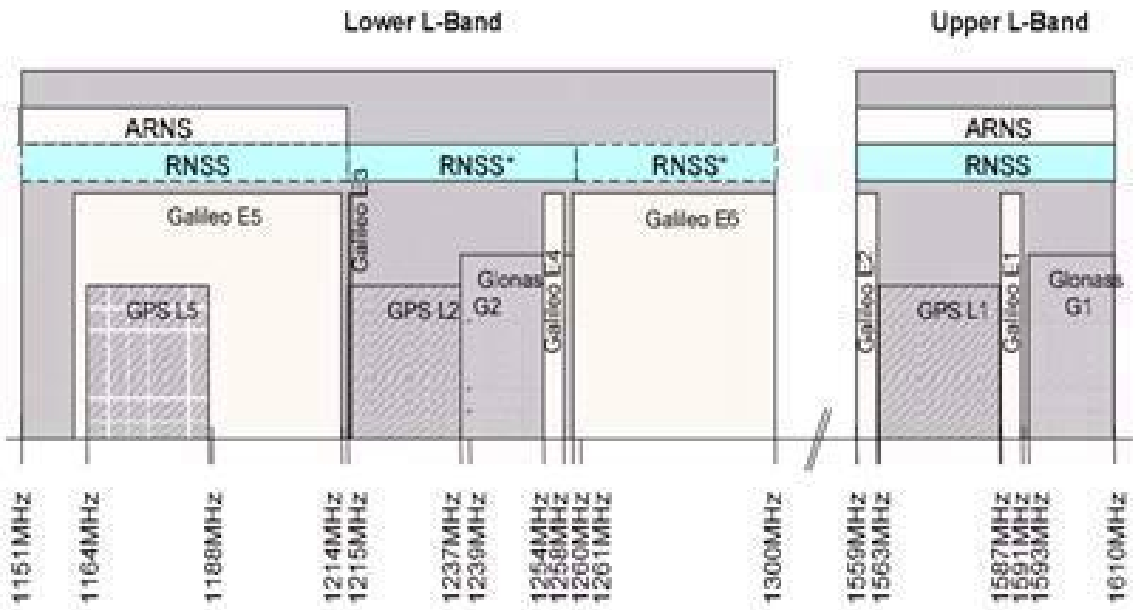

Fig. 2 Frequency spectrum of the proposed SDG [8]

Criteria for optimum sampling frequency according to the Nyquist-Shannon theorem is that it should be at least twice the highest frequency component in the given frequency band [9]. Any frequency lower than this 'Nyquist minimum' will cause aliasing of the frequency band in the digital domain. That is, the frequency band in the digital domain may fold onto itself causing information from two or more distinct channels within the band to interfere when they overlap on one another.

Table 1. Design specifications for bandpass and bandstop filters

Parameter	**Bandpass Filter**	**Bandstop Filter**
Topology	Chebyshev	Chebyshev
Filter order	7	7
Pass band ripple	3dB	3dB
Lower cut-off frequency (f_l)	1164MHz	1300MHz
Upper cut-off frequency (f_u)	1615.5MHz	1559MHz
Pass band IL	≤ 3dB	≤ 3dB
Stop band IL	> 3dB	> 3dB
Input impedance	50 Ohm	50 Ohm
Output	50 Ohm	50 Ohm
Return Loss	≥ 15dB	≥ 15dB

However, aliasing is not always destructive. What if there are certain gaps in between the individual channels within the larger RF band? Lower sampling frequency could be used to ensure intentional aliasing that is not destructive to the original information. That is, ensure that the digitized channels fold on the original RF band, but they fall exactly in the spacing in between individual channels, so that the information in any one channel is retained intact.

Thus, according to the theory of bandpass-sampling, the sampling frequency can be lower than Nyquist criteria and yet (by careful frequency planning) not cause destructive aliasing. The minimum sampling frequency can now be the twice of the bandwidth to be sampled instead of twice of the highest frequency component. Thus, the resulting sampling rate can be significantly reduced. The sampled band is then replicated at every harmonic multiple of the sampling frequency.

The first stage of the proposed SDG is the low noise amplifier. The LNA has already been designed, simulated and implemented on PCB. Its results have been published in [7]. Designed to be unconditionally stable with gain of over 18dB and noise figure of 2dB over a considerable bandwidth of about 450MHz, the achieved results conformed quite well to the specifications. Final implementation results include a gain of 18.5dB at the centre frequency with a nominal variation of ±1.3dB over the desired bandwidth. The noise figure obtained is 2.18dB and the amplifier stability range extends from 0Hz to 9GHz. Very high degree of linearity is achieved with output 1dB compression at +13dB and output third order intercept at +23dB.

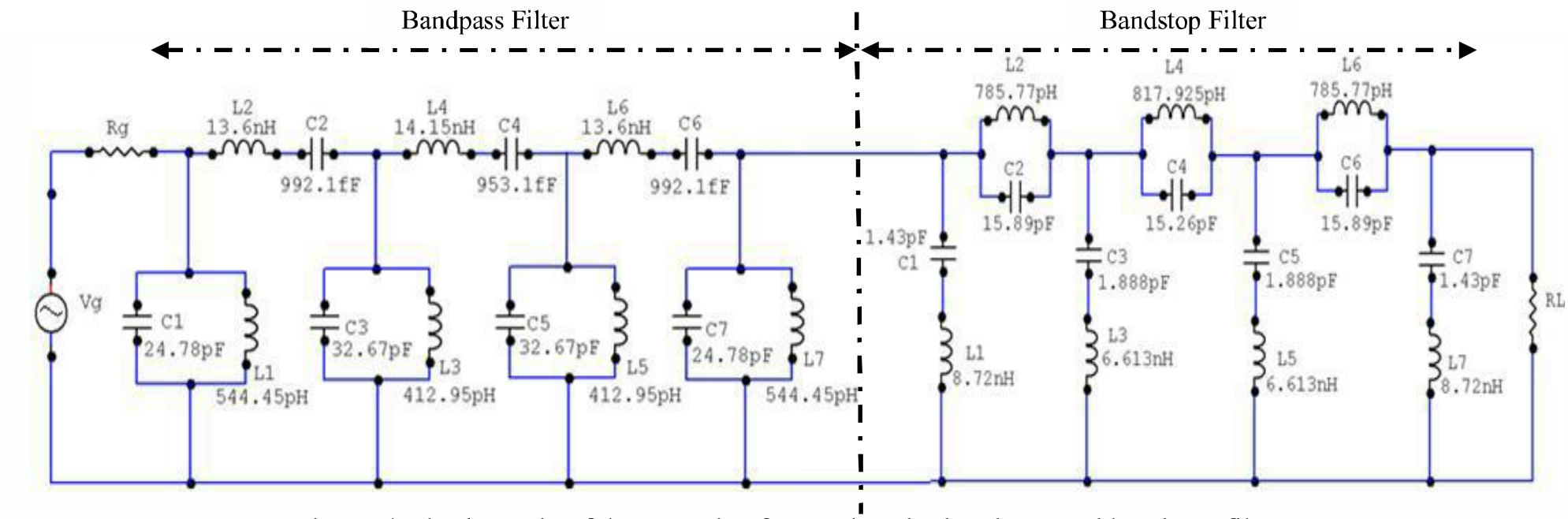

Fig. 3 Final schematic of the cascade of seventh order bandpass and bandstop filters

III. FILTER DESIGN

GNSS frequency bands extend from 1164MHz to 1300MHz and from 1559MHz to 1615.5MHz. Hence to isolate these two bands, it needs one RF bandpass filter (1164MHz to 1615.5MHz) followed by an RF bandstop filter (1300MHz to 1559MHz). To prove the concept, these two filters were designed as seventh-order LC Chebyshev filters.

Table 1 presents the design specifications for the two filters. The design methodology adopted was as follows: first, the seventh-order low pass Chebyshev filter was designed. Next, transformation from low pass to bandpass or bandstop filter was performed using the principle of component transformations. Fig. 3 shows the final schematic of the cascade of the seventh-order bandstop and bandpass filters. The results in graphical format are presented in the Section V.

IV. FREQUENCY PLANNING FOR BANDPASS SAMPLING

Frequency planning was carried out based on the theory presented in [1], [2], [3], [4], [5], [6], [10], [11], and [12]. For a set of two real distinct frequency bands (as in the case of the proposed SDG), appropriate sampling frequency can be computed based on the simultaneous fulfillment of certain conditions. It is possible to prepare a Matlab program to compute all those sampling frequency values which satisfy all these requirements simultaneously. The requirements are given in (1)-(8):

BW of interest (BWoI) = band 1 + band 2

= (1300MHz – 1164MHz) + (1615.5MHz – 1559MHz)

= 192.5MHz (1)

Center frequency of band 1 (f_{c1}) = 1232MHz (2)

Center frequency of band 2 (f_{c2}) = 1587.25MHz (3)

Minimum sampling frequency (f_{smin}) = 2* BWoI (4)

$$IF = f_{IFi} \begin{cases} = \text{Rem}\left(\frac{f_{ci}}{f_s}\right) & \text{if Int}\left[\frac{f_{ci}}{\frac{f_s}{2}}\right] = \text{even} \\ = f_s - \text{Rem}\left(\frac{f_{ci}}{f_s}\right) & \text{if Int}\left[\frac{f_{ci}}{\frac{f_s}{2}}\right] = \text{odd} \end{cases} \quad (5)$$

$$f_{IFi} > \frac{BWi}{2} \quad (6)$$

$$f_{IFi} < \frac{f_{s-BWi}}{2} \quad (7)$$

$$|f_{IF1} - f_{IF2}| \geq \frac{BW_1 - BW_2}{2} \quad (8)$$

Where: Int[x] = largest integer smaller than x (or simply, rounding off to the nearest lower integer)

i = the frequency band number

A Matlab program was written to find out possible values of sampling frequency and intermediate frequencies. These computations are applicable for sampling real GNSS signals. If the GNSS signals are converted into complex/analytic by using Hilbert transformer and then sampled, the sampling frequency requirement is further relaxed. Fig. 4 shows the frequency spectrum of two complex signals with all important frequency points marked on the diagram.

(9)-(12) give the criteria that must be simultaneously satisfied by the sampling frequency in case of complex GNSS signals [5].

$$n_1 \leq \text{Int}\left[\frac{f_{c1}}{B_1 + B_2}\right] \quad (9)$$

$$\text{Int}\left[\frac{n_1 * f_{c2}}{f_{c1}}\right] \leq n_2 \leq \text{Int}\left[n_1 * \left(\frac{f_{c2}}{f_{c1}}\right) + \frac{f_{c2}}{f_{c1}}\right] \quad (10)$$

$$\frac{f_{H2} - f_{L1}}{n_2 - n_1 + 1} \leq f_s \leq \frac{f_{L2} - f_{H1}}{n_2 - n_1} \quad (11)$$

$$\frac{f_{H2} - f_{L1}}{n_2 - n_1} \leq f_s \leq \frac{f_{L2} - f_{H1}}{n_2 - n_1 - 1} \quad (12)$$

(11) should be used if the position of the resulting sampled bands should be as shown in Fig. 5. While if their positions should be as in Fig. 6, then (12) should be used. The solid frequency band denotes spectra of original signal and the dashed frequency band denotes a replica after sampling the original band.

Thus, the procedure for obtaining a range of valid sampling

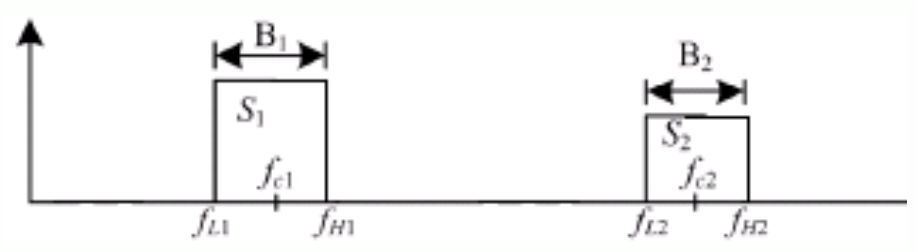

Fig. 4 Frequency spectrum of two complex RF signal bands

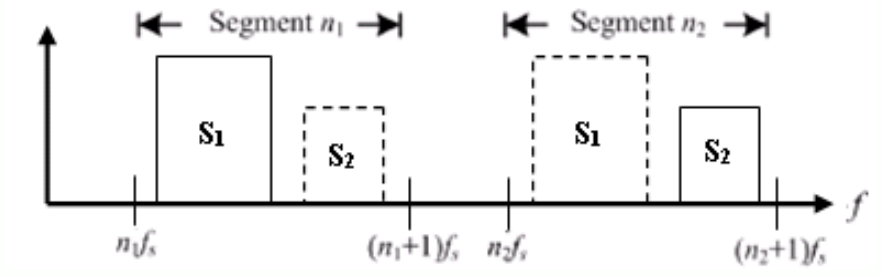

Fig. 5 First possibility of arranging the sampled and original bands

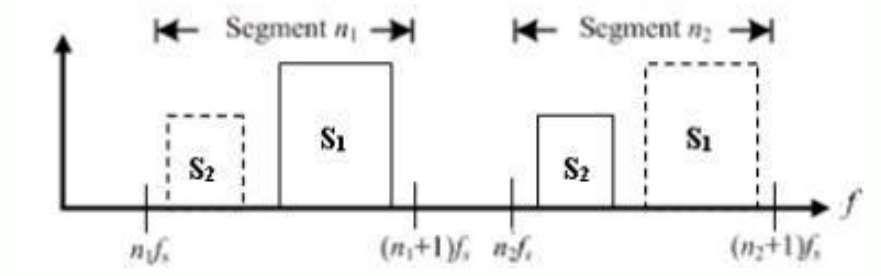

Fig. 6 Second possibility of arranging the sampled and original bands

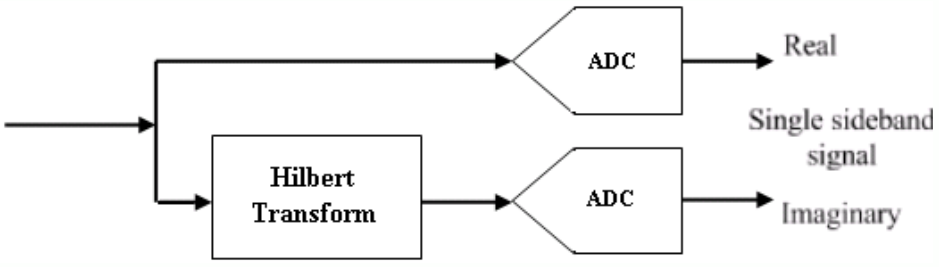

Fig. 7 Block diagram of complex bandpass-sampling

frequencies for two complex RF signals is: first, choose an appropriate n_1 using (9); next, choose an appropriate n_2 using (10), and last, using (11) or (12) compute the range of sampling frequencies. (13) gives the new position of the sampled IF band when complex GNSS signals are considered [5].

$$f_c^m = m*f_s + \mathrm{rem}(f_c, f_s) \qquad (m = 0, \pm1, \pm2, \pm3\ldots\ldots) \qquad (13)$$

Where: f_c^m = Center frequency of the m^{th} replica of the sampled band

$\mathrm{rem}(f_c, f_s)$ = Remainder from the ratio of f_c and f_s

In general, the desired bands can be down-converted using a much lower minimum sampling frequency in case of complex bandpass sampling than real bandpass sampling. Also, the choice of valid sampling frequencies is much narrower in case of real sampling and even a slight deviation from calculated sampling frequency may cause harmful aliasing [5]. However, in case of complex sampling, because there are two signal streams (Inphase & Quadrature), the ADC would need to be replicated in both the signal branches, as shown in Fig. 7.

The limitation due to this additional hardware requirement outweighs the advantage of a relaxed sampling frequency, and hence, using real bandpass sampling is more beneficial. Finally, if this spectrum is passed through a suitable low pass IF filter, it is possible to extract the desired bands downconverted to baseband. This describes the concept of frequency translation by bandpass sampling.

V. Results

Fig. 9 shows the results for the cascade of the bandpass and bandstop filters. Together the two filters effectively isolate the desired GNSS frequency bands (1164MHz to 1300MHz and

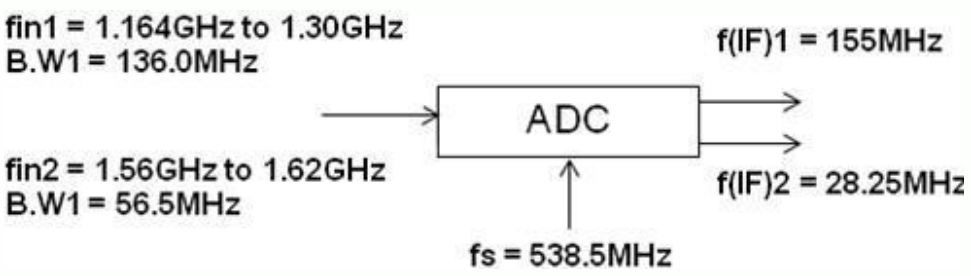

Fig.8 Most convenient sampling frequency and resultant intermediate frequencies.

1559MHz to 1615.5MHz). The phase response shows that the cascade is stable at all frequencies since the gain never exceeds 0dB. The group delay, however, is quite high (around 30nsec) close to the cut-off frequencies and the effect of this group delay on later stages of GNSS signal processing is yet to be determined.

Fig. 8 shows the most convenient values for the sampling frequency and the resulting IF for the two input bands of interest. The required sampling frequency is over 500MHz, which would be stretching the limits of state-of-art ADCs. The implementation of such an ADC is currently under research in the GNSS Receiver Research Group of Tampere University of Technology.

Conclusion

This paper presented an architectural design of a bandpass-sampling based sampled data generator for GNSS applications. After the successful implementation of the LNA, the next logical step was the design and simulation of the filter stage and frequency planning for the bandpass-sampling ADC. By incorporating the theoretical criteria for bandpass-sampling frequency into software, this process is automated for all possible input signal conditions. Both, real and complex sampling is considered. Due to obvious advantage in resource utilization of real bandpass-sampling, its complex equivalent is not considered further. For real sampling, the optimum sampling frequency was computed to be 538.5MHz and the resulting digital intermediate frequencies were 28.25MHz and 155MHz. In spite of the numerous advantages of the direct bandpass-sampling architecture, there are a number of challenges, such as SNR degradation due to Jitter, noise aliasing and quantization or high power consumption and subsequent heating of the ADC due to the extremely large sampling frequency requirement. The effect of these nonlinearities on the final digitized output has yet to be quantified and can be a subject of further research along with possible solutions to mitigate their effects, possibly by efficient digital signal processing of the digitized intermediate frequency signals.

References

[1] R. G. Vaughan, N. L. Scott, & D. R. White, "The Theory of Bandpass Sampling", IEEE Transactions on Signal Processing. Vol. 39, No. 9. September 1991

[2] D. M. Akos, M. Stockmaster, J. B. Y. Tsui, & J. Caschera, "Direct Bandpass Sampling of Multiple Distinct RF Signals", IEEE Transactions on Communications, Vol. 47, No. 7, July 1999

[3] N. Wong & Tung-Sang Ng, "An Efficient Algorithm for Downconverting Multiple Bandpass Signals Using Bandpass Sampling", IEEE International Conference on Communications Proceedings, Helsinki, Finland, June 2001, v. 3, p. 910-914

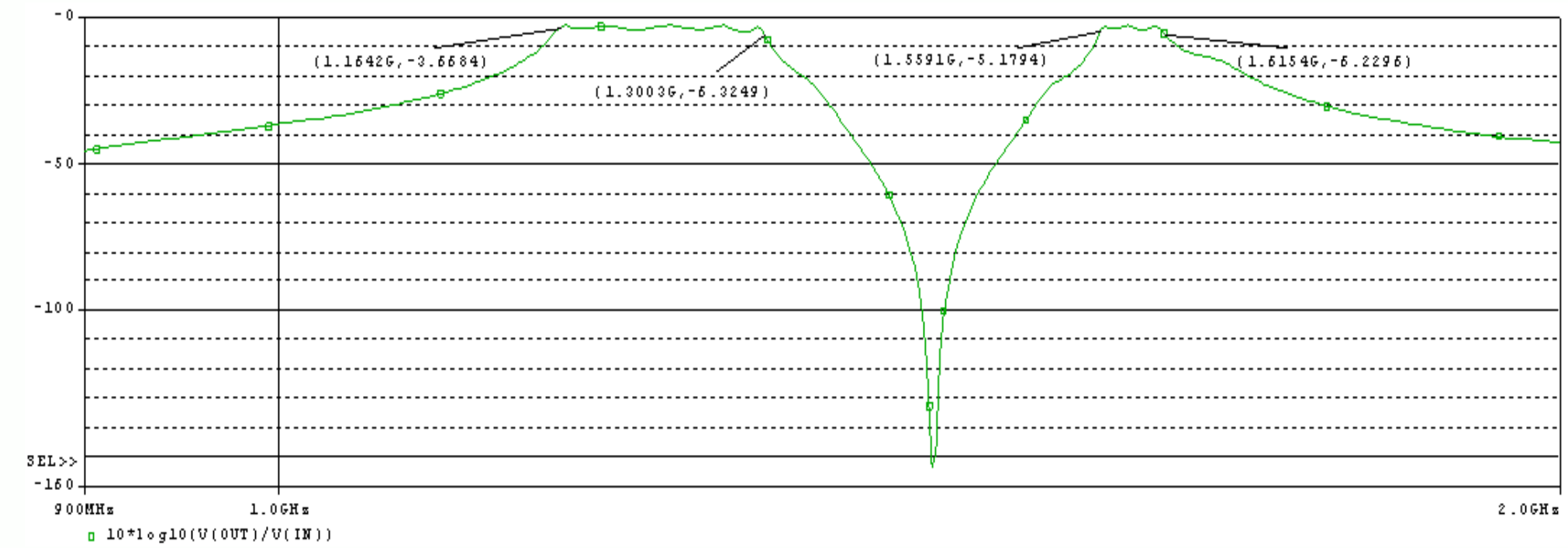

(a)

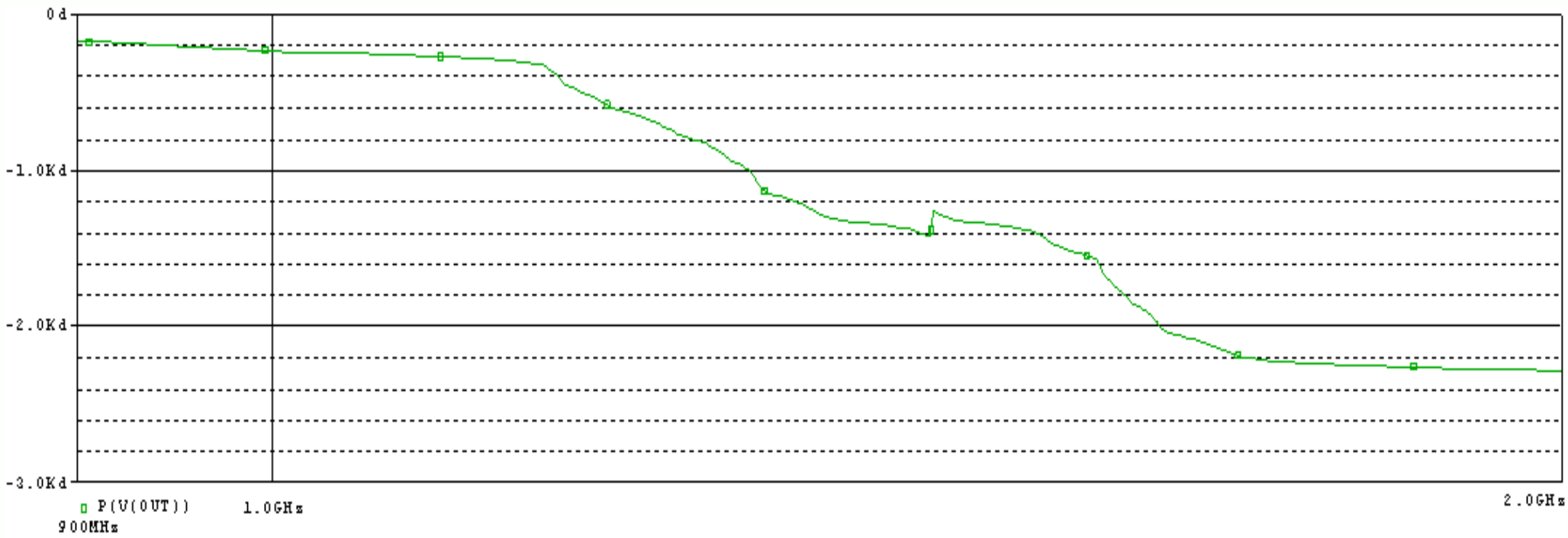

(b)

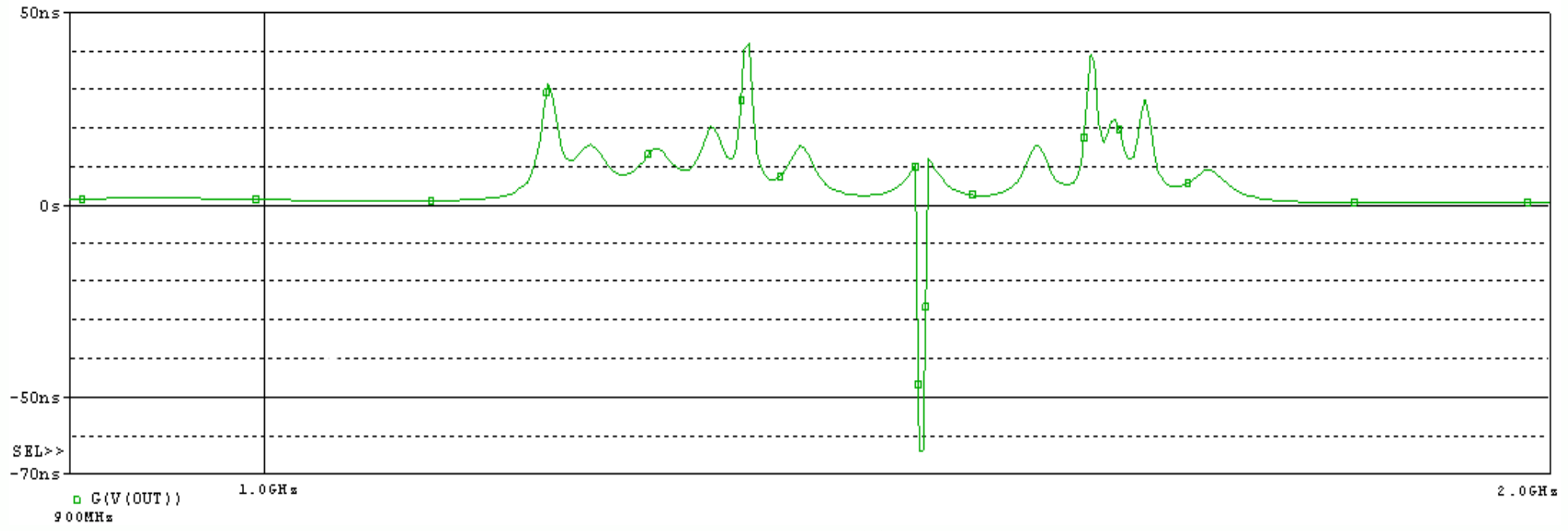

(c)

Fig. 9 Bandpass – bandstop cascade filter results: (a) Amplitude response (b) Phase response (c) Group delay response

[4] Ching-Hsiang Tseng & Sun-Chung Chou, "Direct Downconversion of Multiband RF Signals Using Bandpass Sampling", IEEE Transactions on Wireless Communications, Vol. 5, No. 1, January 2006

[5] Jie-Cherng Liu, "Bandpass Sampling of Multiple Single Sideband RF Signals", ISCCSP 2008, Malta, 12-14 March 2008

[6] M. L. Psiaki, S. P. Powell, H. Jung, & P. M. Kintner, "Design and Practical Implementation of Multifrequency RF Front Ends Using Direct RF Sampling", IEEE Transactions on Microwave Theory and Techniques, Vol. 53, No. 10, October 2005

[7] S. Thombre, H. Hurskainen, J. Nurmi, "Wideband, High Gain, High Linearity, Low Noise Amplifier for GNSS Frequencies with

Compensation for Low Frequency Instability", Proceedings of the 5th Advanced Satellite Multimedia Systems (ASMS) Conference, September 2010 in Cagliari, Italy.

[8] GALILEO (2005). "Mission High Level Definition (HLD) (2002), European Commission Communication Document", W. Doc. 2002/05 - Version 3, 23. September 2002. Available at: http://www.galileoju.com, http://www.esa.int/esaNA/index.html.

[9] C. Shannon, "Communication in the Presence of Noise", Proceedings of the IRE, January 1949

[10] Yi-Ran Sun, "Generalized Bandpass Sampling Receivers for Software Defined Radio", Doctoral Dissertation, Royal Institute of Technology, Stockholm 2006

[11] M. L. Psiaki, D. M. Akos, J. Thor, "A Comparison of Direct RF Sampling and Down-Convert & Sampling GNSS Receiver Architectures", ION GPS/GNSS 2003, 9-12 September 2003, USA

[12] A. Latiri, L. Joet, P. Desgreys, P. Loumeau, "A Reconfigurable RF Sampling Receiver For Multistandard Applications", Académie Des Sciences, 2006

PUBLICATION 4

E. P. Serna, S. Thombre, M. Valkama, S. Lohan, V. Syrjälä, M. Detratti, H. Hurskainen, J. Nurmi, “Local Oscillator Phase Noise Effects on GNSS Code Tracking”, *InsideGNSS*, Nov/Dec 2010, pg 52-62.

The article can be downloaded from http://www.insidegnss.com/auto/novdec10-Thombre.pdf

PUBLICATION 5

S. Thombre, J. Raasakka, M. Valkama, S. Lohan, H. Hurskainen, J. Nurmi, "Local Oscillator Phase Noise Effects on Phase Angle Component of GNSS Code Correlation", Proceedings of the *2011 International Conference on Localization and GNSS (ICL-GNSS 2011)*, June 2011 in Tampere, Finland.

Local Oscillator Phase Noise Effects on Phase Angle Component of GNSS Code Correlation

Sarang Thombre, Jussi Raasakka, Heikki Hurskainen, Jari Nurmi
Department of Computer Systems
Tampere University of Technology (TUT)
Tampere, Finland
{sarang.thombre, jussi.raasakka, heikki.hurskainen, jari.nurmi}@tut.fi

Mikko Valkama, Simona Lohan
Department of Communications Engineering
Tampere University of Technology (TUT)
Tampere, Finland
{elena-simona.lohan, mikko.e.valkama}@tut.fi

***Abstract*— This paper demonstrates the effect of radio frequency (RF) front-end (FE) free-running local oscillator (FRO) phase noise (PN) on the phase component of the Global Navigation Satellite System (GNSS) code correlation product. It is observed that as FE PN increases, it adversely affects the stability of the phase component of the code correlation. The tracking loops in baseband processing of a GNSS receiver attempt to lock on to the frequency, delay and phase of the correlation product. Until these parameters are varying within acceptable bounds, set by the dynamics handling capability of the tracking loops, the tracking loops are able to successfully track the satellite signal. However, PN increases the variation in phase of the correlation product calculated over consecutive epochs and may also cause loss of tracking lock if these variations go beyond phase locked loop (PLL) pull-in range thresholds. This paper studies the relation between FRO PN and phase component of correlation through numerical analysis, and software simulations by artificially contaminating GNSS signal stream with PN of increasing variance and checking the result on the standard deviation (SD) of the phase component of correlation product. Based on these results, this paper recommends certain maximum limits on the FE PN in order to keep the SD of phase component below the one-sigma phase error limits of the PLL used in typical GNSS tracking loops.**

Keywords-Phase noise, phase, correlation, navigation, local oscillator, Phase locked loop

I. INTRODUCTION

In [1], a relation between the FRO PN and code correlation properties was presented. Specifically, the effects on correlation magnitude losses, signal to noise ratio (SNR) and variance were considered. These effects were studied under different pre-detection integrations times (PIT). However, the effect of PN on phase component of correlation product was not discussed. It is now clear that along with magnitude, the phase information of the correlation product is also significant to estimate probability of tracking loop loss of lock. [2] gives a detailed explanation on the different tracking loop measurement errors and specifically 1-sigma tracking errors in the PLL tracking loops. It also provides rule-of-thumb tracking thresholds for these errors. However, it does not give any performance estimates of the phase component of correlation at different levels of input phase noise. Overall it has been observed that there is not much literature available on exact quantification of the harmful effects of FE phase noise on the phase information of GNSS correlation product. This paper aims to fill exactly this void. Fig. 1 shows the block diagram of a typical GNSS receiver considered for this study.

The layout of the paper is as follows: in Section II the phase noise model used for this study has been briefly described. Then a theoretical/numerical relation is made for the phase angle of correlation product in terms of the phase noise variance of a FRO. In Section III, the Matlab model that performs the correlation between phase contaminated and pure pseudorandom (PRN) codes is explained. In Section IV, the negative effects of FE PN on phase component of correlation product are described in more detail. Also, a short description of the tracking loop measurement errors in the PLL and their relation with FE phase jitter is included. In Section V, the results of the numerical and Matlab-based simulations are presented. This section also presents certain recommendations on the maximum limit of allowable front-end PN in order to maintain phase error in code correlation within acceptable threshold of the PLL. Finally, in the conclusion section, the results and key findings are summarized.

II. PHASE NOISE MODEL AND THEORETICAL ANALYSIS

This study uses the same free running oscillator phase noise model as that used in [1]. The oscillator can be represented as in (1).

$$w(t) = A(t)\cos\left(2\pi f_0 t + \varphi(t)\right) \quad (1)$$

Where phase is (φ), amplitude is (A) and frequency is (f_0). In a general case there is phase and amplitude noise, as well as distortion, which makes both A and φ functions of time. For a FRO, the overall phase noise in dBc/Hz at a certain frequency offset f_m in terms of the phase noise variance per unit time (σ_φ^2) is given by (2) [1].

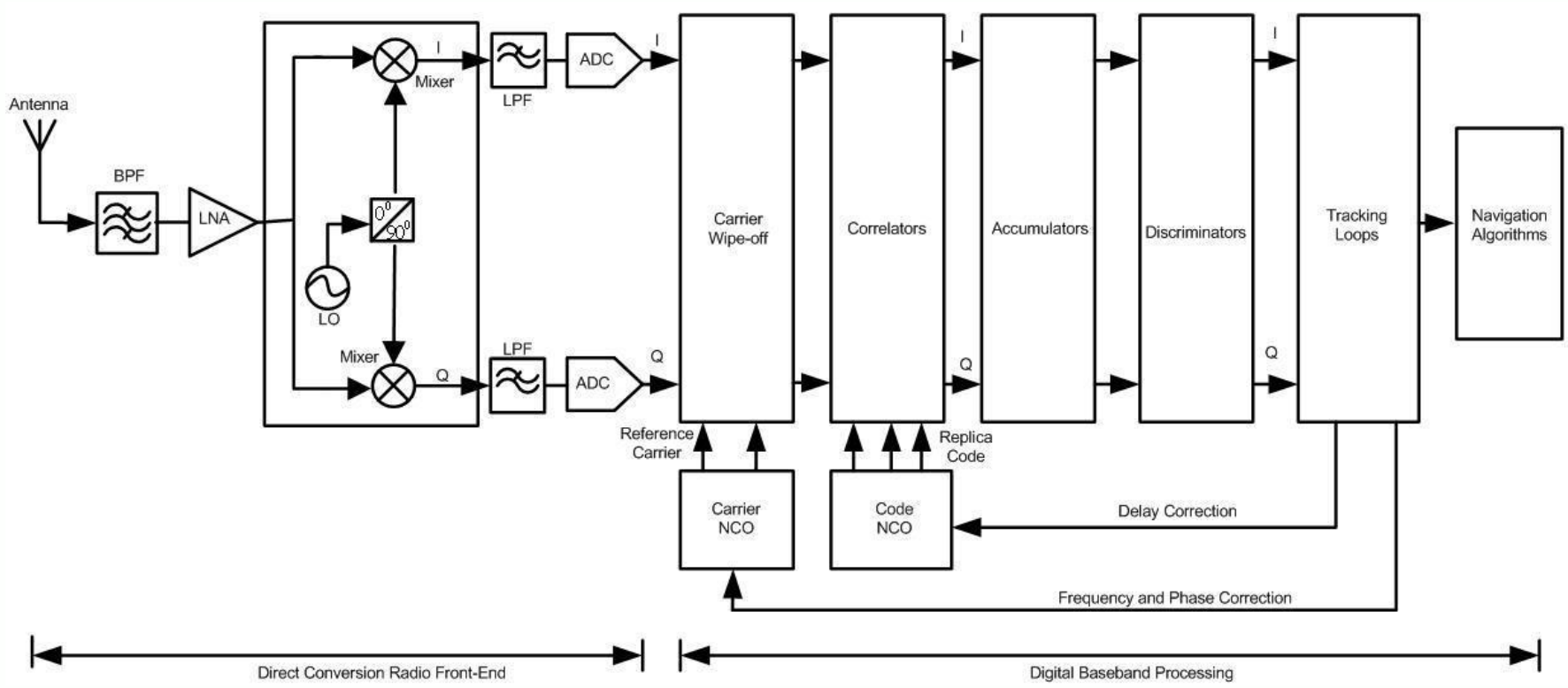

Fig. 1 Block-diagram of a GNSS direct-conversion receiver

$$L(f_m) \approx 10log\left(\frac{\sigma_\varphi^2}{(2\pi f_m)^2}\right) dBc/Hz \quad (2)$$

Where the units of σ_φ^2 are radian^2 per second (Rad^2/sec).

[1] also gives a relation for the maximum value of correlation peak in the frequency domain, which is obtained at zero time lag, as show in (3).

$$R(\tau = 0) = \frac{1}{T}\int_0^T e^{j\Phi(t)}\, dt \quad (3)$$

Where R(τ) is the correlation of the baseband version of the incoming signal with the locally-generated PRN code signal when the local oscillator is affected by phase noise. The value $\tau = 0$ corresponds to a perfect time-match between the codes of the incoming signal and the locally-generated version. T is the PIT and phase noise is represented as a complex exponential of φ(t). As mentioned in [1], the model for phase noise of a free-running oscillator is a cumulative sum of uncorrelated Gaussian random variables over the whole past history (in other words, integral of white Gaussian noise). Such cumulative sum or integral gives a process with linearly-increasing variance over time, and is thus non-stationary. However, the complex exponential of phase noise ($e^{j\varphi(t)}$), in turn is a stationary random variable and hence can be used instead of just phase noise (φ(t)) [3], [4], [5]. Equation (3) can be represented diagrammatically as in Fig. 2 meaning that code correlation peak in the presence of phase noise can be modeled as a filtered random variable ($e^{j\varphi(t)}$), passed through an integrator filter.

The goal is to find a relation for the phase angle of the correlation product. Since R(0) in (3) already represents a complex quantity, it should be enough to represent its angular component as an arctangent of the ratio of its imaginary and real components. Therefore, solving (3) is necessary.

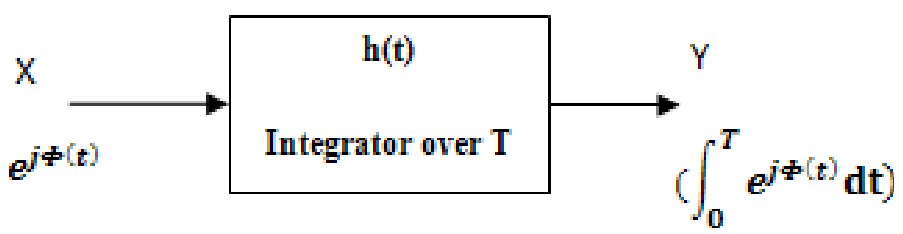

Fig. 2 Equivalent model of phase noise effect

Equation (3) can be simplified by using Euler's theorem for complex numbers.

$$R(0) = \frac{1}{T}\int_0^T (\cos(\varphi(t)) + j\sin(\varphi(t))\, dt \quad (4)$$

$$= \frac{1}{T}\int_0^T (\cos(\varphi(t))\, dt + j\,\frac{1}{T}\int_0^T (\sin(\varphi(t))\, dt \quad (5)$$

Now that R(0) is represented as a complex number in the form ($I + jQ$), the angular component can be represented as the arctangent of the ratio of imaginary component over real component.

$$angle\,[R(0)] = arctan[\frac{\frac{1}{T}\int_0^T (\sin(\varphi(t))dt}{\frac{1}{T}\int_0^T (\cos(\varphi(t))dt}] \quad (6)$$

Cancelling the common multiplier (1/T) and substituting sine and cosine terms by their Taylor series expansions (in terms of φ(t) upto seven co-efficients) gives (7):

$$= arctan[\frac{\int_0^T (\frac{\varphi(t)^1}{1!} - \frac{\varphi(t)^3}{3!} + \frac{\varphi(t)^5}{5!} - \frac{\varphi(t)^7}{7!} + \frac{\varphi(t)^9}{9!} - \frac{\varphi(t)^{11}}{11!} + \frac{\varphi(t)^{13}}{13!})dt}{\int_0^T (1 - \frac{\varphi(t)^2}{2!} + \frac{\varphi(t)^4}{4!} - \frac{\varphi(t)^6}{6!} + \frac{\varphi(t)^8}{8!} - \frac{\varphi(t)^{10}}{10!} + \frac{\varphi(t)^{12}}{12!} - \frac{\varphi(t)^{14}}{14!})dt}] \quad (7)$$

φ(t) being a Gaussian random variable (grv) (since phase noise of a free-running oscillator is a grv), it is not trivial to solve (7) further to obtain a closed-form theoretical solution. Another possibility is to plot the results for angle[R(0)] using numerical analysis of (7). For this, the time domain has to be discretized so that the continuous integral will transform into a summation over the integration interval (T) as shown in (8). The numerical analysis of (8) is further described in Section III.

$$= arctan[\frac{\sum_0^T (\frac{\varphi(t)^1}{1!} - \frac{\varphi(t)^3}{3!} + \frac{\varphi(t)^5}{5!} - \frac{\varphi(t)^7}{7!} + \frac{\varphi(t)^9}{9!} - \frac{\varphi(t)^{11}}{11!} + \frac{\varphi(t)^{13}}{13!})}{\sum_0^T (1 - \frac{\varphi(t)^2}{2!} + \frac{\varphi(t)^4}{4!} - \frac{\varphi(t)^6}{6!} + \frac{\varphi(t)^8}{8!} - \frac{\varphi(t)^{10}}{10!} + \frac{\varphi(t)^{12}}{12!} - \frac{\varphi(t)^{14}}{14!})}] \quad (8)$$

It is possible to represent the relation using numerical and software simulations since the accuracy of (3) has already been proven theoretically in [1] while studying the effect of PN on magnitude of the correlation peak.

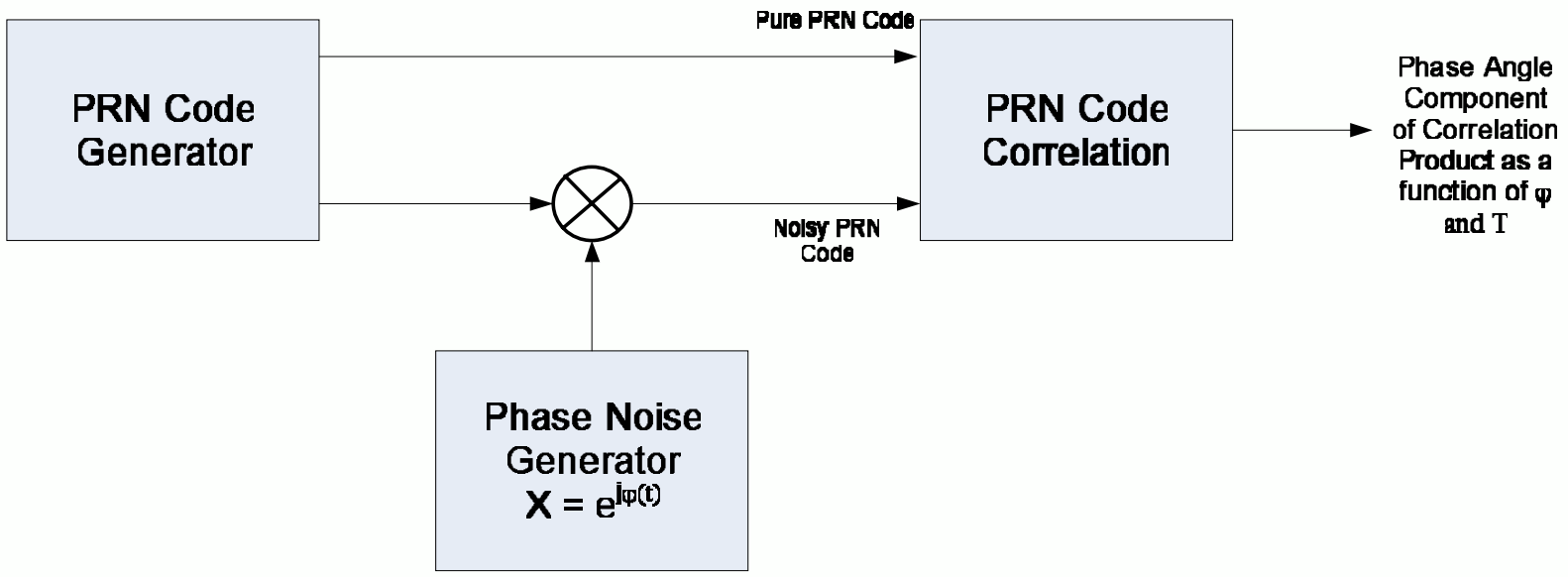

Fig. 3 Matlab model for PRN code correlation

III. Simulation Stage

A Matlab based program was generated which performed correlation between two versions of the same GPS PRN code. The first version was contaminated with different amounts of FRO phase noise in order to replicate a real world PRN code received from the RF front-end and after the carrier strip-off process. The other version of the PRN code was kept 'pure' to mimic the local replica code as generated in every GNSS receiver. The Matlab model is diagrammatically represented in Fig. 3.

The user may select the satellite vehicle number whose PRN code is to be generated. The free running oscillator phase noise was defined in terms of unit time variance (σ_Φ^2). Therefore, the total phase noise variance per chip of the PRN code over the coherent integration period (T) is given by (9):

$$PN_{Variance} = \frac{T\sigma_\Phi^2}{L_{PRN}} \quad (9)$$

Where, L_{PRN} equals to the length of the PRN code. The multiplication of the phase noise with incoming PRN code can be simulated in Matlab as a multiplication of phase noise vector and PRN code vector. A random number 'noise' vector ($\varphi(t)$) with zero mean, unity standard deviation and length of 1023 bits was created and its variance was changed to the required phase noise variance using $PN_{Variance}$ calculated in (9). The overall phase (φ_{k+1}) can be generated as $\varphi_k + w_k$, where k=0,1,2,..., and w_k is a white Gaussian zero-mean sequence with variance σ^2, which is given by $\sigma_\varphi{}^2.T_c$, where T_c is one chip duration.

Now that we have the phase noise vector of the desired length and noise variance, it can be multiplied with a PRN code vector in order to produce a noisy PRN code similar to the one obtained from the RF front-end in a real world GNSS receiver. Correlation of this noisy code is performed with a 'pure' PRN code over multiple iterations and the angular component of correlation result is stored. Once all iterations for one value of phase noise variance are complete, it is possible to calculate the SD of the angular component for the present value of σ_Φ^2. This SD represents the 1-sigma error due to phase jitter in the GNSS baseband tracking loops. σ_Φ^2 is varied from 0 Rad^2/s to 10^4 Rad^2/s on a logarithmic scale and the (SD) of angle of correlation peak is plotted over this range.

Numerical analysis using (8) is performed by using the same phase noise vector $\varphi(t)$ as that used in the simulation set-up described above. Using this vector the Taylor series components are created as in (8) and the numerator and denominator summation terms are generated. Since the length of $\varphi(t)$ vector is already scaled by integration time T, summation over T is equivalent to performing a cumulative sum of all elements of the resultant vectors inside the numerator and denominator summations. Next, the arctangent of the ratio of these summation terms gives the angular component of the correlation peak for that epoch. After calculating the angular component over multiple epochs, the standard deviation is calculated and plotted for every value of input phase noise.

IV. Phase Noise Effects on Phase of Correlation

Figs. 4, 5, and 6 help demonstrate the negative effect of FE PN on phase of correlation peak. In Fig. 4 the instantaneous phase value of correlation peak is plotted over 200 consecutive epochs of code correlation for small and large phase noise variance per unit time values of 10 rad^2/sec and 10000 rad^2/sec, respectively. The phase variations between consecutive epochs are much lower when PN from front-end is low. The limited variation in phase can be better observed in the polar I/Q plot of Fig. 5. Therefore, if such a correlation product is fed to the tracking loop PLL, it will be able to maintain lock as the phase variations between consecutive epochs may be within its pull-in range. When the FE phase noise is increased, the correlation peak phase variations are distinctly higher as shown in Fig. 6. In case such a signal is fed to the tracking loop PLL, it would not be able to track such random and huge changes in phase over consecutive epochs. Comparing polar plots of Figs. 5 and 6, it is noticed that the amplitude of the correlation results is degraded when the phase noise is higher. It proves that the front-end phase noise has an adverse effect to the correlation peak magnitude [1].

The real parameter of interest is the 1-sigma tracking loop measurement error, in degrees, for the PLL. Equations (10) and (11) give the rule-of-thumb threshold for this error for a PLL considering navigation data-less & with-data signals respectively [2].

$$\sigma_{PLL(data-less)} = \sqrt{\sigma_{tPLL}^2 + \sigma_v^2 + \theta_A^2} + \frac{\theta_e}{3} \leq 30° \quad (10)$$

$$\sigma_{PLL(with-data)} = \sqrt{\sigma_{tPLL}^2 + \sigma_v^2 + \theta_A^2} + \frac{\theta_e}{3} \leq 15° \quad (11)$$

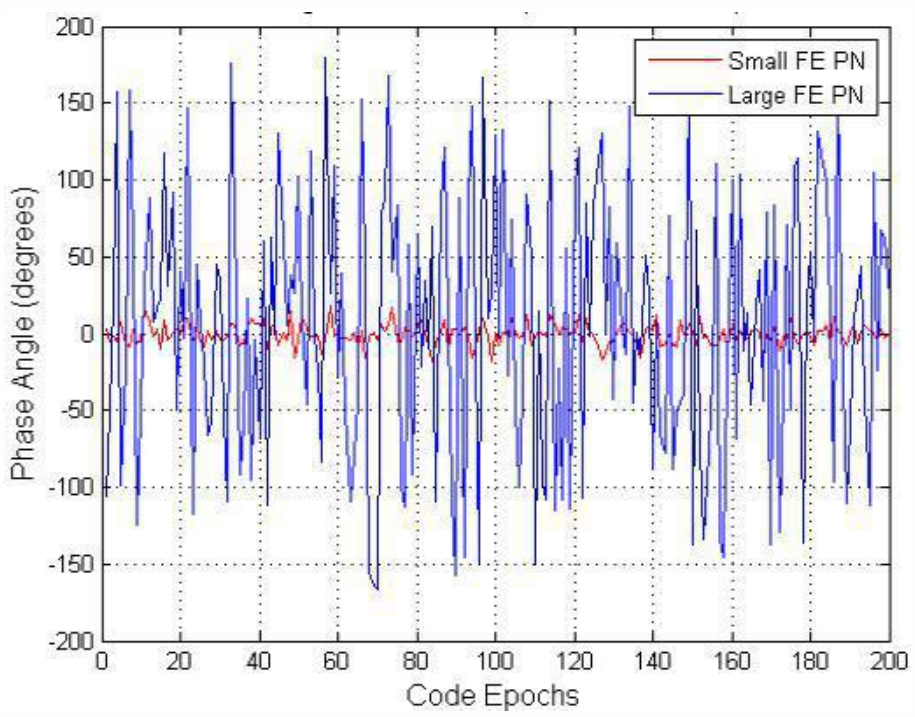

Fig. 4 Phase angle of correlation peak over 200 consecutive epochs for small and large FE PN

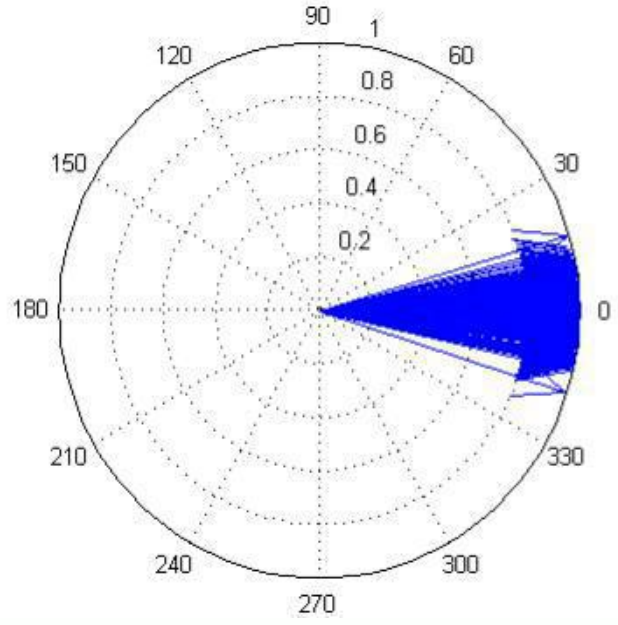

Fig. 5 Polar I/Q plot of the correlation peak over 200 consecutive epochs for small FE PN

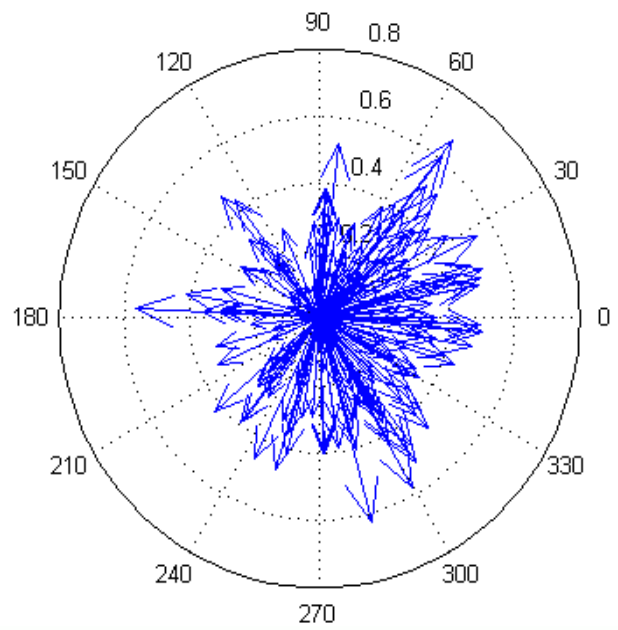

Fig. 6 Polar I/Q plot of the correlation peak over 200 consecutive epochs for high FE PN

Where, σ_{tPLL} is the 1-sigma PLL thermal noise in degrees, σ_v is the 1-sigma vibration induced oscillator jitter in degrees, θ_A= Allan variance induced oscillator jitter and $\theta_e$is dynamic stress error. For simplicity if we assume typical values for σ_v = 1.4 degrees and θ_A = 1.4 degrees and θ_e = 15 degrees, we can derive rule-of-thumb thresholds for 1-sigma PLL thermal noise in degrees so that overall PLL noise remains below 30

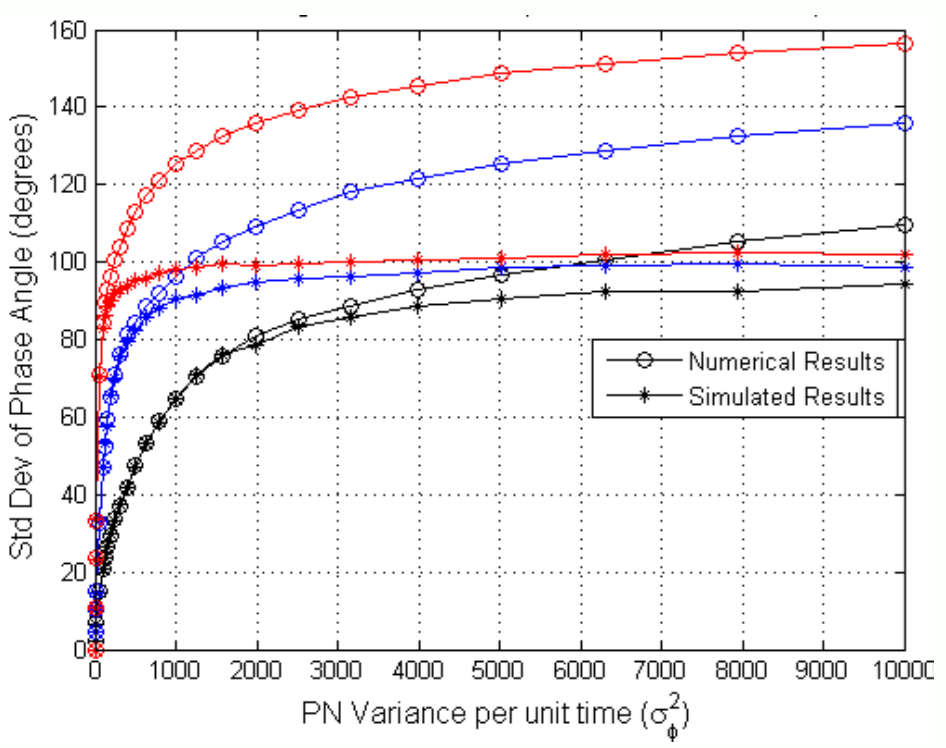

Fig. 7 Linear plot of standard deviation of phase component of correlation peak versus PN variance per unit time for different PIT values

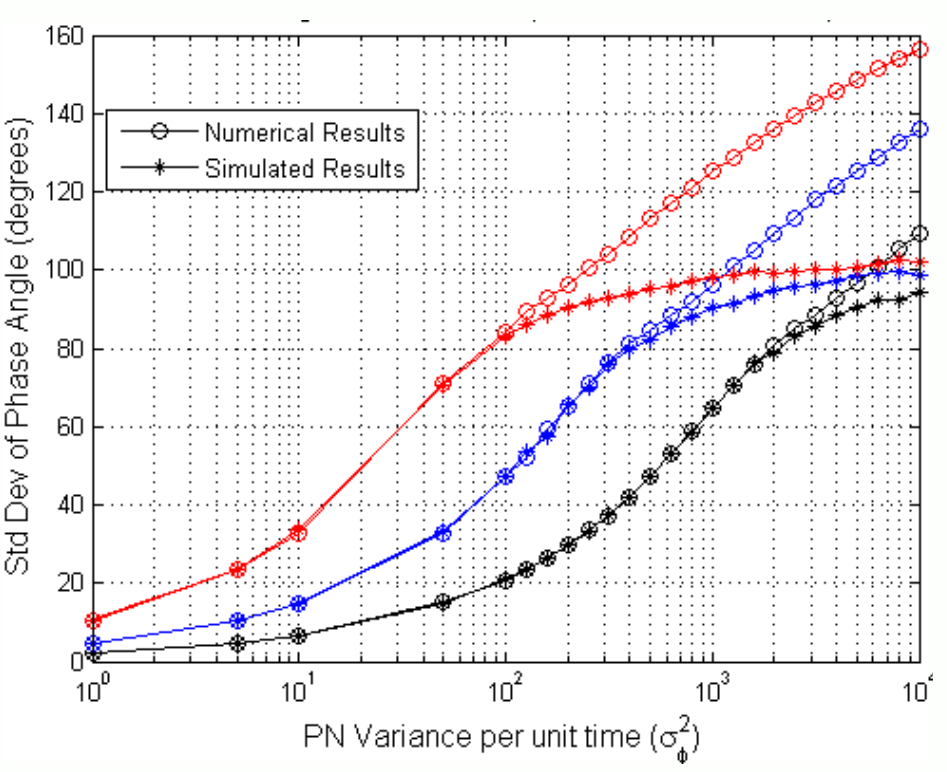

Fig. 8 Logarithmic plot of standard deviation of phase component of correlation peak versus PN variance per unit time

degrees (data-less) as in (12) and below 15 degrees (with-data) as in (13).

$$\sigma_{tPLL(data-less)} \leq 10^{o} \quad (12)$$

$$\sigma_{tPLL(with-data)} \leq 25^{o} \quad (13)$$

Therefore, now that we know the maximum allowed phase error for a PLL to be able to keep track, we can easily locate the front-end PN at which the SD of phase component of correlation (which is equivalent to the 1-sigma PLL thermal noise phase error σ_{tPLL}) increases beyond 10 degrees.

V. RESULTS AND MATHEMATICAL ANALYSIS

This section gives details of the results obtained from software simulation of code correlation by correlating two versions of the same PRN code: one contaminated with phase noise and the other in its original uncontaminated state. The phase angle of correlation product is of focus and more specifically, the SD of this angular component over multiple consecutive code epochs. Fig. 7 shows the SD of phase component versus phase noise variance per unit time for three

TABLE 1. Maximum FE PN to maintain Std. Dev. of phase angle below 10°

(Navigation data is present)

PIT (msec)	Maximum Phase Noise (dBc/Hz)	
	f_m = 10KHz	f_m = 1MHz
4	-83	-123
20	-89	-129
100	-96	-136

TABLE 2. Maximum FE PN to maintain Std. Dev. of phase angle below 25°

(Navigation data is absent)

PIT (msec)	Maximum Phase Noise (dBc/Hz)	
	f_m = 10KHz	f_m = 1MHz
4	-74	-114
20	-82	-122
100	-88	-128

different PIT values: 4 msec, 20 msec and 100 msec. Fig. 8 shows the same curves but now the noise variances (x-axis) is plotted on a logarithmic scale to enlarge the effects at lower values of phase noise. This is because the phase angle deviations already increase well beyond 10 degrees at quite low values of phase noise. The figures show that the phase SD increases with increasing phase noise, until it saturates at around 100 degrees. Further increase in phase noise has no effect on the phase variations. The figures also show the effect of increasing PIT on the phase errors. Greater the value of PIT, greater is the SD of phase for the same amount of FE PN.

Tables 1 and 2, show the maximum front-end phase noise (in dBc/Hz at frequency offsets of 10 KHz and 1 MHz), in order to maintain SD of phase angle below 10 degrees and 25 degrees respectively. The results show that, for 4 msec PIT, to maintain the phase angle SD of 10 degrees (navigation data present), maximum FE PN allowed (at 1 MHz offset) is -123 dBc/Hz. But if the PIT is increased to 20 msec, maximum PN requirements become more stringent by around 6 dB. If the phase noise were measured at 10 KHz offset, maximum PN requirements are scaled by around 40 dBs. If the maximum allowed PLL phase error is 25 degrees (navigation data absent), the phase noise requirements can be relaxed by 7-9 dB for each of the PIT values respectively. One can also see that the results for maximum FE PN obtained in this study are comparable to the values obtained in the initial study performed in [1], where effect of PN on magnitude, SNR and variance of correlation product were studied.

The results obtained from the numerical analysis match very closely to the simulated curves for most values of phase noise. At higher noise levels however, the numerical results continue to degrade, thus diverging from the simulated results as they saturate around 100 degrees (after all, the Taylor series expansion is an approximation of sine and cosine terms). This also proves that the results obtained are theoretically, numerically, and technically sound.

One point to remember is that the PN source used for this study is a free-running local oscillator. Noise performance of such a device is quite poor. In practical receiver front-ends there may be a free-running local oscillator to heterodyne the receiver signal from RF to baseband and the resulting complex signal will be tracked by a phase-locked loop which tries to follow the phase noise. This tracking is successful at least for the noise components inside the PLL bandwidth. But the noise components with higher frequencies cannot be tracked conveniently and may lead to loss of phase lock. Nevertheless, the overall noise performance of such a device is far superior and hence the threshold for maximum FE PN to maintain thermal noise PLL error below 10 degrees or 25 degrees would be much higher. Further studies on comparing the effects of free-running oscillator and realistic frequency sources on correlation parameters are currently being performed in our Department.

CONCLUSION

The standard deviation of phase angle component of correlation is the same as the 1-sigma thermal phase error of the PLL in the GNSS baseband tracking loops. The current paper presented an initial approximation of the effects of FE PN on this phase error of the PLL. Simulated correlation results are supported by theory and numerical methods. The results of this study can be used by designers of RF front-end local oscillators as it establishes a conservative upper bound on the phase noise originating from these devices in order to maintain the phase error in the baseband tracking loops below a certain threshold under specific conditions of coherent integration periods. The results obtained are comparable to those obtained in an earlier study on the effects of FE PN on magnitude losses and SNR of correlation peak, and hence can be considered an alternative method of determining the maximum front-end phase noise in a GNSS receiver. Future work could include the study of PN originating from more realistic frequency sources, for example, PLL in the RF FE.

ACKNOWLEDGMENT

The research leading to these results has received funding from the European Community's Seventh Framework Programme (FP7/2007-2013) under the GRAMMAR project, grant agreement number 227890. This work has been partly supported also by the Academy of Finland. Prof. Robert Pichè of the Department of Mathematics, Tampere University of Technology has provided assistance in the numerical analysis.

REFERENCES

[1] E. P. Serna, S. Thombre, M. Valkama, S. Lohan, V. Syrjälä, M. Detratti, H. Hurskainen, J. Nurmi, “Local Oscillator Phase Noise Effects on GNSS Code Tracking”, InsideGNSS, Nov/Dec 2010, pg 52-62.

[2] E.D. Kaplan, C. Hegarty, “Satellite Signal Acquisition, Tracking and Data Demodulation”, in *Understanding GPS: Principles and Applications*, 2nd ed., Artech House Inc, Norwood USA, 2006, pp 183-191

[3] T. Schenk, “Phase Noise”, in *RF Imperfections in High-rate Wireless Systems*, Springer 2008, ISBN: 978-1-4020-6902-4, Chapter 4

[4] V. Syrjälä, M. Valkama, N.N. Tchamov, J. Rinne, “Phase Noise Modelling and Mitigation Techniques in OFDM Communication

Systems", Wireless Telecommunication Symposium, 2009, WTS 2009, April 2009, Pages1-7

[5] A. Demir, "Computing Timing Jitter from Phase Noise Spectra for Oscillators and Phase-Locked Loops with White and 1/f Noise", IEEE Transactions on Circuits and Systems-I, vol. 53, no. 9, Sept 2006.

[6] G. Casella, R. Berger, "Common Families of Distributions" in *Statistical Inference*,2nd ed., Duxbury 2002, Pacific Grove, USA, Chapter 3, pp-102

[7] Dartmouth College, "The Gaussian (Normal) Distribution", Lecture Notes of *Engs 27 — Discrete and Probabilistic Systems*, Lecture 20, Winter 2003.

[8] S.Male, "Double Exponential Transformation Methods in Numerical Integration with Applications in Volterra Integral Equations", Department of Mathematics of the University of Portsmouth, May 2006, Chapter 2, pp 20-21

PUBLICATION 6

S. Thombre, N. N. Tchamov, S. Lohan, M. Valkama, J. Nurmi, “Effects of Radio Front-end PLL Phase Noise on GNSS Baseband Correlation”, accepted to *NAVIGATION, Journal of the Institute of Navigation*, March 21, 2014.

Effects of Radio Front-end PLL Phase Noise on GNSS Baseband Correlation

Sarang Thombre, Nikolay N. Tchamov, Simona Lohan, Mikko Valkama, and Jari Nurmi

Department of Electronics and Communications Engineering

Tampere University of Technology, Korkeakoulunkatu 1, Tampere 33720, Finland.

{sarang.thombre, nikolay.n.tchamov, elena-simona.lohan, mikko.e.valkama, jari.nurmi}@tut.fi

Phone: +358 404 819 476

Keywords: code tracking, charge-pump PLL, reference oscillator, VCO, loop filter, signal to noise ratio, thermal noise, power spectral density.

Acknowledgements: This research work has received support from the Tampere Doctoral Programme in Information Science and Engineering (TISE), and Nokia Foundation. It has also been partially supported by the Academy of Finland (under the projects: 251138 "Digitally-Enhanced RF for Cognitive Radio Devices", and 256175 “Cognitive Approaches for Location in Mobile Environments”). We wish to gratefully acknowledge each of these institutions.

Abstract

This article presents a study of Global Navigation Satellite System (GNSS) receiver correlation performance in the presence of phase noise (PN) originating from the radio front-end's phase-locked loop (PLL). Various constituent PLL sub-blocks, such as the reference oscillator (RO), phase & frequency detector (PFD), voltage controlled oscillator (VCO), loop filter and frequency dividers contribute to the overall PN of the PLL. The PLL phase noise modeling is covered in detail. Correlation performance of GNSS baseband tracking loops is then calculated as a function of several PLL design parameters such as, the VCO thermal PN, loop filter bandwidth (BW), frequency division ratio (FDR) and the receiver correlator's pre-detection integration times (PIT). The effects of these parameters on the signal to noise ratio (SNR) of the correlation product are described and simulated. Based on the results of these simulations, we present guidelines for radio front-end PLL circuit design in order to maintain a minimum baseband correlation performance within the GNSS receiver.

Introduction

The phase variations due to phase noise originating from the local frequency synthesizer and imposed on the PRN codes will adversely affect the code correlation product [1]. However, the magnitude of this correlation loss has not yet been quantified in existing literature. It should be noted that phase noise from diverse sources such as, the radio frequency front-end (RF FE) PLL, the baseband tracking PLL [2], assumed neighboring channel signal powers and distant blocker powers (through reciprocal mixing [14]) may cause problems to GNSS correlation. However, in this article, only the RF FE PLL case is addressed. In two prior works [3][4], the phase noise of a free-running oscillator (FRO) from the RF FE has been analyzed and shown to deteriorate GNSS

receiver performance in terms of code and carrier correlation. In both its analytical and empirical forms, these studies concentrate on the scenario of using a simple FRO as the frequency synthesizer. The articles showed that the derived results are valid for FROs and stipulated to their validity for low-bandwidth PLL where the phase noise of the PLL-enclosed VCO is dominant. Unfortunately, the FRO model is not well suited to represent practical receiver frequency synthesizers [5], [6], [12] and hence, its direct use for specification of receiver designs is not appropriate.

Therefore, this paper presents the subsequent observations of receiver performance by utilizing the PLL as a practical frequency synthesizer. The results reveal that, there are both quantitative and qualitative differences in performance when compared to the FRO scenario. More specifically, this article will re-iterate [8] that the variance of PLL excess phase does not necessarily increase linearly with time, as in the case of FRO [3], but rather saturates with increasing pre-detection integration times. This phenomenon allows for a relaxed design of the frequency synthesizer as compared to FRO-only based synthesizer. It is shown that a decreased design effort and manufacturing cost can be achieved through careful PLL parameter selection.

Thus, the goal of this article is to provide, in both theoretical and empirical terms, guidelines and specifications for practical design of frequency synthesizers for GNSS receiver RF FE in terms of allowable phase noise power spectral density (PSD) masks. The differences in results obtained compared to the basic case of FRO are discussed throughout the length of the article. The results aim to benefit both academic and industrial research. Primarily, the approach is useful for the optimization of vendor-specific GNSS receiver designs. Specifications for the phase noise PSD of the PLL are derived for a large set of PLL parameters. The results are thus more exhaustive and useful than the boundary case of FRO, equivalent to a zero-bandwidth PLL. To adequately

represent practical frequency synthesizer performance, we have utilized a model for an integer charge-pump PLL (CHPLL) [6], [7], [12].

The structure of the article is as follows. Firstly, the CHPLL modeling and excess phase variance calculations are presented. The next section describes the theoretical stipulation on the relation between CHPLL PN and performance of the baseband code correlation. Further, numerical evaluations and simulations are performed to determine the effect of CHPLL PN on code correlation to prove the accuracy and efficiency of the theoretical stipulations. Based on numerical evaluations from the results obtained, performance bounds are set and recommendations are made for FE designs in terms of allowable PN PSD masks that their PLL can have in order to maintain a minimum code correlation performance in the GNSS baseband signal processing. This is the defining contribution of the article.

PLL Modeling

This section addresses two major points of the study. Firstly, the CHPLL phase noise model developed [11] is reviewed shortly and used here for analytical and empirical study of the GNSS receiver-end correlation. Secondly, the CHPLL excess phase variance calculations are presented to give preliminary stipulations for the design guidelines of CHPLL with respect to several GNSS pertinent parameters.

PLL Basics and Existing Phase Noise Models

A PLL encloses a FR VCO in a feedback loop where the VCO phase difference to a more stable RO phase is minimized [6]. In Fig. 1, a third-order CHPLL circuit diagram together with a linear time-invariant (LTI) phase-domain model [6] is presented. In Fig. 1 the PFD, charge-pump (CHP), loop filter (LF), VCO, and RO are represented through their transfer functions and

inherent noise sources. Publicized PLL phase noise models [6], [7], [11] often rely on LTI phase-domain representation or stochastic differential equation approach [9]. In this work, the LTI phase-domain approach is selected for its simplicity and interpretability of individual noise contributors.

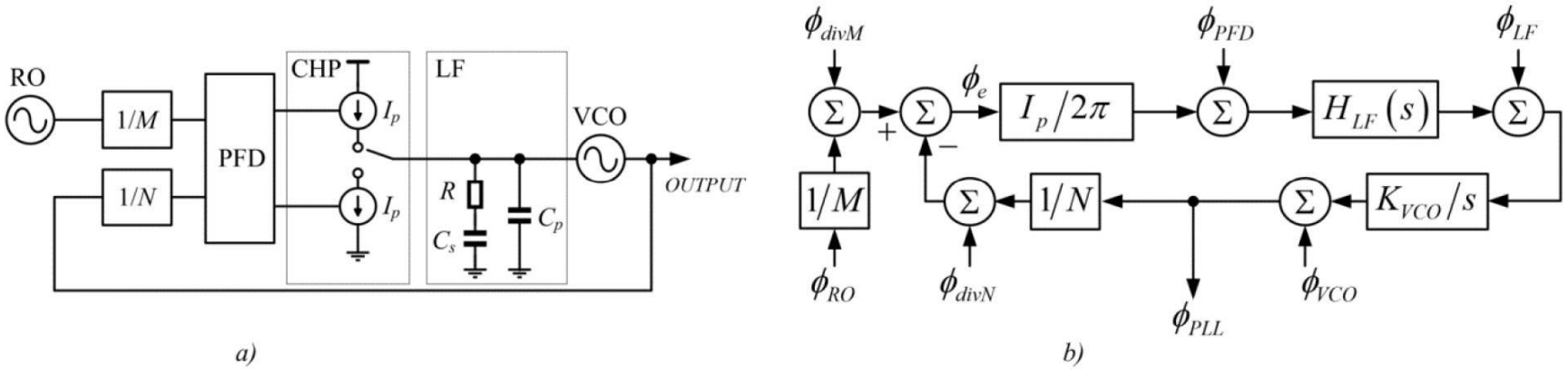

Fig. 1 Charge-pump PLL: a) block diagram, b) phase-domain LTI model.

Proposed Implementation of the LTI Phase-Domain Model of a CHPLL

We next summarize the proposed implementation [11] of the LTI phase-domain modeling of the CHPLL for use in the system-level simulations. The block diagram of a 3rd-order CHPLL is presented in Fig. 1a, while in Fig. 1b we present the LTI phase-domain model [6]. Each component is represented by its transfer function and associated noise source. To represent the major contributions to CHPLL phase noise, we include the VCO, RO, and PFD as the three major noise contributors. We note that in cases of severe adjacent channel interference [7], [12], also the PLL output buffering should be taken into account. Using the notations in Fig. 1, the contributions of these three noise sources to the CHPLL output Φ_{OUTPUT} are described by the loop transfer functions:

$$H_{VCO,PLL}(f) = \frac{\Phi_{OUTPUT}(f)}{\Phi_{VCO}(f)} = \frac{j2\pi fN}{j2\pi fN + I_p K_{VCO} H_{LF}(f)}, \quad (1)$$

$$H_{RO,PLL}(f)=\frac{\Phi_{OUTPUT}(f)}{\Phi_{RO}(f)}=\frac{NI_pK_{VCO}H_{LF}(f)}{M\left(j2\pi fN+I_pK_{VCO}H_{LF}(f)\right)}, \tag{2}$$

$$H_{PFD,PLL}(f)=\frac{\Phi_{OUTPUT}(f)}{\Phi_{PFD}(f)}=\frac{2\pi NK_{VCO}H_{LF}(f)}{j2\pi fN+I_pK_{VCO}H_{LF}(f)}. \tag{3}$$

In (1)-(3), we have denoted the loop filter response as:

$$H_{LF}(f)=\frac{1+j2\pi fRC_1}{j2\pi f\left(C_1+C_2+j2\pi fRC_1C_2\right)}, \tag{4}$$

where M, N, I_p, K_{VCO}, R, C_1, and C_2 represent the RO frequency division factor, the VCO frequency division factor, the charge-pump current, VCO tuning gain, and the loop filter passive components, respectively. The intrinsic noise contributions from the PFD before inclusion in the loop are assumed to be thermal noise, whereas the noise FR-RO and FR-VCO PSDs (due to thermal noise perturbations only) are the result of integrated thermal noise [3],[8].

The excess phase $\Phi_{PLL}(t)$ of the CHPLL is generated as discrete time series in the Matlab environment as follows [11]. Firstly, bilinear transform from *s*-domain to *z*-domain of the transfer functions (1)-(3) provides a bank of filters whose inputs are independent Gaussian random processes, as shown in Fig. 2. The branches implementing the VCO and RO excess phases consist of two cascaded filters, the first of which acts as an ideal integrator for the Gaussian random processes [4][10][11], scaled to properly represent the VCO and RO, respectively. As the intrinsic noise of the PFD/CP is represented here by thermal noise, its branch consists of a single filter. Secondly, the RO, VCO, and PFD individual contributions are summed together to form the total CHPLL output excess phase $\Phi_{PLL}[n]$.

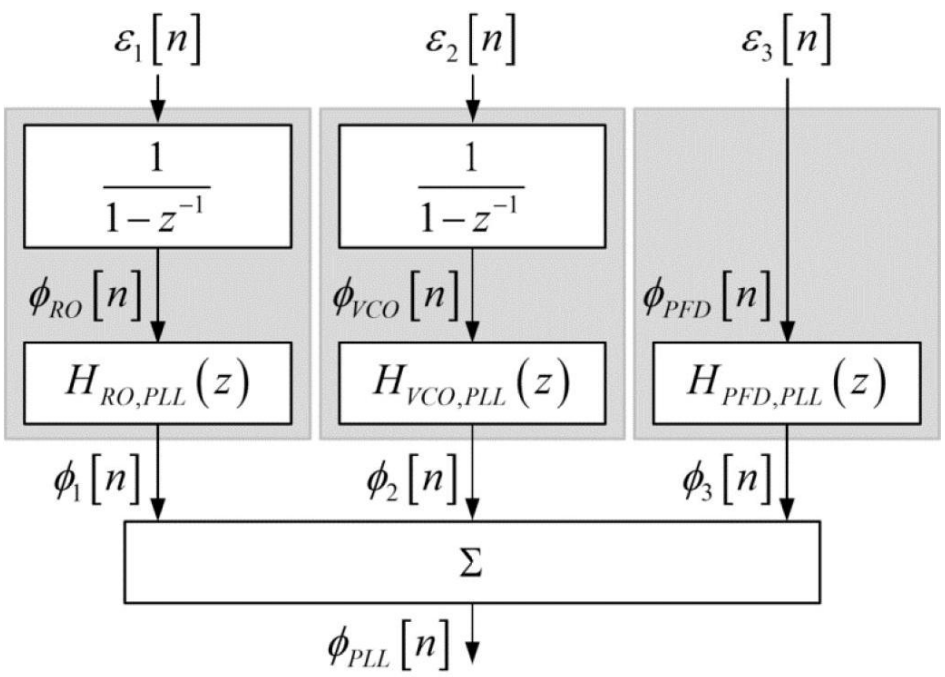

Fig. 2 Filter bank model for generating CHPLL output, taking into account the excess phase characteristics of reference oscillator, voltage controlled oscillator and phase-frequency discriminator.

The resulting CHPLL phase PSD, denominated by $P_{\Phi}(f)$ is then calculated as:

$$P_{\Phi}(f) = P_{\Phi,VCO-in-PLL}(f) + P_{\Phi,RO-in-PLL}(f) + P_{\Phi,PFD-in-PLL}(f), \tag{5}$$

where:

$$P_{\Phi,VCO-in-PLL}(f) = \left|H_{VCO}(f)\right|^2 \left|H_{ii,sr}(f)\right|^2 4\pi^2 f_{c,VCO}^2 c_{w,VCO}, \tag{6}$$

$$P_{\Phi,RO-in-PLL}(f) = \left|H_{RO}(f)\right|^2 \left|H_{ii,sr}(f)\right|^2 4\pi^2 f_{c,RO}^2 c_{w,RO}, \tag{7}$$

$$P_{\Phi,PFD-in-PLL}(f) = \left|H_{PFD}(f)\right|^2 c_{w,PFD}, \tag{8}$$

In (6)-(7) $f_{c,VCO}$ and $f_{c,RO}$ specify the oscillation frequencies of the VCO and RO, while the thermal noise scaling coefficients [10] are:

$$c_{w,VCO} = \frac{f_w^2}{f_{c,VCO}^2} 10^{\frac{L_{VCO}(f_w)}{10}}, \tag{9}$$

$$c_{w,RO} = \frac{f_w^2}{f_{c,RO}^2} 10^{\frac{L_{RO}(f_w)}{10}}, \tag{10}$$

$$c_{w,PFD} = 10^{\frac{L_{PFD}}{10}}. \tag{11}$$

where $L_{VCO}(f_w)$, $L_{RO}(f_w)$, and L_{PFD} represent the spot phase noise measurements [7][11] defining the PSDs of the free-running VCO, RO, and PFD, respectively.

Examples of the loop responses generated with the proposed model are shown in Fig. 3(left) for typical component values of R = 1580 Ω, C_1 = 200 pF, C_2 = 1 pF, K_{VCO} = 10 MHz/V, N = 42, M = 1, I_p = 200 μA and $f_{c,RO}$ = 16 MHz. The component values are chosen so as to represent average performance in state-of-the-art integrated CMOS PLL structures, e.g. in [5], [12], [13]. In Fig. 3(right) we have also generated examples of the VCO, RO, and PFD noise PSDs as stand-alone and PLL-enclosed components. The PSD spot measurement for the thermally perturbed RO is L_{RO}(1MHz) = -140 dBc/Hz, whereas the VCO is perturbed by thermal noise with L_{VCO}(1MHz) = -120 dBc/Hz. The PFD spectral density is flat at L_{PFD} = -235 dBc/Hz. We note that the VCO PSD components above the loop bandwidth are mostly preserved, while its lower-offset components are attenuated. The other noise sources from the loop illustrated in Fig. 1, other than the VCO, are visible at frequency offsets lower than the loop bandwidth and are moreover amplified, as seen in Fig. 3 (right).

PLL Excess Phase Calculation

The variance of the CHPLL excess phase $\theta[n]$, denoted by σ_n^2, as attributed to the VCO, RO, and PFD separately is given by [8], where T is the PIT:

$$\sigma_{\phi,VCO}^2(T) = \int_{-\infty}^{+\infty} \frac{\left|H_{VCO}(f)\right|^2 \sin(\pi f T)^2 \, 4\pi^2 f_{c,VCO}^2 c_{w,VCO}}{(\pi f)^2} df, \tag{12}$$

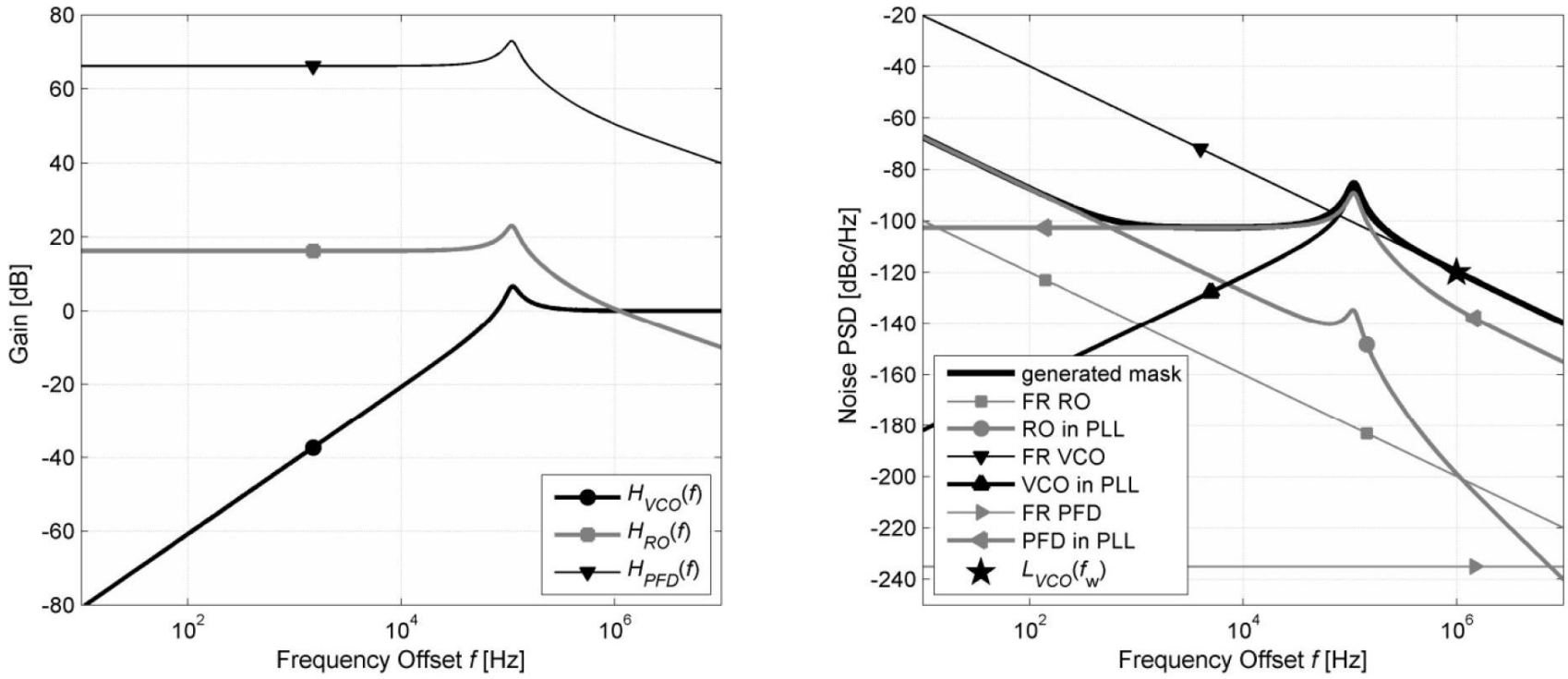

Fig. 3 Charge-pump PLL: left – example VCO and RO excess phase transfer functions, right – output PSD and individual contributors.

$$\sigma^2_{\phi,RO}(T) = \int_{-\infty}^{+\infty} \frac{\left|H_{RO}(f)\right|^2 \sin(\pi f T)^2 \, 4\pi^2 f^2_{c,RO} c_{w,RO}}{(\pi f)^2} df, \tag{13}$$

$$\sigma^2_{\phi,PFD}(T) = \int_{-\infty}^{+\infty} \left|H_{PFD}(f)\right|^2 c_{w,PFD} df, \tag{14}$$

$$\sigma^2_{\phi}(T) = \sigma^2_{\phi,VCO}(T) + \sigma^2_{\phi,RO}(T) + \sigma^2_{\phi,PFD}(T), \tag{15}$$

Analytical solution of (12) and (13) within a 3rd-order CHPLL is not possible; however numerical integration can still be used [8]. In the next Section of this article, we discuss the effects of the CHPLL model on the GNSS correlation properties and provide a qualitative expectation for the simulation results.

Theory on the Relation between CHPLL PN and GNSS Code Correlation

In the GNSS radio interface, which relies on direct sequence spread spectrum (DSSS) to achieve high receiver sensitivity, the received signal is compared with a replica of its corresponding code until the correlation is maximized for a given delay which in turn provides an indirect measurement of the range of the satellite. One of the performance limiting factors of GNSS receivers is the imperfection of the RF-FE PLL. This imperfection is translated into random deviations in its instantaneous phase or frequency and is typically modeled as a phase imperfection, and therefore referred to as a phase noise [3]. This phase noise from the receiver front-end PLL affects both, the carrier and code tracking loops in the baseband processing. It affects the phase stability of the correlation product, making it increasingly challenging for the baseband tracking loop PLL to maintain carrier lock, and it also adversely affects the signal to noise ratio of the code correlation product, which in turn degrades the receiver sensitivity. Furthermore, longer integration intervals ideally mean higher sensitivity. Phase noise however is translated into rotations in the complex I/Q plane that are expected to make integration (correlation) comparatively less effective as this interval increases.

Firstly, we look into the variance of the excess phase of the CHPLL. For the purposes of this work, the expressions in (12)-(15) are of fundamental importance. Comparison with the FRO variance, as given in [3], shows a significant difference in behavior – whereas the variance of the free-running oscillator phase increases linearly with time [10]:

$$\sigma^2_{\phi,FRVCO}(T) = c_{VCO}T, \tag{16}$$

The output phase variance of the oscillator-within-the-CHPLL may not necessarily behave this way. In Fig. 4, we give an example with the VCO excess variance as a function of time once

inserted in the PLL. With the FRVCO case, i.e. equivalent to zero-bandwidth PLL [3], the variance follows the straight line as given in (16). However, when enclosed in the CHPLL loop, the excess phase variance component of the VCO saturates within one loop time-constant [8]. The effect of PLL bandwidth on the variance contributions of the PLL blocks is qualitatively demonstrated in Fig. 5, where we give two examples of CHPLL output variances with corresponding variance contributions from the VCO, RO and PFD. As can be observed, the variance of the excess phase at the output of the CHPLL saturates after the one PLL loop time constant, unlike the free-running oscillator phase variance. Moreover, when the bandwidth increases, the RO becomes more dominant and it appears as the free-running version of itself, while when the PLL bandwidth decreases, the VCO contribution becomes more dominant. The results in Fig. 4 and Fig. 5 stem from numerical evaluation using the analysis performed in the previous section.

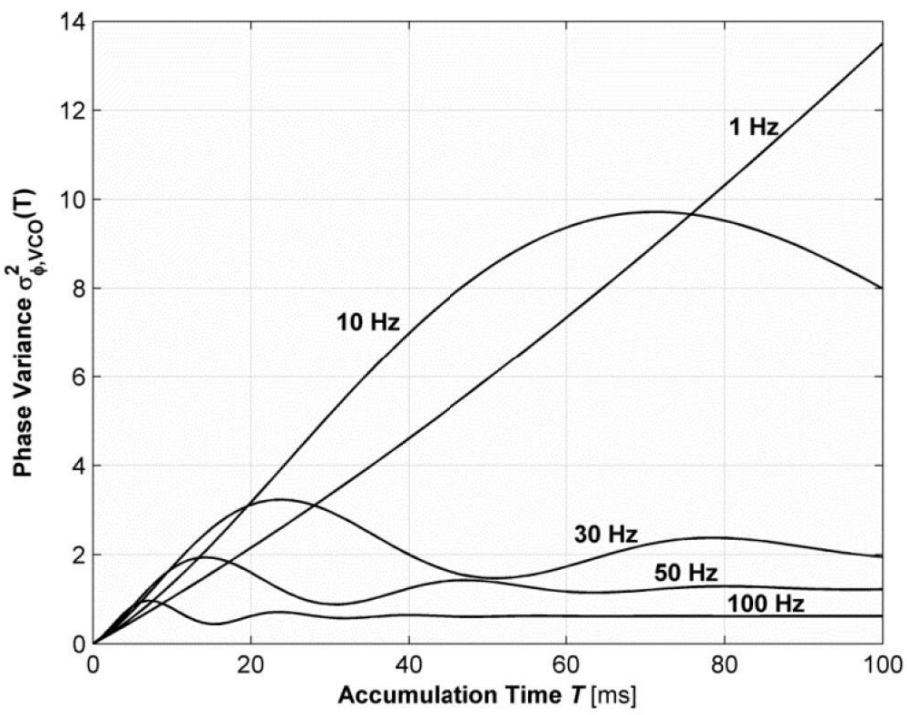

Fig. 4 VCO excess variance as a function of time with different PLL bandwidths.

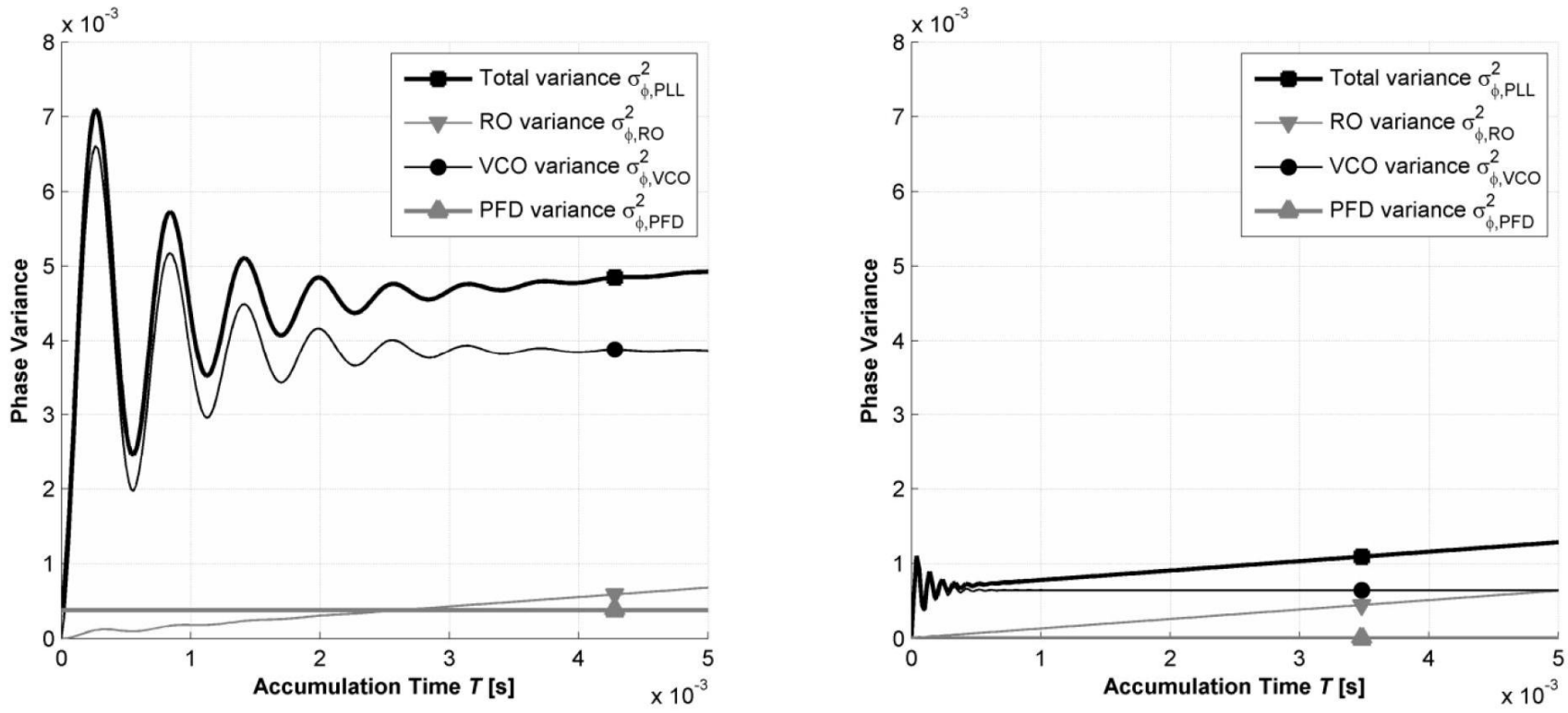

Fig. 5 Components of CHPLL excess phase variance: left – small bandwidth, right – large bandwidth.

In the presented study, the effects of the VCO, RO, and PFD are being investigated. As summarized in Fig. 4, after one loop constant, the PLL VCO contribution to the phase variance is constant. This is a major difference from the variance of a FRO, which is a linear function (16) of accumulation time [3][8]. Due to this phenomenon, the PLL VCO contribution alone would not deteriorate the correlation with increasing integration time. In general, this gives the freedom to utilize large integration times without the penalty from PLL VCO phase noise. On the other hand, the PLL RO retains the same phase variance behavior as the free-running VCO and will be a source of degradation with increasing integration times for example, up to 100 ms. As the PLL RO seems to be the dominant source of degradation with large integration times, a good design approach would entail minimizing $H_{RO,PLL}(f)$ in (2) and consequently minimizing the PLL RO variance from (13). As is clear from (2), smaller division ratios N are one possibility given that the input frequency to the PFD, equal to each of the terms $f_{c,RO}/M$ and $f_{c,VCO}/N$, permits a reliable PFD circuit design.

The parameters of the GNSS code correlation that are studied in this article are the SNR and the variations or instability in the phase angle component of the correlation product. The complex PRN code correlation output Y(τ) (with magnitude |Y|) at the receiver is obtained by correlating the incoming down-converted signal with a local reference code delayed by τ seconds. In general, phase noise has two effects on the signal. First, there is an energy loss, as the expected value of |Y| decreases with noise. Second, the variance of |Y| - which is ideally 0 if no other error effects are considered - increases [3]:

$$\mathrm{E}\left[|Y|\right] = \mathrm{E}\left[\sqrt{I^2 + Q^2}\right] \equiv \mu_Y \leq 1 \tag{17}$$

$$\mathrm{var}\left[|Y|\right] = \mathrm{E}\left[|Y|^2\right] - \left[|Y|\right]^2 \equiv \sigma_Y^2 \geq 0 \tag{18}$$

where μ_Y denotes the mean or expected value of |Y| and σ_Y^2 denotes the variance of |Y|. Therefore, the post-correlation SNR_C due to phase noise is defined by (19) [15], [16].

$$SNR_C \equiv 20\log_{10}\left(\frac{\mu_Y}{\sigma_Y}\right) \tag{19}$$

Additionally, the instability (IPA_C in radians) in the phase angle component of the correlation product (θ_C) is given by its standard deviation:

$$IPA_C \equiv \mathrm{std.}\left(\theta_C\right) \tag{20}$$

Next, we look into the mean of the correlation peak as defined in [3]. If we take into account the phase noise of the local oscillator, the correlation output can be written as:

$$Y\left(\tau\right) = \frac{1}{PIT}\int_0^T c\left(t\right)e^{j\Phi(t)} * c^*\left(t-\tau\right)dt \tag{21}$$

where $e^{j\Phi(t)}$ equals time dependant phase noise effect, $c^*(t-\tau)$ equals time delayed local code, $\Phi(t)$ equals non-stationary random variable modeling the phase noise effect, PIT = T = pre-detection integration time over which code correlation is performed. The correlation peak has maximum value at τ = 0 when the time delay between the incoming signal and the local replica is zero, in other words, when the two signals are perfectly aligned in time domain.

$$\begin{aligned} Y(0) = R(\tau = 0) &= \frac{1}{PIT}\int_0^T c(t)\, e^{j\Phi(t)} * c^*(t-\tau)\, dt \\ &= \frac{1}{PIT}\int_0^T \left|c(t)\right|^2 e^{j\Phi(t)} dt \\ &= \frac{1}{PIT}\int_0^T e^{j\Phi(t)} dt \end{aligned} \tag{22}$$

where PRN code c(t) is essentially a sequence of +1 and -1. Equation (22) shows that the correlation peak fluctuates randomly, according to $\Phi(t)$ and also that the effect of correlation peak in the presence of noise can be modeled as a filtered random variable equals to $e^{j\Phi(t)}$ passed through an integrator filter whose impulse response is a rectangular pulse of width T, and therefore, its frequency response is given by the well-known sinc function:

$$H(f) = \frac{\sin(\pi fT)}{\pi fT} \tag{23}$$

The PSD of the output random process Y(0) is denoted by $P_Y(f)$ and given by (24):

$$P_Y(f) = P_X(f)\left|H(f)\right|^2 \tag{24}$$

where $P_X(f)$ is the PSD of the frequency synthesizer output. The average power of the correlation peak is E(Y^2(0)) is given by integrating the $P_Y(f)$ over all frequencies (please refer to Fig. 6):

$$E\left(Y^2(0)\right) = \int_{-\infty}^{\infty} P_X(f)\left|H(f)\right|^2 df \tag{25}$$

Results and Analyses

Numerical Evaluation Scenarios

The CHPLL model described earlier is used to create sampled phase noise signal vectors (called 'realizations'), each of length 200 ms. These signal vectors are created for different combinations of a range of typical GNSS front-end PLL parameters, as described in Table 1. This allows us to study the effect of each PLL parameter upon the baseband GNSS correlation performance. One hundred such realizations are generated for every combination so that the results can be averaged over a considerable size of data samples. The nature of PLL phase noise data used for these simulations is as follows:

Table 1. Constituent blocks of a PLL and typical values of their significant design parameters

Constituent Block	Important Parameter	Typical Value(s)/Range
Crystal RO	PN (at 10 kHz offset)	-150 dBc/Hz
PFD	PN (at 1 MHz offset)	-265 dBc/Hz
Loop Filter	Order	2^{nd} order
	Bandwidth	1 kHz → 100 kHz
VCO	PN (at 1 MHz offset)	-130 dBc/Hz → -100 dBc/Hz
FD	Division Ratio (N)	64, 200

The overall PLL phase noise is dependent on the sum of phase noise contributions of its constituent blocks. The contribution of each block is in turn dependent upon various parameters, as shown in Table 1. In each realization, only one parameter is varied while keeping all others

constant, so that the effect on code correlation due to that parameter (and hence due to that constituent block) can be studied. The method of adding the PN into the signal stream and simulation of code correlation is the same as in [3].

Result Analyses – Mean and SNR of correlation peak versus VCO PN

Figs. 6 and 7 show the effect of PLL phase noise on the mean and SNR of baseband correlation for PLL frequency division ratios of (a) 64 and (b) 200 respectively. Each band represents a given CHPLL bandwidth that is commonly found in practical implementations. The PIT is varied from 4 ms (weak boundary) to 100 ms (bold boundary). It can be observed that, increasing the PLL loop bandwidth generally improves the mean correlation and its SNR for a given quality of VCO. Increasing the PIT degrades the mean value of correlation peak for a given PLL loop bandwidth, however this effect is generally reversed if the SNR is considered. This is because, with increasing PIT (which effectively means more averaging), the variance of the correlation peak reduces which results in the higher SNR. Interestingly, as evidenced in Fig. 7, with large PLL bandwidths and very good VCO, increasing PIT may not provide any SNR benefit as opposed to a poor VCO case. This is due to the PLL phase noise being dominated by the phase noise of the RO, which is almost unmitigated, i.e. appears as a free-running due to the large PLL bandwidth. As discussed in [3], increasing PIT with a free-running oscillator results in a lowering of the SNR. Such an example in Fig. 7 is the case of the 100 kHz band (and also observable in the 30 – 100 kHz bandwidth range) where there exists a point at which the boundaries intersect and exchange places. To the left of this ‘knot’ we have a situation in which increasing PIT actually decreases the correlation SNR.

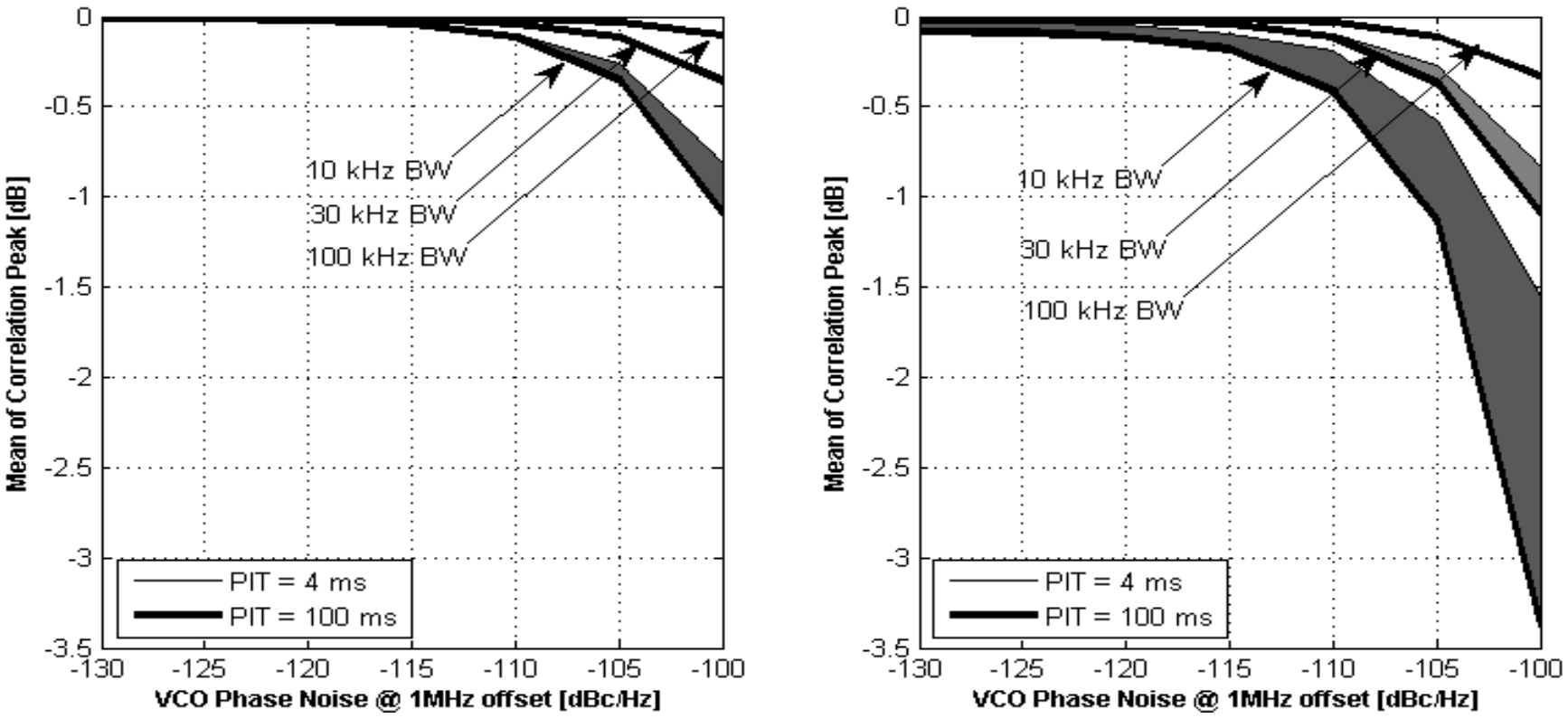

Fig. 6 Mean of Correlation Peak vs VCO PN with (a) N = 64 and (b) N = 200. PIT is varied from 4 ms (weak boundary) to 100 ms (bold boundary). Mean values computed using equation (25).

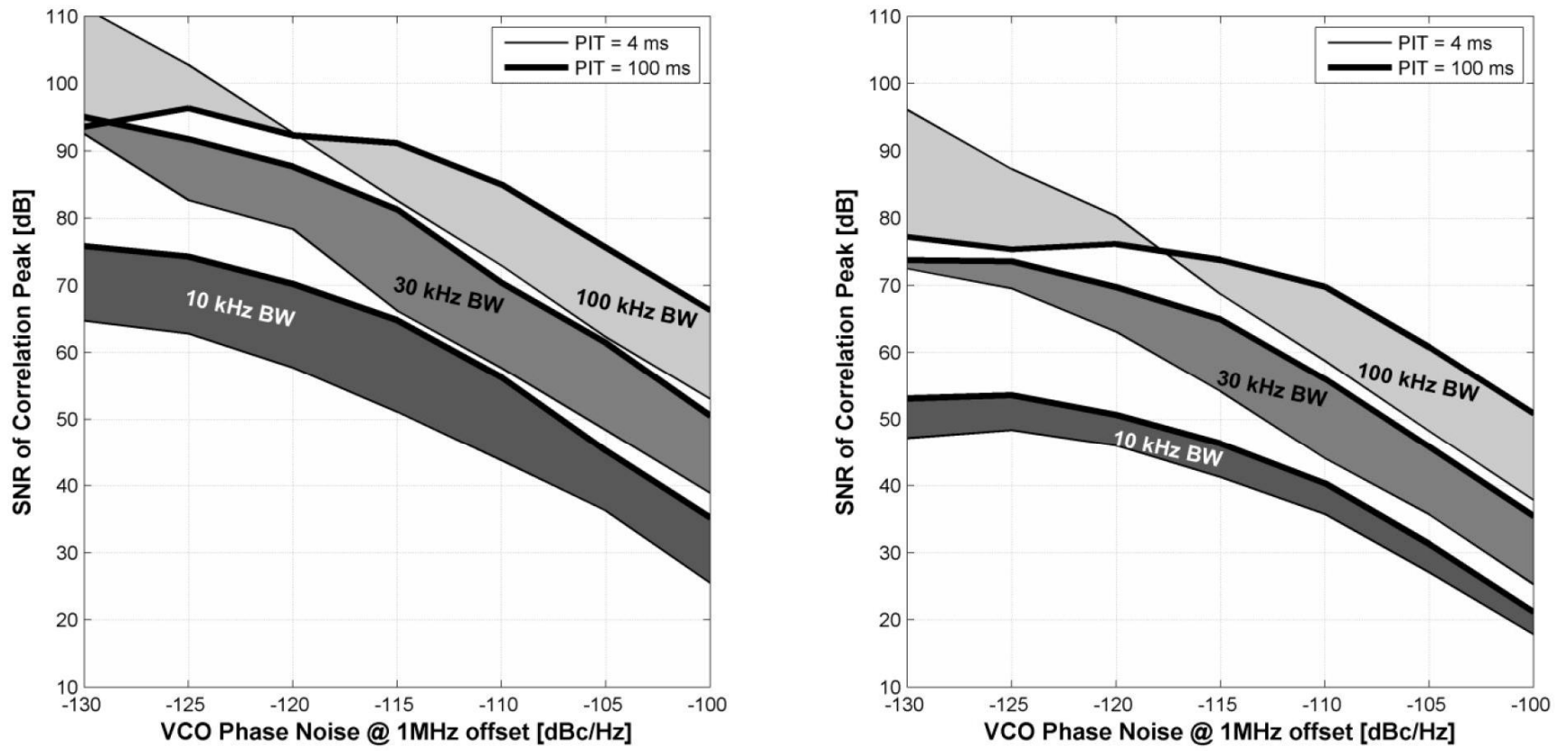

(a) (b)

Fig. 7 Correlation SNR vs VCO PN with (a) N = 64 and (b) N = 200. PIT is varied from 4 ms (weak boundary) to 100 ms (bold boundary).

This scenario is strongly related to the scenario in [3], where the PN PSD is mainly due to the FRO PSD and where increasing PIT was found to deteriorate the correlation SNR. Hence, PIT increase is useful only when the PLL PSD is not dictated mainly by the FR RO PSD. The intersection occurs for larger bandwidths of the PLL where VCO PN is mitigated, while RO PN is unmitigated at the output of the PLL. In this situation, the overall PLL phase noise is mainly the RO phase noise, which appears as free-running. Therefore, the conclusions of [3] for a free-running oscillator apply and we expect the larger PIT to result in smaller SNR.

The intersection point of the 4 and 100 ms PITs is therefore, important to the specification of the receiver – if a large PLL BW and a clean VCO are used on the circuit-side, increasing PIT on the system side may not necessarily be beneficial. Finally, comparing Figs. 6a and 6b it can be observed that the mean and SNR performance of every band degrades and the PLL phase noise requirement becomes more stringent if the FDR is increased from 64 to 200. Hence, we conclude that Fig. 7 provides distinct radio front-end CHPLL design options for the desired baseband correlation SNR value, i.e. the bandwidth, VCO PSD, and PIT can be adjusted to values commanding the best receiver design, production, and performance cost.

CHPLL Circuit-Design Guidelines

In absence of front-end phase noise, the correlation would exhibit a linearly increasing SNR as the integration period is increased [3]. However, phase noise from the front-end sets a practical upper-bound to the integration period, after which effective correlation SNR degrades. This phenomenon is clearly visible in Fig. 8, which shows the relation between correlation SNR and integration period by varying the PLL's (a) frequency division ratio, keeping filter BW = 30 kHz

and VCO PN = -115 dBc/Hz (b) Filter BW, keeping VCO PN = -115 dBc/Hz and N = 64 (c) VCO PN, keeping N = 64 and Filter BW = 30 kHz.

The significant contribution of this article is that, the well-established relation between correlation SNR and integration period is presented in terms of front-end PLL design parameters. This makes the results applicable not only for designers of baseband tracking algorithms but also for designers of front-end frequency synthesizers. For example, if it is desired to have a minimum correlation SNR of 75 dB using 100 ms integration time, looking at Figs. 8 (a), (b) and (c), an engineer can estimate that the front-end PLL parameters should be approximately, an N = 64, filter BW of 30 kHz and VCO PN of not more than -115 dBc/Hz at 1MHz offset. Furthermore, as each plot within Fig. 8 displays a maxima point, it is possible to allow for tolerances in the front-end frequency synthesizer design parameters by specifying a minimum threshold for SNR around this maxima point for the baseband correlation SNR.

Alternatively, to obtain direct circuit-design specifications for CHPLL parameters we use the curves in Fig. 7 to obtain the dependence between the VCO phase noise at 1 MHz offset and the required PLL bandwidth in order to maintain a given SNR of the correlation peak. As an example, selecting correlation peak SNR = 60 dB yields the dependence given in Fig. 9.

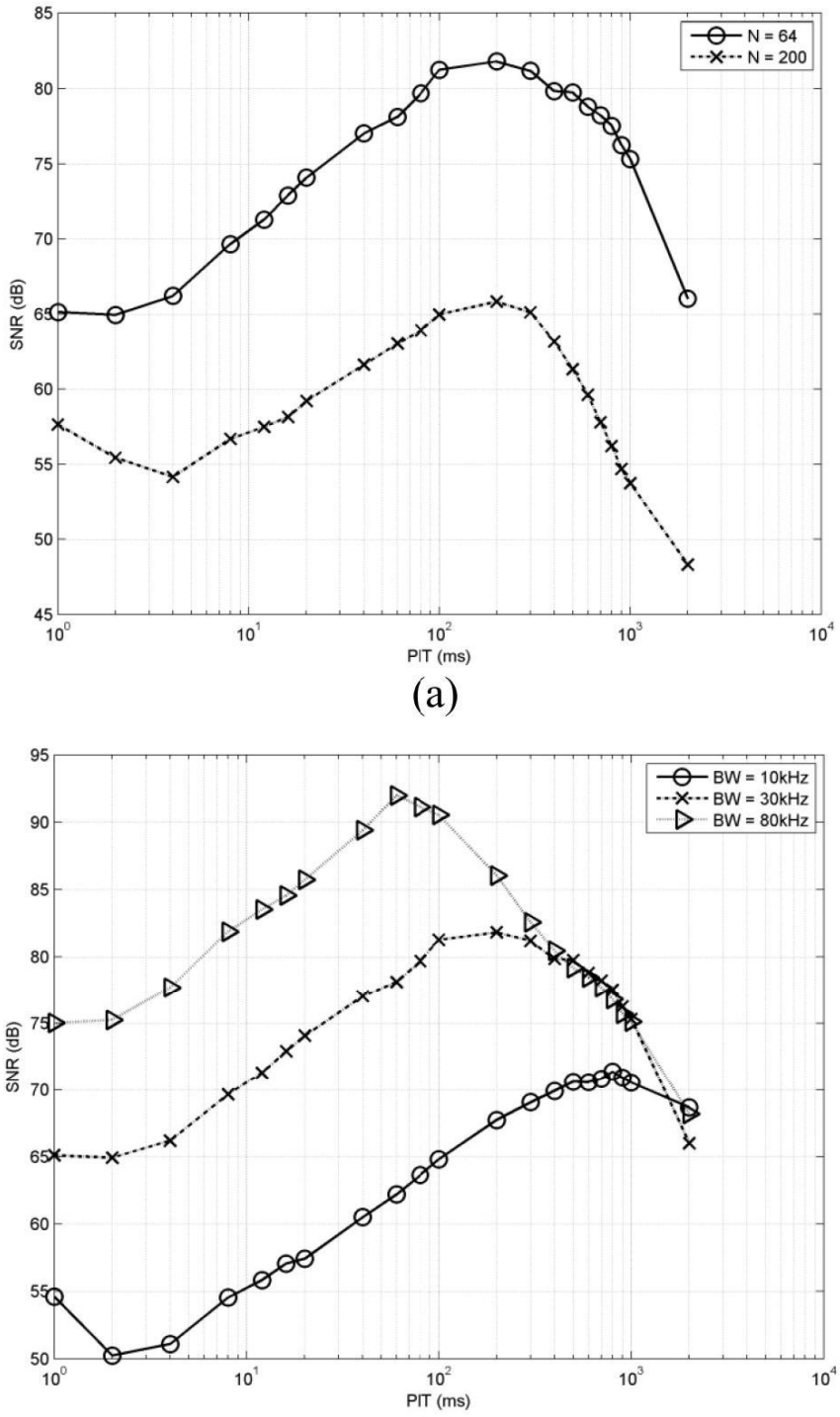

(a)

(b)

(c)

Fig. 8 Correlation SNR VS PIT by varying the PLL's (a) FDR *N* (BW = 30 kHz and VCO PN = -115 dBc/Hz) (b) Filter BW (VCO PN = -115 dBc/Hz and N = 64) (c) VCO PN (offset 1 MHz, N = 64 and Filter BW = 30 kHz).

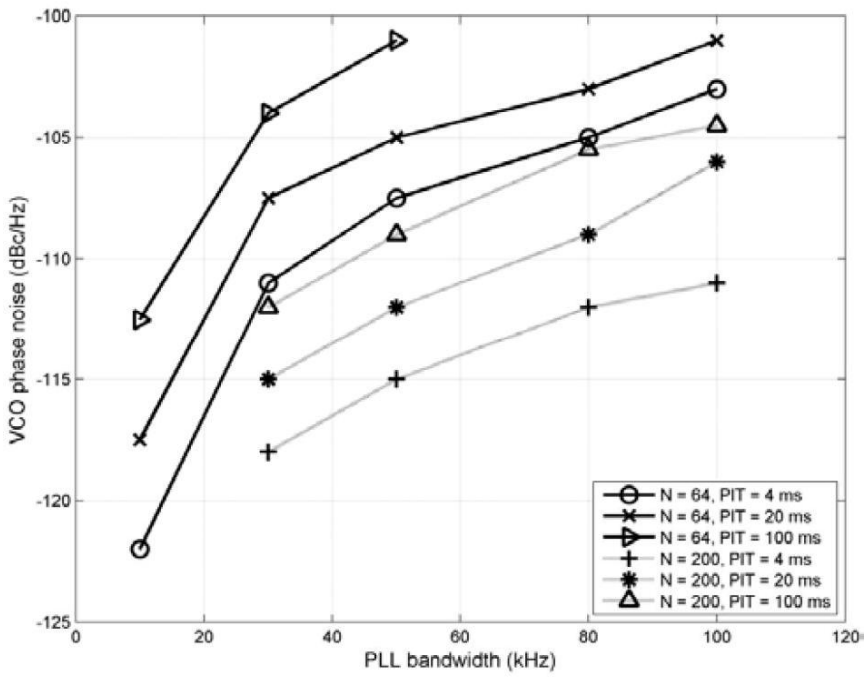

Fig. 9 Circuit design requirements for PLL filter BW and VCO PN assuming minimum SNR requirement of 60 dB.

Conclusion

This article is a substantial extension, with practical emphasis, to [3] and [4] where the effect of free running local oscillator thermal phase noise on GNSS code tracking performance was considered. However, since a FRO is not well suited to mimic practical receiver frequency synthesizers, it is necessary to perform the same study using a more real-world frequency source, the phase locked loop, and this has been the main contribution of this article. First, a PLL phase noise model was constructed which included PN contributions from each of its constituent building blocks. This PLL model is designed to accommodate direct circuit specifications of frequency synthesizers used in state-of-the-art GNSS receivers. Next, an analytical relationship was derived between this phase noise and code correlation properties. Numerical evaluations were performed to verify the findings of the analytical study. The effect of PLL loop bandwidth, thermal phase noise, frequency division ratio, and correlator integration time were observed on SNR of the code correlation product. Through mathematical interpretations of the results, performance bounds to designers of radio front-ends were provided as they attempt to meet

baseband performance requirements during the design of frequency synthesizers. The results can be refined for any given PLL design by varying the constants of RO, PFD noise contributions, and additionally providing PLL buffering noise contribution.

We hope to continue this study in the future. The next step is to convert the PLL phase noise model, presently in Matlab, into a physical device using programmable hardware logic and VHDL coding. This physical PLL (P-PLL) would then be integrated with a VHDL-based GNSS signal simulator and their combined signals will be studied using the TUTGNSS receiver already developed in our University. It would be interesting to compare the results of this study with the results obtained in the present article using the Matlab-based PLL model. Also interesting would be to perform a similar study in presence of for example, white noise due to the other front-end components and further refining the PLL PN model by introducing reference oscillator phase noise as an additional variable.

References

[1] Diggelen F. V., “Standard GPS Review”, Chapter 2 of *A-GPS: Assisted GPS, GNSS, and SBAS*, Artech House, 2009, ISBN-13: 978-1-59693-374-3.

[2] Curran J. T., Lachapelle G., Murphy C. C., “Digital GNSS PLL Design Conditioned on Thermal and Oscillator Phase Noise”, *IEEE Transactions on Aerospace and Electronic Systems*, Vol. 48, Issue 1, Jan. 2012, pp. 180 - 196.

[3] Serna E. P., Thombre S., Valkama M., Lohan S., Syrjälä V., Detratti M., Hurskainen H., Nurmi J., “Local Oscillator Phase Noise Effects on GNSS Code Tracking”, *InsideGNSS*, Nov/Dec 2010, pp. 52-62.

[4] Thombre S., Raasakka J., Lohan E-S., Valkama M., Hurskainen H., Nurmi J., "Local Oscillator Phase Noise Effects on Phase Angle Component of GNSS Code Correlation", Proceedings of the *International Conference on Localization and GNSS (ICL-GNSS 2011)*, June 2011.

[5] Congyin S., Chuan W., Le Y., Huailin L., "−99dBc/Hz@10kHz 1MHz-step dual-loop integer-N PLL with anti-mislocking frequency calibration for global navigation satellite system receiver", *IEEE International Symposium on Circuits and Systems (ISCAS 2011)*, 15-18 May 2011, pp.1876-1879.

[6] Gardner F., “Charge-pump phase-lock loops”, *IEEE Transactions on Communications*, Vol. 28, Issue 11, Nov. 1980, pp. 1849-1858.

[7] Tchamov N. N., Rinne J., Syrjala V., Valkama M., Yaning Z., Renfors M., "VCO phase noise trade-offs in PLL design for DVB-T/H receivers", *IEEE International Conference on Electronics, Circuits, and Systems (ICECS 2009)*, Dec. 2009, pp.527-530.

[8] Demir A., "Computing Timing Jitter from Phase Noise Spectra for Oscillators and Phase-Locked Loops with White and 1/f Noise", *IEEE Transactions on Circuits and Systems I: Regular Papers*, Vol.53, Issue.9, Sept. 2006, pp.1869-1884.

[9] Mehrotra A., "Noise analysis of phase-locked loops," *IEEE Transactions on Circuits and Systems I: Fundamental Theory and Applications*, Vol.49, Issue.9, Sep 2002, pp. 1309- 1316.

[10] Demir A., “Phase noise and timing jitter in oscillators with colored-noise sources”, *IEEE Transactions on Circuits and Systems I: Fundamental Theory and Applications*, Vol. 49, Issue 12, 2002, pp. 1782-1791.

[11] Mathecken P., Riihonen T., Tchamov N. N., Werner S., Valkama M., Wichman R., “Characterization of OFDM Radio Link Under PLL-Based Oscillator Phase Noise and Multipath Fading Channel”, *IEEE Transactions on Communications*, Vol. 60, Issue 6, 2012, pp. 1479 - 1485.

[12] Cheng K. W., Natarajan K., Allstot D. J., "A Current Reuse Quadrature GPS Receiver in 0.13μm CMOS," *IEEE Journal of Solid-State Circuits*, Vol.45, Issue.3, Mar. 2010, pp.510-523.

[13] Torre V. D., Conta M., Chokkalingam R., Cusmai G., Rossi P., Svelto F., "A 20 mW 3.24 mm^2 Fully Integrated GPS Radio for Location Based Services," *IEEE Journal of Solid-State Circuits*, Vol.42, Issue.3, Mar. 2007, pp.602- 612.

[14] Jin S. (ed.), *Global Navigation Satellite Systems: Signal, Theory and Applications*, InTech, ISBN: 978-953-307-843-4, February 2012.

[15] Proakis J. G., *Digital Communications*, 4th Edition, McGraw hill Publishers, ISBN-10: 0072321113, ISBN-13: 9780072321111, 1989.

[16] Lohan E. S., Renfors M., "Performance analysis of the RAKE receiver in the presence of multipath delay estimation errors and Rician fading channels", *European Transactions on Telecommunications*, Vol. 14, Issue5, pp. 435-447, 2003.

PUBLICATION 7

S. Thombre, J. Raasakka, T. Paakki, F. Della Rosa, M. Valkama, J. Nurmi, "Automated Test-bench Infrastructure for GNSS Receivers – Case Study of the TUTGNSS Receiver", Proceedings of the *Institute of Navigation's GNSS+ (ION GNSS+ 2013)*, Nashville, Tennessee, USA, September 16-20, 2013.

Reprinted with kind permission.

Automated Test-bench Infrastructure for GNSS Receivers – Case Study of the TUTGNSS Receiver

Sarang Thombre, Jussi Raasakka, Tommi Paakki, Francescantonio Della Rosa, Mikko Valkama[†], Jari Nurmi
Department of Electronics and Communications Engineering,
Tampere University of Technology, Finland.
{firstname.lastname, [†]mikko.e.valkama}@tut.fi

Keywords: data capture tool, multi-frequency, multi-constellation, performance, testing, analysis, GPS, accuracy, sensitivity

Biography

Sarang Thombre is a Research Scientist, Teacher and a Doctoral Candidate at the GNSS Research Group of the Tampere University of Technology (TUT), Finland. He completed his Bachelor's in Electronics and Telecommunication from University of Pune, India in 2003 and Master's in Radio Frequency Electronics from TUT in 2009, both with Distinction. He is currently Chairman of the IEEE Signal Processing and Circuits & Systems Joint Chapter of the Finland Section and a Member of Board (Alternate) at the Nordic Institute of Navigation. His research interests include automated testing solutions for GNSS receivers, radio front-end designs for multi-frequency, multi-constellation receivers and study of phase noise effects on baseband correlation performance.

Jussi Raasakka is currently a GNSS R&D Scientist at Honeywell International s.r.o. Previously, he was a Teaching Associate at the Department of Electronics and Communications Engineering in Tampere University of Technology (TUT). He received his Master's degree in 2009 from TUT. His current research interests include GNSS receiver baseband algorithms, SDR architectures for future GNSS receivers, and interference detection/mitigation algorithms for GNSS receivers.

Tommi Paakki received his MSc degree at Tampere University of Technology in 2008. He is currently a teaching assistant and a doctoral student at the Department of Electronics and Communications engineering. His research interests and expertise are in the areas of GNSS receiver navigation algorithms, emerging GNSS constellations, multi-GNSS receivers, receiver software and hardware implementation, and receiver characterization on FPGA platforms. He has worked in national and international collaboration for the development of the TUTGNSS receiver reference design, and has authored and co-authored several publications related to that work.

Francescantonio Della Rosa received the M.Sc. degree in Electrical and Electronic Engineering, with specialization in Mobile Communications, from Aalborg University (AAU), Aalborg, Denmark, in June 2007. Currently, he is the Project Manager of the Multitechnology Positioning Professionals (MULTI-POS) Marie Curie (ITN) and Research Scientist at Tampere University of Technology (TUT), pursuing his PhD on hybrid positioning solutions.

Mikko Valkama received the M.Sc .and Ph.D. Degrees (both with honours) in electrical engineering (EE) from Tampere University of Technology (TUT), Finland, in 2000 and 2001, respectively. In 2002 he received the Best Ph.D. Thesis -award by the Finnish Academy of Science and Letters for his dissertation entitled, "Advanced I/Q signal processing for wideband receivers: Models and algorithms". In 2003, he was working as a visiting researcher with the Communications Systems and Signal Processing Institute at SDSU, San Diego, CA. Currently, he is a Full Professor and Department Head at the Department of Communications Engineering at TUT, Finland. He has been involved in organizing conferences, like the IEEE SPAWC'07 (Publications Chair) held in Helsinki, Finland. His general research interests include communications signal processing, estimation and detection techniques, signal processing algorithms for software defined flexible radios, cognitive radio, digital transmission techniques such as different variants of multicarrier modulation methods and OFDM, radio localization methods, and radio resource management for ad-hoc and mobile networks.

Jari Nurmi is a Professor at TUT since 1999, at the Department of Electronics and Communications Engineering. His research interests include positioning receivers, wireless localization, software-defined radio, embedded computing systems, and high-level design methodology,. He held various research, education and management positions at TUT since 1987, was the Vice President of VLSI Solution Oy 1995-1998, and is a co-founder of a start-up Ekin Labs Oy since 2013. He was one of the recipients of Nokia Educational Award 2004, won the Tampere Congress Award 2005, was an Academy of Finland Research Fellow 2007-2008, and was the co-recipient of IIDA Innovation Award 2011. He is a steering

committee member of five international conferences. He has edited two Springer books, and published over 270 international conference and journal articles and book chapters.

Abstract

Testing of Global Navigation Satellite System (GNSS) receivers requires active participation of humans to initiate, control, record results of, and terminate the test cases. These manual operations are often inefficient and inaccurate, rendering the test results unreliable. Furthermore, accessing the internal signals of the receiver at different stages of processing is necessary to pinpoint the exact location of anomalies. Using traditional black-box testing techniques, it is only possible to test the final outputs of the receiver. This paper describes the automated test-bench developed at our University for analyzing the overall performance of multi-frequency multi-constellation GNSS receivers. The proposed test-bench includes a data capture tool (dCAP) to extract internal process information, and the overall controlling software, called automated performance evaluation tool (AutoPET), that is able to communicate between all modules for hands-free, one-button-click testing of GNSS receivers. The paper also describes the application of these tools through single frequency GPS L1 performance testing of the TUTGNSS receiver.

Introduction

The prototype Global Navigation Satellite System receiver (TUTGNSS) [1], developed at the Department of Electronics and Communications Engineering of Tampere University of Technology (TUT), is now in the performance testing phase. TUTGNSS is a GPS L1/L5 + Galileo E1/E5a dual-frequency dual-constellation receiver jointly developed by TUT and its international partners under 2 European Union Framework Programme research grants.

During the manual testing of the receiver, it was noticed that the results were often contaminated with errors due to imprecise time-keeping and inconsistent test environments. It was also strenuous and time consuming to perform repetitive tests over multiple iterations, with decreasing personnel efficiency as the number of iterations increased. The aforementioned problems led to the results being deemed unreliable and unrepeatable. There was thus a need to innovate and automate the testing process and environment. In addition, there was also the need to study the signals as they flowed through the internal signal processing chain, so that the exact location of anomalies could be detected.

Currently, there are very few solutions available in the commercial and academic domain which can perform end-to-end fully automated, yet customizable testing of GNSS receivers [2], [3]. A couple of commercial testing tools [4], [5] were recently unveiled, which claim to perform similar automated testing of GNSS receivers. However, these are not fully customizable by the end-user, having the limitation that they can be used only with their parent company's own proprietary signal simulators. Other commercial automated testing tools [6], [7], [8] are available nowadays. However, they are targeted towards electronic systems other than GNSS receivers. It was due to these reasons that we decided to implement an in-house solution. Consequently, an automated performance evaluation tool, called AutoPET was devised, along with a data capture tool, called dCAP.

The AutoPET is implemented completely in software (Qt, C++) and communicates with the Receiver Under Test (RUT) via RS-232 and NMEA protocol and with a commercial GNSS signal simulator via an RS-232 link. It holds the GNSS test-cases with user-defined iterations and other system settings. The AutoPET has already been used for making test runs on the TUTGNSS receiver with positive results. It is possible to initiate the overall testing of the receiver with a single button-click and the results are stored in the computer without any human intervention. Test scenarios currently included in the 'library' of the tool are: time-to-first-fix (TTFF), position accuracy, acquisition sensitivity, tracking sensitivity, and reacquisition time. By changing the scenarios in this library, the tool can be used with different simulator models. Another innovative aspect of the AutoPET is that it uses multi-threading to perform the receiver testing. Multiple software processing threads are necessary to keep track of the receiver operations and simulator feeds simultaneously, so that an appropriate interrupt can be generated when the receiver has performed the desired operation. This feature is explained in further detail in Section 1.

The dCAP is a hybrid (software controlled hardware) entity capable of extracting the user-defined internal process data from the different modules (acquisition, tracking, bit decoding, etc.) of the GNSS RUT and stores it in a computer via a 100 Mbps Ethernet link. The dCAP hardware is independent of the receiver module (although implemented on the same softcore) and operates through minimal interference with the receiver operation. This data can then be post-processed to monitor and record the behavior of the receiver and to investigate for any anomalies in its intermediate stages. An experimental version of the dCAP has already been used to monitor the carrier to noise ratio (C/No), carrier Doppler, and code delay from the internal tracking channels, and the raw GNSS signals in I/Q format entering the baseband processing unit (BPU) of the TUTGNSS receiver from its radio front-end.

Benefits of the AutoPET over the state-of-art are that it is portable (software platform independent), easy to use,

suitable for testing most receivers using variety of simulators (provided each of them can communicate with the outside world using some form of communication protocol), and its operational parameters are easy to modify through an external configuration file. The dCAP is currently designed specifically for the TUTGNSS receiver; however it can be easily replicated for most experimental embedded system receivers. Once implemented, the dCAP offers a clear view of the internal operation of the receiver by accessing intermediate signals between the input and output terminals. The speed and size of data capture are limited only by the type of Ethernet connection and the size of the internal and external memories. Additional details of the AutoPET and dCAP are provided in Sections 1 and 2 of the paper, while Section 3 describes the application of these tools in testing the GPS L1 operation of the TUTGNSS receiver.

1. Automated Performance Evaluation Tool (AutoPET)

The automated performance evaluation tool (AutoPET) is a software program in the Qt platform and C++ language that communicates between the GNSS receiver, signal simulator and its associated computer through a remote PC that houses the AutoPET. The set-up is shown in Fig. 1. This figure also denotes the different communication protocols used between the different modules.

At the center is the GNSS receiver, which accepts RF signals from the GNSS signal simulator. These signals represent signals from the sky in accordance with the scenario currently loaded in the simulator and therefore, represent uni-directional communication. On the other hand, the receiver communicates with the remote PC housing the AutoPET using NMEA-183 protocols [9]. This is a bi-directional communication, as the receiver continuously updates its status via NMEA messages to the AutoPET, and in turn the AutoPET sends a response/control command to the receiver. The receiver sends the $GPGGA NMEA message every 1 second (format shown in Fig. 2 (a)), and through reading this message, the AutoPET can determine the current status (acquisition, tracking, position fix etc.) of the receiver.

The TUTGNSS receiver has the capability to perform a cold-start to initiate the next test iteration when commanded by the AutoPET. For this purpose, we have designed a very simple custom message string which can be identified by the TUTGNSS receiver as a cold start command. In response, the receiver sends a custom NMEA message, $GPTXT (format shown in Fig. 2 (b)) which identifies that it has successfully performed a cold-start. Performing a cold-start involves erasing all a-priori navigation related information from the receiver memory. This includes erasing the ephemeris, almanac and timing information, and ensuring that all satellite tracking is lost.

AutoPET communicates with the GNSS signal simulator through its controlling computer, called the Sim-PC (which runs the control software for the simulator). This communication is bi-directional using a 100 Mbps Ethernet link. The AutoPET library holds the scenario files, through which it remotely controls the simulator. In turn, the Sim-PC returns responses or error messages in the form of XML strings to the AutoPET. The communication between the Sim-PC and the simulator is through its proprietary protocols.

Fig. 3 shows the overall operation of the AutoPET in the form of a flowchart. AutoPET makes extensive use of multi-threading. The receiver, AutoPET and the simulator function autonomously of each other and hence are independently controlled using their own processing threads running in parallel. Examples of some processing threads are; **Thread 1** monitors the receiver operation through the received NMEA messages. This thread is responsible to identify for example, if the receiver achieves a position fix or if it performs a successful cold start. **Thread 2** monitors the simulator through the received XML error messages and response messages from the Sim-PC. It is responsible to identify for example, if the simulator scenario is successfully set-up or if the satellite signals are turned ON and OFF when demanded by the test-case. **Thread 3** monitors the internal operation of the AutoPET itself for example, if a timer has expired or if the user performs any operation on the GUI during the progress of a test. Each thread generates an internal software ‘interrupt’ within the AutoPET, based on which the future course of action has to be dynamically determined.

Later in the paper, the application of the AutoPET for single frequency, single constellation operation and testing of the TUTGNSS receiver is described. However, it can just as easily be applied for more complex, multi-frequency, multi-constellation testing. The scenarios are stored in the “library” of the AutoPET, and they can be easily updated without requiring any changes in the tool itself. On the other hand, the receiver operation needs to be updated to perform position fix with multiple signals and constellations. If the receiver allows updating its operation mode using software commands, as is the case in TUTGNSS, these commands can also be included within the AutoPET.

In the case of TUTGNSS, two configuration settings control the mode of operation and the manner in which it has to be turned ON (cold, warm, or hot start) via a 32 bit control word. Table 1 describes the various options and the digital control word corresponding to each option. There are 8 possible modes of operations which would require 3 bits to be uniquely represented. However, we have assigned 5 bits in order to accommodate any planned future increase in operating modes. Similarly, there are

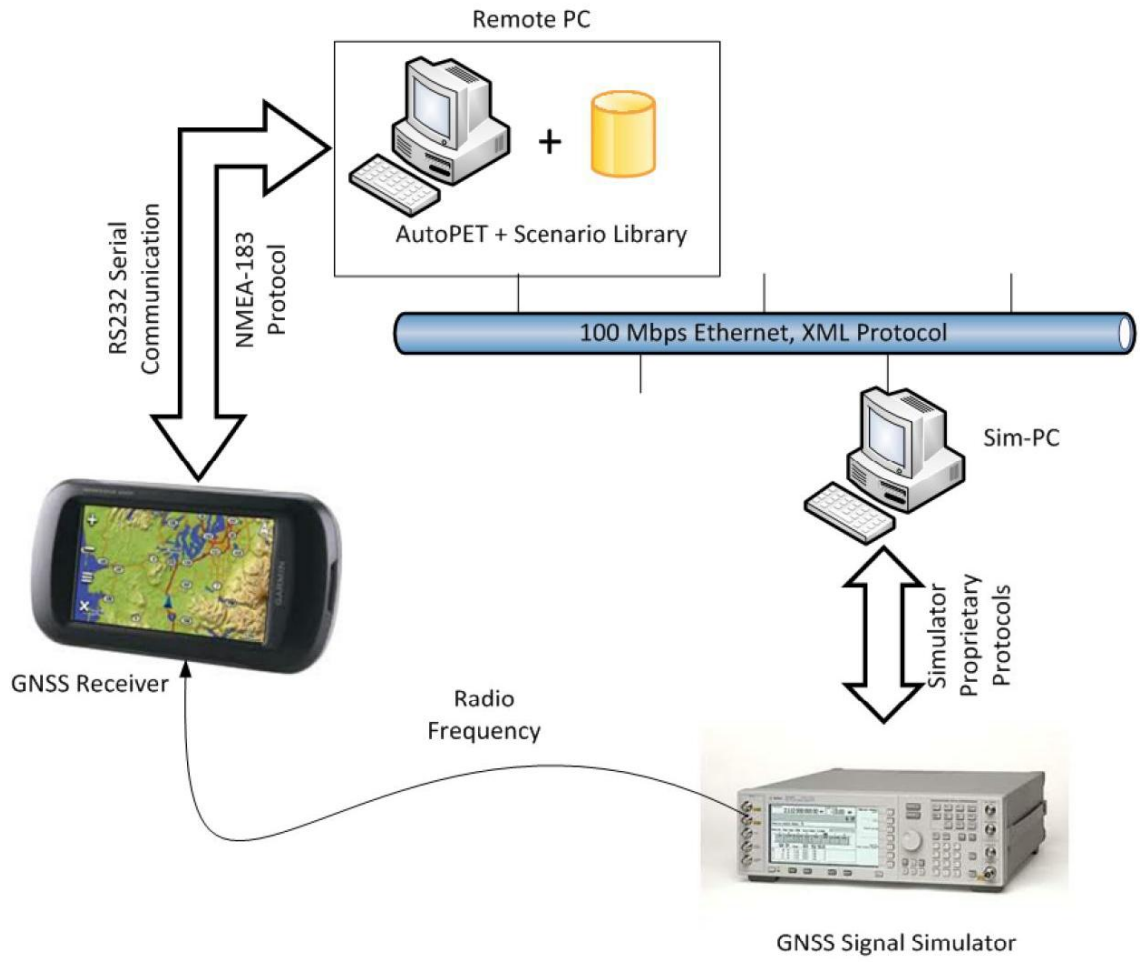

Fig. 1 Block-schematic of the AutoPET assembly

	ColdStart Msg	Checksum
$GPTXT	ResettingGPS	, *64

(a)

GPS Fix Code
1 = GPS, 2 = DGPS, 4 = RTK (Fixed), 5 = RTK (Float)

	Time										
	18:17:35	Latitude		Longitude		# of Satellites Tracking	HDOP	Orthometric Height		Geoid Height wrt WGS84	Checksum
$GPGGA	181735.00	4522.89368 , N		07540.33529 , W	1	05	2.3	78.9 , M		-33.9 , M	, *64

(b)

Fig. 2 Format of the NMEA messages (a) $GPGGA and (b) $GPTXT

three ways to turn ON the TUTGNSS receiver, and they can be uniquely represented by 2 bits. Therefore, out of the 32 available bits, only 7 bits are currently utilized. The rest of the bits are in reserve for future use. The mode selection bits are in least significant bit (LSB) position of the control word. For example, if the receiver should perform position fix after a warm start using GPS L1 and Galileo E1 signals, the 32 bit control word would be "00000000_0000000_00000000_00100010". Using this control word at the beginning of every test, the AutoPET can be used for a simple single constellation or more advanced multi-constellation testing of the receiver.

2. Data Capture Tool (dCAP)

The overall set-up of the dCAP is shown in Fig. 4. The TUTGNSS receiver consists of the radio front-end and the Baseband processing Unit (BPU) implemented on an

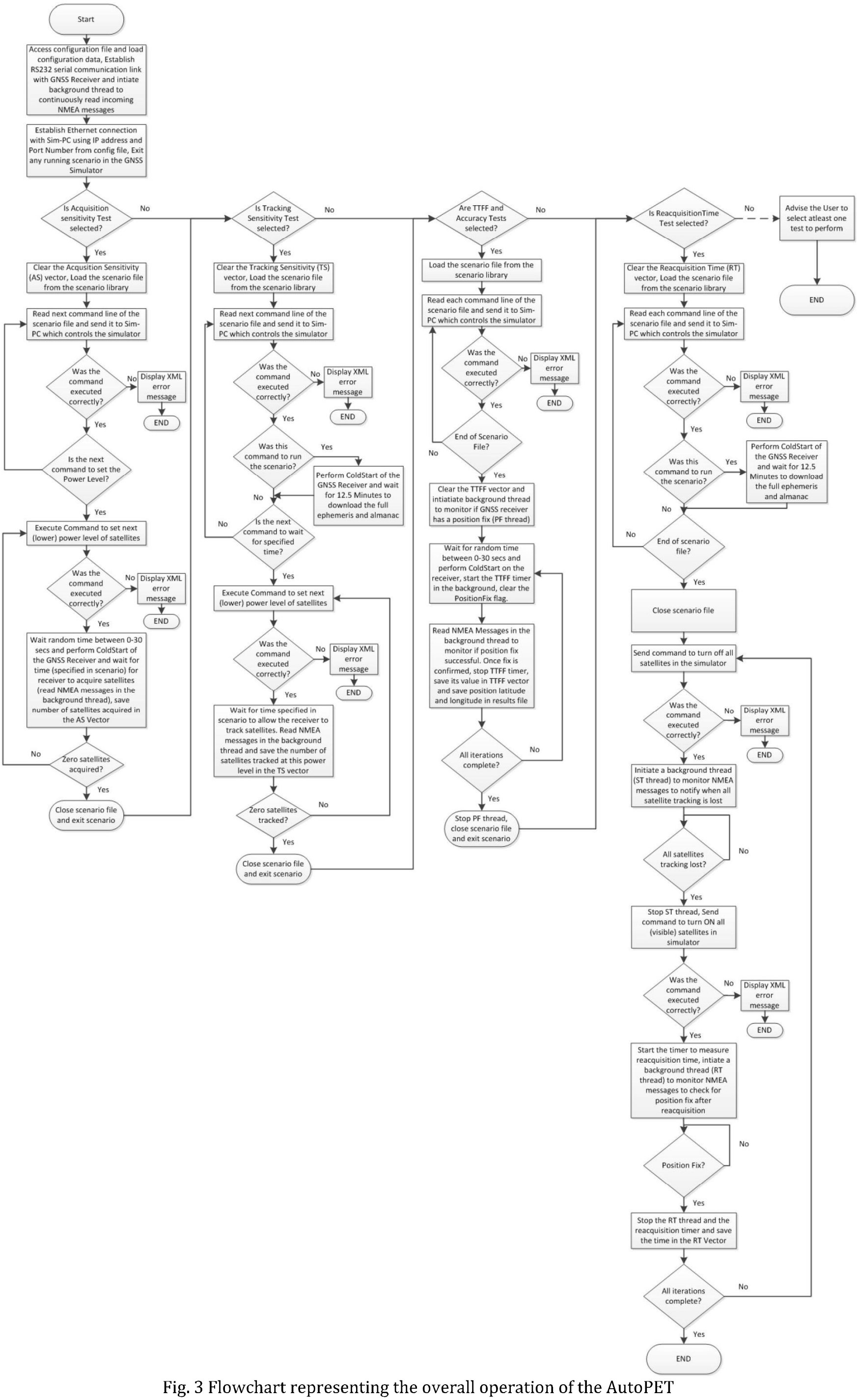

Fig. 3 Flowchart representing the overall operation of the AutoPET

Table 1 Control Word for multi-frequency, multi-constellation testing of TUTGNSS

Control	Individual Options	Digital Representation
Frequency and Constellation	GPS L1 only	00000
	Galileo E1 only	00001
	GPS L1 + Galileo E1	00010
	GPS L1 + GPS L5	00011
	Galileo E1 + Galileo E5a	00100
	GPS L1 + Galileo E1 + GPS L5 + Galileo E5a	00101
	GPS L1 + Galileo E1 + GPS L5	00110
	GPS L1 + Galileo E1 + Galileo E5a	00111
Turn ON method of TUTGNSS	Cold Start	00
	Warm Start	01
	Hot Start	10

Altera Stratix-II development board. This board consists of the NIOS-II softcore controlled by the MicroC operating system. The hardware is programmed using VHDL and consists of the System entity and a few peripheral entities, such as phase-locked loop (PLL) which are not shown in the figure for sake of simplicity. The System entity consists of (among others) two software-controlled hardware entities, one for the TUTGNSS receiver BPU and the other for the dCAP server, called CPU-0 and CPU-1 respectively. The Control-PC is responsible for the overall programming of the FPGA board through a USB link. It also holds a Qt-based user interface acting as the dCAP client implementation.

The dCAP client (in the Control-PC) establishes an Ethernet connection with the dCAP server (on the FPGA) and requests for a user-specified internal data sample. As an example, let us assume the user requests for raw I/Q samples input to the TUTGNSS BPU from the radio front-end. The dCAP server software communicates with the TUTGNSS software, which in turn allows the dCAP server hardware access to the requested data from the appropriate region of the TUTGNSS hardware, quite similar to how a signal across a resistor on a dense printed circuit board (PCB) is viewed by placing the oscilloscope probes across it. The only limitation with dCAP is that the user has to predict in advance which internal data parameters are of interest and create access points within the correct hardware entities. The dCAP server hardware will connect to the respective access point when demanded by the client.

This data snapshot is first buffered in the local shared memory entity on the FPGA board due to the requirements of speed, size and time synchronization. The dCAP server software is responsible for transferring this data from the internal memory to the Control-PC through the Ethernet link. The data is stored on the Control-PC hard-drive in the form of a *.bin file. Therefore, the size of each data-packet that can be accessed at a time is limited by the size of the FPGA memory entity, while the total data size is limited only by the size of the hard-drive of the Control-PC. The speed of data capture is restricted by the maximum speed of Ethernet link between the dCAP client and server.

In Fig. 5, the internal operation of the dCAP server is demonstrated, assuming that we would like to access the raw samples from the radio front-end. The first block that the samples enter inside the TUTGNSS BPU is the Baseband Converter Unit (BCU). This is where the dCAP hardware “probes listen in” on the signal samples. Through these “probes”, the signals are diverted to the first-in-first-out (FIFO) data collector on the dCAP server (CPU-1) in addition to their usual route through the further baseband processing blocks of the receiver. After the FIFO, the data undergoes clock arbitration, time synchronization, and master-slave synchronization, before being buffered into the on-chip SDRAM memory, where it waits until the dCAP server transfers it through the Ethernet-based local network to the requesting dCAP client within the Control-PC. In the case where a different internal data has to be monitored, the “probes” simply reorienteer to the correct access point within the correct hardware entity (for example, to monitor the signal C/No, the probes access the tracking loops).

3. Application of the AutoPET and dCAP in Performance Testing of the TUTGNSS Receiver

During the GPS L1 performance testing of the TUTGNSS receiver, the reference position in the simulator was set (randomly) to 10° 27’ N, 10° 51’E, 0.0 m Height, which is equivalent to x = 6160896.38 m, y = 1180826.81 m, z = 1149232.10 m. Ionosphere and troposphere errors were turned OFF in the simulator. On average, 100 iterations

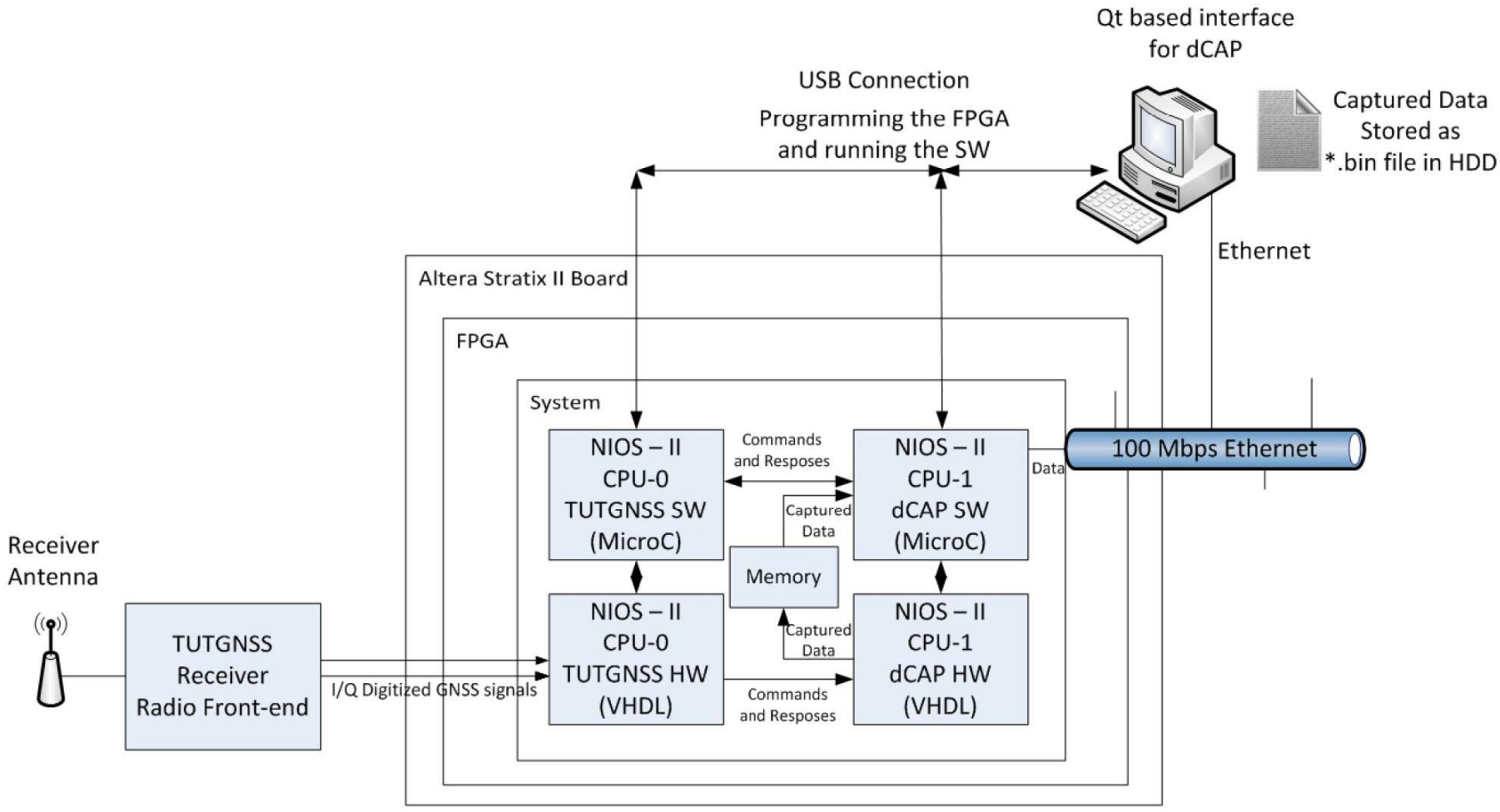

Fig. 4 Overall block schematic of the dCAP assembly

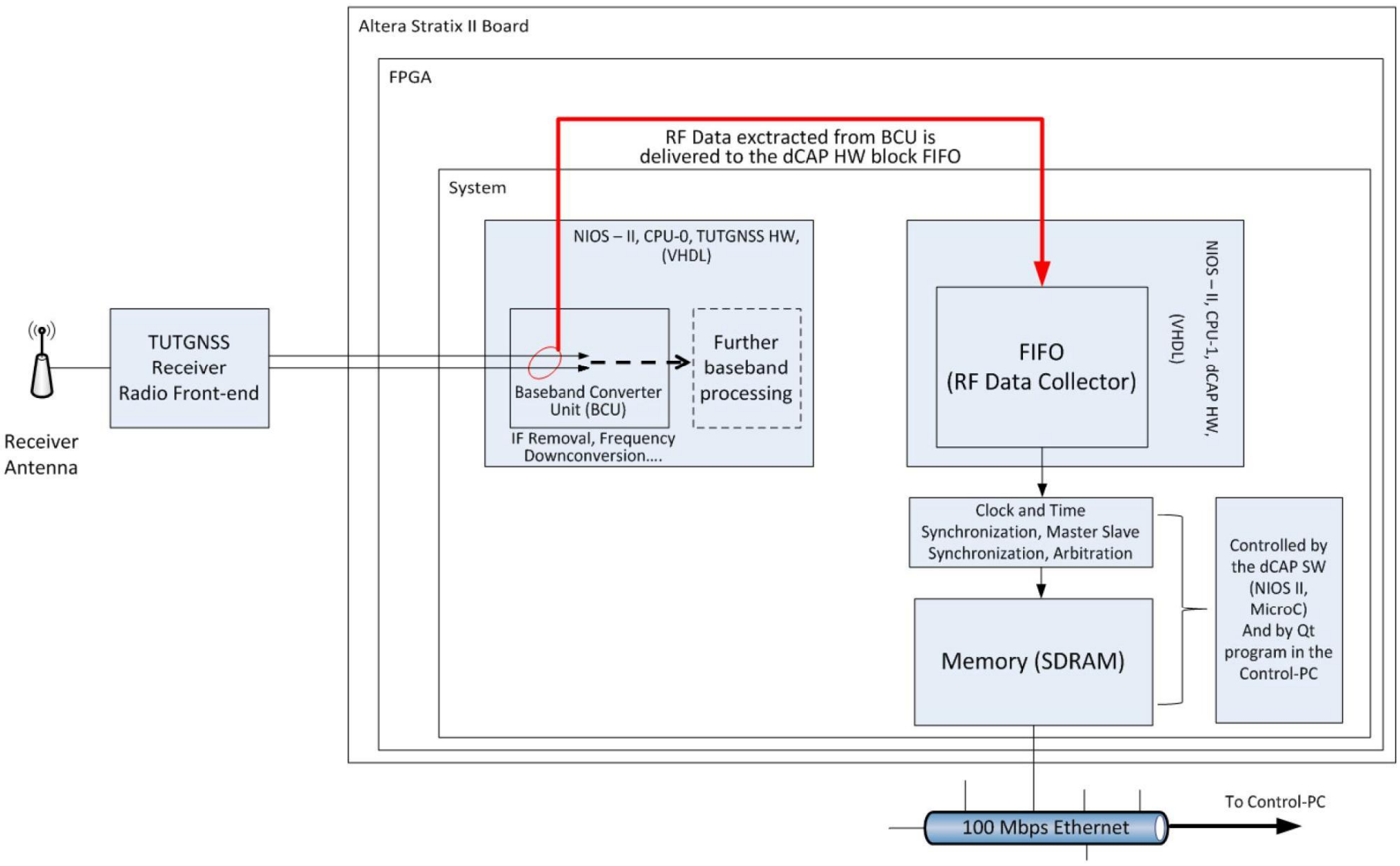

Fig. 5 Block schematic of an example of the dCAP internal operation

were performed for each test, and the total duration to complete all tests was two weeks. The dCAP was used in monitoring the tracking channels and extracting information such as the C/No, carrier Doppler and code delay estimates for the satellites being tracked. Access to these parameters enabled testing the acquisition and tracking sensitivity of the TUTGNSS receiver, thus confirming the results of the tests performed using the AutoPET.

3.1 Acquisition Sensitivity

Acquisition sensitivity for the TUTGNSS receiver was measured to be -141.5 dBm via the AutoPET and -141dBm via the dCAP. Each coherent integration interval was of 4 ms and 256 such intervals were integrated non-coherently. Using the AutoPET, 100 acquisition iterations were performed at every power level and the average number of satellites acquired was recorded, as shown in Fig. 6. It can be observed that, no satellites were acquired at -142dBm. Acquisition sensitivity test using the dCAP involved extracting the carrier Doppler and code delay estimates. A successful acquisition was assumed only if the code delay estimate error was less than ±1 chip (300 m) and the carrier Doppler estimate error was less than ±150 Hz. Based on these criteria, 96.72% of acquisitions were found to be successful when the satellite power was maintained at -141 dBm in the simulator as shown in the histograms in Fig. 7 and Fig. 8.

3.2 Tracking Sensitivity

Tracking sensitivity for the TUTGNSS receiver was measured to be -151 dBm via both the tools, assuming a coherent integration interval of 20 ms. Using the AutoPET,

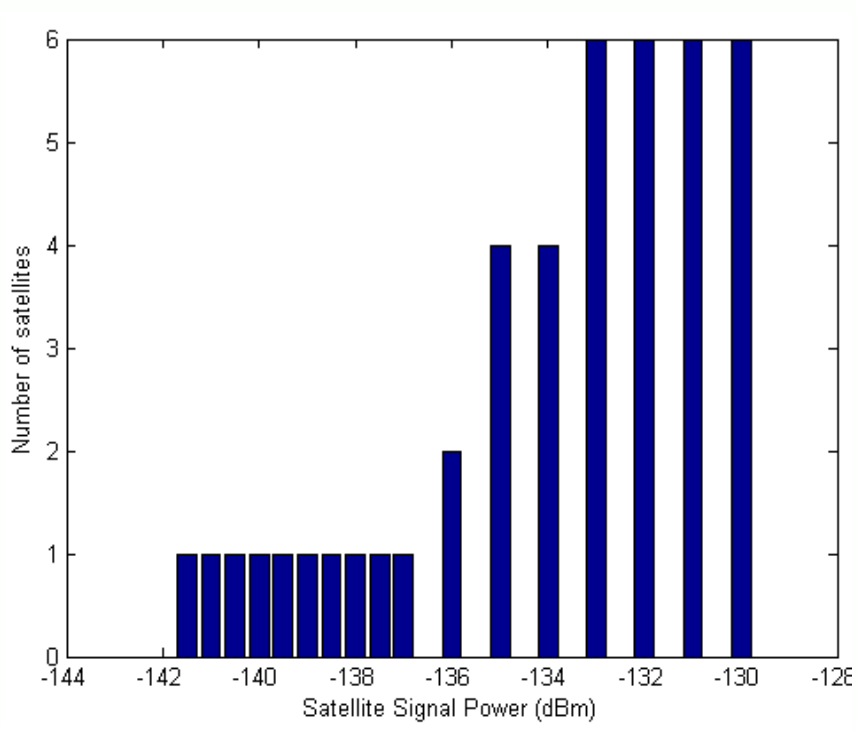

Fig. 6 TUTGNSS acquisition sensitivity using the AutoPET

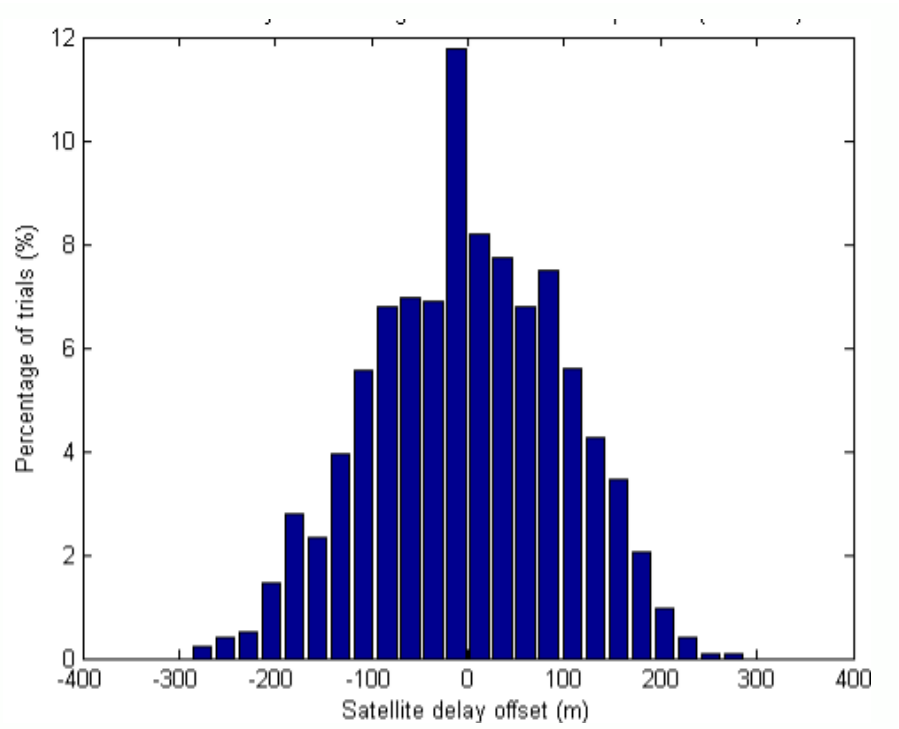

Fig. 7 Code delay estimate within ±1chip (300 m)

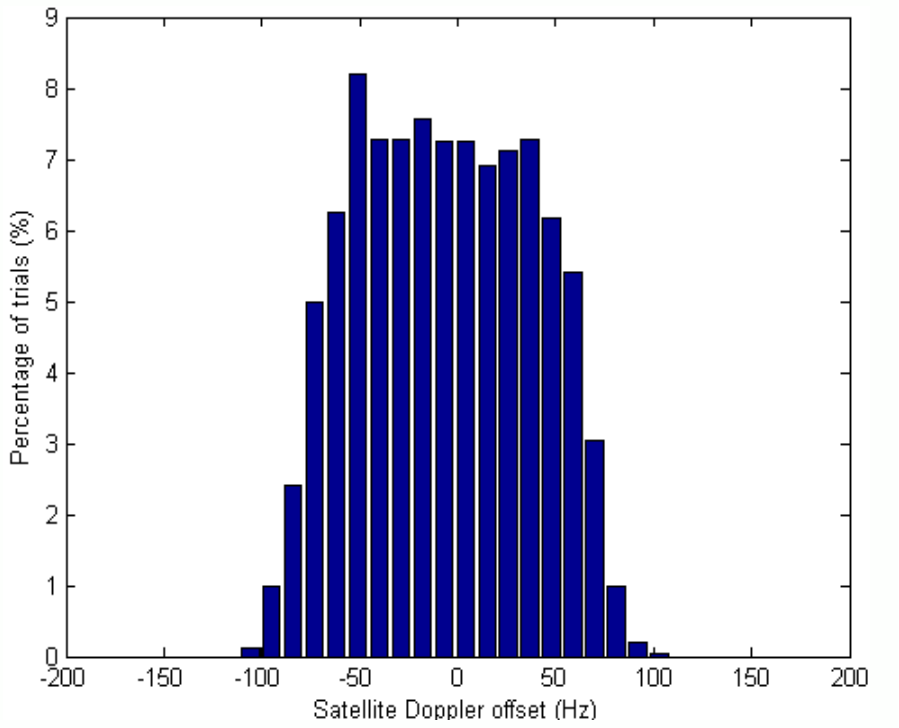

Fig. 8 Carrier Doppler estimate within ± 150Hz

100 tracking iterations were performed at every power level and the average number of satellites tracked was recorded as shown in Fig. 9. Using the dCAP, this test was performed by selecting one satellite and observing how the receiver C/No tracked this satellite during high and low signal power conditions. 20 tracking iterations of 90 seconds each were performed for a particular satellite. In each iteration, the satellite power in the simulator was maintained at the nominal condition of -130 dBm (equivalent to 38 dB C/No in the receiver) for the first 30 seconds. Subsequently, the power of the satellite was dropped to -151 dBm (equivalent to 17 dB C/No in the receiver).

As visible from Fig. 10, the receiver was able to continue tracking the satellite at -151 dBm in 19 out of the 20 iterations. In the case where tracking was lost, the C/No

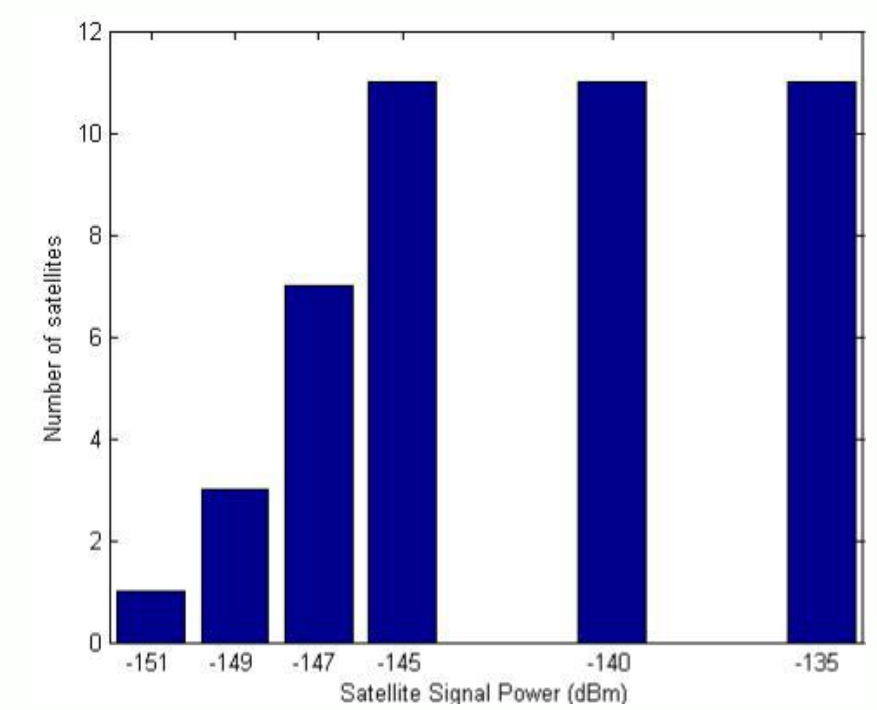

Fig. 9 TUTGNSS tracking sensitivity using the AutoPET

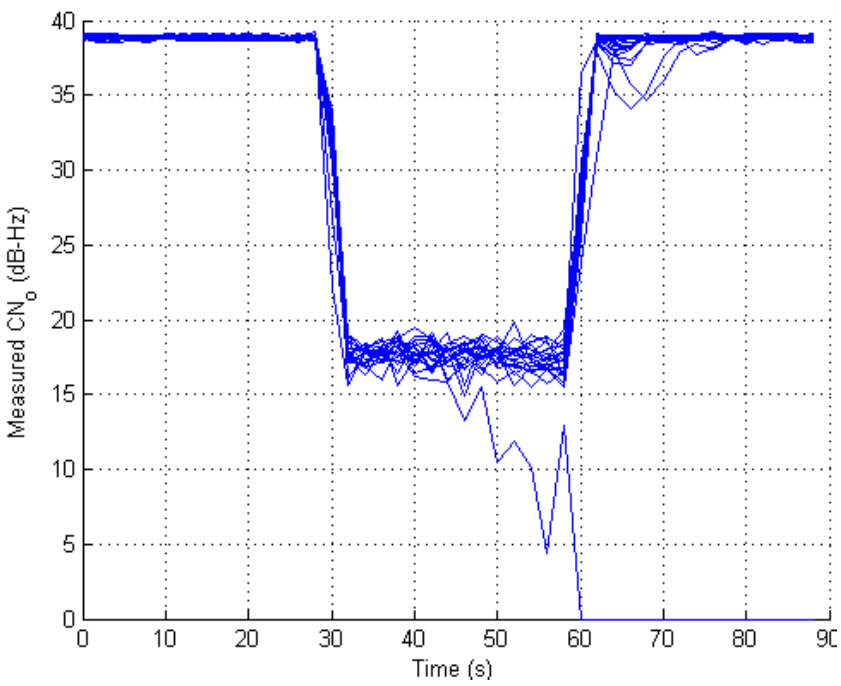

Fig. 10 Tracking the C/No in one tracking channel using the dCAP

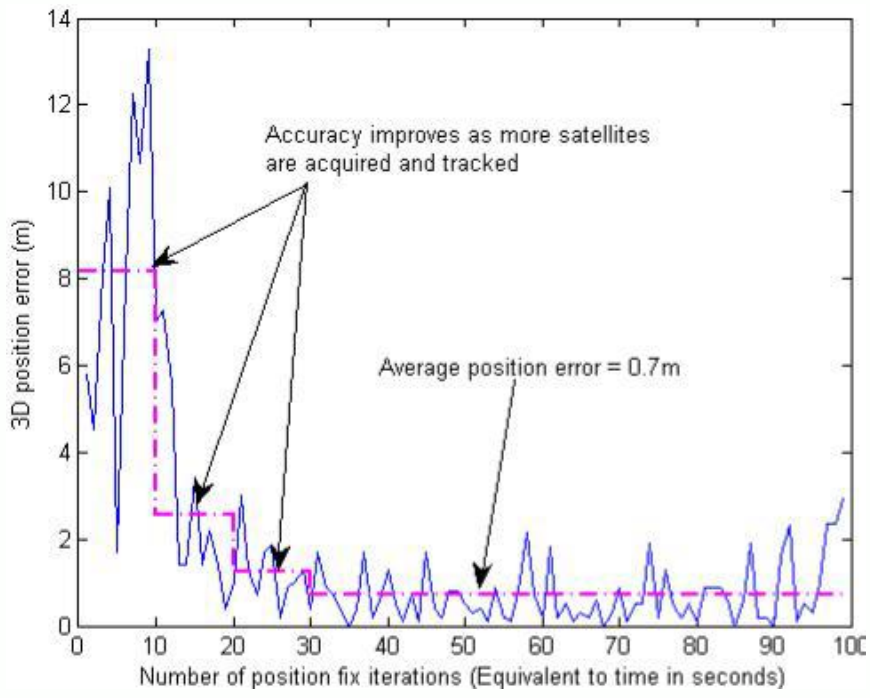

Fig. 11 TUTGNSS 3D position accuracy using the AutoPET

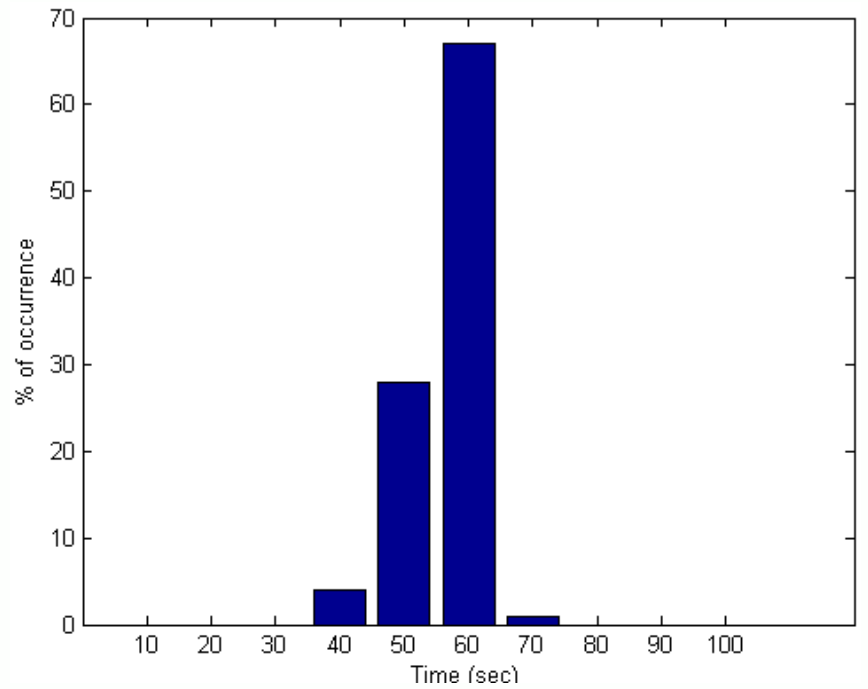

Fig. 12 TTFF distribution using the AutoPET

can be seen to diverge rapidly to 0. To make sure that in the rest of the 19 cases the receiver was really tracking the satellite at low power, the power of the satellite was increased again after an additional 30 seconds. In each of the 19 cases, the receiver successfully continued to track the satellite.

3.3 3D Position Accuracy & Time to First Fix

Computation of the position fix was performed using Least Squares algorithm without any filtering. Using only the AutoPET, 100 position fix iterations were performed and the average 3D error in meters was computed. Within the same test-case, the time for achieving position fix was also recorded. As shown in Fig. 11, the initial (0 – 30 sec) position fix estimates are not very accurate. This is because only the first 4 acquired satellites are used for the position computation. As more satellites are acquired and tracked, their inclusion into the computation gradually improves the position accuracy to within 1 meter. Fig. 12 shows the distribution of TTFF on a time-scale divided into decades of seconds. The average TTFF was computed to 60.59 sec.

3.4 Validity of C/No Estimator

Fig. 13 and Fig. 14 present a comparison of C/No measurements between the TUTGNSS receiver (extracted using the dCAP) and a commercial receiver [10]. For Fig. 13, the input power from the simulator was varied between -130 dBm and -151 dBm with steps of around 2 dB for 10 seconds each. The C/No readings from the two receivers were measured at each power level and plotted on the same

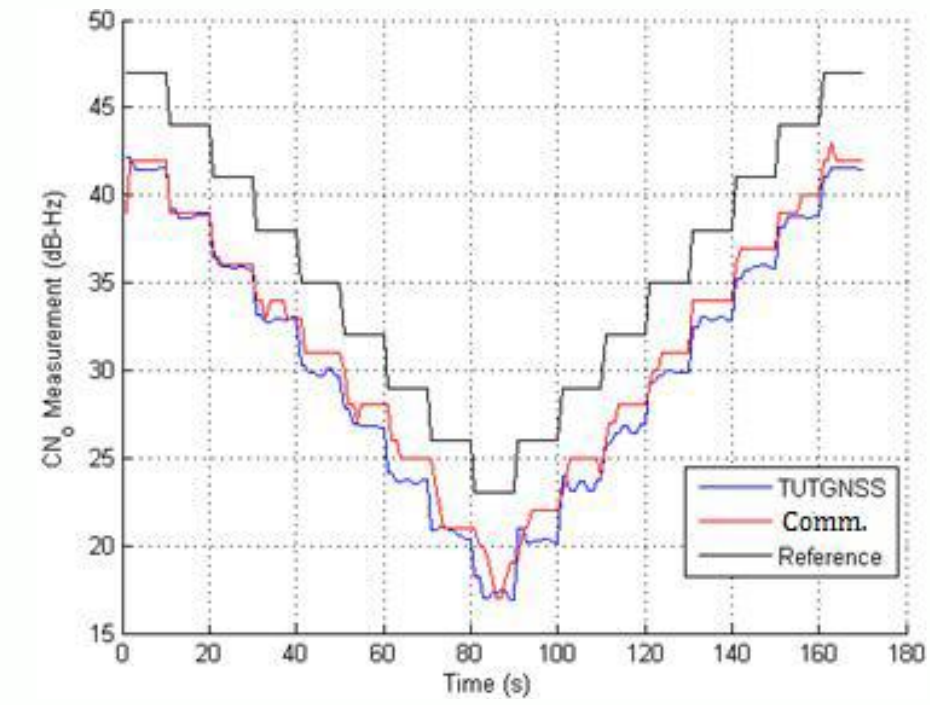

Fig. 13 C/No measurement using the dCAP – Comparison between TUTGNSS, a Commercial and a hypothetical receiver

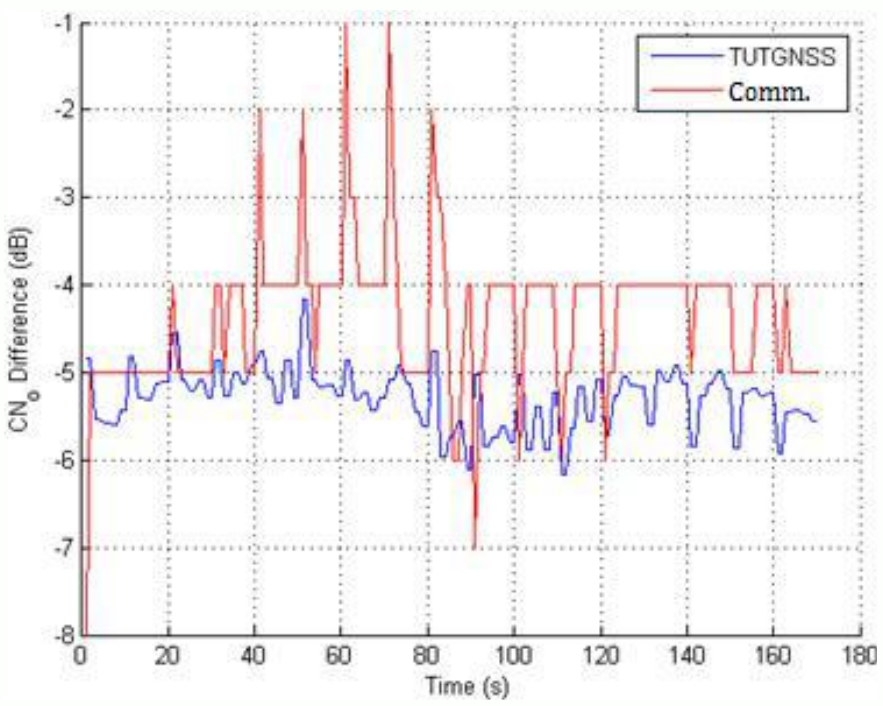

Fig. 14 Blue = TUTGNSS Rx C/No – Hypothetical Rx C/No
Red = Commercial Rx C/No – Hypothetical Rx C/No
(Difference between the C/No as shown in Fig. 13)

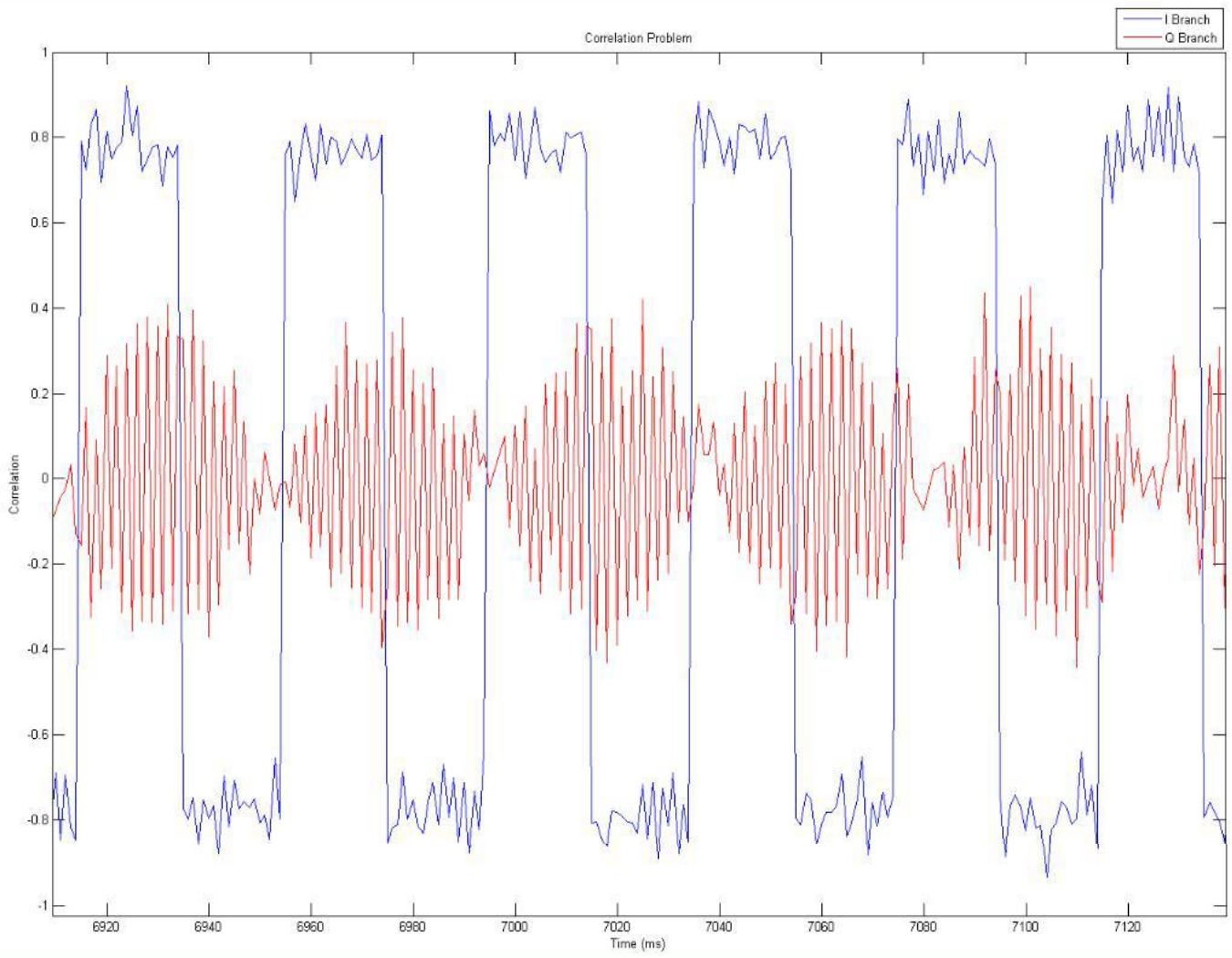

Fig. 15 Signal anomaly in the Q-branch signal due to insufficient clock buffering in the experimental RF FE – detected using the dCAP

scale. The reference power level represents the C/No readings of a hypothetical (ideal) receiver with zero radio FE losses. As the figure shows, on average there is close conformance between the estimated values of C/No in the two receivers. The difference between the two receivers and the reference is approximately 5 dB, which includes Radio FE noise and other losses. Fig. 14 shows the instantaneous difference in C/No between the reference and each of the two receivers taken at every power level. The figure shows that the TUTGNSS receiver displays lower C/No estimation peak-to-peak inconsistency than the commercial receiver.

3.5 Other uses of dCAP

During initial prototype validation, it was noticed that the satellite tracking was inconsistent even under high SNR conditions. The dCAP was used to extract detailed baseband tracking information that helped to identify the source of the problem - signal anomalies due to insufficient clock buffering on experimental RF FE, as shown in Fig. 15. Such anomalies would have been impossible to detect with traditional black-box testing practices. Once the problem was rectified, the dCAP was used once again to monitor the RF FE signals and performance of the baseband tracking loops, where Figs. 16-20 show a marked improvement in the receiver signal processing and satellite tracking performance.

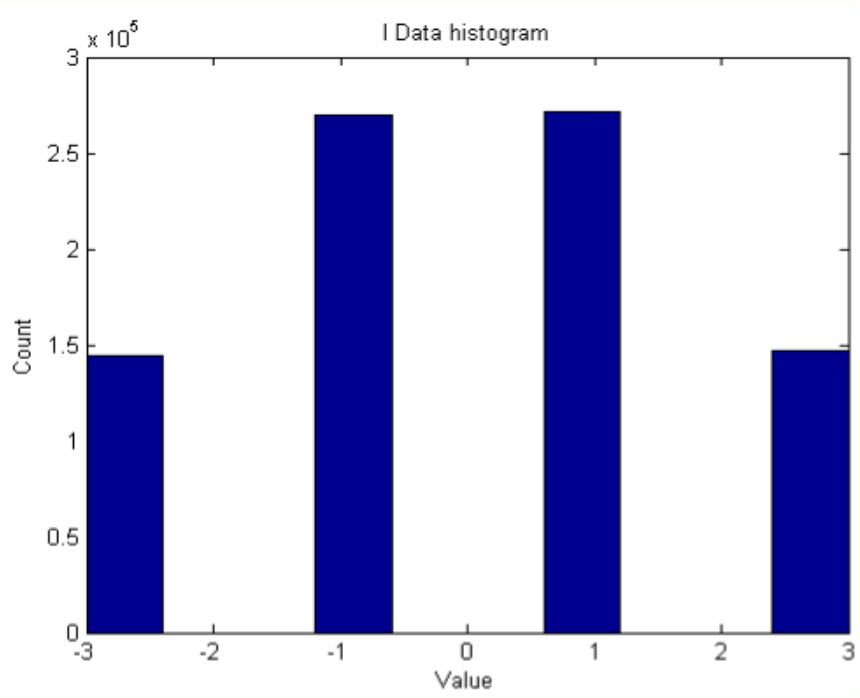

Fig. 16 Histogram of I-branch raw samples from the RF FE captured by the dCAP

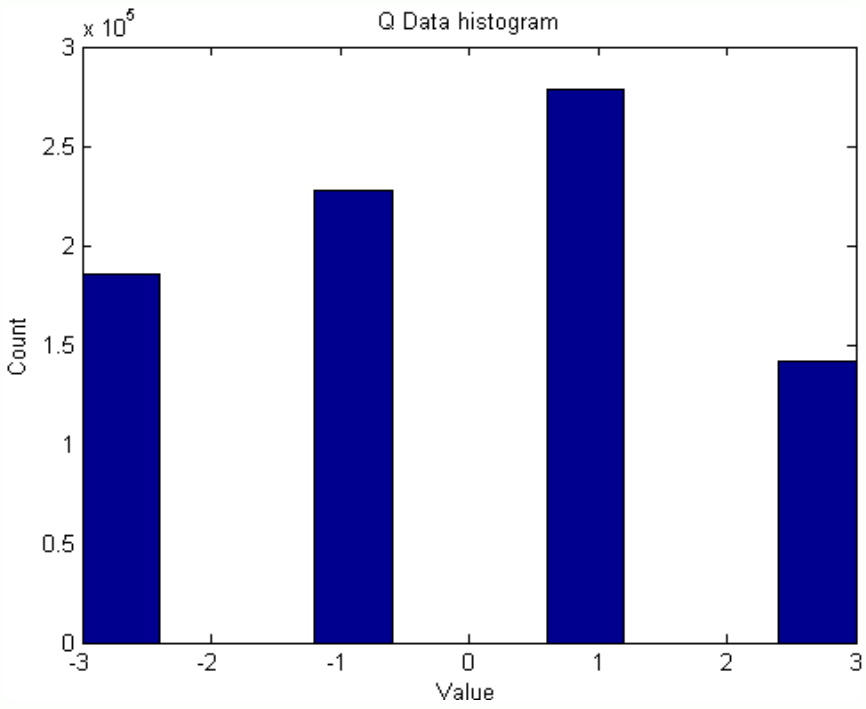

Fig. 17 Histogram of Q-branch raw samples from the RF FE captured by the dCAP

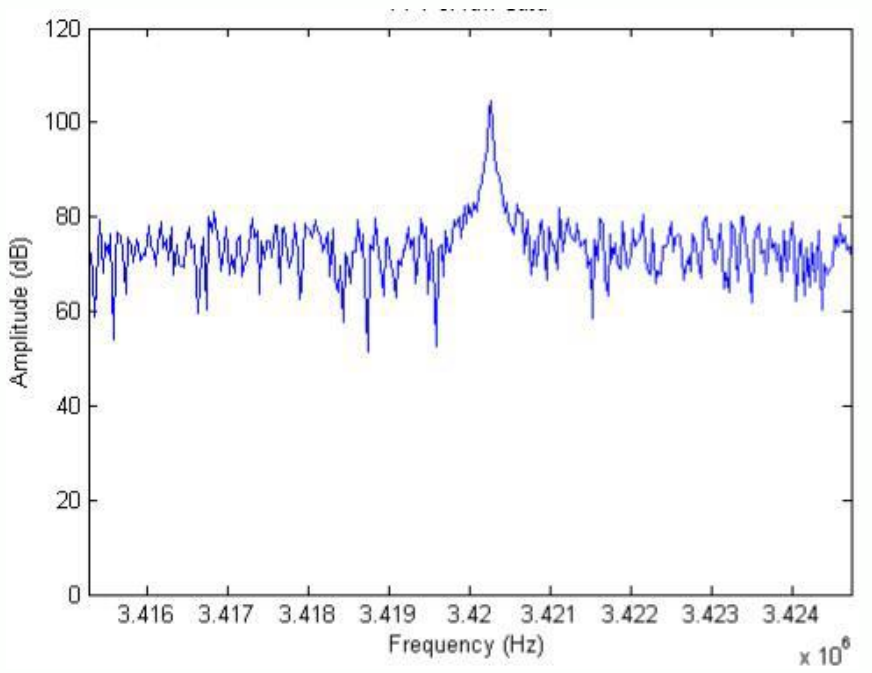

Fig. 18 FFT of the raw samples from the RF FE captured by dCAP (IF = 3.42MHz)

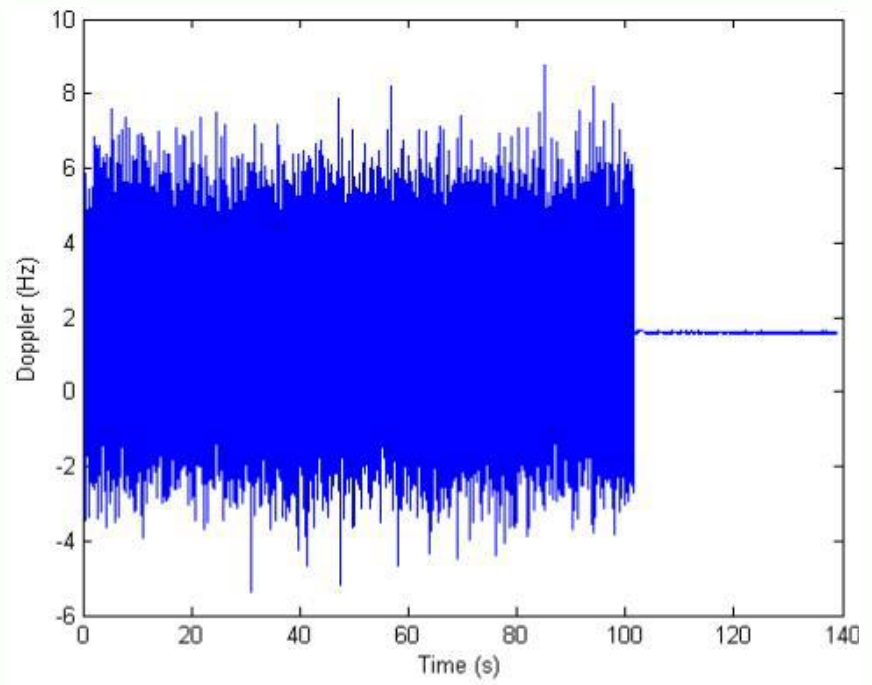

Fig. 19 Code Doppler extracted from one tracking loop

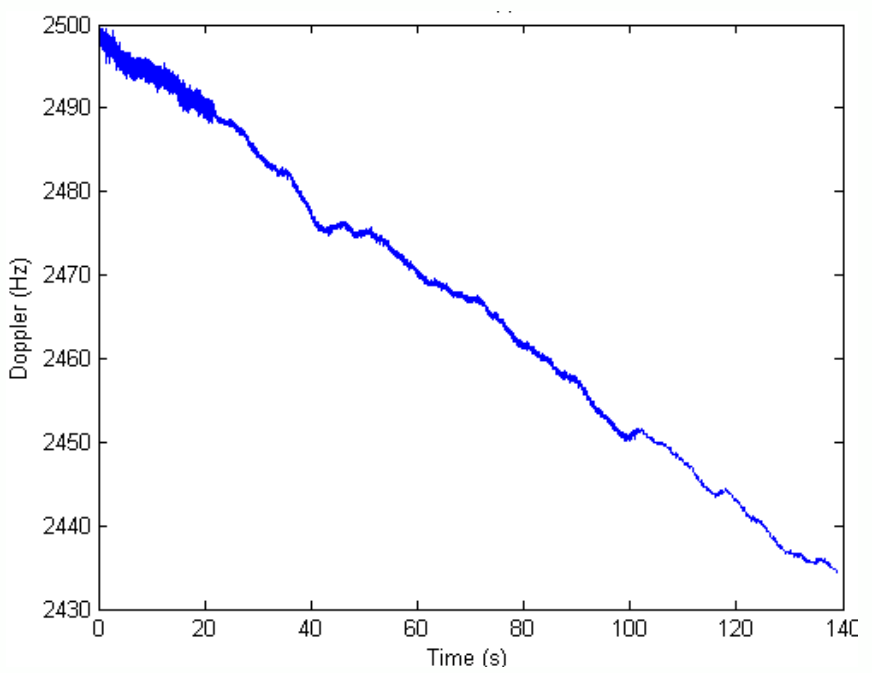

Fig. 20 Carrier Doppler extracted from one tracking loop using the dCAP

Conclusions

In this paper we have demonstrated the results of the TUTGNSS prototype receiver testing using the AutoPET and dCAP. Results were presented, analyzed and conclusions drawn for the GPS L1 performance of the receiver. Furthermore, the procedures can be easily replicated through software modifications for testing more advanced multi-frequency, multi-constellation modes of the receiver.

Added to the benefits of automation in terms of improved accuracy and personnel efficiency, the proposed AutoPET is a cost-effective solution to anyone working on GNSS receiver technology to understand its most important performance parameters. This tool is portable (software platform-independent), easy to install and execute on any computer with the basic scientific software. From an academic point of view, the dCAP is useful for teaching the spectral characteristics of GNSS signals at every stage from deep inside the receiver to researchers or university students in laboratory exercises. Together, these tools have assisted in the complete characterization of the TUTGNSS receiver at our University, and can be easily adapted, enhanced and applied to other research-based receivers as well. In other words, the proposed research has an academic as well as practical appeal.

Acknowledgements

This research work has received support from the Tampere Doctoral Programme in Information Science and Engineering (TISE), Nokia Foundation, and the Ulla Tuominen Foundation. It has also been partially supported by the Academy of Finland (under the projects: 251138 "Digitally-Enhanced RF for Cognitive Radio Devices", and 256175 “Cognitive Approaches for Location in Mobile Environments”). We wish to gratefully acknowledge each of these institutions.

References

[1] T. Paakki, J. Raasakka, F. Della Rosa, H. Hurskainen, J. Nurmi, *TUTGNSS University based hardware/software GNSS receiver for research purposes*, Ubiquitous Positioning Indoor Navigation and Location Based Service (UPINLBS), 2010 , vol. 1, no. 6, pp. 14-15, Oct. 2010

[2] S. Thombre, E. S. Lohan, J. Raquet, H. Hurskainen, J. Nurmi, *Software-based GNSS Signal Simulators: Past, Present and Possible Future*, Proceedings of the European Navigation Conference (ENC GNSS 2010), October 2010 in Braunschweig, Germany.

[3] P. Boulton, R. Borsato, B. Butler, K. Judge, *GPS Interference Testing: Lab, Live, and LightSquared*, InsideGNSS, July/August 2011. Available at: http://www.insidegnss.com/node/2674

[4] Spirent Communications UK, *TestDrive GNSS: Simplify testing, reduce cost, increase efficiency of GNSS test*, Product Datasheet, March 2012. Available at: http://www.spirent.com/~/media/Datasheets/Positioning/TestDrive%20GNSS.pdf

[5] Rohde & Schwarz, *GPS, GLONASS, Galileo Receiver Testing Using a GNSS Signal Simulator (R&S®SMBV100A)*: Application Note - 1GP86_1E, Available at: http://www.insidegnss.com/special/elib/RS_GNSS_Receiver_Testing.pdf

[6] VALTES, *Digital Broadcasting Receiver Test Solutions*, Available at: http://www.valtes.co.jp/en/testing_field/digital_broadcasting/index.html

[7] Agilent Technologies, *N5990A Test Automation Software Platform - Multi-Bus Stimulus/Response Test Software*, Data Sheet, Version 3.1, Available at: http://cp.literature.agilent.com/litweb/pdf/5989-5483EN.pdf

[8] Tektronix, *BSAPCI3 - PCI 3.0 Receiver Test Software*, Datasheet, Available at: http://www.tek.com/sites/tek.com/files/media/media/resources/BSAPCI3-PCI-3.0-Receiver-Test-Software-Datasheet_65W-28485-0.pdf

[9] Tronico, *The NMEA 0183 Protocol*, Available at: http://www.tronico.fi/OH6NT/docs/NMEA0183.pdf. Official website of the National Marine Electronics Association: http://www.nmea.org/

[10] u-blox, EVK-5 u-blox 5 Evaluation Kits - EVK-5P u-blox 5 Evaluation Kit with SuperSense®, Available at: http://www.amtechs.co.jp/2_gps/pdf/EVK-5.pdf

Tampereen teknillinen yliopisto
PL 527
33101 Tampere

Tampere University of Technology
P.O.B. 527
FI-33101 Tampere, Finland

ISBN 978-952-15-3259-7
ISSN 1459-2045